

NASA Conference Publication 2172

NASA
CP
2172
c.1

Advanced Aerodynamics and Active Controls

Selected NASA Research



LOAN COPY: RETURN TO
AFRL TECHNICAL LIBRARY
KIRTLAND AFB, N.M.



*Contributions from NASA Research Centers
to the Fourth Annual Status Review of the
NASA Aircraft Energy Efficiency (ACEE)
Energy Efficient Transport Program held at
Ames Research Center, Mountain View, California
October 7-9, 1980*

NASA



NASA Conference Publication 2172

Advanced Aerodynamics and Active Controls

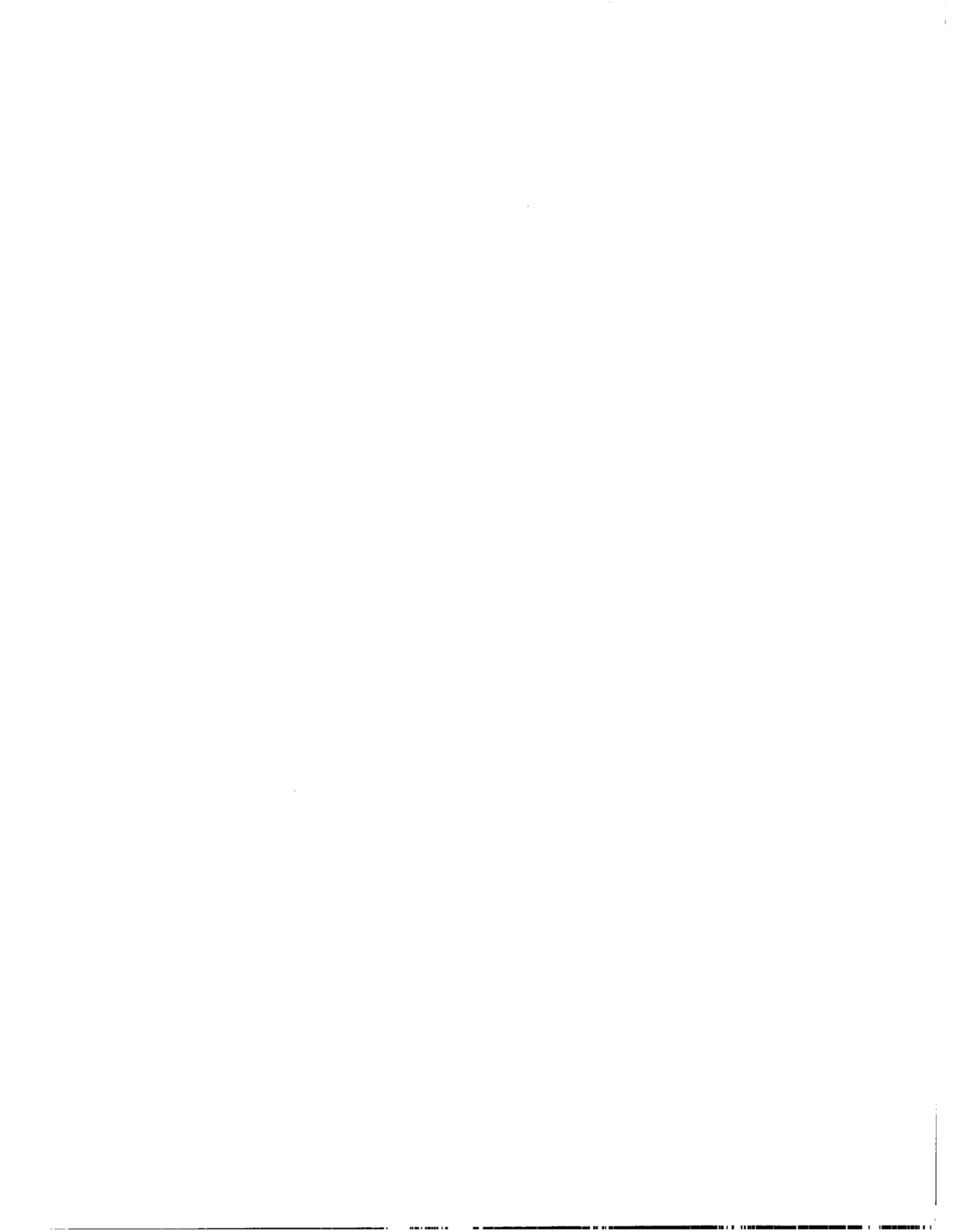
Selected NASA Research

Contributions from NASA Research Centers
to the Fourth Annual Status Review of the
NASA Aircraft Energy Efficiency (ACEE)
Energy Efficient Transport Program held at
Ames Research Center, Mountain View, California
October 7-9, 1980

NASA

National Aeronautics
and Space Administration

**Scientific and Technical
Information Office**



FOREWORD

The NASA Aircraft Energy Efficiency (ACEE) Energy Efficient Transport Program has made significant progress in developing technology required for application of advanced aerodynamic and active control concepts to commercial transport aircraft. Under NASA sponsorship, commercial airframe manufacturers are four (4) years into programs to develop aerodynamic and active control concepts which will lead to significant fuel savings for both near-term derivatives and future new aircraft. Timely dissemination of technical information acquired in these programs is achieved through distribution of written final reports and through annual status reviews.

The fourth annual status review of the ACEE Energy Efficient Transport (EET) Program was held October 7-9, 1980, at the NASA Ames Research Center in Mountain View, California. The conference included comprehensive reviews of major contracts by the ACEE EET contractors: Boeing Commercial Airplane Company, Douglas Aircraft Company, and Lockheed-California Company. In addition, two special sessions included selected papers describing NASA sponsored research in advanced aerodynamics and active controls. These latter presentations are collected in this NASA Conference Publication.

Individual authors prepared their narrative and figures in a form that could be directly reproduced in this volume. The material is in facing page format and is essentially the same material used in the oral presentations at the review. This status review (fourth annual) is the first to be documented by a NASA Conference Publication.

Use of trade names or names of manufacturers in this report does not constitute an official endorsement of such products or manufacturers, either expressed or implied, by the National Aeronautics and Space Administration.

Ray V. Hood
Conference Chairman
Langley Research Center

CONTENTS

Foreword	iii
1. Langley Research Center Contributions in Advancing Active Control Technology I. Abel and J. R. Newsom	1
2. Status and Future Plans of the Drones for Aerodynamic and Structural Testing (DAST) Program Harold N. Murrow	21
3. Transport Aircraft Flying Qualities Activities Martin T. Moul	37
4. In-Flight Direct Strike Lightning Research Felix L. Pitts	43
5. Ground and Flight Test Experience With a Triply Redundant Digital Fly-by-Wire Control System Calvin R. Jarvis and Kenneth J. Szalai	67
6. Small Transport Aircraft Technology Thomas L. Galloway	85
7. Status Report on an Investigation of Powered Nacelles on a High Aspect Ratio NASA Supercritical Wing - Phase II Stuart G. Flechner; James C. Patterson, Jr.; and Paul G. Fournier	105
8. Status Report on the EET Horizontal Tails Investigation and the EET Lateral Controls Investigation Peter F. Jacobs and Dennis W. Bartlett	123
9. Natural Laminar Flow Flight Experiment Louis L. Steers	135
10. KC-135 Winglet Flight Results Lawrence C. Montoya	145
11. Overview of Advanced Wing Design Raymond M. Hicks	157
12. Advanced Turboprop Installation Aerodynamics R. C. Smith	171

LANGLEY RESEARCH CENTER CONTRIBUTIONS IN ADVANCING
ACTIVE CONTROL TECHNOLOGY

I. Abel and J. R. Newsom
NASA Langley Research Center

ABSTRACT

The application of active control technology to reduce aeroelastic response of aircraft structures offers a potential for significant payoffs in terms of aerodynamic efficiency and weight savings. To reduce technical risks, research was begun at NASA in the early 1970's to advance this concept. This presentation describes some of the contributions of the Langley Research Center in advancing active control technology. Contributions are categorized into the development of appropriate analysis tools, control law synthesis methodology, and experimental investigations aimed at verifying both analysis and synthesis methodology. The work reported herein was either performed in-house or under contract to the Structures Directorate at LaRC.

CONTRIBUTIONS

This chart lists three of the areas to which the LaRC has made contributions advancing active control technology. The following charts will expand on each of these areas.

- ANALYSIS
- CONTROL LAW SYNTHESIS
- EXPERIMENTS

Figure 1

STABILITY ANALYSIS

This chart describes the difficulty in performing a stability calculation for an actively controlled flexible aircraft including the effects of unsteady aerodynamics. The structural quantities are defined in terms of the generalized masses [M], the structural damping coefficients [C], and the structural stiffnesses [K]. The control law is normally expressed as a transfer function which relates control surface motion to aircraft response and is written as a ratio of polynomials in the Laplace variable S. The unsteady aerodynamics are computed for simple harmonic motion at specific values of reduced frequency and can not be cast into the form shown on the chart. The problem facing the analyst is to develop a set of constant coefficient differential equations where the unsteady aerodynamics, the control law, and the structural terms are compatible. Once the equations are cast into this form, a number of synthesis and analysis methods developed for other applications may be utilized.

● EQUATIONS OF MOTION

$$\begin{aligned} & [M]\{\ddot{q}\} + [C]\{\dot{q}\} + [K]\{q\} && \text{STRUCTURE} \\ + & [C_1]\{\delta\} + [C_2]\{\dot{\delta}\} + [C_3]\{\ddot{\delta}\} && \text{CONTROLS} \\ + & [A_0]\{q\} + [A_1]\{\dot{q}\} + [A_2]\{\ddot{q}\} + \dots = 0 && \text{AERODYNAMICS} \end{aligned}$$

● STABILITY

CONSTANT COEFFICIENT DIFFERENTIAL EQUATIONS

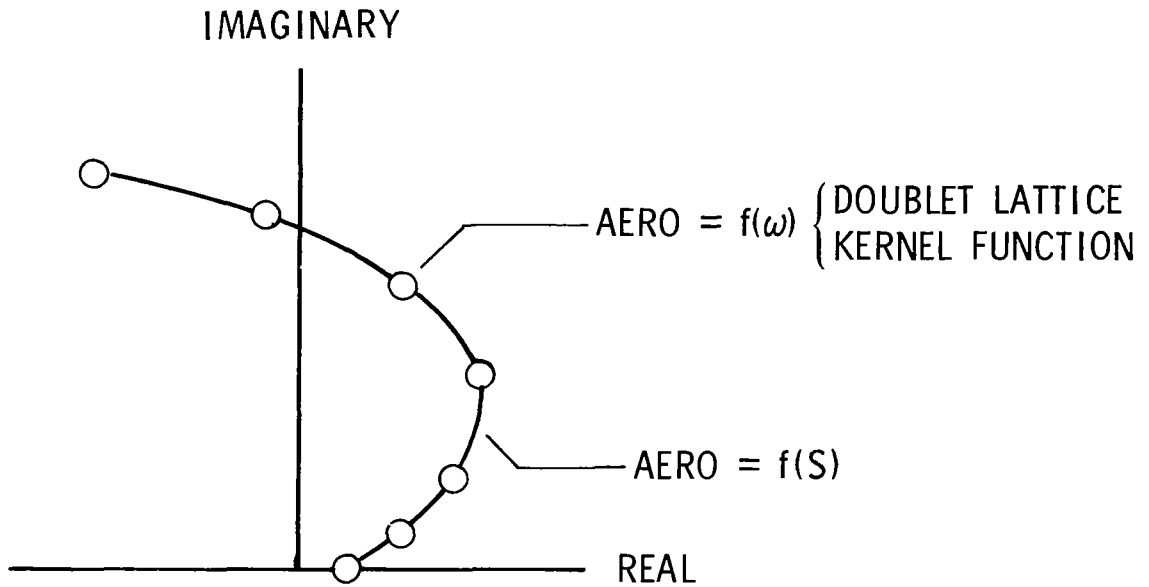
$$\{\dot{q}\} = S\{q\} \quad \{\ddot{q}\} = S^2\{q\} \dots$$

● UNSTEADY AERODYNAMICS NOT IN THIS FORM

Figure 2

UNSTEADY AERODYNAMIC APPROXIMATION

In lieu of developing a completely new aerodynamic theory, the approach taken is to allow the variation of the aerodynamic forces with frequency to be approximated by a rational function in the variable S . The form of the function presented permits an approximation of the time delays inherent in unsteady aerodynamics subject to: denominator roots in the left-hand plane, and a good approximation of the complex unsteady aerodynamic terms at $S = j\omega$. The approximating coefficients (A_0, A_1, \dots, A_6) are evaluated by a least-squares curve fit through the values of complex aerodynamic terms at discrete values of frequency. The chart illustrates a typical fit. The solid curve represents the approximating function. This technique is similar to that described in reference 1.



$$AERO(S) = A_0 + A_1 S + A_2 S^2 + \sum_{m=3}^6 \frac{A_m S}{S + \beta_{m-2}}$$

Figure 3

TYPICAL DYNAMIC PRESSURE ROOT LOCUS

Using the aerodynamic approximating functions, the stability problem is solved by calculating the roots of the characteristic equation. This chart presents a typical root locus of the flexible mode roots as a function of dynamic pressure for the DAST ARW-1 vehicle (arrows indicate increasing dynamic pressure). The solid line represents the no control case. A classical flutter behavior is apparent since the frequency of flexible modes 1 (wing bending) and 2 (wing torsion) tend to coalesce as mode 1 crosses into the unstable region. Calculations performed for the wing with flutter suppression (dashed line) indicate that the flutter can be delayed to dynamic pressures approaching 100 percent above the no control case. Analyses of this type are of extreme value to the designer since he can see graphically the manner in which the control system is modifying the behavior of the flexible mode roots. A description of this analysis method is presented in reference 2.

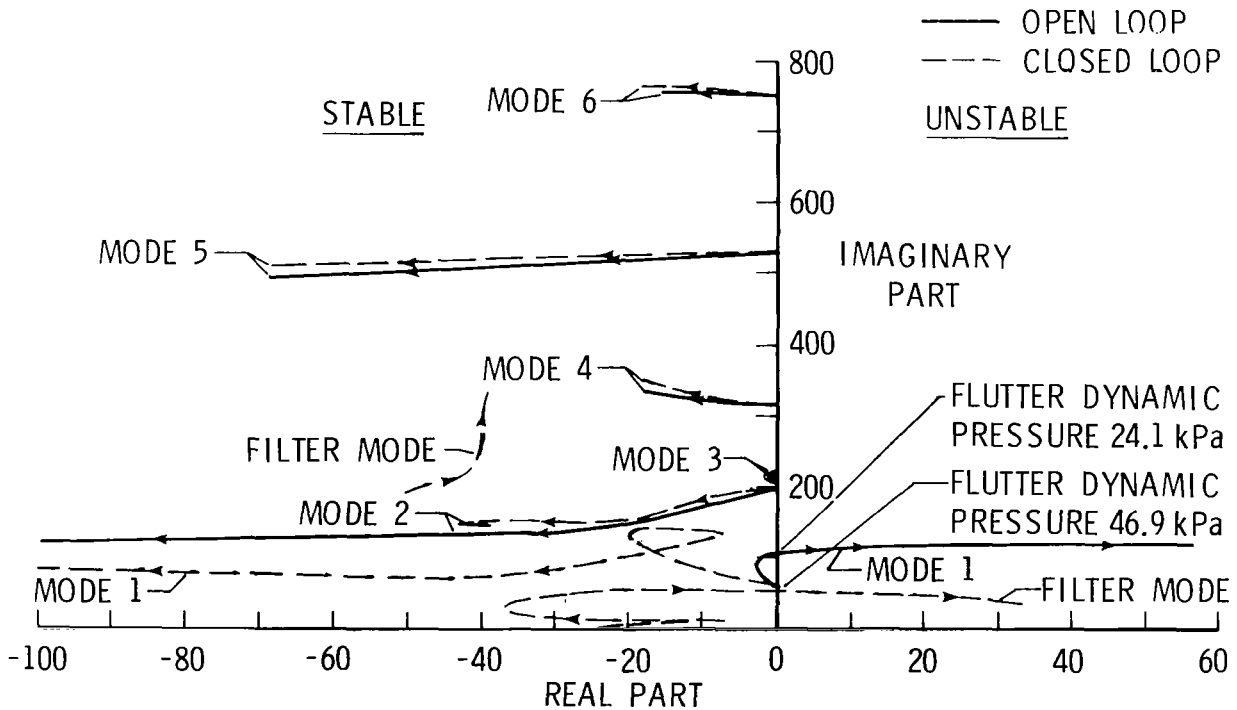


Figure 4

DYLOFLEX

DYLOFLEX is an integrated system of stand-alone computer programs which performs dynamic loads analyses of flexible airplanes with active controls. DYLOFLEX incorporates a wide range of analysis capabilities which include calculating dynamic loads due to (1) continuous atmospheric turbulence, (2) discrete gusts, and (3) discrete control inputs. The input to DYLOFLEX consists of externally generated structural data, vehicle geometry, a transfer function representation of the active control system, and flight condition information. The output consists of either statistical quantities or time histories of the dynamic loads. DYLOFLEX is well documented and available from COSMIC (Computer Software Management and Information Center). It was developed under contract by the Boeing Company, Seattle, Washington. An overview of its capabilities is presented in reference 3.

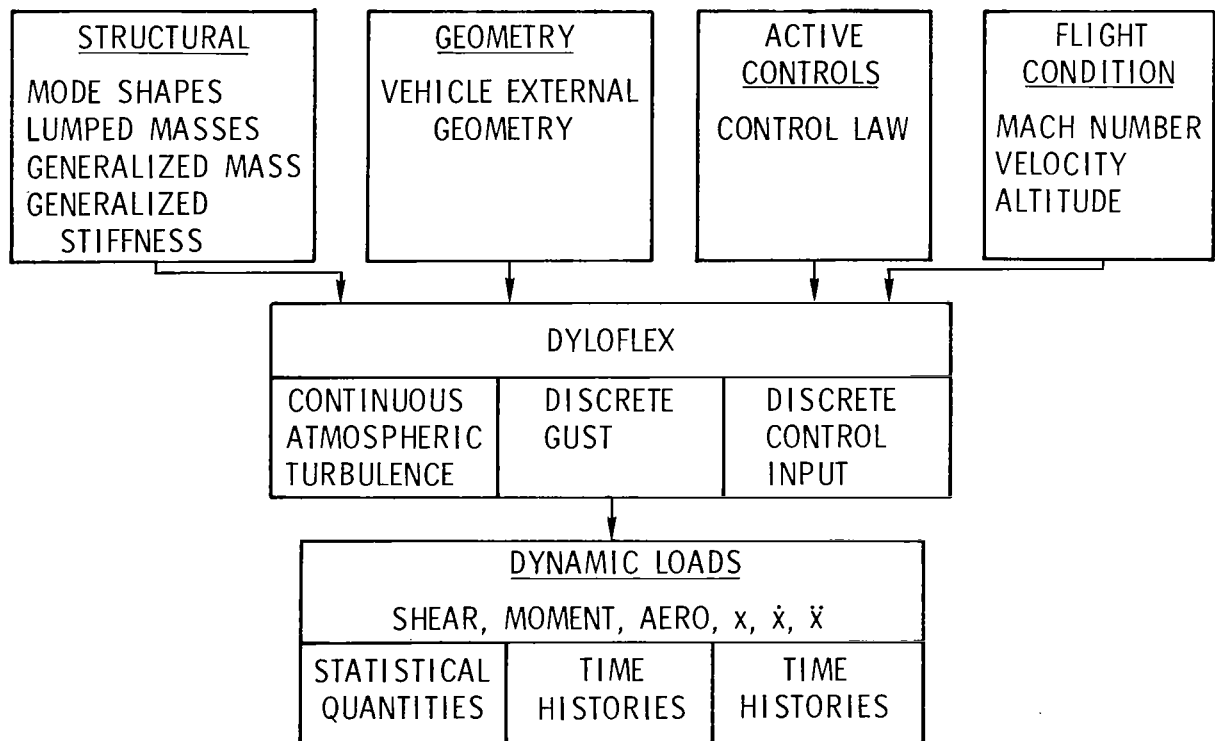


Figure 5

TYPICAL DYLOFLEX RESULTS

A typical example of DYLOFLEX's capability is presented on this chart. A wind-tunnel model of a DC-10 derivative wing was analyzed. Predicted gust loads, both with and without an active control system, were calculated. Structural input data were provided by the Douglas Aircraft Company. Turbulence was modeled as a Dryden spectrum fitted to measured wind-tunnel data. Results are presented in terms of the rms values per unit gust velocity of wing acceleration and wing bending moment as a function of wing semispan.

DYLOFLEX has also been applied to several other aircraft configurations, both at NASA and within the aircraft industry. It has been shown to be suitable for both preliminary and final design studies.

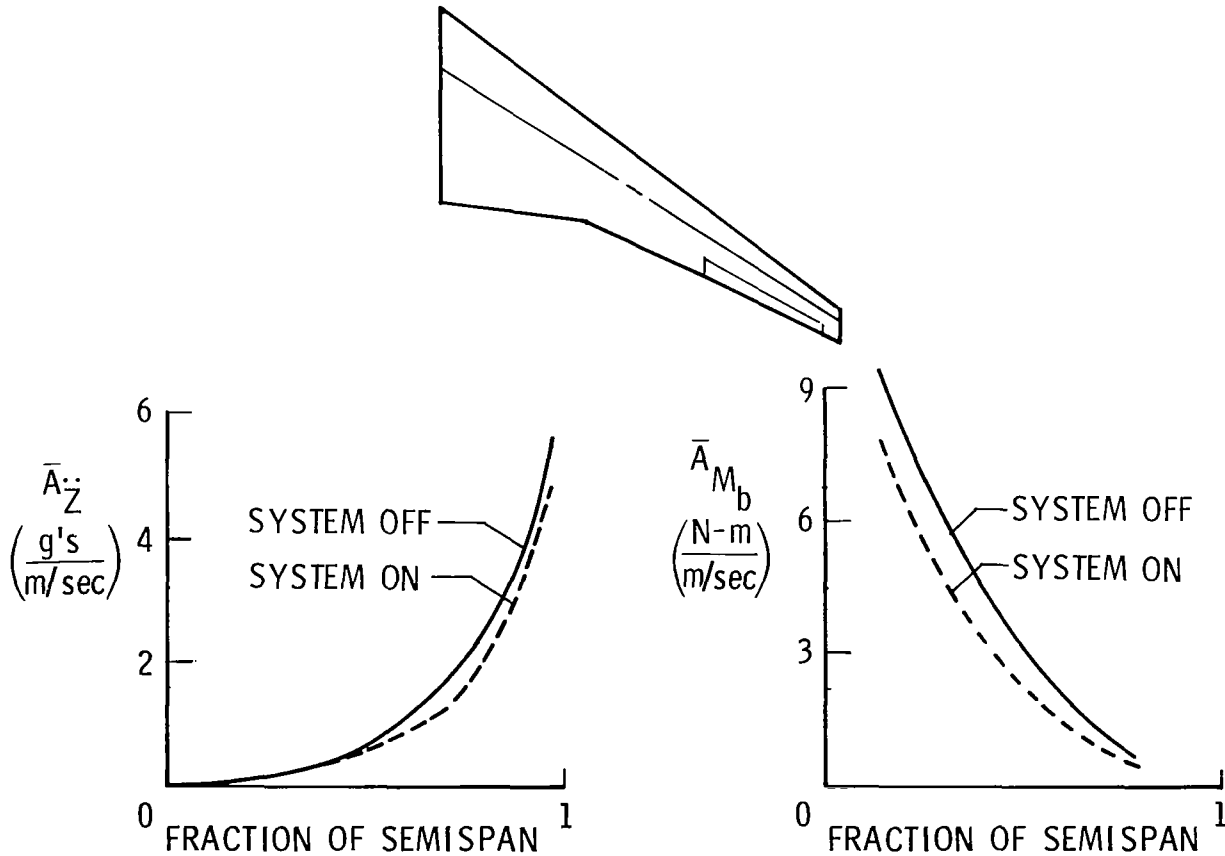


Figure 6

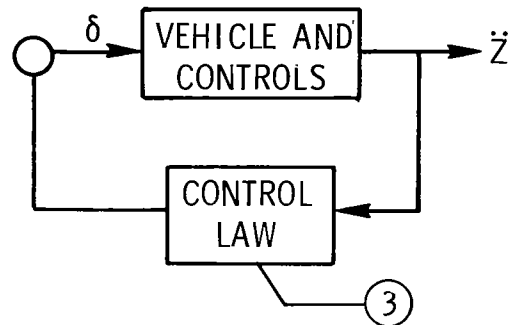
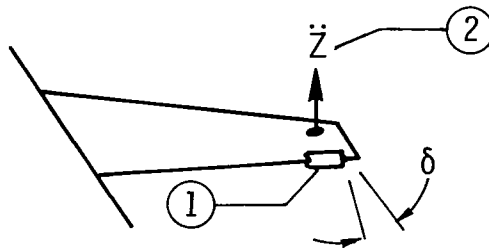
CONTROL LAW SYNTHESIS

Through the proper selection of (1) control surfaces and (2) sensors, (3) control laws can be synthesized to:

- o Increase flutter speed
- o Reduce loads due to gusts
- o Reduce wing loading during maneuvers
- o Reduce acceleration levels within the crew and passenger compartments
- o Augment the basic aircraft stability

Due to its impact on safety of flight, flutter suppression is probably the active control concept furthest from realization and is therefore an area of primary emphasis within NASA. The synthesis methods which will be described deal primarily with active flutter suppression but the methodology can also be extended to other active control functions.

PROBLEM:



FOR:

- FLUTTER SUPPRESSION
- GUST LOAD ALLEVIATION
- MANEUVER LOAD CONTROL
- RIDE QUALITY CONTROL
- RELAXED STATIC STABILITY

Figure 7

SYNTHESIS METHODS

Three methods for synthesizing active control systems that the authors have used and are familiar with are listed on this chart. All three methods have been applied to the flutter suppression problem.

- CLASSICAL
- AERODYNAMIC ENERGY
- OPTIMAL CONTROL THEORY

Figure 8

CLASSICAL CONTROL THEORY

This chart describes the basic steps used when applying classical control theory. The first two steps are common to all three methods and normally begin with a parametric investigation, at a design point, to establish the number and location of control surfaces and sensors needed to provide the increased stability. In many cases, this step is a result of engineering judgment or the constraint that existing control surfaces be used. Once the number and location of control surfaces and sensors are fixed, a control law is designed using a combination of classical techniques including gain root loci, Nyquist diagrams, trial and error, and engineering judgment. The stability of the system is now evaluated over a range of flight conditions. If the system is unstable at off-design conditions, the control law is modified. At this point in the design process, the forced response of the system to a realistic gust environment is evaluated. If the control surface activity is beyond the capability of the actuator, either the control law is modified or the control surface is resized. In this method, stability and forced response analyses are sequential and can lead to time consuming iterations. Once the system meets both stability and gust criteria, the design is complete.

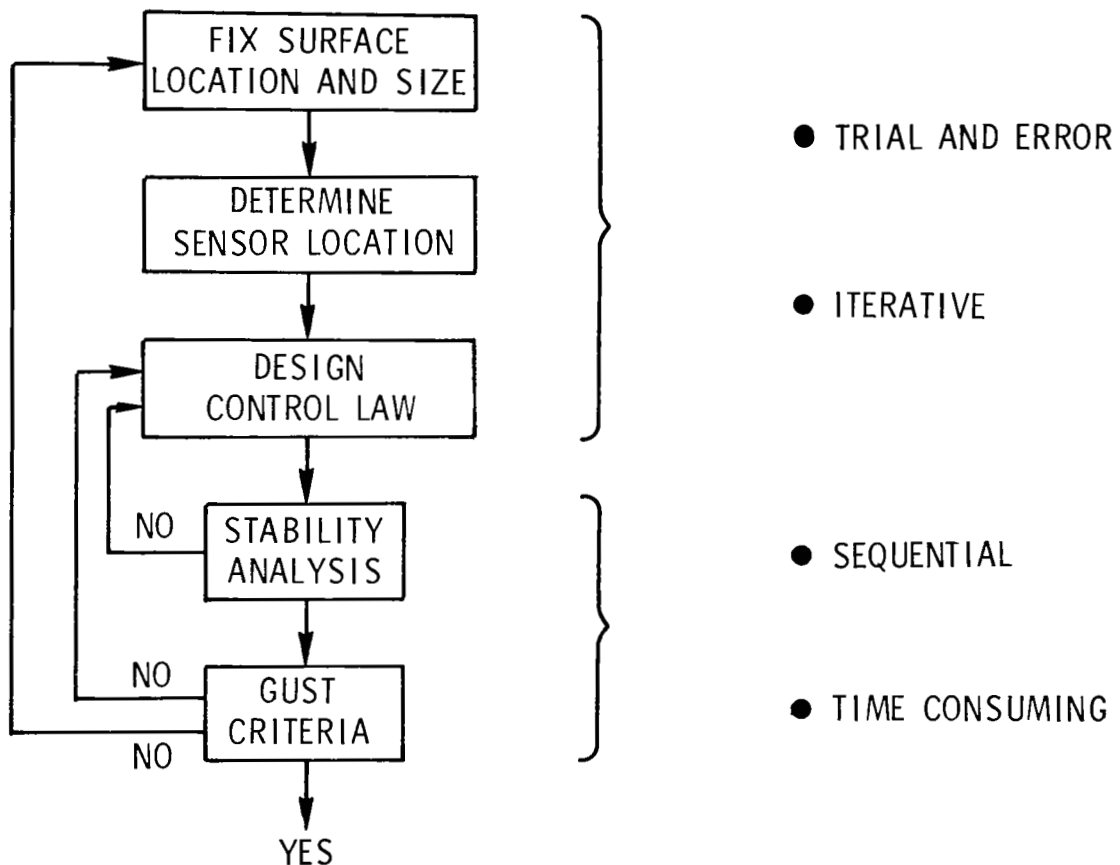


Figure 9

AERODYNAMIC ENERGY PRINCIPLE

This chart presents the steps used when applying the relaxed aerodynamic energy method to the simplest case of a single trailing-edge control surface and a single second-order transfer function. (The most general case uses a pair of leading- and trailing-edge control surfaces, two accelerometers, and two fourth-order transfer functions.) The first step is to fix the control surface location and size. This is normally done using engineering judgment. The location of the accelerometer is fixed with respect to the control surface. The basic form of the control law has "free parameters" a , ζ , and ω which enables it to be tailored to a specific application. This is accomplished by assigning initial values to the free parameters which stabilize the system at the required design point. This step is performed by trial and error. Experience has shown that if the system is initially stable, and the free parameters are changed in a way to reduce stability, the control surface activity in a gust environment increases. Therefore, the final values of the free parameters are determined by minimizing the forced response of the system to a gust input. By placing constraints on the free parameters as shown in reference 4, the resulting control law will be insensitive to changing flight conditions. In this method, the gust response and stability problems are handled simultaneously and the resulting control law is optimal with respect to control surface activity for the given control surface size, location, and order of the control law.

If, after this process is completed, the maximum control surface activity is unacceptable, then the control surface must either be repositioned, increased in size, or more controls added and the process repeated. It has been the author's experience that when this method is combined with classical design techniques, control laws can be synthesized which are near optimal and have excellent stability margins. (See reference 5)

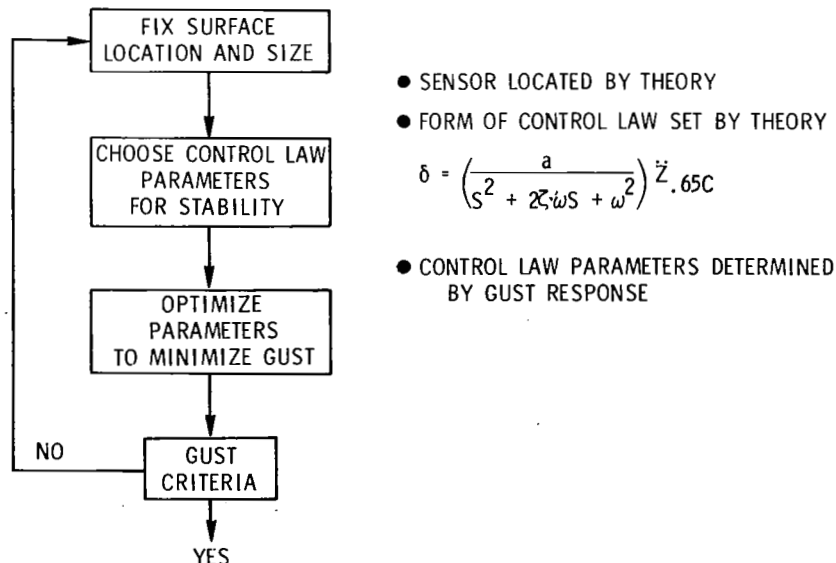
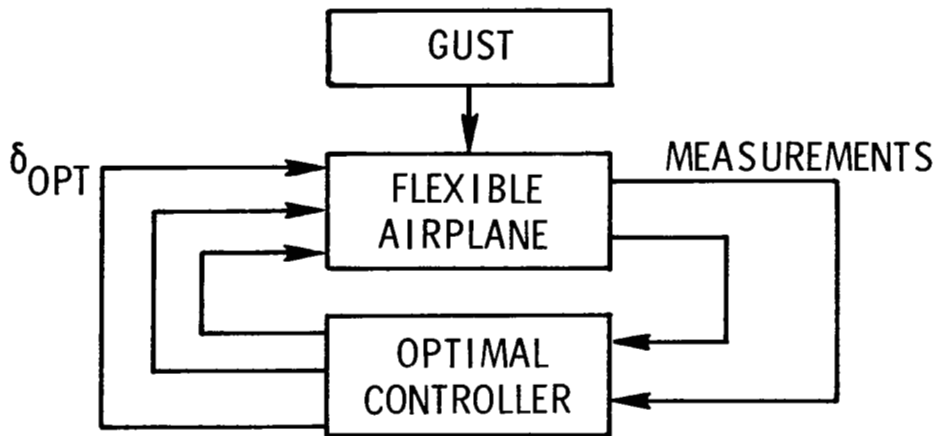


Figure 10

OPTIMAL CONTROL THEORY

Optimal control theory provides an excellent basis for a systematic approach to the control law synthesis problem. The theory is based on the design of a controller which minimizes a performance function. Since the performance function can be defined in terms of such quantities as control deflection, bending moment, acceleration, etc., the method can be adapted quite easily to multiple control tasks. The difficult problem of synthesizing control laws that involve multiple sensors and controls can be handled readily with this method. It also provides the very attractive feature of directly synthesizing digital control laws.



- OPTIMIZATION CRITERIA
 - CONTROL DEFLECTION
 - BENDING MOMENT
- MULTIPLE SENSORS/CONTROLS SIMULTANEOUSLY
- MULTIPLE CONTROL TASKS
- ADAPTABLE TO DIGITAL DESIGN/ANALYSIS

Figure 11

OPTIMAL CONTROLLER DESIGN

The Linear-Quadratic-Gaussian (LQG) method has become the most widely accepted means of synthesizing optimal controllers (ref. 6). However a shortcoming of this method, in particular for high-order systems (characteristic of flexible airplanes), is the requirement that the control law be of the same order as the system being modeled. That is, all states of the system must be estimated. Not only is this unnecessarily complex, but this full-order control law is often sensitive to small changes in the system parameters and very difficult to implement in a flight computer. The usual method for designing a low-order control law from optimal control theory is to approximate the full-order control law through order reduction techniques such as truncation, residualization, and transfer function matching (refs. 7, 8, and 9). These techniques all result in low-order control laws that are not optimal.

A new approach has been developed for designing low-order optimal control laws (ref. 10). The basic concept is to begin with a full-order controller. Using engineering judgment, a few key states and their associated design variables and initial values are selected from the full-order solution. A nonlinear programming algorithm is then used to search for the values of the control law variables which minimize the performance function. The resulting low-order control law is optimal for the states selected. The method is direct and results in a control law that is much easier to implement in a flight computer. Comparative features of the new method to the LQG method are given in the chart.

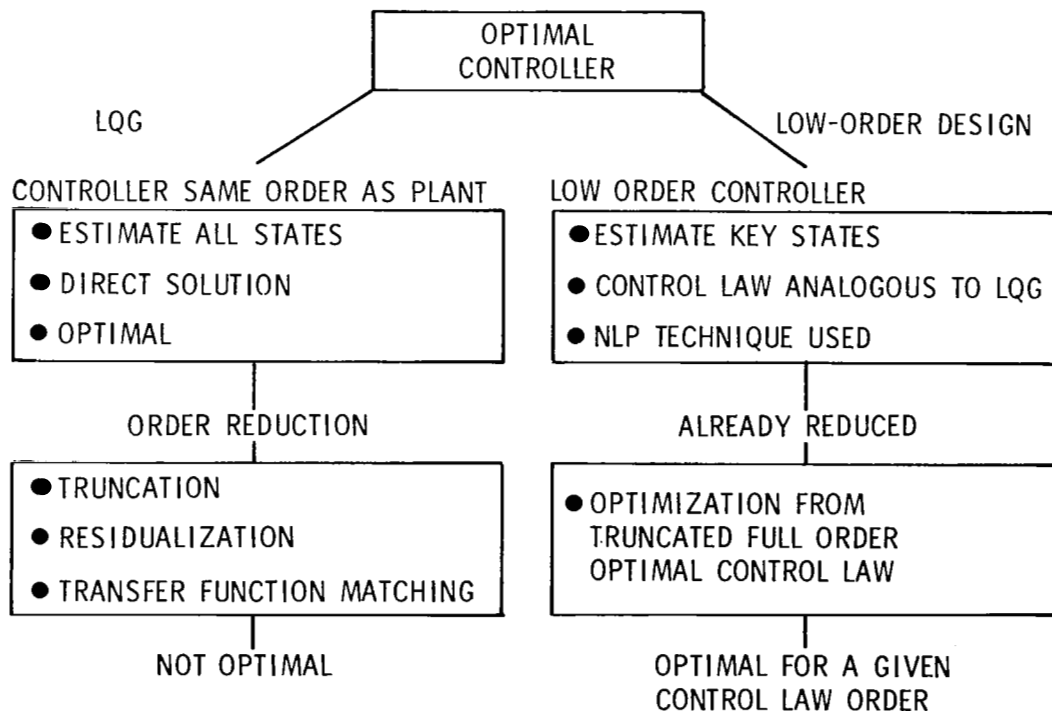


Figure 12

WIND-TUNNEL STUDIES

Wind-tunnel studies of aeroelastic models are a cornerstone of the NASA research program. Presented on this chart are a number of models that have been used to demonstrate active control concepts on a variety of configurations. The Delta-wing model was the first experimental demonstration of flutter suppression in this country (ref. 11). The B-52 model was tested in support of a USAF/Boeing flight study on active controls (ref. 12). Wing load alleviation was studied in support of a USAF/Lockheed program using a C-5A model (ref. 13). The DAST ARW-1 model was used for a variety of flutter suppression studies including an evaluation of the control system that would ultimately be tested on the DAST flight vehicle. Control laws were synthesized and tested on the model using classical, aerodynamic energy, and optimal methods (ref. 5). The F-16 and YF-17 model tests have shown active flutter suppression to be a promising method for preventing wing/external store flutter (refs. 14 and 15). Active controls is especially attractive for fighters because of the multitude of possible store configurations. These studies are part of a cooperative effort with the Air Force Flight Dynamics Laboratory/General Dynamics/Northrop/NASA. The last study was a cooperative effort with the McDonnell Douglas Corporation on a DC-10 derivative wing. The broad objectives were to allow NASA the opportunity to apply in-house control law synthesis methods to a realistic transport configuration with engines on the wing and at the same time provide a rapid transfer of research technology to industry. Increases in flutter speeds in excess of 26 percent were demonstrated. These studies are an extension of those reported in reference 16.

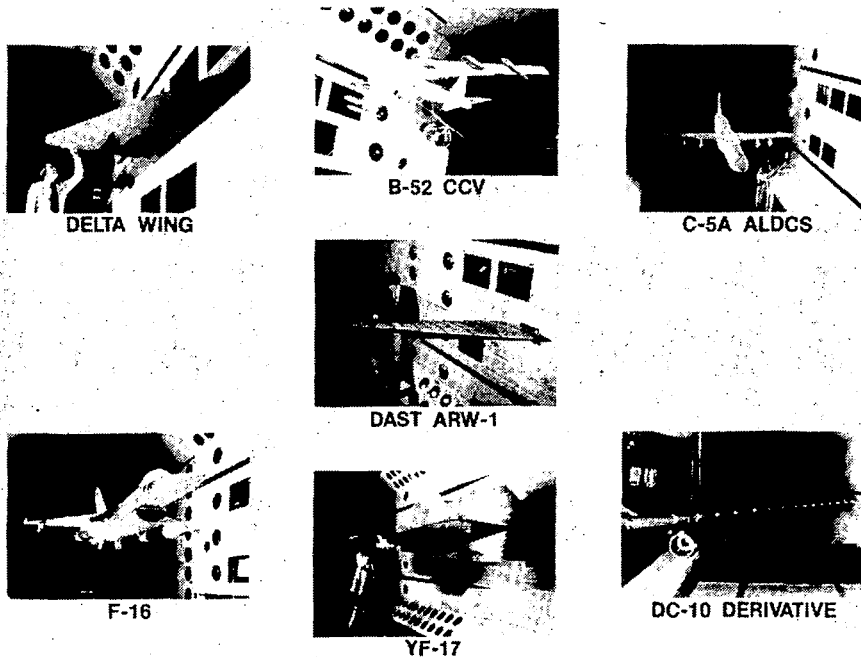


Figure 13

FLUTTER SUPPRESSION DESIGN STUDY

The objective of the wind-tunnel study was to provide a 44 percent increase in flutter dynamic pressure for the aeroelastic model shown on the chart through the use of active controls. Two control laws were designed. One control law is based on the aerodynamic energy method, and the other is based on the results of optimal control theory. Tests were performed in the Langley Transonic Dynamics Tunnel. Both control laws were implemented on an analog computer. The performance of the flutter suppression systems is illustrated by the oscillograph records of wing acceleration and control surface position presented on the chart. The test condition was a dynamic pressure 10 percent above the system-off boundary at $M = 0.90$. The trace begins with the system turned on. The system was then turned off for approximately 4.5 seconds and then turned on again. During the time the system was turned off, the wing began to flutter as evidenced by the rapid buildup of acceleration. The effect of turning the system on again was a rapid suppression of the oscillatory motion. Results of these tests are reported in reference 5.

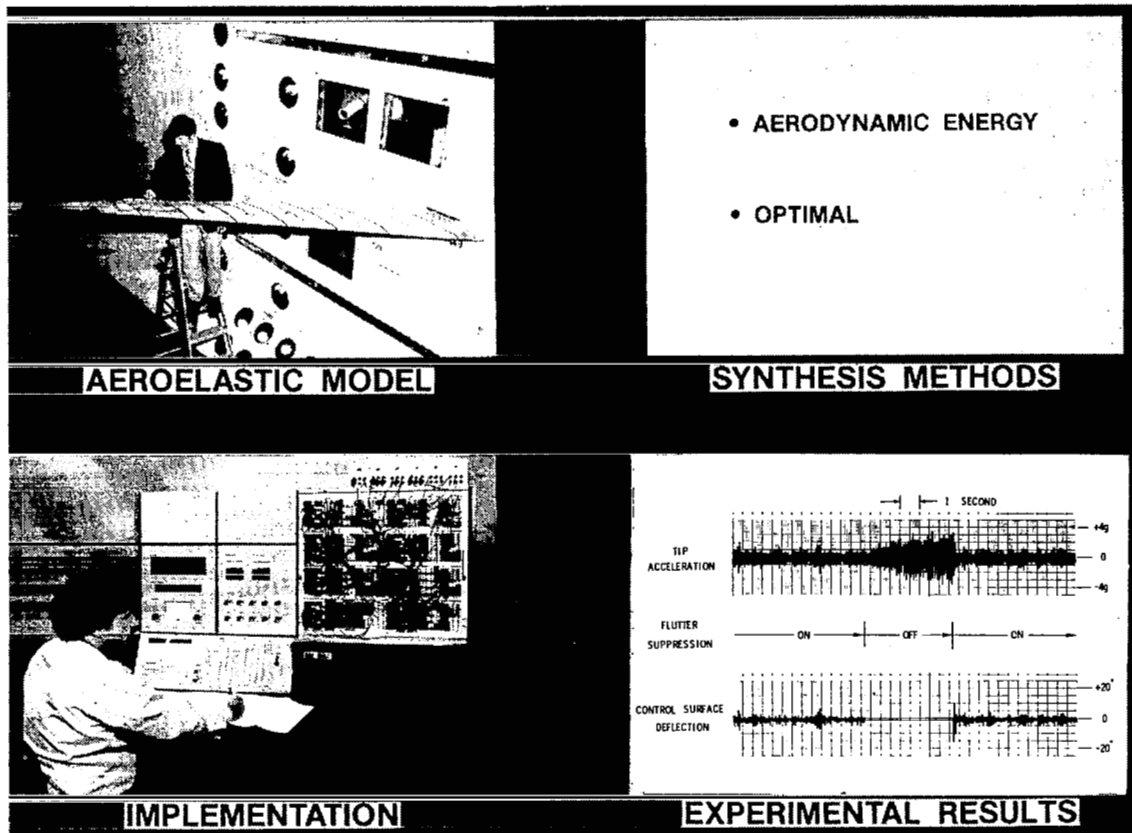
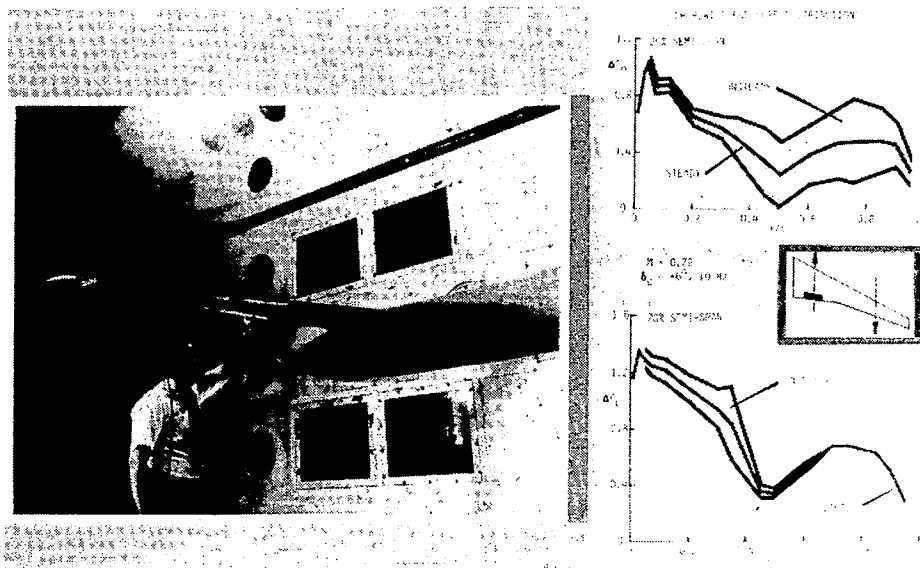


Figure 14

TRANSONIC AIRLOADS

The application of active control technology to advanced airplane designs, such as energy efficient transports, requires the understanding of both steady and unsteady transonic aerodynamics. No theory has yet been developed that can accurately predict unsteady aerodynamic characteristics at transonic speeds. Consequently, a wind-tunnel program has been initiated at the Langley Research Center to experimentally determine the transonic aerodynamic characteristics of a representative energy efficient transport wing with emphasis on oscillating control surfaces. This test is part of a much larger experimental program to acquire unsteady pressure measurements for a wide range of aircraft configurations. The results from this study will serve two purposes. One purpose is to provide a comprehensive data base of measured pressure data that can be used in airplane design; the other purpose is to provide high quality data that can be used to validate theoretical methods being developed in companion programs.

A photograph of the aspect-ratio-10.76 model mounted in the Transonic Dynamics Tunnel is shown on the chart. The model has a supercritical airfoil section and is equipped with ten control surfaces, five along the trailing-edge and five along the leading-edge. Some representative results obtained by oscillating an inboard trailing-edge control surface are shown on the right in the chart. Both steady and unsteady chordwise lifting pressure distributions are presented for two spanwise locations. The data show that the unsteady pressures produced by oscillating the control surface are relatively large when compared to the steady pressures (no control surface oscillation). Even though the outboard station is far removed from the control surface, significant unsteady pressures are produced forward of the midchord at this station. Results of this investigation are presented in reference 17.



CONCLUSIONS

LESSONS LEARNED

- UNSTEADY AERO THEORY NEEDS
 - CONTROL SURFACE
 - ARBITRARY MOTION
- ACCURATE DEFINITION OF ACTUATOR DYNAMICS
- ACCURATE TURBULENCE MODEL
- CLOSER COOPERATION BETWEEN AEROELASTICIAN AND CONTROLS ANALYST

FUTURE THRUSTS

- TRANSONIC TIME PLANE UNSTEADY AERO
- SYSTEMATIC METHODS FOR LOCATING CONTROL SURFACES AND SENSORS
- APPLY FLUTTER SUPPRESSION METHODOLOGY TO OTHER ACTIVE CONTROL FUNCTIONS
- SYNTHESIS OF MULTIPLE ACTIVE CONTROL SYSTEMS
- CONTROL CONFIGURED VEHICLES

Figure 16

REFERENCES

1. Roger, K. L.: Airplane Math Modeling Methods for Active Control Design. Structural Aspects of Active Controls, AGARD-CP-228, August 1977.
2. Abel, I.: An Analytical Technique for Predicting the Characteristics of a Flexible Wing Equipped With an Active Flutter-Suppression System and Comparison With Wind-Tunnel Data. NASA TP-1367, February 1979.
3. Perry, B. III; Kroll, R. I.; Miller, R. D.; and Goetz, R. C.: DYLOFLEX: A Computer Program for Flexible Aircraft Flight Dynamic Loads Analyses with Active Controls. J. Aircraft, vol. 17, no. 4, April 1980, pp. 275-282.
4. Nissim, E.: and Abel, I.: Development and Application of an Optimization Procedure for Flutter Suppression Using the Aerodynamic Energy Concept. NASA TP-1137, February 1978.
5. Newsom, J. R.; Abel, I.; and Dunn, H. J.: Application of Two Design Methods for Active Flutter Suppression and Wind-Tunnel Test Results. NASA TP-1653, May 1980.
6. Athans, Michael: The Role and Use of the Stochastic Linear-Quadratic-Gaussian Problem in Control System Design. IEEE Trans. Autom. Control, vol. AC-16, no. 6, December 1971, pp. 529-552.
7. Gangsaas, Dagfinn; and Ly, Vy-Loi: Application of Modified Linear Quadratic Gaussian Design to Active Control of a Transport Airplane. AIAA Paper No. 79-1746, August 1979.
8. Mahesh, J. K.; Stone, C. R.; Garrard, W. L.; and Hausman, P. D.: Active Flutter Control for Flexible Vehicles. NASA CR-159160, November 1979.
9. Newsom, Jerry R.: A Method for Obtaining Practical Flutter Suppression Control Laws Using Results of Optimal Control Theory. NASA TP-1471, August 1979.
10. Mukhopadhyay, V.; Newsom, J. R.; and Abel, I.: A Direct Method for Synthesizing Low-Order Optimal Feedback Control Laws With Application to Flutter Suppression. AIAA Paper No. 80-1613, August 1980.
11. Sandford, M. C.; Abel, I.; and Gray, D. L.: Development and Demonstration of a Flutter Suppression System Using Active Controls. NASA TR-450, December 1975.
12. Redd, L. T.; Gilman, J., Jr.; Cooley, D. E.; and Sevart, F. D.: A Wind-Tunnel Study of B-52 Model Flutter Suppression. AIAA Paper No. 74-401, April 1974.

13. Doggett, R. V., Jr.; Abel, I.; and Ruhlin, C. L.: Some Experiences Using Wind-Tunnel Models in Active Control Studies. NASA TM X-3409, August 1976, pp. 831-892.
14. Peloubet, R. P., Jr.; Haller, R. L.; and Bolding, R. M.: F-16 Flutter Suppression System Investigation. AIAA Paper No. 80-0768, May 1980.
15. Hwang, C.; Johnson, E. H.; and Pi, W. S.: Recent Developments of the YF-17 Active Flutter Suppression System. AIAA Paper No. 80-0768, May 1980.
16. Winther, B. A.; Shirley, W. A.; and Heimbough, R. M.: Wind Tunnel Investigation of Active Controls Technology Applied to a DC-10 Derivative. AIAA Paper No. 80-0771, May 1980.
17. Sandford, M. C.; Ricketts, R. H.; Cazier, F. W., Jr.; and Cunningham, H. J.: Transonic Unsteady Airloads on an Energy Efficient Transport Wing With Oscillating Control Surfaces. AIAA Paper No. 80-0738, May 1980.

STATUS AND FUTURE PLANS OF THE DRONES FOR AERODYNAMIC AND STRUCTURAL TESTING (DAST) PROGRAM

Harold N. Murrow
NASA Langley Research Center

ABSTRACT

This paper will review the past year's progress in the NASA DAST program. Emphasis will be given to presenting results from flight tests of the ARW-1 research wing. Preliminary loads data and experiences with the active control system for flutter suppression will be included along with comparative results of test and prediction for the flutter boundary of the supercritical research wing and on performance of the flutter suppression system. Status will be given of the ARW-2 research wing. Finally, future plans for a third research wing resulting from solicitation of recommendations from industry and recent study results will be presented.

CONTENTS

- BACKGROUND
- ARW-1 RESULTS TO DATE
- ARW-2 STATUS
- FUTURE PLANS

Figure 1

DAST OBJECTIVES

The DAST program objectives, which have not changed, will be reviewed. The concept of the DAST program is to provide a focus for evaluation and improvement of synthesis and analysis procedures for aerodynamic loads prediction and design of active control systems for load alleviation on wings with significant aeroelastic effects. Major challenges include applications to wings with supercritical airfoil, and tests emphasizing the transonic speed range. The program requires complete solutions to real-world problems since research wings are designed and flight tested. Because of the risky nature of the flight testing, especially with regard to flutter, target drone aircraft are modified for use as test bed aircraft and development of an appropriate test technique has been required. Principal flight vehicle modifications have included the flight control system, data acquisition system, and receiving and transmitting antennas. A test pilot controls the vehicle from a ground cockpit with appropriate displays and experimenters control the flutter system, command wing excitation with sweeps and pulses, and monitor flutter characteristics from a facility specially tailored for this task.

DRONES FOR AERODYNAMIC AND STRUCTURAL TESTING (DAST)

PROVIDE FLIGHT DATA FOR COMPARISON WITH ANALYSIS (AND FOR CASES WHERE ANALYSIS IS INADEQUATE)

DEVELOP TEST TECHNIQUE AND FLIGHT FACILITY FOR "RISKY" FREE FLIGHT TESTING

PRINCIPAL RESEARCH AREAS

AERODYNAMIC LOADS MEASUREMENT

ACTIVE CONTROL SYSTEMS EVALUATIONS

STRUCTURAL INVESTIGATIONS

STABILITY AND PERFORMANCE STUDIES

EMPHASIS

TRANSONIC REGION

AEROELASTIC EFFECTS

Figure 2

FEATURES OF DAST RESEARCH WINGS

Again by way of review, a brief description is given of the two transport-type research wings in the currently approved program. The first wing, Aeroelastic Research Wing No. 1 (ARW-1), was designed for $M = 0.98$ cruise and 2.5 g maneuver, and was purposely designed for flutter with a rapid onset within the flight envelope. Flights are aimed at acquiring data emphasizing validation of a flutter suppression system (FSS) design and aeroelastic effects on aerodynamic loads.

The wing fabrication and test for the second research wing (ARW-2) are sponsored by the ACEE-EET program. This design involved what is believed to be the first exercise of an iterative procedure integrating aerodynamics, structures, and controls technologies in a design loop resulting in flight hardware. Evaluation of multiple active controls systems operating simultaneously, the operation of which is necessary to preserve structural integrity for various flight conditions, is the primary objective of the flight tests on this fuel-conservative-type wing.

ARW-1

- AEROELASTIC WING EXHIBITS "EXPLOSIVE" FLUTTER WITHIN FLIGHT ENVELOPE
- ACTIVE CONTROL FLUTTER SUPPRESSION SYSTEM
- SUPERCRITICAL AIRFOIL

ARW-2

- FUEL CONSERVATIVE WING DESIGN
 - HIGH ASPECT RATIO ($AR = 10.3$)
 - LOW SWEEP ($\Lambda = 25^0$)
 - ADVANCED SUPERCRITICAL AIRFOIL
- FIRST REAL EXERCISE OF INTEGRATED DESIGN PROCEDURES RESULTING IN FLIGHT HARDWARE
- MULTIPLE ACTIVE CONTROLS CRITICAL TO FLIGHT OPERATION

Figure 3

ARW-1 FLIGHT TESTS

Three flights were made with the first research wing in the past year. The first flight in October 1979 principally involved overall flight systems evaluations and results led to further work with the flight control system. Good loads data were obtained. The second flight was made in March 1980 and was highly successful. The third flight was conducted in June 1980 and following receipt of data at four data points increasing in Mach number at 4.6 km altitude, flutter was inadvertently encountered in advancing to the fifth data point. The right wing separated from the aircraft, and due to excessive damage to the parachute on emergency deployment, impact velocity was excessive and the airframe was damaged beyond repair.

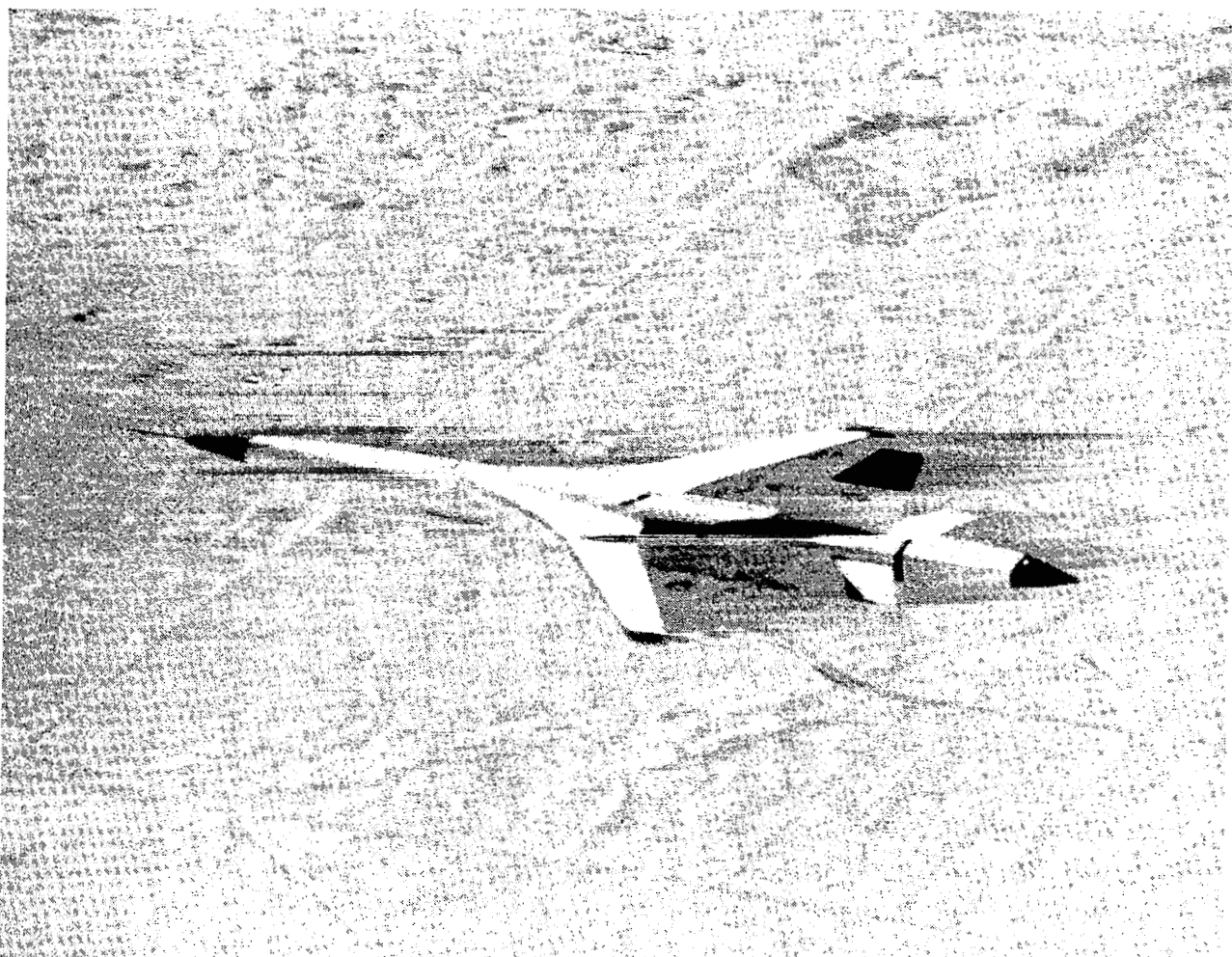


Figure 4

FLUTTER SUPPRESSION SYSTEM CONTROL LAW

The evolution of the flutter suppression system has required numerous modifications, including a major change to the control law prior to the third flight. Effects of higher frequency modes (structural and hydraulic system) resulted in the incorporation of a number of notch filters to compensate for undesirable structural and fluid modes to allow for system stabilization in the hangar. In addition, actuator frequency response was significantly different than the math model used in the earlier analyses. At this time significant parameters affecting actuator frequency response (include effects of mounting and control surface) are not clearly identified; therefore, empirical data must be fed back into the analysis after hardware implementation. As a result of these two factors (added filters and actuator characteristics), it became obvious that the original control law could not provide the goal of 20 percent margin above open loop boundary.

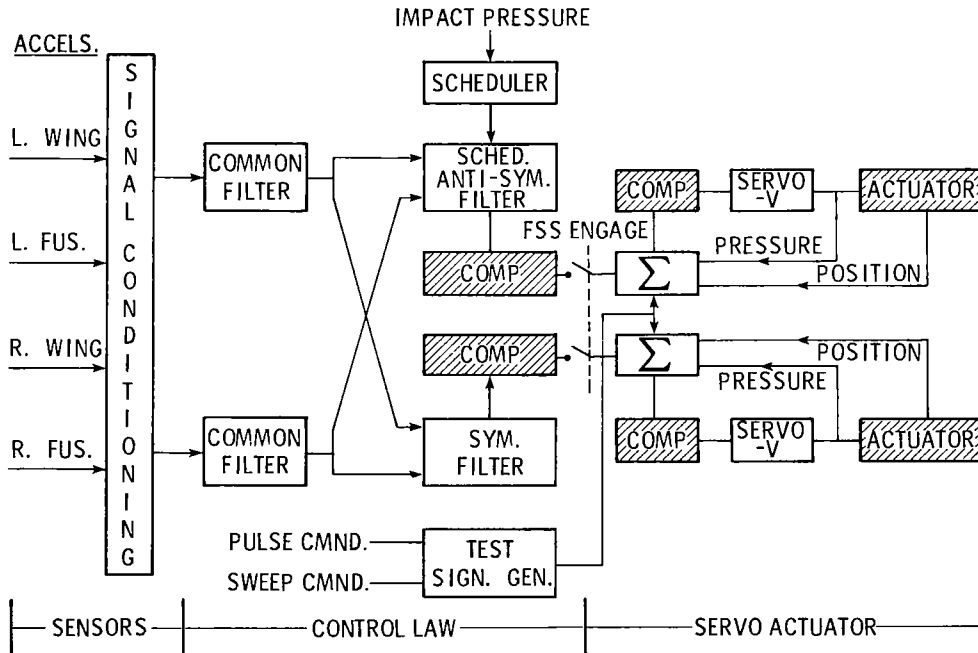


Figure 5

TYPICAL TIME HISTORIES FROM FREQUENCY SWEEPS

The flight data from DAST flights are remarkably free from contamination of any kind. Detailed active control system evaluations in the NASA Transonic Dynamics Tunnel have been difficult due to the high turbulence content in the airflow. Because of the high quality flight data, reliable results can be determined from short (6.8 sec) log sine sweeps from 10-40 Hz. This is very important, since, due to fuel limitations, flights are limited to 20-30 minutes.

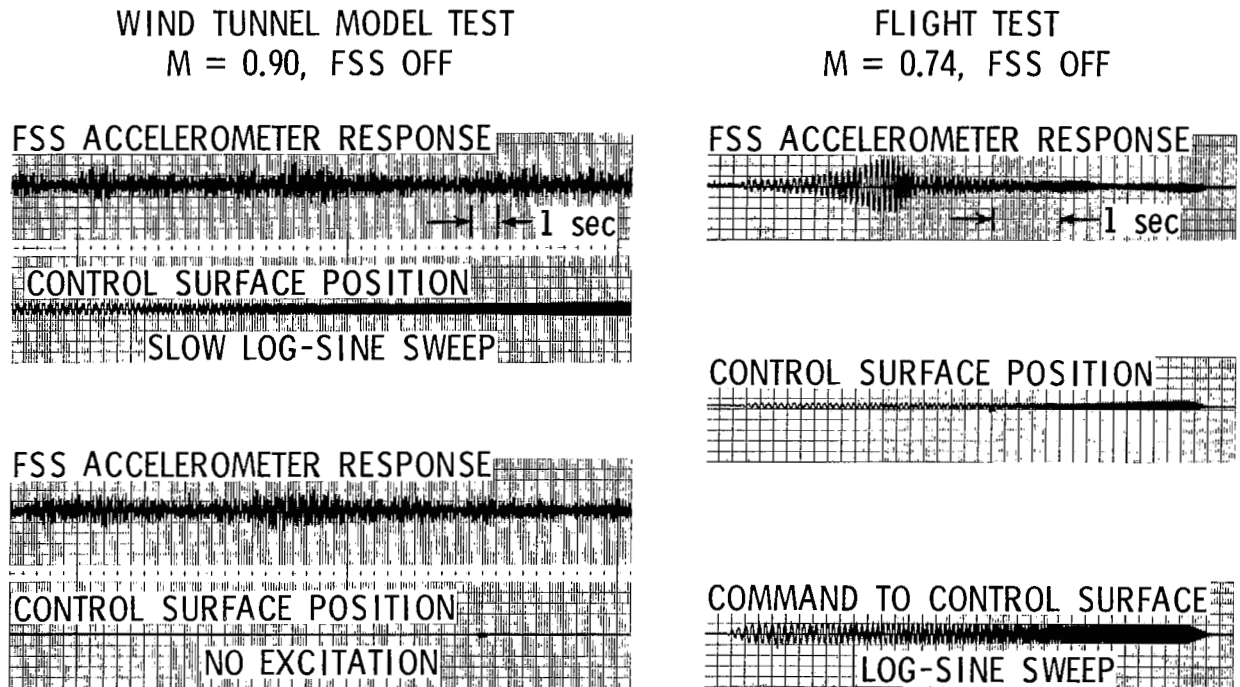


Figure 6

ANALYTICAL-EXPERIMENTAL DATA CORRELATION

Frequency and damping data from the March flight at 6.1 km altitude for the basic wing (FSS off) for both the symmetric and antisymmetric flutter modes indicate that flutter will be encountered at a lower Mach number than predicted analytically. This corresponds to earlier results in the wind tunnel for a supercritical wing at Mach numbers above 0.9. Post-flight analyses indicate improvement in the prediction if (1) the lift curve slope measured on the rigid wind tunnel model is used in place of that resulting from doublet-lattice analysis and (2) modal frequencies derived from the NASTRAN structural model are used rather than matching ground vibration test frequencies with the NASTRAN-derived mode shapes. The reason for the latter is not yet well understood.

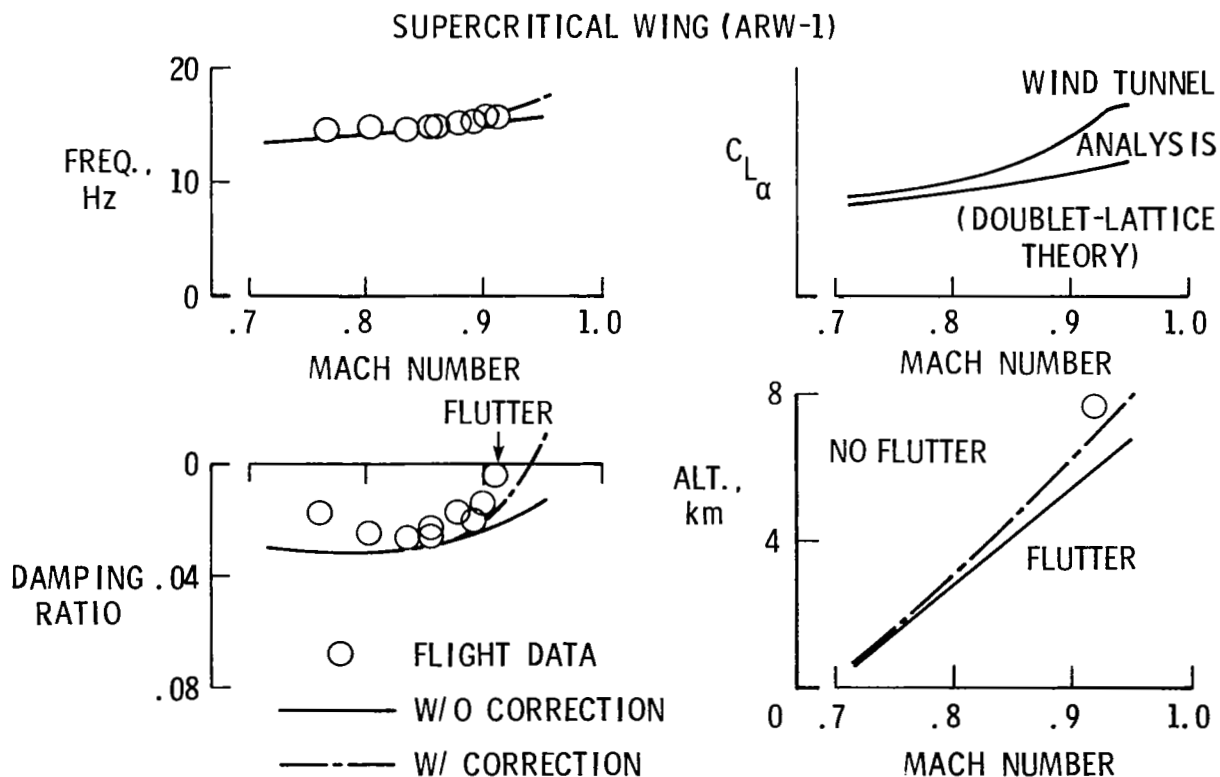


Figure 7

FLUTTER ONSET TIME HISTORY

Flutter was encountered as speed was being increased from one test point to another at a Mach number slightly above 0.8. The procedure was to excite the wing with a symmetric sine sweep and an antisymmetric sine sweep, process to the next higher test point while exciting the wing every 3-4 seconds with symmetric and antisymmetric pulses and observing the response on the strip chart of the wing accelerometer output. The time history of wing tip acceleration during flutter onset can be observed from the FSS accelerometer output scaled to ± 10 g peak and subsequently by another accelerometer located at the wing tip which was scaled to ± 68 g peak. It was observed that a frequency shift (from about 19 Hz to about 14.5 Hz) occurred at a time corresponding to when control surface amplitude saturation was reached. Since this event would effectively reduce gain and the gain setting was one-half nominal, the frequency shift probably corresponds to a shift to essentially the open-loop condition. Subsequent to this time, the amplitude quadrupled in two cycles. An aft-located mass, designed to be released in emergencies, was released, but apparently due to the rapid buildup was not effective in stopping flutter.

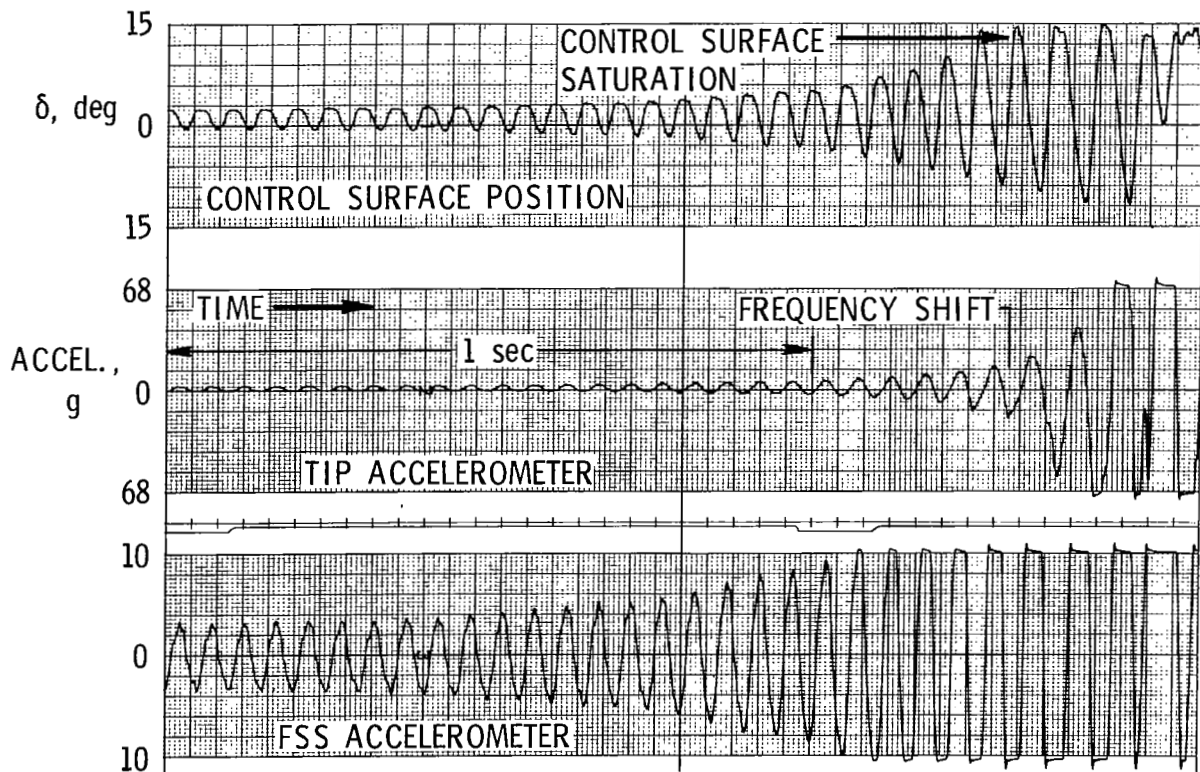


Figure 8

CORRELATION OF SYSTEM ON- AND OFF-FLIGHT DATA WITH PREDICTION

It has been determined that one-half the nominal gain was inadvertently implemented in the flight hardware for the third flight. Post-flight analyses have indicated the system to become unstable at a Mach number above 0.8 at one-half nominal gain if the NASTRAN model is used to describe the structural characteristics. A comparison of predicted frequency and damping with analysis indicates that even at Mach numbers well below 0.9, in this case near 0.8, analysis is unconservative. Frequency predictions are very close to measured values. (A significant note to be made is that the analysis does not predict instability at one-half nominal gain if ground vibration test frequencies are used with mode shapes of the NASTRAN model.)

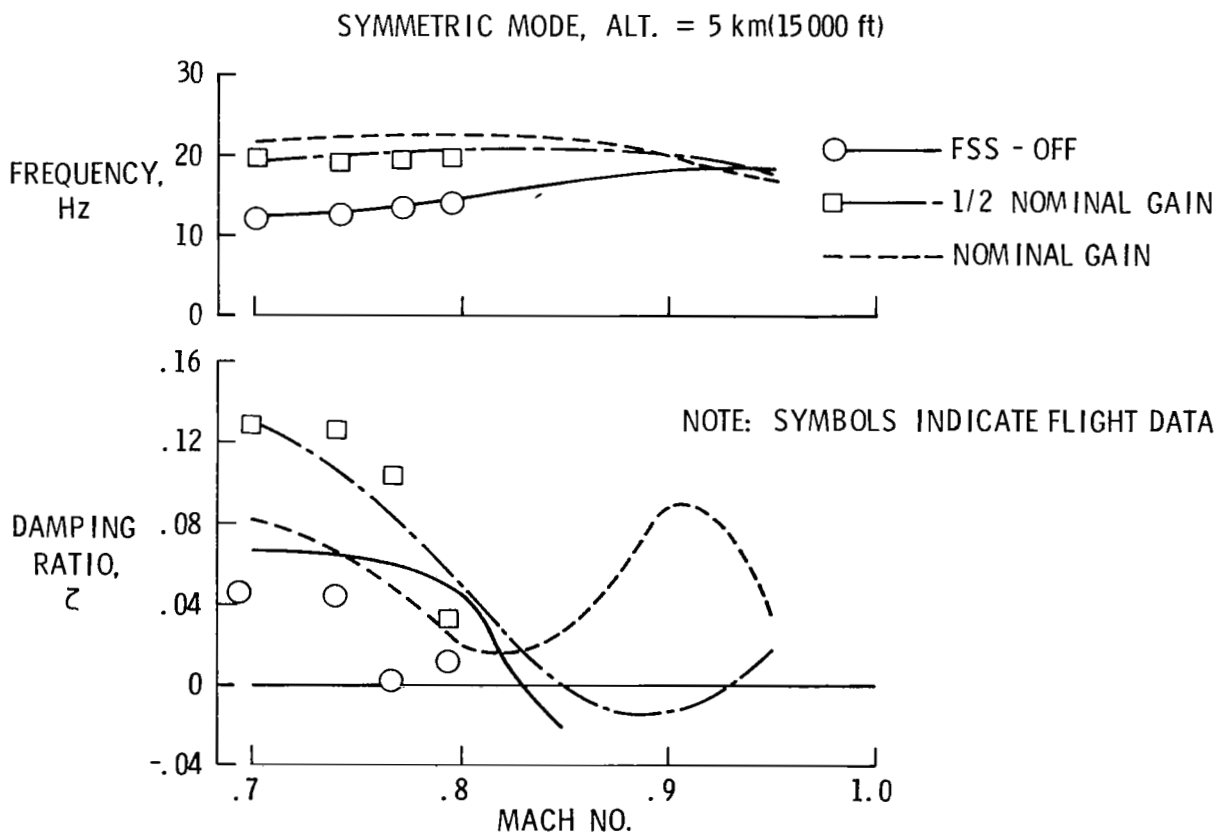


Figure 9

DETERMINATION OF SYSTEM-OFF CHARACTERISTICS WITH SYSTEM ON

Early in the program it was planned that suitable system-off (open loop) data would be obtained with the system on (closed loop), using transfer function analyses, if the data were uncontaminated by noise. This procedure has been recently demonstrated for some store flutter investigations in the wind tunnel, but was unsuccessful on the DAST ARW-1 dynamically scaled wind-tunnel model, apparently due to high turbulence content in the airflow. Flight results to date are encouraging, although scatter is seen in the two damping estimates closest to the zero damping axis on the one set of data.

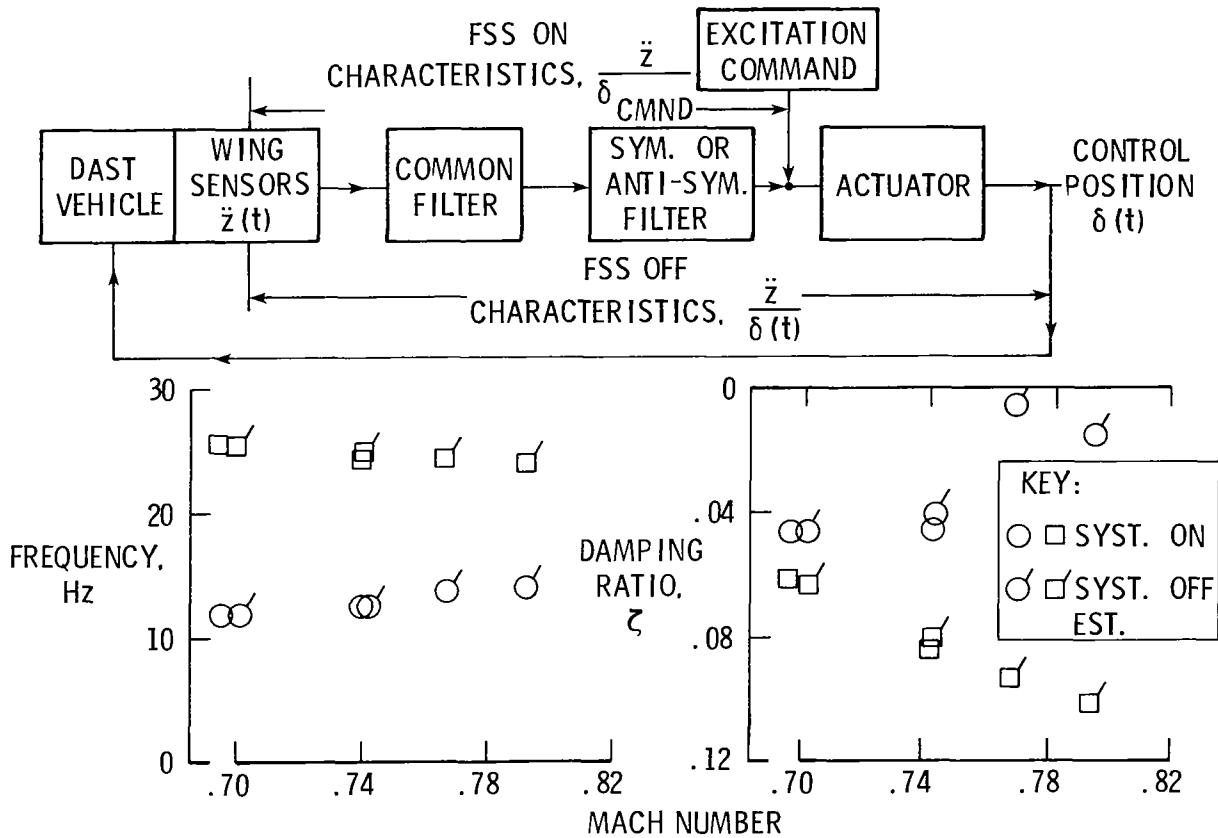


Figure 10

ARW-1 STATUS

Activity is underway to rebuild the ARW-1 and re-establish flight status as quickly as possible. Essentially all electronic equipment, for both controlling vehicle functions and the FSS, is reusable. A significant number of spare parts are on hand and another Firebee II target drone will be modified for ARW-1 tests. System improvements under consideration include a refinement to speed control of the flight vehicle, adjustment in criteria for tip ballast release, and tailoring the parachute deployment sequence to be more adaptable to emergency situations.

- WING IS BEING REBUILT USING SPARES AND MAXIMUM USE OF REFURBISHABLE COMPONENTS
- ANOTHER FLIGHT VEHICLE IN PREPARATION
- VEHICLE SYSTEM MODIFICATIONS UNDER CONSIDERATION
 - SPEED CONTROL
 - PARACHUTE DEPLOYMENT SEQUENCE
 - FLUTTER ARRESTER

Figure 11

ARW-2 ACTIVITY

The DAST ARW-2 design is complete and fabrication is continuing. The design includes maneuver load alleviation (MLA), gust load alleviation (GLA), flutter suppression (FSS), and relaxed static stability (RSS). The high aspect ratio supercritical wing has both inboard and outboard active control surfaces; vehicle control is through a differentially moving horizontal tail. Two major contracts have been implemented to provide the active control systems and machined components for the wing. Fabrication of the wing skins, hydraulic system, instrumentation system, and wing assembly will all be performed at Langley. The wing will be instrumented to measure quasi-steady loads with calibrated strain gage bridges, and pressure orifices; in addition, one row of orifices near the tip will be employed to measure unsteady surface pressures. The test vehicle and flight control system will be developed by the Dryden Center. A means of drag enhancement, probably a speed brake arrangement, will be incorporated in the vehicle systems in order to expand the level flight envelope of the ARW-2 configuration.

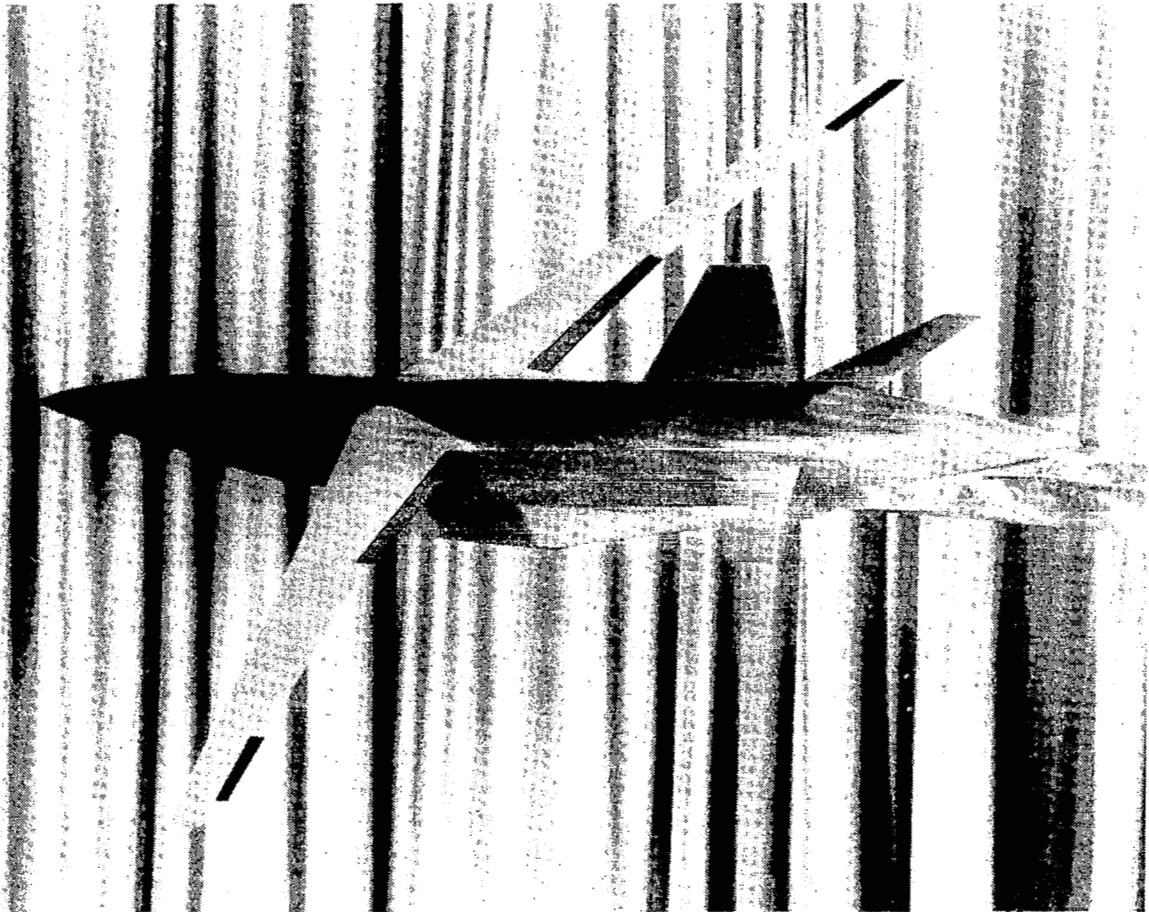


Figure 12

ARW-2 TEST CONDITIONS

The principal flight test conditions selected for ARW-2 include the MLA test point of $M = 0.4$ at 3.0 km (10 000 ft), the GLA test point of $M = 0.6$ at 2.1 km (7000 ft), the FSS test point of $M = 0.86$ at 4.6 km (15 000 ft), and the RSS test point of $M = 0.80$ at 13.7 km (45 000 ft). Balsa flow vanes will be used on the pitot head to sense turbulence input and turbulence encounters will be necessary to evaluate the GLA. These were selected to correspond as closely as possible to the various design conditions. Other test points will be selected within the flight envelope for loads evaluations and the active control systems will be evaluated at those test points also.

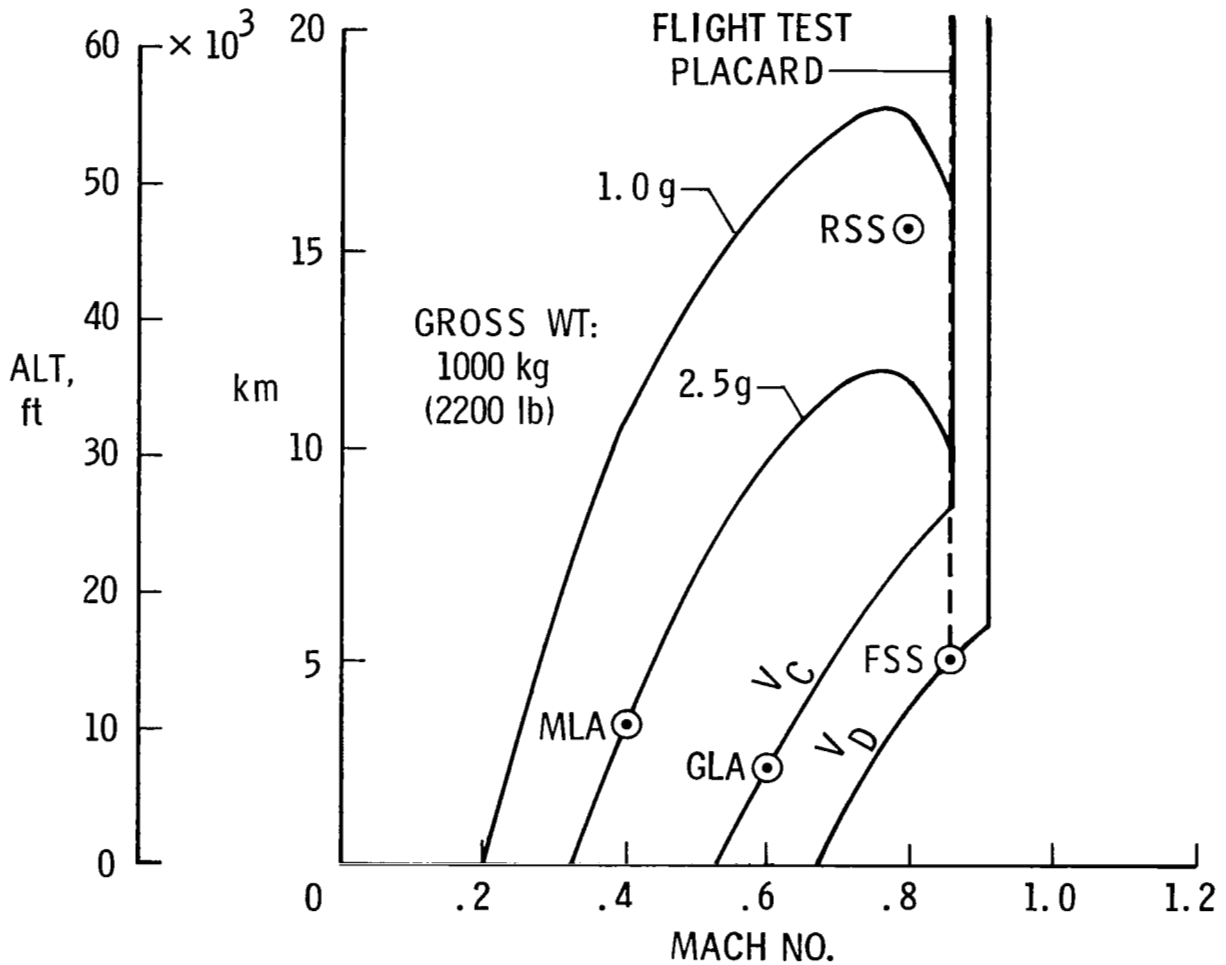


Figure 13

UNSTEADY PRESSURE MEASUREMENTS ARE CONTINUING

The rigid semispan model of an EET-type wing ($M = 10.3$, supercritical airfoil) equipped with leading- and trailing-edge control surfaces has had two test entries to date in the Langley Transonic Dynamics Tunnel. Results from the first test series which included one inboard and one outboard trailing-edge control surface are in the process of being published. Additional data were acquired from trailing-edge control surfaces and one outboard leading-edge control surface in an entry completed in August of this year. The next entry is planned for mid-year 1981.

PURPOSE

- EFFECTS OF OSCILLATING CONTROL SURFACES ON UNSTEADY AERODYNAMIC PRESSURES
- DATA BASE FOR DESIGN AND VALIDATION OF THEORY

STATUS

- INITIAL TESTS COMPLETED SPRING 1979
 - ONE INBOARD AND ONE OUTBOARD T. E. CONTROL SURFACE
- SECOND TEST SERIES COMPLETED AUGUST 1980
 - ADDITIONAL T. E. DATA AND ONE OUTBOARD L. E. SURFACE
 - DATA REDUCTION UNDERWAY
- NEXT ENTRY PLANNED FOR MID-1981

Figure 14

FUTURE DAST STUDIES

In cooperation with the Aerospace Flutter and Dynamics Council, solicitations were made to all pertinent segments of the aerospace community to determine consensus on DAST contributions and appropriate follow-on research. A compilation of responses resulted in consensus that NASA should conduct research in the areas of tailored composite structures combined with continued active controls studies with some emphasis on acquiring unsteady pressure measurements in flight. From the standpoint of pursuing energy-efficient transport technology, a configuration with aspect ratio higher than ARW-2 with simulated engines and nacelles (mass and aerodynamic effects), designed with load control through use of tailored orientation of composite laminates in combination with active controls, would appear to be a good candidate. Some preliminary design studies are planned during the next year.

- HIGH PRIORITY TECHNOLOGY AREAS IDENTIFIED
 - UNSTEADY PRESSURE MEASUREMENTS
 - TAILORED COMPOSITE STRUCTURES
 - ACTIVE CONTROLS

- TRANSPORT CONFIGURATION
 - HIGH ASPECT RATIO (~12)
 - SIMULATED ENGINES AND NACELLES
 - COMBINED ACTIVE CONTROLS AND TAILORED COMPOSITES

Figure 15

DAST STATUS SUMMARY

- **THREE FLIGHTS COMPLETED WITH ARW-1**
 - FLIGHTS TO RESUME LATE 1981
- **ARW-2 FABRICATION PROGRESSING**
 - FLIGHTS EXPECTED TO BEGIN LATE 1982
- **DAST FOLLOW-ON FOCUS IDENTIFIED**

Figure 16

TRANSPORT AIRCRAFT FLYING QUALITIES ACTIVITIES

Martin T. Moul
NASA Langley Research Center

ABSTRACT

Three research efforts of interest to transport airplane designers are reviewed. The first study is one in which the optimal-control model for pilot-vehicle systems was used to develop a methodology for predicting pilot ratings for commercial transports. The method was tested by applying it to a family of transport configurations previously evaluated by the Douglas Aircraft Company on their motion-base simulator, and for which subjective pilot ratings were obtained.

The second study is an extension of the first in which specific attention will be given to the development of the simulator program and procedures so as to yield objective and subjective performance data useful for a critical evaluation of the analytical method. This study was started in September 1980

The third activity is a proposed program for investigating the influence of flexible modes on transport aircraft flying qualities. This activity will include control system design, analysis of vehicle dynamics (open and closed loop), motion-base simulator studies, and variable-stability airplane tests.

AIRPLANE LONGITUDINAL STABILITY CHARACTERISTICS

The pilot rating prediction method was tested by applying it to a number of subsonic transport configurations evaluated by Douglas Aircraft Company on a motion-base simulator and for which pilot opinion data had been reported in NASA TM X-73. The configurations typified airplanes with varying degrees of longitudinal stability, and the short-period modal characteristics vary from the conventional oscillatory and well-damped mode to two aperiodic modes with varying divergence rates. Flight path stability, dy/dV , ranged from stable (negative) values to divergent values, and the mean pilot ratings varied from satisfactory (2.5) to unacceptable (8.3). The mission simulated was an ILS approach with cockpit motion and turbulence and with constant, satisfactory lateral-directional characteristics.

$V = 140$ knots

$W = 1\ 560\ 000$ N

CONFIG. NUMBER	ω_{sp}	ξ_{sp}	n/α	dy/dV	PILOT RATING
1	0.846	0.628	3.80	-0.040	2.5
3	(-0.633)	(-0.307)	4.14	-0.049	4.3
4	(-0.811)	(+0.090)	4.20	-0.051	4.2
5	(-0.909)	(+0.158)	4.24	-0.053	5.3
8	0.811	0.662	4.04	+0.339	8.3
15	(-0.991)	(+0.225)	4.29	-0.055	6.7
16	(-1.061)	(+0.291)	4.35	-0.057	7.7
21	0.441	0.665	1.05	+0.285	6.2

CONSTANT, SATISFACTORY LATERAL-DIRECTIONAL CHARACTERISTICS

ILS TRACKING TASK

COCKPIT MOTION AND TURBULENCE

PARENTHESES SIGNIFY FIRST-ORDER FACTOR

Figure 1

PROCEDURE FOR PREDICTING PILOT RATING

There are five basic elements in the methodology for predicting pilot rating. Task definition requires specification of aircraft configuration, mission, such as landing approach, and atmospheric environment. Subtasks are those elements of the task which may be independently analyzed and evaluated by the pilot and for this study included altitude station keeping, glide slope capture, and glide slope tracking. Definition of performance criteria involves the specification of terms to be included in the quadratic performance index as well as the weighting constants. Performance is then predicted as a function of workload which in this method is defined as mental workload and is synonymous with attention. Several candidate pilot rating expressions for linear combinations of performance and workload were evaluated through comparison with the simulation results.

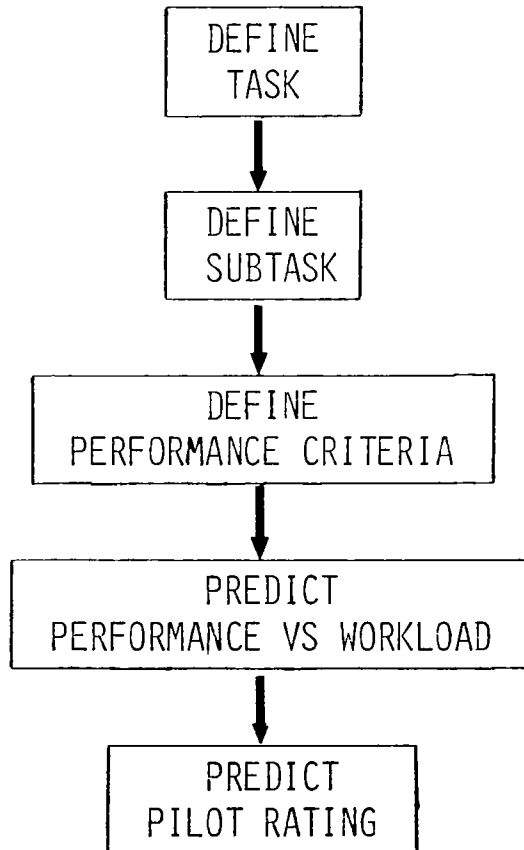


Figure 2

COMPARISON OF PREDICTED AND EXPERIMENTAL RATINGS

Experimental mean pilot ratings and their standard deviations are presented for the test configurations along with predicted values. For most of the test configurations the agreement between the mean experimental rating and the predicted rating is less than one rating number which is certainly good for subjective results. The standard deviations of experimental ratings are unfortunately large for many of the configurations as a result of a small data set and render some obscurity to the comparisons. No explanation is available for the apparent large discrepancy in the data for configuration 8 in which the pilot rating exceeded the predicted value by about 2 1/2 units.

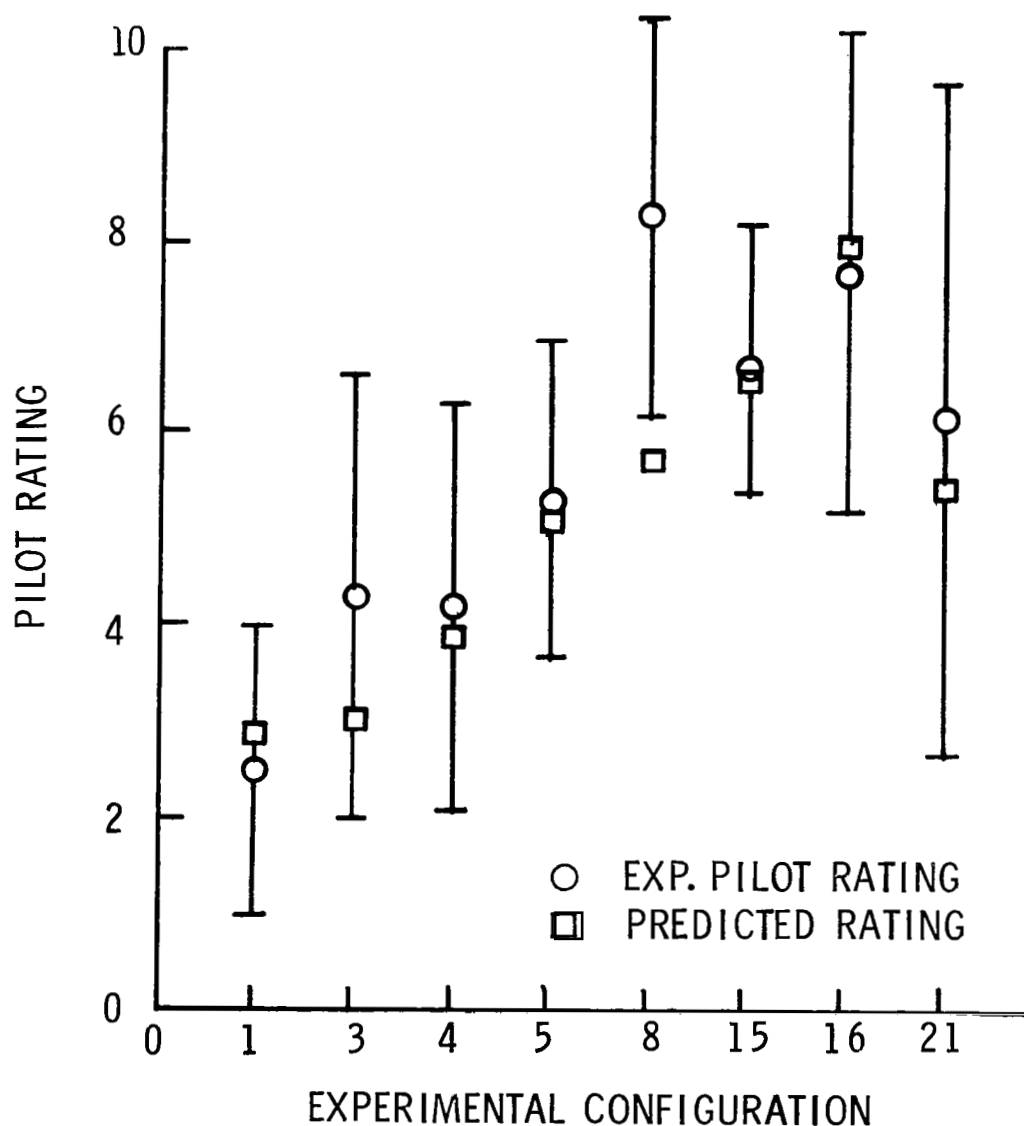


Figure 3

BOLT BERANEK AND NEWMAN/DOUGLAS AIRCRAFT CO. PHASE II STUDY

The results obtained in comparing the pilot rating prediction method with the subjective pilot opinion data from the Douglas study were encouraging and have prompted a follow-on effort in which simulator test procedures will be designed to produce both objective and subjective results in a form compatible to the analytical method. Subtasks will be selected for rating by the pilots, and an attempt will be made to standardize the test maneuvers and the method used in arriving at a composite rating. Performance criteria, or expectations, will be obtained from pilot questionnaires and interviews, and efforts will be made to arrive at a common set of criteria. In all this effort, a significant test pilot participation is essential. A major addition to this program will be the acquisition of quantitative data, which will provide another basis on which to test the analytical method.

EXPERIMENT DESIGN

SUBTASKS

PERFORMANCE CRITERIA

PILOT ROLE

DATA OUTPUT

TIME HISTORIES OF AIRPLANE MOTIONS, CONTROLLER INPUTS
MEAN AND STANDARD DEVIATIONS OF PERTINENT VARIABLES

Figure 4

INFLUENCE OF FLEXIBLE MODES ON TRANSPORT AIRCRAFT
FLYING QUALITIES, RIDE QUALITIES, AND PILOT OPINION

Within the Advanced Controls RTOP a program has been initiated to investigate the flying qualities and ride qualities of flexible transport airplanes. This activity will include control system design, analysis of vehicle dynamics (open and closed loop), motion-base simulator studies, and variable-stability airplane tests. The initial effort will be a study of flexible vehicle dynamics for advanced transports to identify flexible and rigid body modes; to ascertain which structural modes influence flying qualities, ride qualities, and control; to determine reduced-order math models of vehicle dynamics for use in piloted simulator studies; and to evaluate capability or limitations of motion-base simulators to replicate vehicle motions. The entire effort is expected to extend over about four years.

MILESTONES:

- o ANALYSIS OF VEHICLE DYNAMICS AND PRELIMINARY FLYING QUALITIES CRITERIA, FY 81-82
- o DEVELOPMENT OF MOTION-BASE SIMULATOR MATH MODEL, FY 81-82
- o CONDUCT MOTION-BASE SIMULATION PROGRAM, FY 82
- o DEVELOPMENT OF CANDIDATE CONTROL LAWS FOR FLEXIBLE TRANSPORT, FY 82-83
- o CONDUCT IN-HOUSE MOTION-BASE SIMULATOR STUDY TO VALIDATE CRITERIA, FY 83-84
- o FSAA OR VARIABLE-STABILITY AIRPLANE TESTS OF FLYING QUALITIES, FY 84-85

Figure 5

IN-FLIGHT DIRECT STRIKE LIGHTNING RESEARCH

Felix L. Pitts
NASA Langley Research Center

EXPANDED ABSTRACT

In future aircraft, the projected use of digital avionic systems, along with composite aircraft structure, compounds lightning related problems. Digital avionic systems are potentially more susceptible to upset by electrical transients than previous generation systems, and the composite structure may not provide electrical shielding equivalent to that provided by metal aircraft. Future design processes will thus require lightning protection assessment techniques for digital avionic systems operating in electromagnetically nonoptimum structures. A necessary requirement of potential assessment techniques (which may range from purely analytical, through simulation, to actual hardware tests) is a refined definition of the lightning electromagnetic hazard. Recent ground-based measurements have indicated that the rise times of lightning electromagnetics are around one order of magnitude faster than is used in current lightning protection criteria.

The NASA Langley Research Center is performing in-flight direct strike lightning research to better define the lightning-generated electromagnetic environment affecting aircraft. The research program uses an NASA F-106B aircraft which operates in a thunderstorm environment and is specially instrumented for lightning electromagnetic measurements. This presentation reviews the instrumentation system and presents typical results recorded by the research instrumentation, during simulated-lightning ground tests performed for a safety survey, along with several examples of direct strike data obtained during the summer of 1980.

INTRODUCTION

The NASA Langley Research Center is performing in-flight direct strike lightning research to better define the lightning-generated electromagnetic environment affecting aircraft. The research program uses an NASA F-106B aircraft which operates in a thunderstorm environment and is specially instrumented for lightning electromagnetic measurements. This presentation reviews the instrumentation system and presents typical results recorded by the research instrumentation, during simulated-lightning ground tests performed for a safety survey, along with several examples of direct strike data obtained during the summer of 1980.

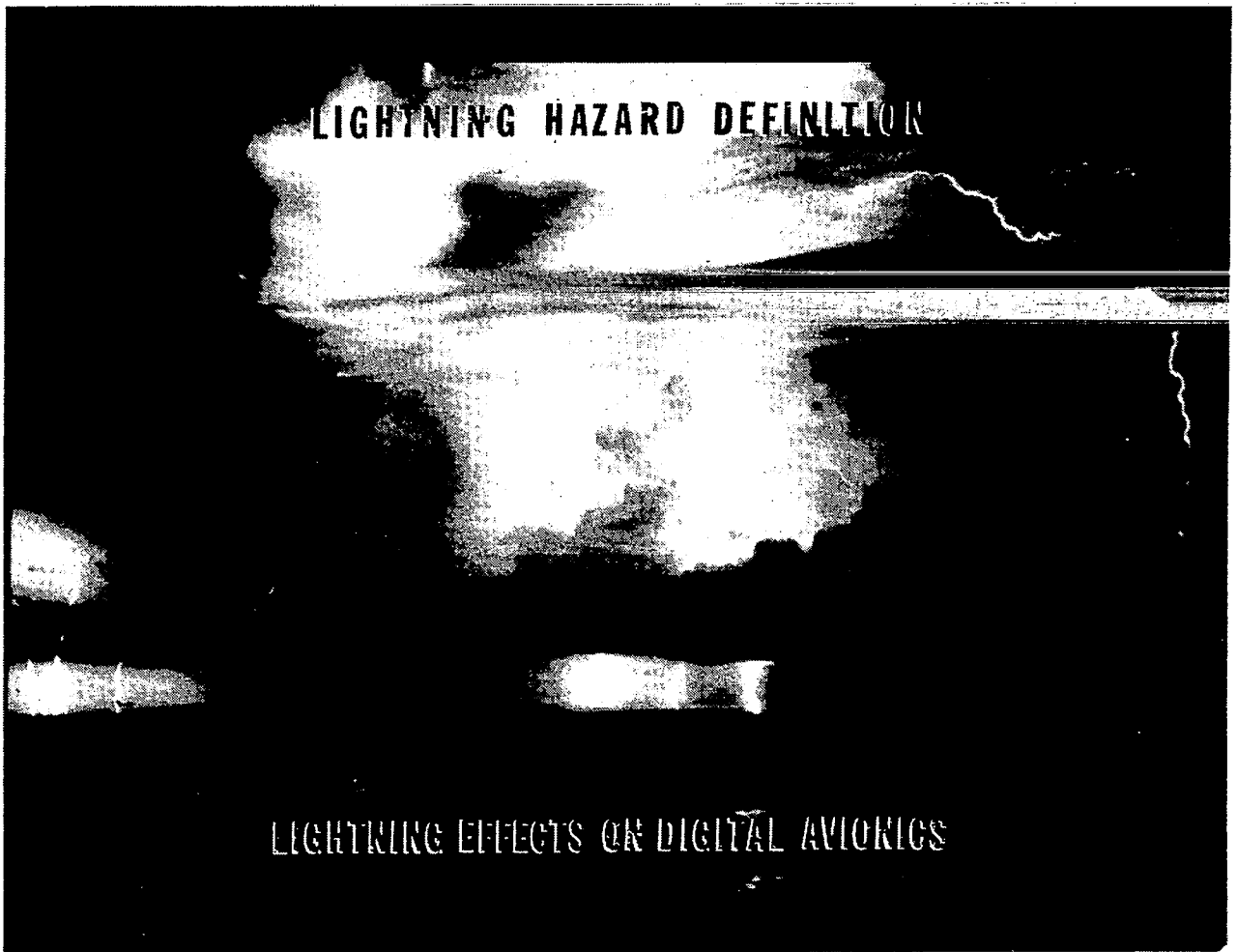


Figure 1

MOTIVATION FOR LIGHTNING RESEARCH

In future aircraft, the projected use of digital avionic systems, along with composite aircraft structure, compounds lightning related problems. Digital avionic systems are potentially more susceptible to upset by electrical transients than previous generation systems, and the composite structure may not provide electrical shielding equivalent to that provided by metal aircraft. Future design processes will thus require lightning protection assessment techniques for digital avionic systems operating in electromagnetically nonoptimum structures. A necessary requirement of potential assessment techniques (which may range from purely analytical, through simulation, to actual hardware tests) is a refined definition of the lightning electromagnetic hazard. Recent ground-based measurements have indicated that the rates of rise of lightning electromagnetics are around one order of magnitude faster than is used in current lightning protection criteria.

LIGHTNING EFFECTS ON DIGITAL SYSTEMS

- COMPOSITE STRUCTURE SHIELDING INEFFECTIVENESS
- DIGITAL SYSTEM SUSCEPTIBILITY TO DISTURBANCE BY ELECTRICAL TRANSIENTS
 - MOMENTARY ANOMALIES - GLITCHES
 - UPSETS - ANOMALIES REQUIRING RESET OR RELOAD
 - PERMANENT DAMAGE - COMPONENT FAILURE
- LIGHTNING CAN SIMULTANEOUSLY AFFECT ALL CHANNELS OF REDUNDANT SYSTEMS

Figure 2

SIMPLIFIED LIGHTNING MODEL

This lightning model illustrates several lightning electromagnetic concepts even though the model is grossly simplified in that it assumes the charge Q is uniformly distributed in a single, straight, vertical, non-tortuous channel. E and B are the electric and magnetic fields, respectively, generated by the lightning current (which is the time rate of change of Q , noted by \dot{Q}). H is height of the channel, D is distance from the channel, t is time, c is the speed of light, ϵ_0 and μ_0 are the permittivity and permeability of free space. The argument $(t - D/c)$ illustrates the traveling wave nature of the radiation. The magnetic field has no static term; the radiation and induction terms are inversely proportional to the first and second power, respectively, of D .

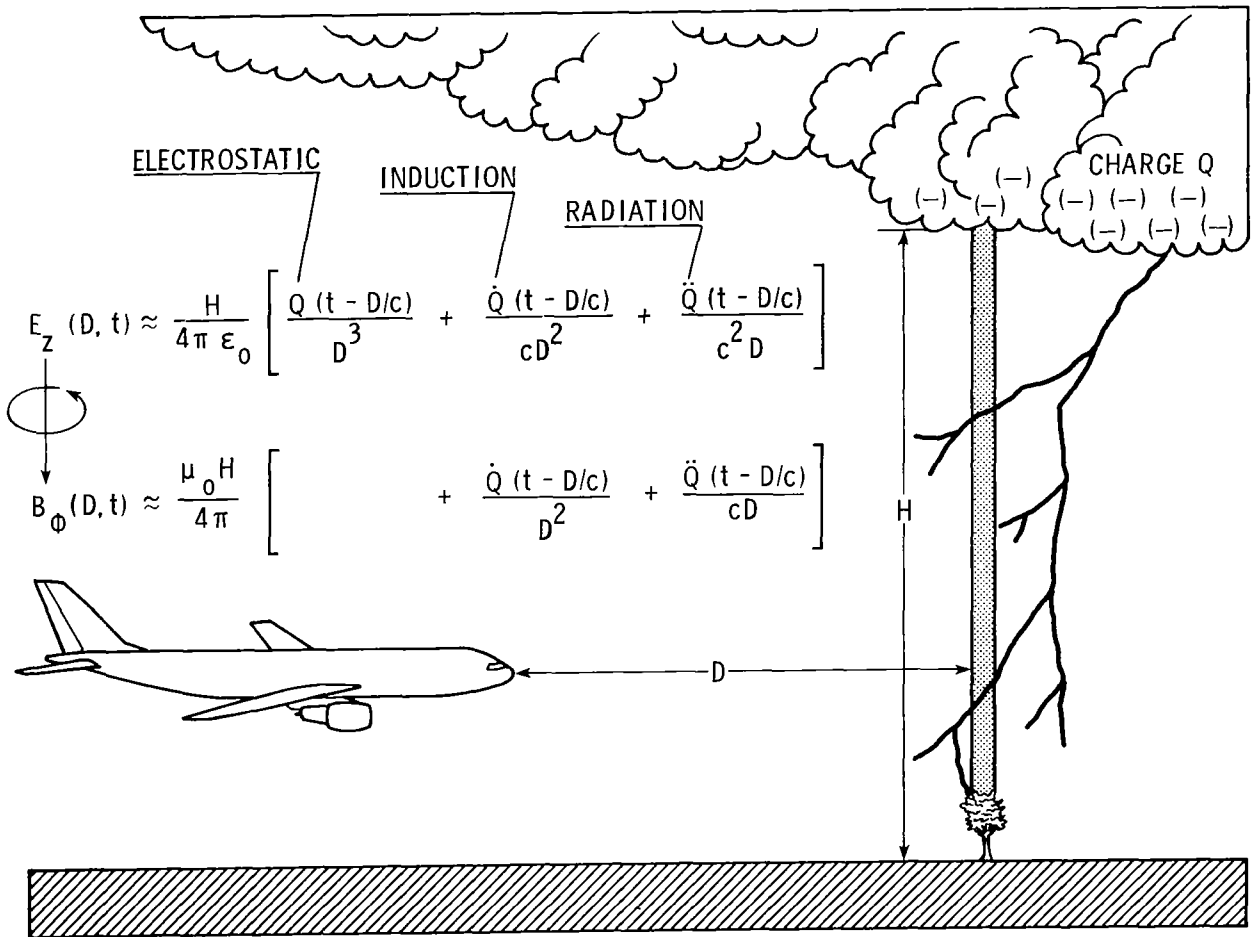


Figure 3

RESEARCH INSTRUMENTATION CONCEPT

The instrumentation concept consists of a number of electromagnetic sensors which measure the electromagnetic fields during the lightning strike to the aircraft. The data are recorded in a shielded, isolated instrumentation enclosure.

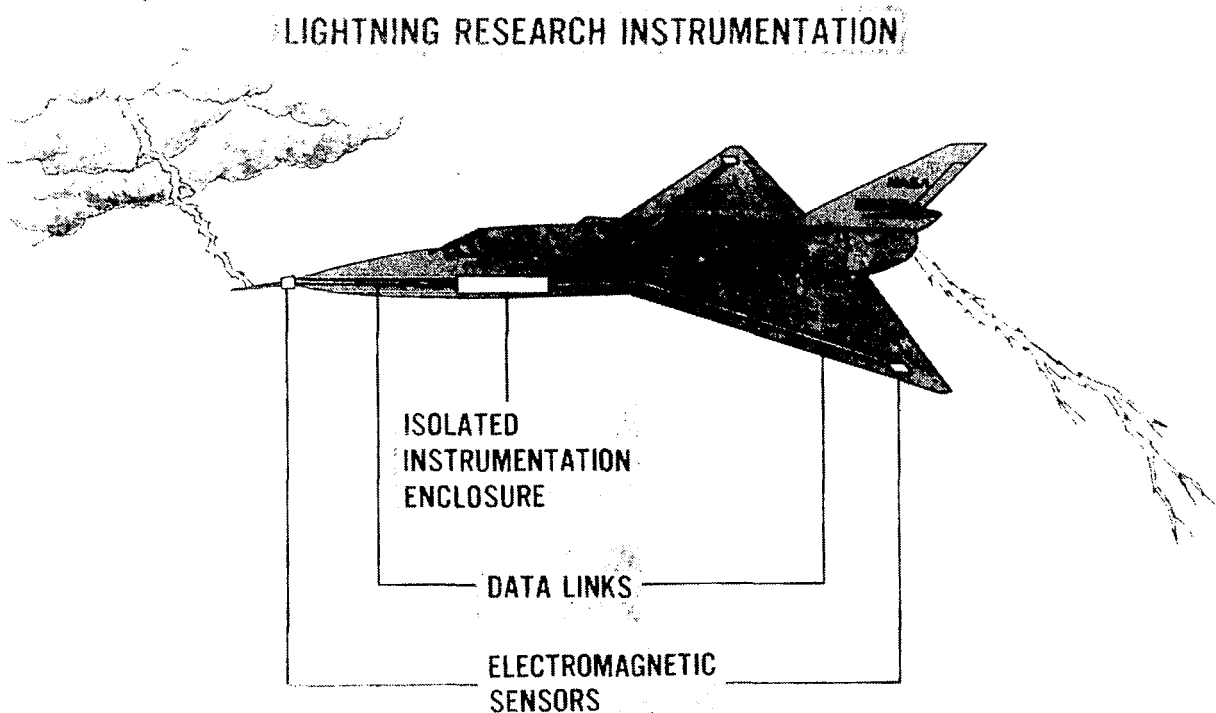


Figure 4

RESEARCH MEASUREMENTS

D-Dot, B-Dot, and I-Dot are the measurements of choice as determined by a group of technical experts representing industry, academe, and government. D-Dot is related to rate of change of electric field as $\dot{D} = \epsilon_0 \dot{E}$, I-Dot is rate of change of strike current to the boom, and B-Dot is rate of change of magnetic flux density. The amplitude ranges are based on a nominal strike with 10 000 amperes and 500 000 volts per meter changes in 0.1 microsecond. The B-Dot range corresponds to that B-Dot generated by the above current at 1-meter radius.

<u>MEASUREMENT</u>	<u>SYMBOL</u>	<u>AMPLITUDE RANGE</u>	<u>SENSOR TYPE</u>
RATE OF CHANGE OF ELECTRIC FLUX DENSITY	\dot{D}	50 A/M ²	FLUSH PLATE DIPOLE
RATE OF CHANGE OF MAGNETIC FLUX DENSITY	\dot{B}	2 X 10 ⁴ TESLA/SEC	MULTIGAP LOOP
RATE OF CHANGE OF CURRENT	\dot{i}	10 ¹¹ A/SEC	INDUCTIVE CURRENT PROBE

Figure 5

MEASUREMENT LOCATIONS

The electromagnetic sensors are located on the aircraft in regions where the field strengths are greatest. Lightning currents contain frequency components high enough to excite the electromagnetic resonances of the aircraft; thus, the strongest fields occur at the antinode points of the resonances. For the lowest frequency resonances, the charge, and therefore the electric field, antinodes occur at the extremities of the aircraft and the current and magnetic field antinodes occur at the center. Thus, the D-Dot sensors are located near the ends of the nose, tail, and wings, and the B-Dot sensors are located near the center of the fuselage. Practical considerations, such as the location of access panels, dictate the exact sensor locations.

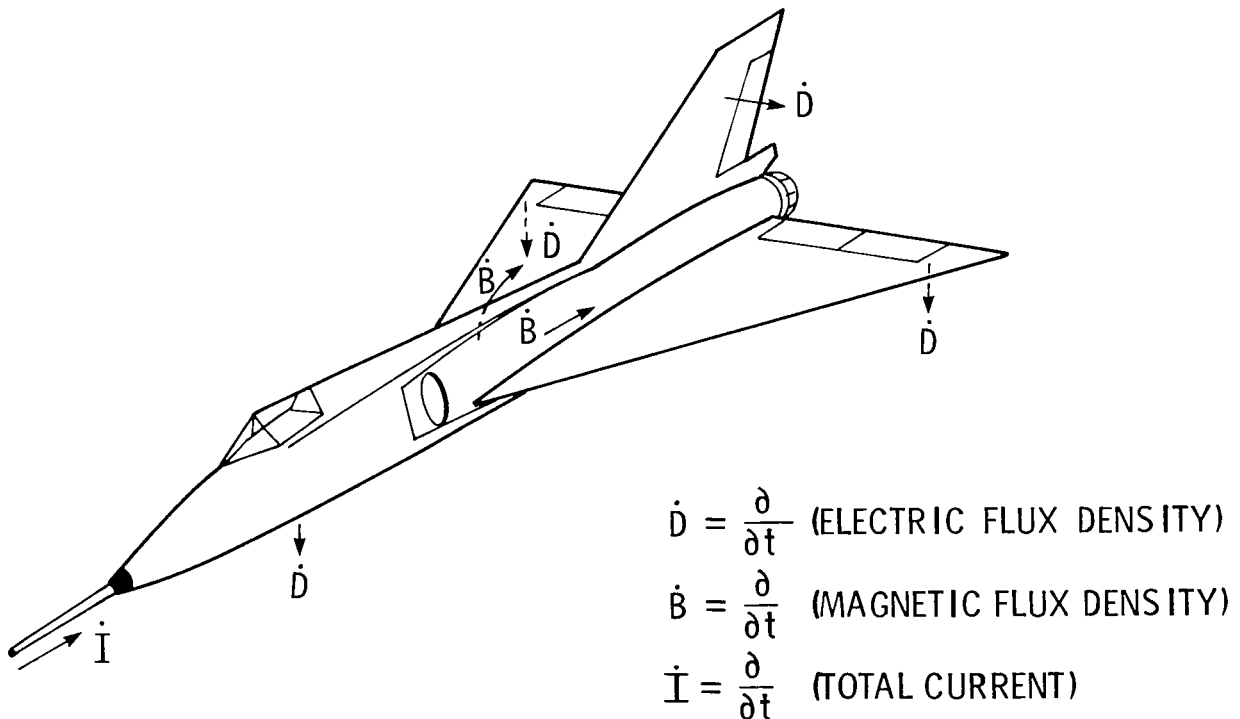


Figure 6

ELECTROMAGNETIC SENSORS

The sensors used in the lightning instrumentation system are derived from designs developed for nuclear electromagnetic pulse measurements. The sensor response to rates of change of the lightning electromagnetic characteristics (as opposed to the current and fields, directly) accentuates the recording of the higher frequency components of the lightning process. Since the magnitudes of induced voltages (and currents) are proportional to rates of change of the lightning electromagnetic characteristics, enhanced definition of the more interesting (from an induced effects viewpoint) portion of the spectrum is obtained. The sensor sensitivity is calculated based on sensor geometry and then checked using a parallel-plate transmission line calibrator. Following are photographs of the I-Dot, B-Dot, and D-Dot sensors, respectively, and a photograph of the flat-plate transmission line calibrator.

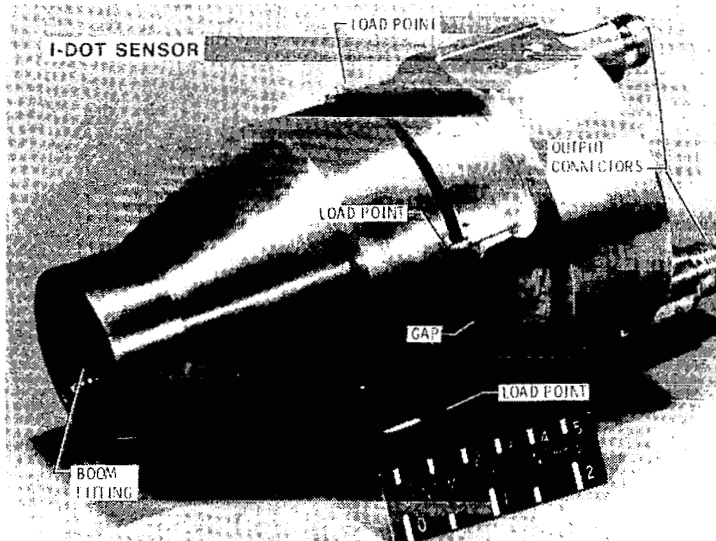


Figure 7

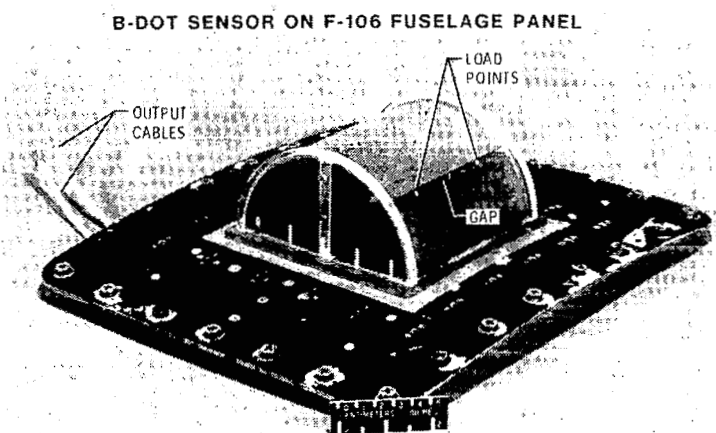


Figure 8

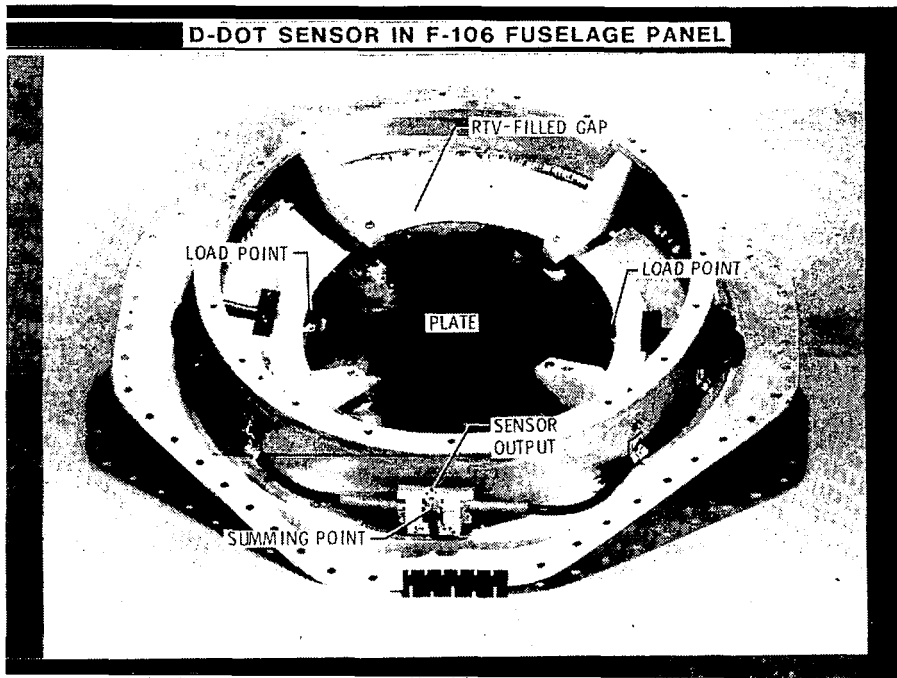


Figure 9

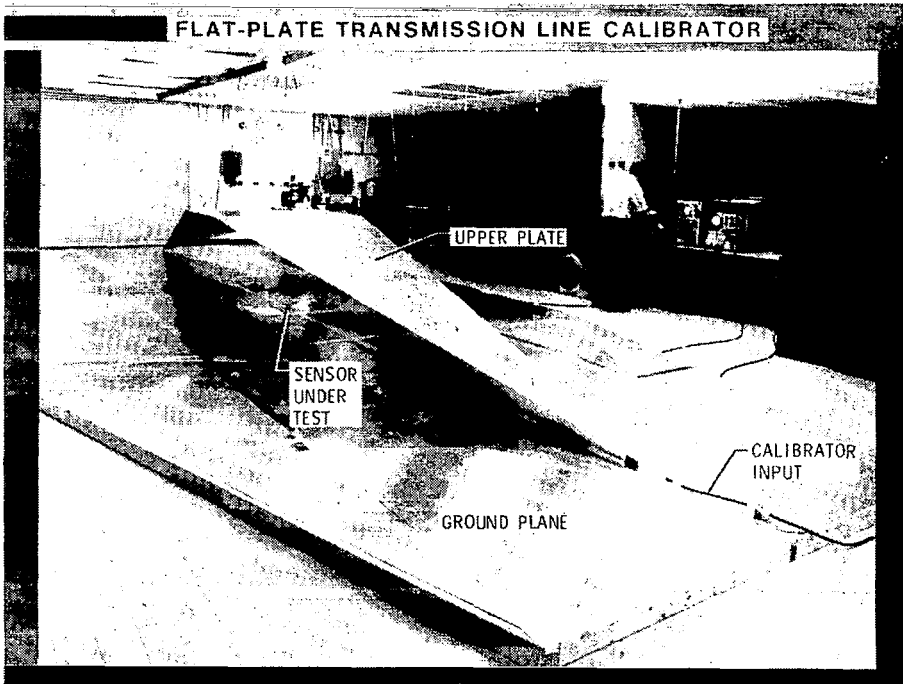


Figure 10

INSTRUMENTATION SYSTEM

This is the instrumentation system with the cover removed. The system is approximately 2-1/4 m x 1-1/2 m x 1/2 m and weighs about 450 kg (1000 pounds).

Specially expanded Biomation transient waveform recorders provide a unique capability for recording lightning electromagnetic transients. The transient recorders have solid-state memories which are continually updated with 6-bit data samples each 10 nanoseconds. Upon occurrence of a lightning strike, an internally generated trigger signal causes the recording to momentarily stop, temporarily storing the acquired lightning waveform in the memory. The memory contents are then formatted and recorded in the instrumentation tape recorder for permanent storage. The system then automatically resets for the next strike. The basic Biomation Model 6500 recorder memory was increased in an in-house development by over two orders of magnitude to allow a significant data window recording of 1300 microseconds of data at 10 nanoseconds resolution.

The wideband RCA Adviser video recorder has 6-MHz bandwidth and is capable of recording continuously for 24 minutes. This continuous recorder provides information on the overall lightning scenario to supplement the data "snapshots" recorded by the transient waveform recorders.

Power system isolation for the instrumentation is obtained using a motor-generator set. A 3-phase, 208-V, 400-Hz, 13-kVA electric motor external to the enclosure drives a nonconducting flexible coupler to a 12.5-kVA, 120/208-V, 3-phase, 400-Hz AC generator located within the enclosure to power the system.

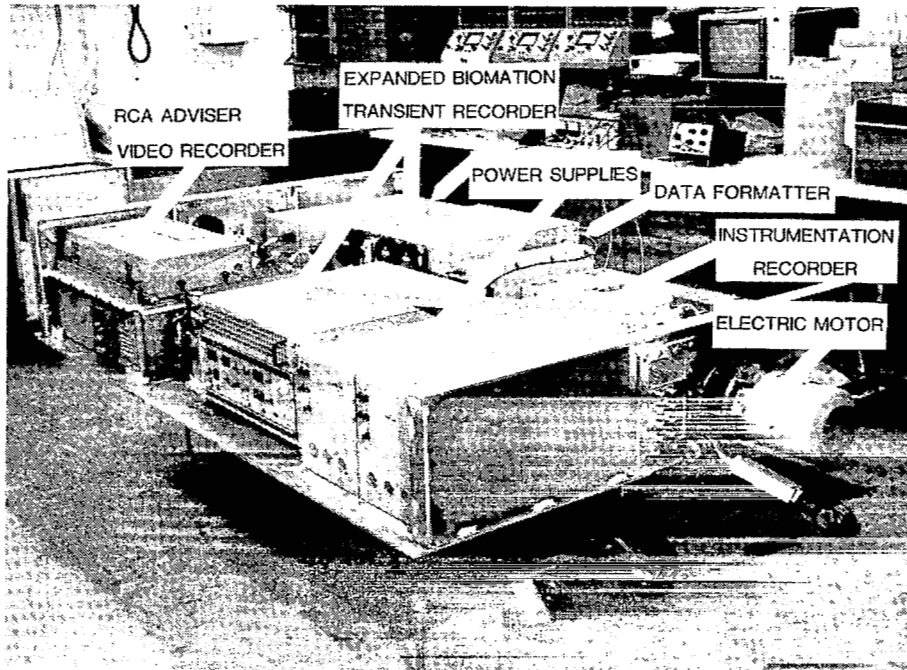


Figure 11

TRANSIENT RECORDER BLOCK DIAGRAM

The key feature of the transient recorder is the expanded memory which provides 131 072 data samples at 10 nanosecond sample intervals. The memory uses an interleaved architecture to achieve this speed with Intel 2147-3 RAM integrated circuits with a 55 nanosecond write-cycle period.

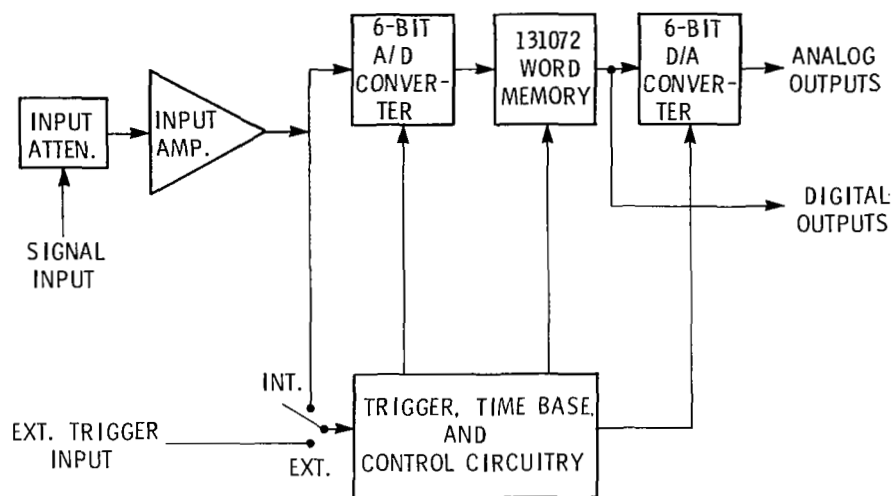


Figure 12

EXPANDED TRANSIENT WAVEFORM RECORDER FEATURES

- 6-BIT AMPLITUDE RESOLUTION (1.56%)
- FREQUENCY RESPONSE - DC TO 50 MHz
- 131072 (2^{17}) DATA WORD CAPACITY
- SAMPLE RATES UP TO 100 MHz
- DATA WINDOW LENGTH OF 1310 MICROSECONDS AT 100 MHz
- INTERNAL OR EXTERNAL TRIGGERING
- DATA WINDOW SELECTION WHICH IS BEFORE, DURING, OR AFTER TRIGGER EVENT

Figure 13

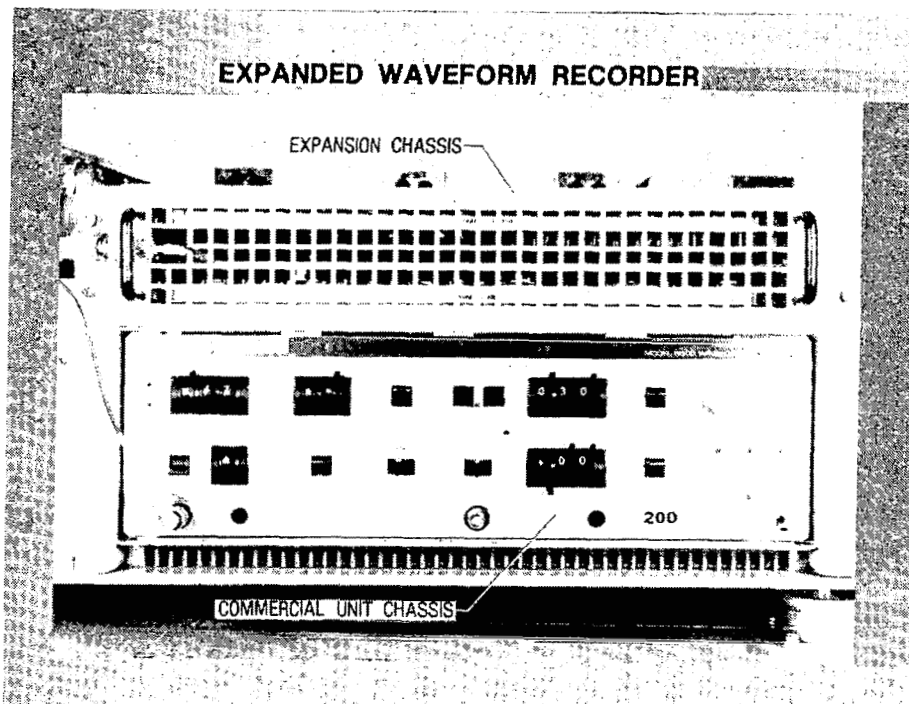


Figure 14

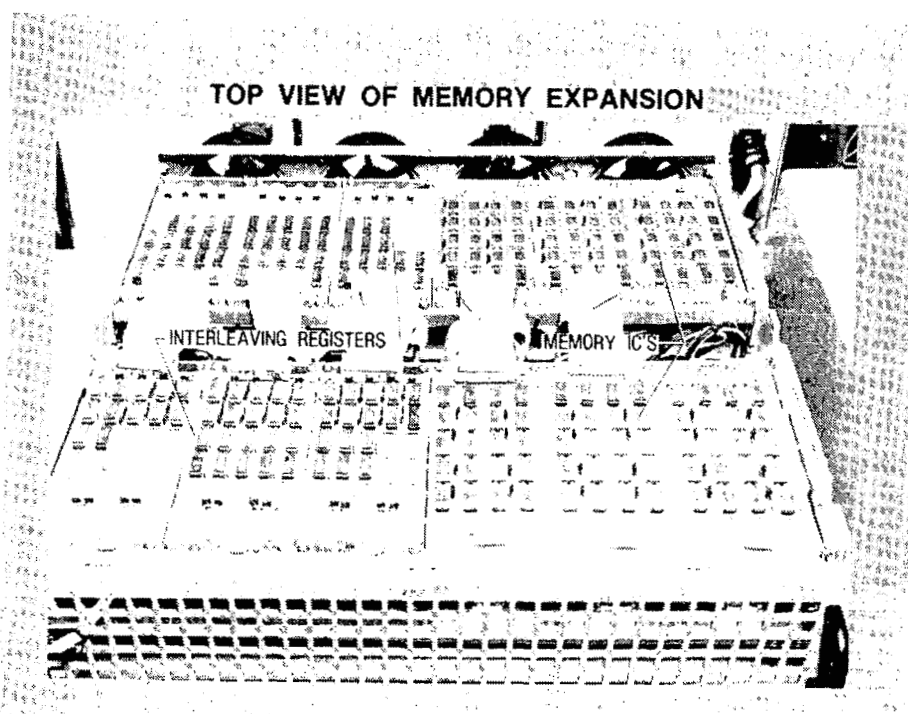


Figure 15

INSTRUMENTATION SYSTEM WITH COVER

This is the instrumentation system ready for mounting in the aircraft missile bay.

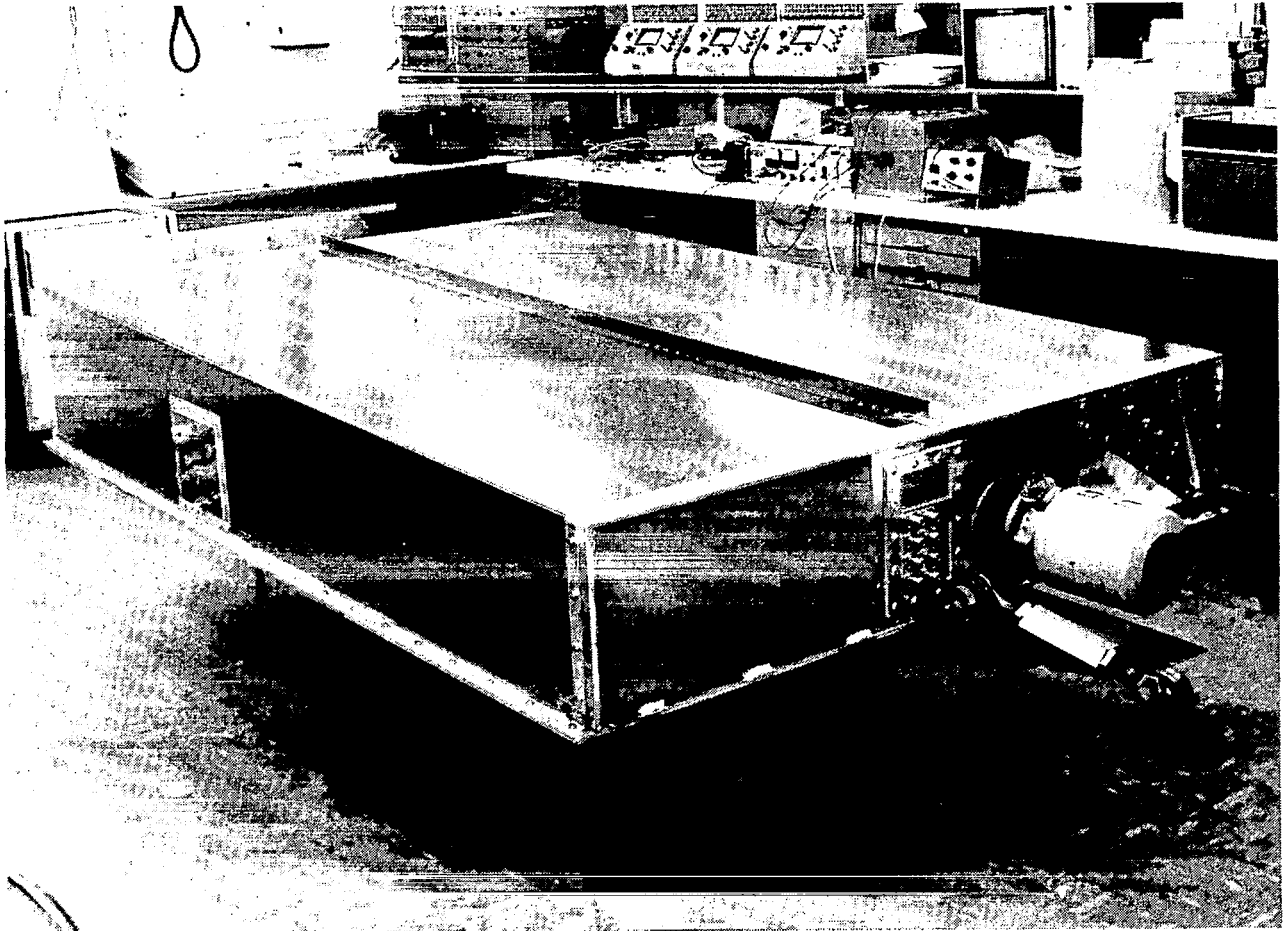


Figure 16

D-DOT SENSOR MOUNTED UNDER AIRCRAFT CHIN



Figure 17

D-DOT SENSOR MOUNTED ON VERTICAL FIN

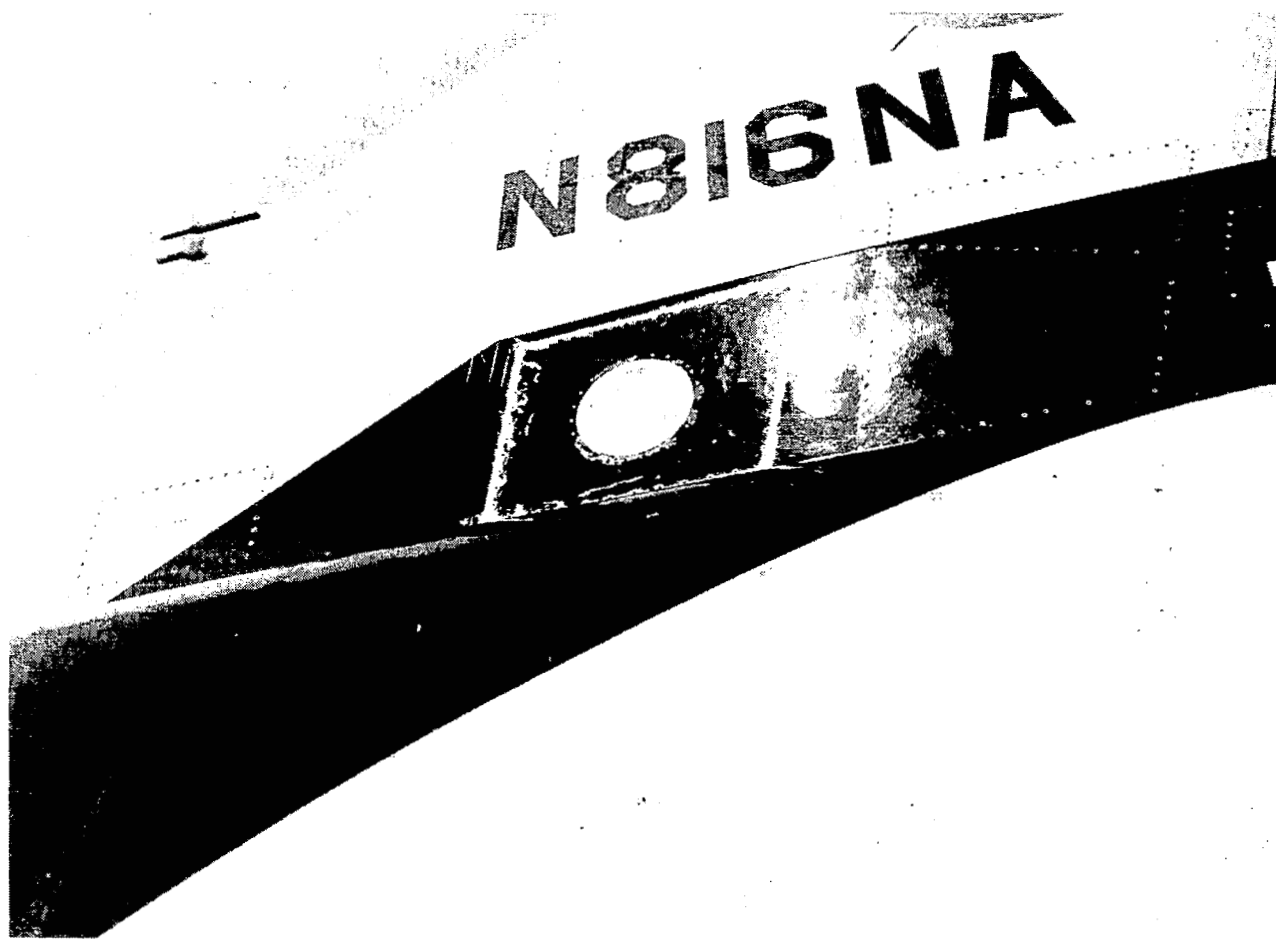


Figure 18

B-DOT SENSOR MOUNTED ON FUSELAGE

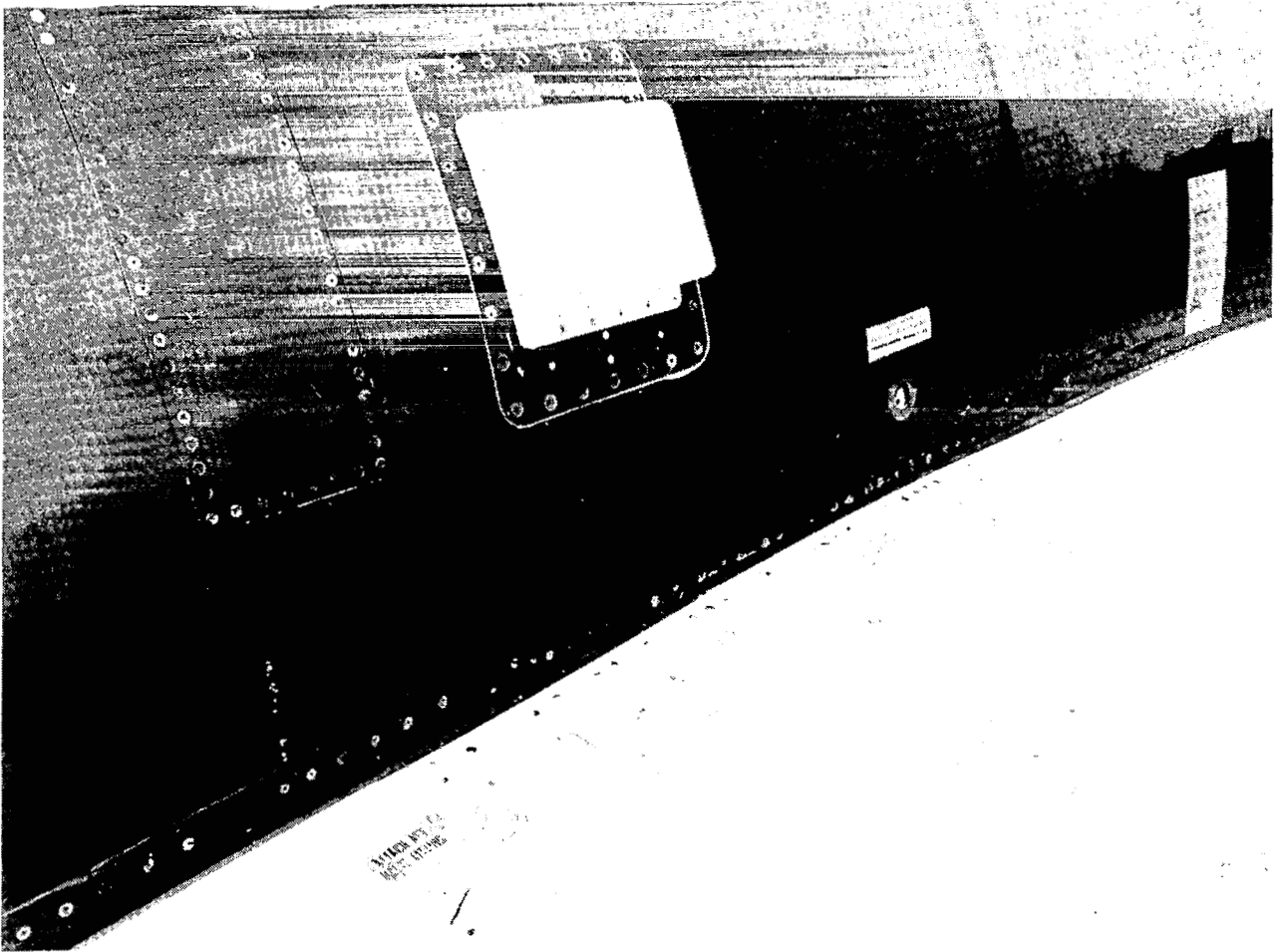


Figure 19

SIMULATED LIGHTNING SAFETY TEST

A simulated lightning safety survey test was performed on the aircraft to assess potential problems concerning aircraft systems safety. These tests were conducted by Lightning Technologies, Inc., and no safety hazards were disclosed by the tests. The safety survey tests also provided an opportunity for "end-to-end" instrumentation system fidelity and noise immunity tests. The tests were performed with the aircraft engine running and all flight systems operating on aircraft power. The instrumentation system measured and recorded the fields and currents on the aircraft in response to a current pulse of known amplitude and waveform (as determined from an external current transformer measurement) which was generated with a high-voltage capacitor discharge apparatus attached to the noseboom. The current exited from the aircraft tail and was returned to the generator using symmetrical return wires as shown in the test set-up photograph.

During subsequent tests, sensor cables were terminated in dummy 50-ohm loads, in lieu of the sensors, to investigate the noise immunity of the instrumentation system. The system did not respond during these tests, indicating that the noise level would be at least one order of magnitude below the flight configuration threshold.

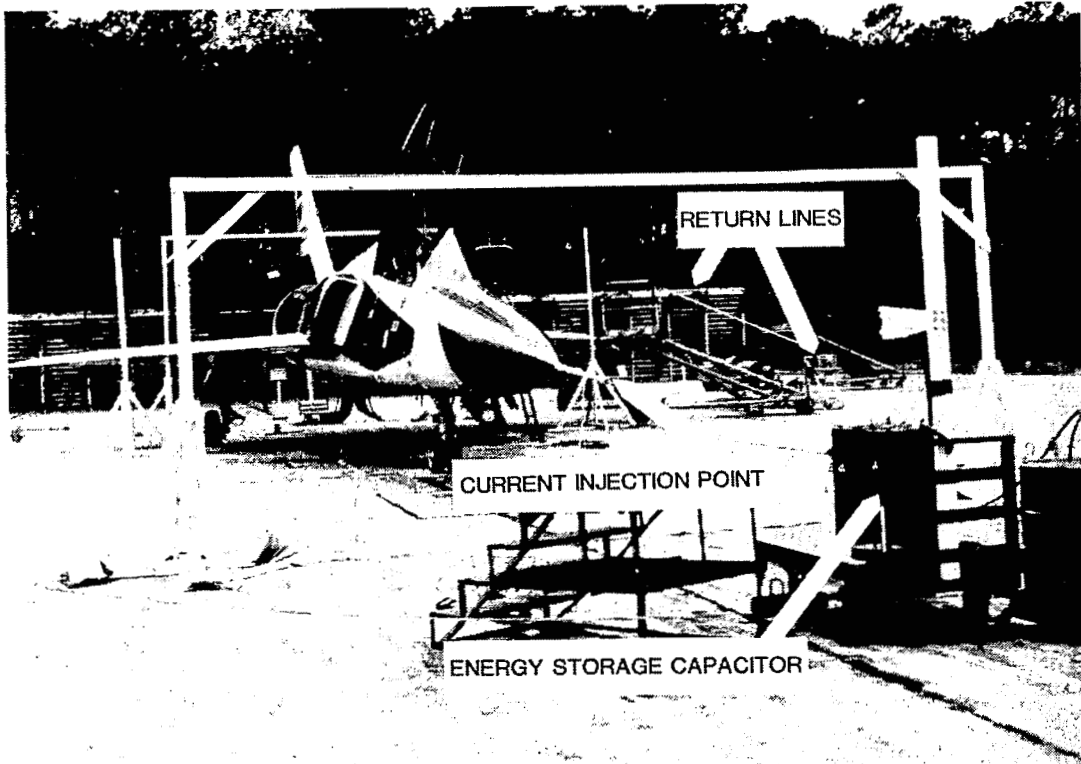


Figure 20

I-DOT SENSOR RESPONSE

This waveform shows typical I-Dot sensor response to an input current to the noseboom, recorded during the safety test. The input was a damped sinusoidal current oscillating at 86 000 Hz, with a peak amplitude of 10.500 amperes. The I-Dot measurement agrees with the rate of change of input current within about 10 percent.

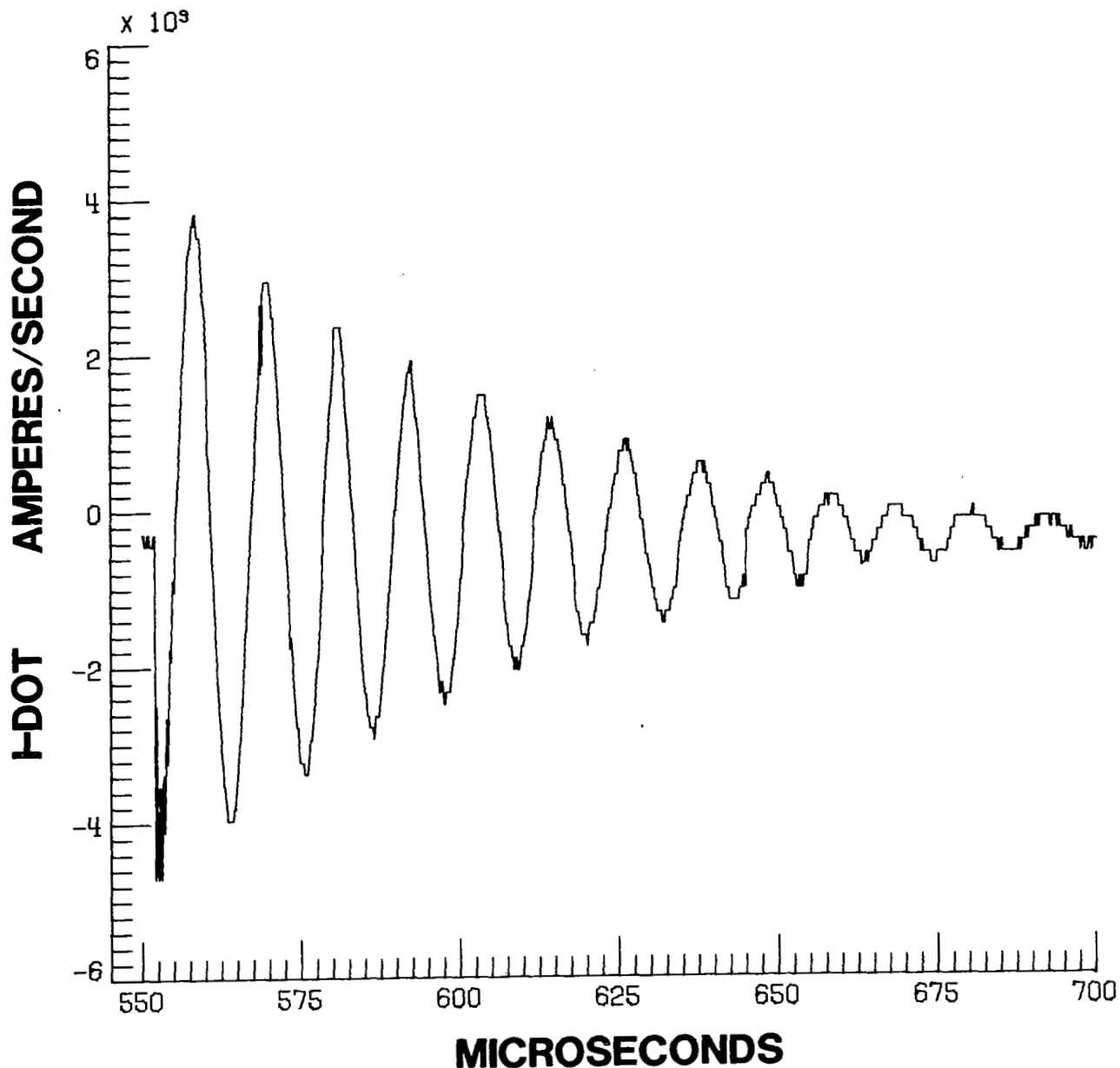


Figure 21

DIRECT STRIKE LIGHTNING DATA

The aircraft sustained three strikes while in the vicinity of the National Severe Storms Laboratory, Norman, Oklahoma, on June 17, 1980. The strikes occurred with the aircraft at an altitude of 4 800 meters (16 000 feet) at a speed of 154 meters per second (300 knots); the approximate freezing level was at the aircraft operating altitude. These strikes were not particularly energetic in that the magnetic characteristics (I-Dot, B-Dot) did not exceed system thresholds and only information from the forward D-Dot sensor was recorded. The portions of the above strike data records with the largest rates of change of electric flux density follow (fig. 23). The electric field changes for these data have been calculated as $1/\epsilon_a$ times integral of D-Dot and also follow (fig. 24). Interpretation and analysis of the data are continuing; the following observations are offered at this point: (1) the utility of the derivative (D-Dot) sensor is clearly demonstrated by comparing the amplitude resolution of the "faster" changing portions of the D-Dot data with its integral during the first microsecond of the event; (2) the data indicate significant changes in the strike electric characteristics during submicrosecond intervals; and (3) a large electric field change accompanies the strike.



Figure 22

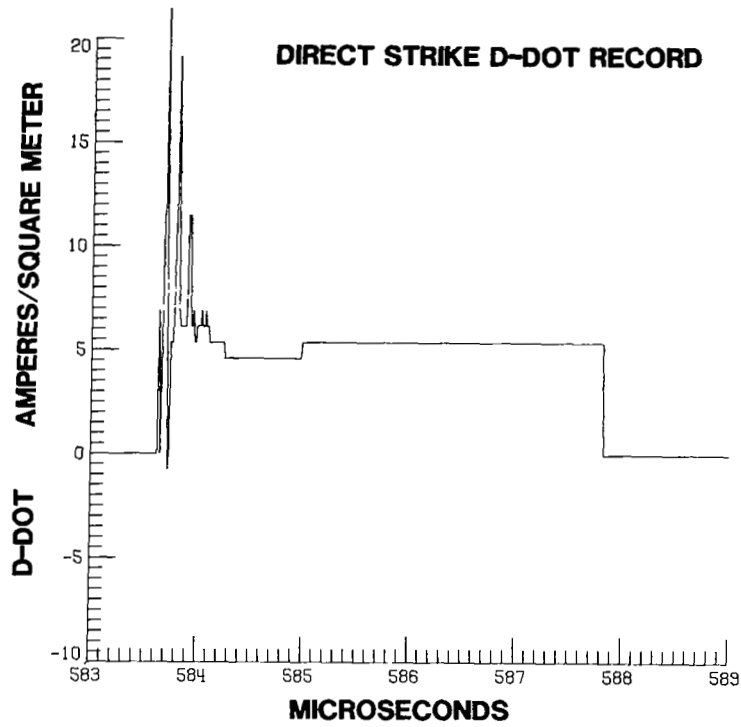


Figure 23

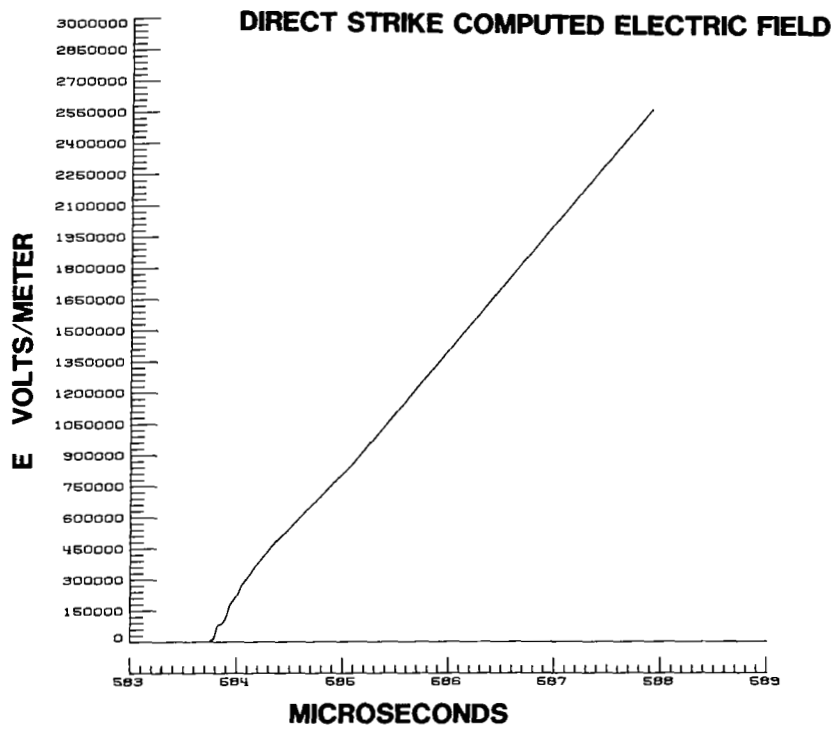


Figure 24

SUMMARY OF LIGHTNING EXPERIMENTS ON NASA F-106B AIRCRAFT

- LANGLEY RESEARCH CENTER DIRECT STRIKE
- BOEING DATA LOGGER EVALUATION
- LANGLEY RESEARCH CENTER ATMOSPHERIC CHEMISTRY (N₂O, CO)
- NATIONAL SEVERE STORM LABORATORY OPTICAL SIGNATURE
- UNIVERSITY OF WASHINGTON X-RAY EMISSION

Figure 25

FY 81 PLANS

- CONTINUE DIRECT STRIKE FLIGHT TESTS
 - 12 CHANNEL DIGITAL TRANSIENT RECORDER
 - 15 MHz VIDEO RECORDER

- DATA INTERPRETATION/ANALYSIS

REFERENCES

1. Weidman, C. D.; and Krider, E. P.: Submicrosecond Risetimes in Lightning Radiation Fields. Lightning Technology, NASA CP-2128, 1980, pp. 29-38.
2. Pitts, F. L., et al.: In-Flight Lightning Characteristics Measurement System. Federal Aviation Administration - Florida Institute of Technology Workshop on Grounding and Lightning Technology, FAA-RD-79-6, Mar. 1979, pp. 105-111.
3. Baum, C. E., et al.: Sensors for Electromagnetic Pulse Measurements Both Inside and Away From Nuclear Source Regions. IEEE Trans. Electromagn. Compat., vol. EMC-20, no. 1, Feb. 1978.
4. Trost, Thomas F. ; and Zaepfel, Klaus P.: Broadband Electromagnetic Sensors for Aircraft Lightning Research. Lightning Technology, NASA CP-2128, 1980, pp. 131-152.
5. Thomas, Robert M., Jr.: Expanded Interleaved Solid-State Memory for a Wide Bandwidth Transient Waveform Recorder. Lightning Technology, NASA CP-2128, 1980, pp. 119-129.
6. Pitts, Felix L.; and Thomas, Mitchel E.: Initial Direct Strike Lightning Data. NASA TM-81867, 1980.

GROUND AND FLIGHT TEST EXPERIENCE WITH A TRIPLY REDUNDANT
DIGITAL FLY-BY-WIRE CONTROL SYSTEM

Calvin R. Jarvis and Kenneth J. Szalai
NASA Dryden Flight Research Center

ABSTRACT

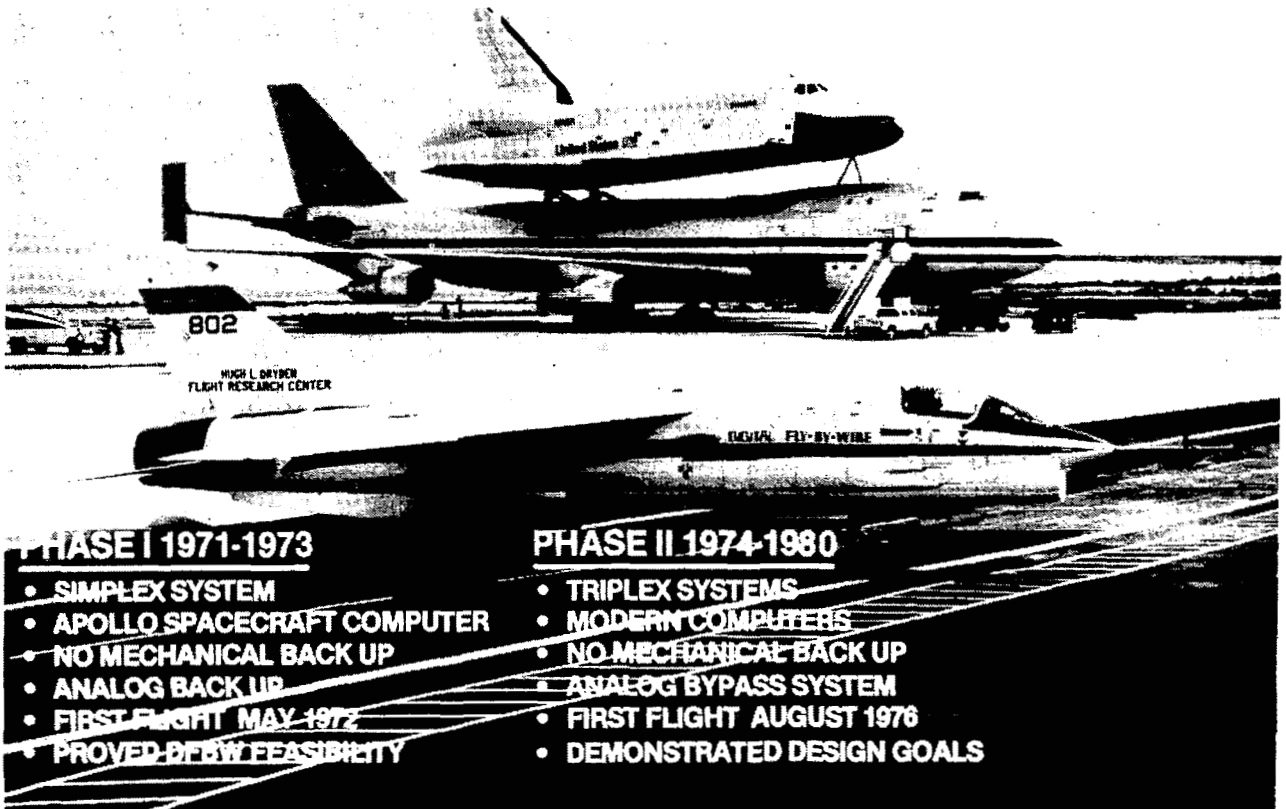
The National Aeronautics and Space Administration (NASA) is conducting research in digital fly-by-wire (DFBW) flight control for aircraft. The primary impetus for this work has come from the projected flight control system requirements for advanced military and commercial aircraft, particularly in the area of active controls. Such systems must have extremely high levels of reliability and computational capacity.

From 1972 to 1980, the NASA Dryden Flight Research Center (DFRC) conducted flight tests of a DFBW control system in an F-8C aircraft.

A triplex digital fly-by-wire flight control system was developed and then installed in the aircraft to provide fail-operative, full authority control. Hardware and software redundancy management techniques were designed to detect and identify failures in the system. Control functions typical of those projected for future actively controlled vehicles were implemented.

NASA F-8 DIGITAL FLY-BY-WIRE PROGRAM

NASA has been conducting research in aircraft digital fly-by-wire control at the Dryden, Langley, Ames, Lewis, and Johnson centers. The primary objective of this work is the development of highly reliable flight control systems that permit the implementation of active control functions, which contribute to energy efficiency and high maneuverability. A major flight experiment at the Dryden Flight Research Center involves the use of a Navy F-8C testbed aircraft that was modified to incorporate full authority digital fly-by-wire controls. The vehicle has a triplex fail-operational digital fly-by-wire primary flight control system and an analog emergency backup control system.



F-8/DFBW LIGHTNING SUSCEPTIBILITY TESTS

To learn more about possible lightning effects on digital fly-by-wire systems, a series of NASA-sponsored research programs were conducted by Lightning Technologies Inc. and the Air Force Flight Dynamics Laboratory at Wright Patterson, using the F-8/DFBW aircraft. This research led to development of a nondestructive method, now known as the lightning transient analysis (LTA) test, for determining the level of lightning-induced voltages in aircraft electrical circuits. These test results were widely distributed in industry and prompted positive efforts to design lightning protection into other aircraft being designed with fly-by-wire control systems, including the USAF/General Dynamics F-16, the USN/McDonnell Douglas F-18 and the NASA space shuttle.

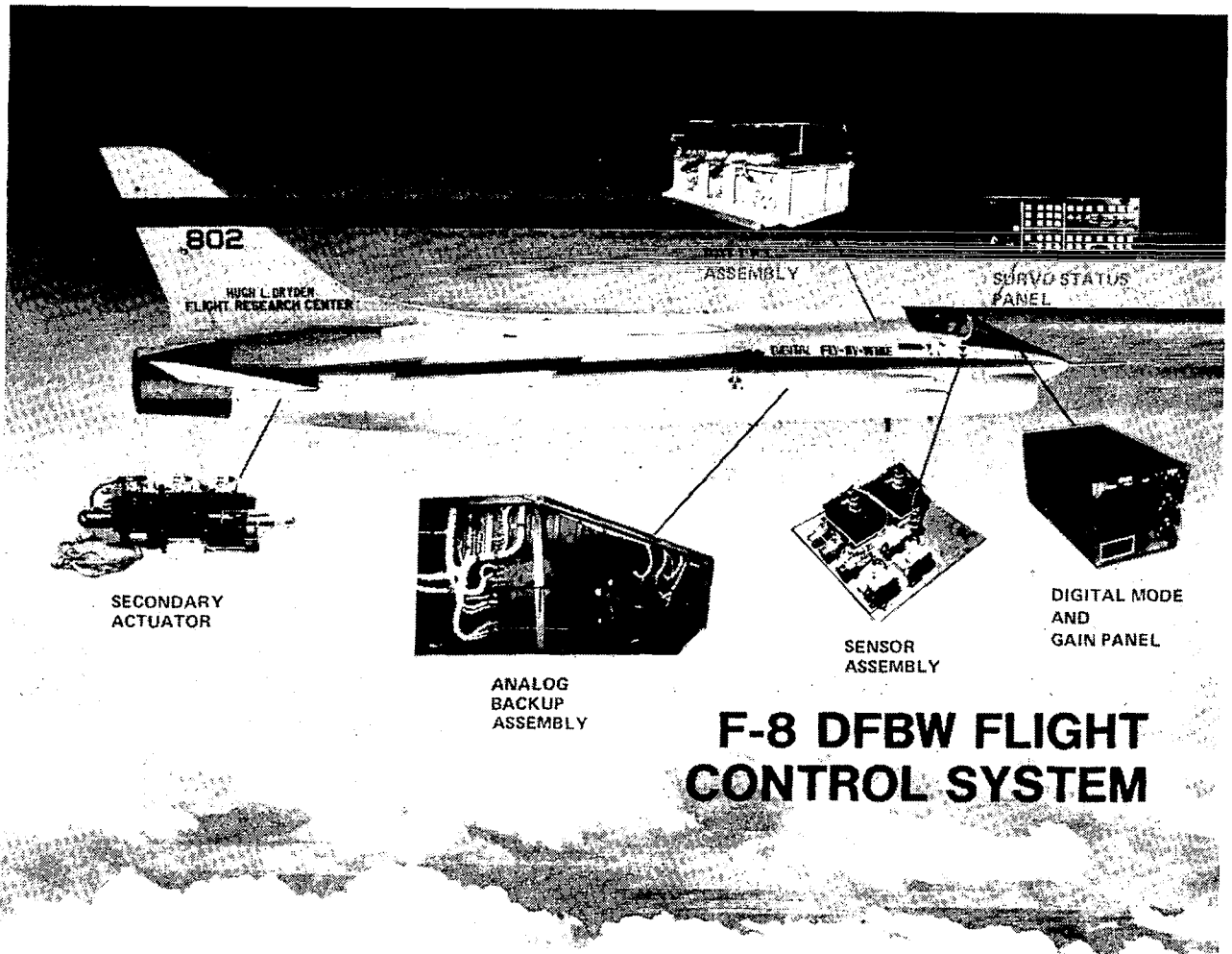


**50,000 Volt Simulated Lightning
Strike Induced on Nose Boom
Of Digital-Fly-By-Wire Aircraft**

**F-8/DFBW LIGHTNING
SUSCEPTIBILITY TESTS**

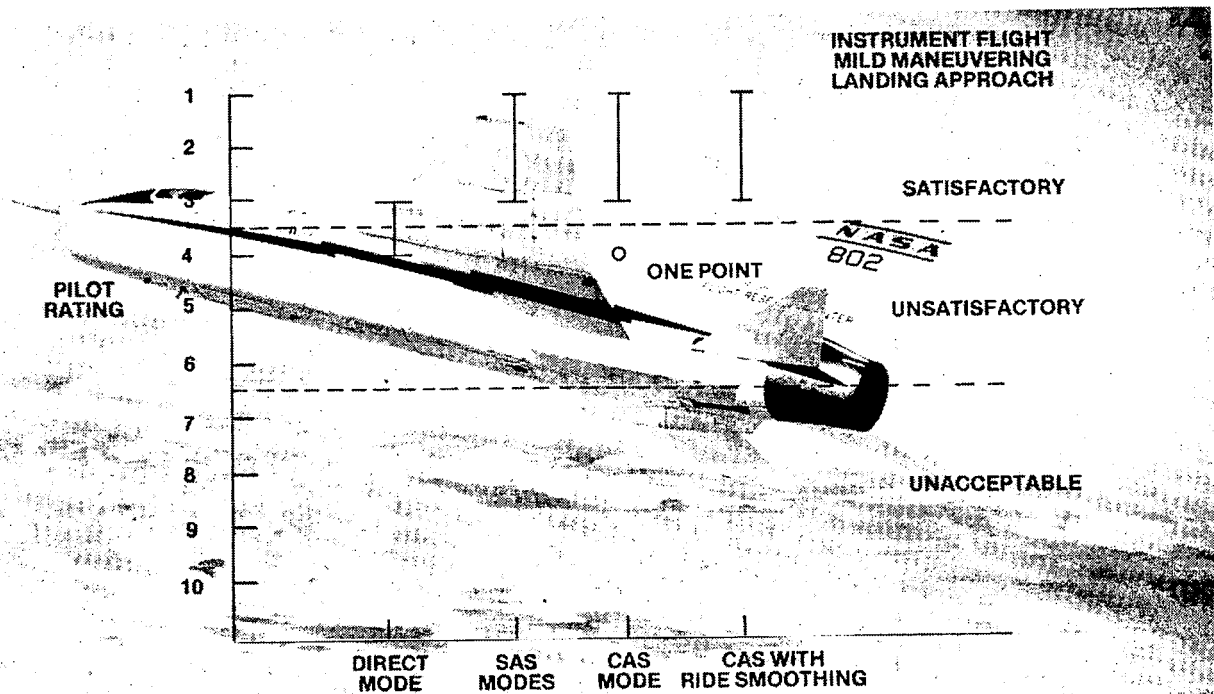
F-8/DFBW FLIGHT CONTROL SYSTEM MAJOR COMPONENTS

The heart of the F-8/DFBW flight control system is the triplex computer and interface unit assembly mounted on a removable pallet for easy access. A digital mode and gain panel located in the cockpit provides the pilot with system status information. Similar data are provided for the redundant actuators on a servo status panel. Analog backup electronics are located in the aircraft fuselage section as are the redundant rate gyro and accelerometer sensors. Each aircraft control surface is operated through a redundant servoactuator assembly that is commanded via the digital computers.



F-8/DFBW HANDLING QUALITIES SUMMARY

Handling qualities ratings by pilots for all control modes, based on the Cooper-Harper rating scale, have been satisfactory and above for all augmented modes and borderline for direct modes with no augmented feedback parameters. Ratings did not tend to vary for instrument flight, mild maneuvering and landing approach tasks.



PREFLIGHT TEST PROGRAM EXPERIENCE

All test flights are preceded by preflight tests comprised of hangar tests to verify system gains and scale factors, and automated flight-line tests that take approximately 5 minutes. The flight software program is generally loaded into the redundant computers during the hangar test, but can also be loaded during flight-line operations. Automated flight-line tests generally require pilot participation for switch operations and control inputs. No significant problems have been experienced with the integrity of the preflight procedures.



PREFLIGHT TEST PROGRAM EXPERIENCE

NASA
DFRC80-482

- COMPLETE HANGAR PREFLIGHT TAKES APPROXIMATELY ONE HOUR
- DIGITAL PORTION OF FLIGHT-LINE PREFLIGHT TAKES 5 MINUTES

- NO PROBLEMS WITH TAPE LOAD IN HANGAR AND RAMP POWER-UP
- SURFACE TOLERANCES ARE WIDER THAN DESIRED TO ACCOMMODATE RIGGING
- MID-STICK END-TO-END GEARING CHECK OCCASIONALLY FAILS DUE TO PROCEDURAL PROBLEMS, BUT IS A SENSITIVE TEST
- NO SIGNIFICANT DEVELOPMENT PROBLEMS ENCOUNTERED

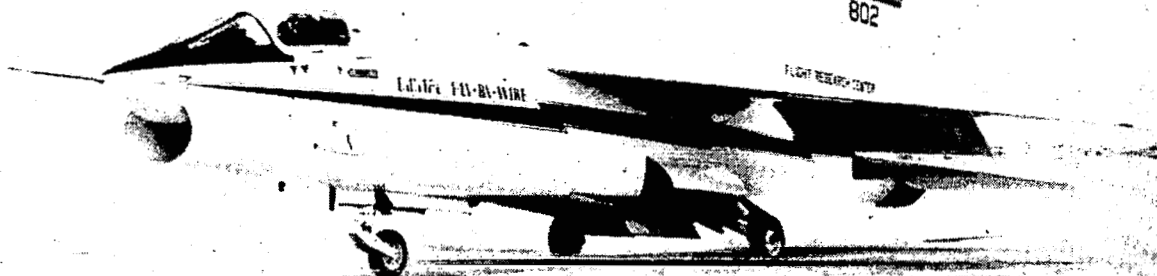
GROUND AND FLIGHT QUALIFICATION TESTS

The iron bird facility was used to a much greater extent than the actual aircraft for ground and flight qualification testing. The actual aircraft was used primarily to validate results established using the iron bird, except for ground resonance and structural coupling testing which required the presence of valid vehicle structural modes. The importance of an iron bird facility as a cost effective means of accomplishing these types of tests cannot be over emphasized.

PERCENTAGE OF TESTING IRON BIRD AIRCRAFT

NASA
DFRC 80-487

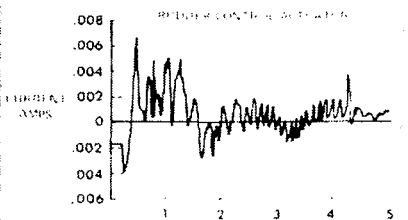
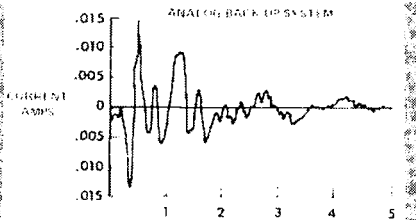
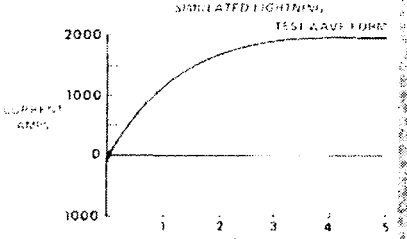
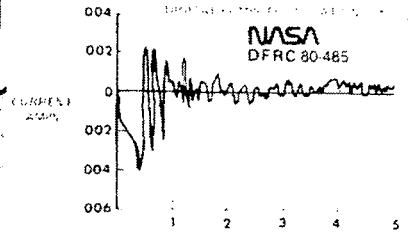
● SOFTWARE VERIFICATION	98	2 (PREFLT TEST)
● FMEA DEMONSTRATION	90	10
● SYSTEM INTEGRATION	75	25
● GROUND RESONANCE		100
● PILOT FAMILIARIZATION	95	5
● EMI	90	10
● LIGHTNING SUSCEPTABILITY		100



INDUCED-CURRENT MEASURED DURING F-8/DFBW LIGHTNING TRANSIENT ANALYSIS TESTS

A wide range of lightning test conditions were applied to the F-8/DFBW aircraft, reaching potentials of up to 50,000 volts and simulated lightning currents of up to 8,000 amps. One of the more significant findings of this first series is that at the instant test voltage is applied to the aircraft, traveling wave currents are established that "ring" back and forth along the aircraft at the speed of light, much as mechanical vibrations are set up in an airplane when it encounters a gust of wind. These currents precede the flow of return stroke current and are considerably higher than it in frequency. The magnetic fields produced by these high frequency currents thus induce higher voltages in internal electrical circuits.

Induced Currents Measured During F-8/DFBW Lightning Transient Analysis Tests



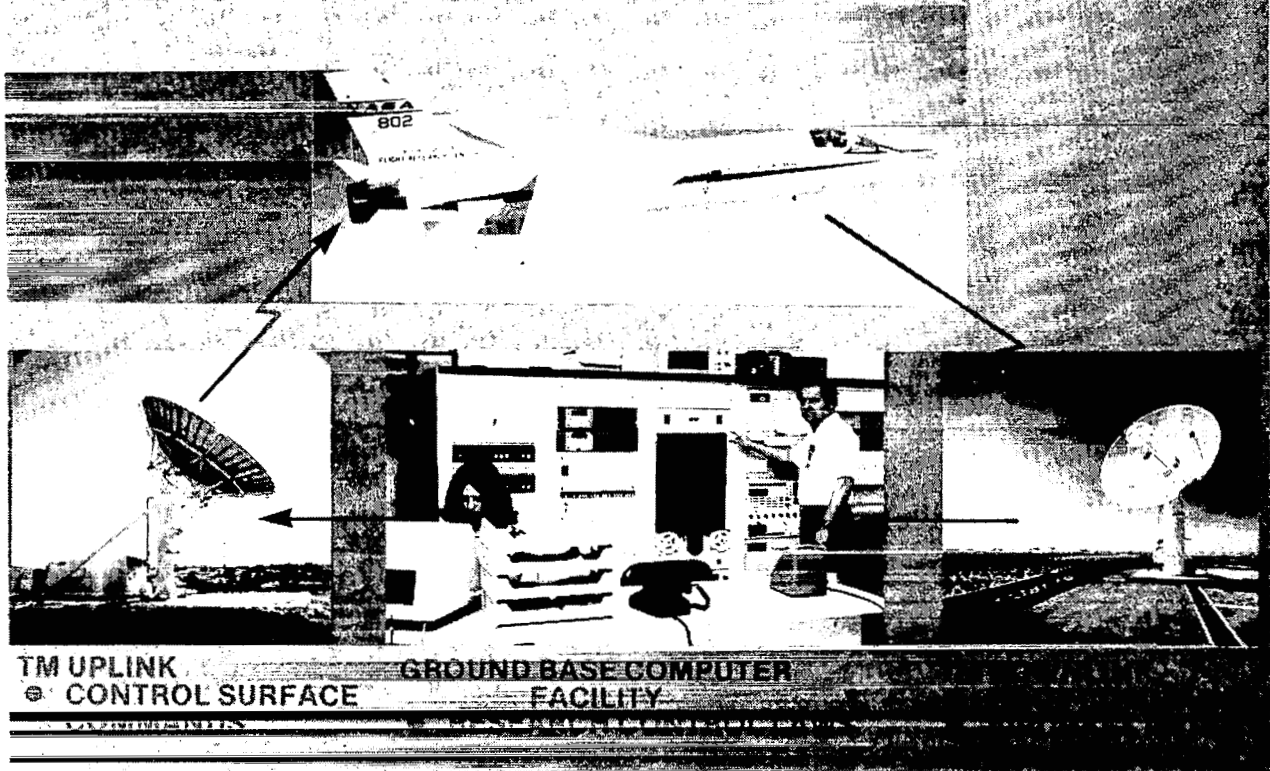
REMOTELY AUGMENTED VEHICLE TEST FACILITY

The F-8/DFBW aircraft can also be operated in a unique control law evaluation mode. By selecting special on-board software, the pilot can bypass the on-board flight computer, and have his normal control commands transmitted via downlink to a special receiving antenna. The commands are then processed in special control law algorithms programmed on a ground-based computer, and computed surface commands are uplinked to the aircraft. The pilot, in effect, flies the aircraft through the ground-based control laws. This approach greatly simplifies the level of verification required to man rate research control laws for flight test purposes and becomes a very low cost means of flight testing advanced control law algorithms.

REMOTELY AUGMENTED VEHICLE (RAV) TEST FACILITY

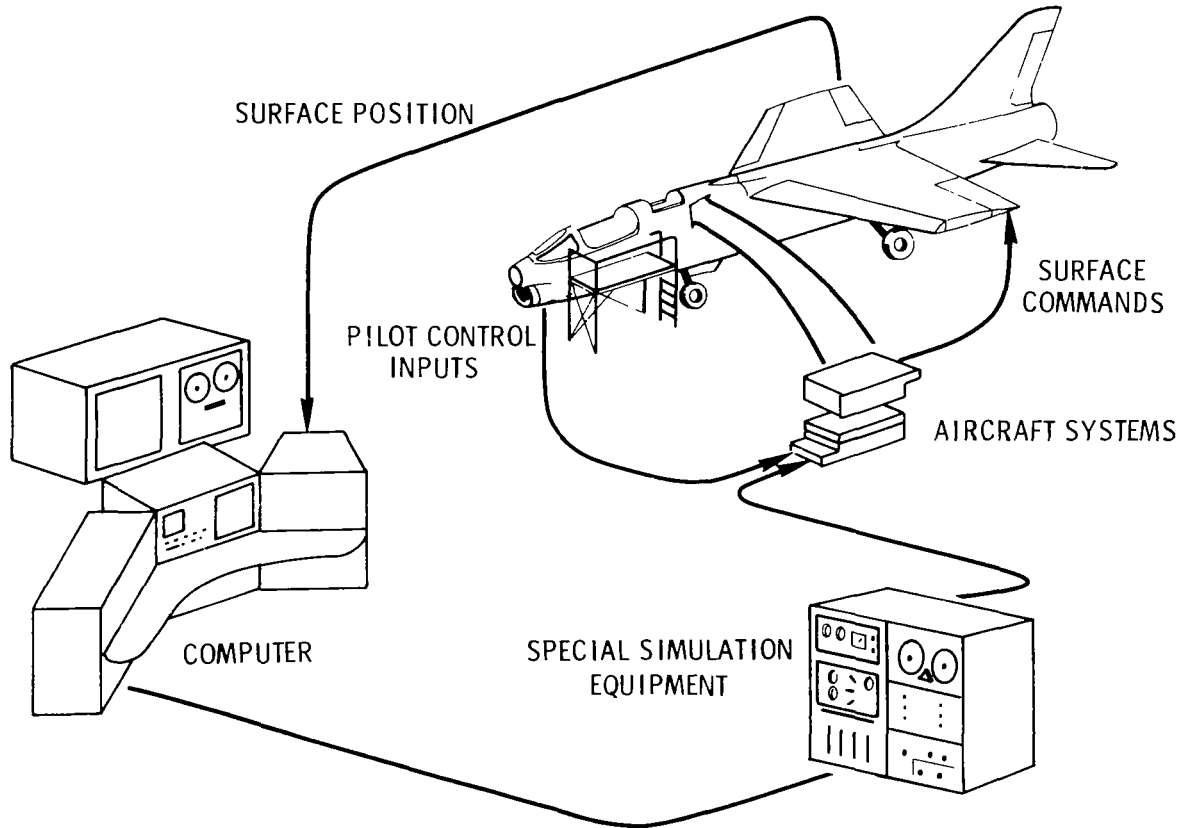
NASA
DFRC 10-88

UNIQUE FACILITY FOR TESTING ADVANCED CONTROL LAW CONCEPTS



IRON BIRD TEST FACILITY

An iron bird test facility was used in carrying out the many tests to support software and hardware verification. The facility consisted of an actual F-8 aircraft and all associated electric, electronic and hydraulic systems. A complete set of DFBW electronics and actuators were installed in the iron bird which was coupled to a six-degree-of-freedom closed-loop simulation of the F-8 dynamics. In addition to supporting ground verification and validation tests, the iron bird was also used for pilot training, pilot-in-the-loop failure mode, effects testing, and EMI testing.

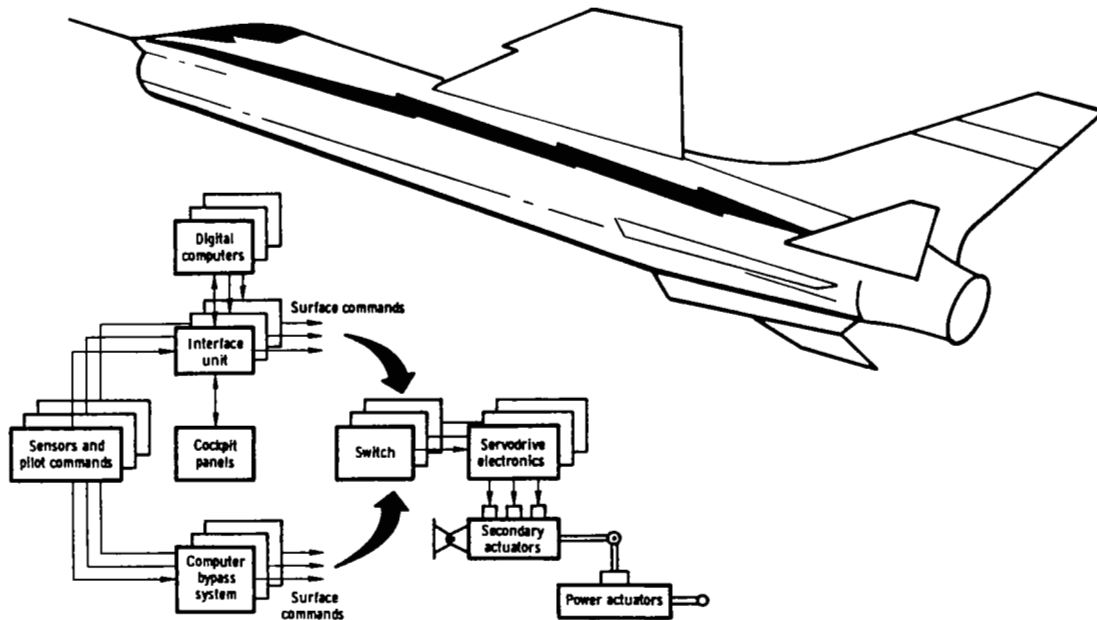


F-8 DIGITAL FLY-BY-WIRE SYSTEM DESCRIPTION

The overall mechanization of the F-8 DFBW control system is shown in this figure. A triplex digital computer set containing control law and system redundancy management software communicates with a specially designed interface unit (IFU). The IFU processes input data, which consist of pilot commands and aircraft sensor signals, and output data, which consist of surface commands, cockpit displays, and telemetry data. Surface commands are routed through a switching mechanism to the servodrive electronics and then to the force-summed secondary actuators, which are installed in series with the existing F-8C power actuators. There are five actuator sets: one for each aileron and horizontal stabilizer surface and one for the rudder.

The triplex analog computer bypass system provides the pilot with an emergency unaugmented command path to the control surfaces in the event of a total primary digital system failure. This path was provided primarily to protect against a common-mode software failure in the infant stages of flight test. The switching mechanism allows either the primary system or the bypass system to drive the secondary actuators based on pilot selection or automatically, according to fault status.

Electrical power is provided to three independent flight control buses by an engine-driven dc generator. Each bus is protected by a 40-ampere-hour battery, which would allow approximately 90 minutes of operation in the event of a loss of generator power. Secondary actuator hydraulic power is provided by the aircraft's three hydraulic systems, each of which supplies one of the triple chambers of each actuator.



IN-FLIGHT SYSTEM PERFORMANCE SUMMARY

Over 80 research missions have been flown with the F8/DFBW system. All take-offs and landings have been accomplished with the primary digital system. No automatic reversion to the analog bypass system has ever been required. Four computer hard failures have occurred on separate flights resulting in loss of one of the three digital channels. In each case, the aircraft was operated on the remaining two channels. All failure detection, identification and recovery operations have been according to design.

Although software errors have been discovered after initiation of the flight test program, no software errors have resulted in terminating a flight or aborting a mission, although this could have been the case had the right sequence of events occurred.

Several control law refinements were required to improve overall flying qualities, especially about the roll axis. Roll control was initially extremely sensitive about neutral stick positions for precision control tasks such as formation flying.

Very few cases of sensor failures have been noted, either hard or transient fails.

All failures that have occurred have been detected and properly resolved.

- **ALL TAKE-OFFS AND LANDINGS MADE WITH PRIMARY DIGITAL FLY-BY-WIRE SYSTEM**
- **NO AUTOMATIC REVERSION TO ANALOG BY-PASS SYSTEM HAS OCCURRED**
- **FOUR IN-FLIGHT COMPUTER FAILURES**
- **ONE TRANSIENT FAILURE IN-FLIGHT RESETTABLE**
- **NO FLIGHT ABORTS DUE TO SOFTWARE FAULTS**
- **SEVERAL CONTROL LAW REFINEMENTS NECESSARY**
- **SOME SOFTWARE ERRORS DISCOVERED DURING FLIGHT TEST PROGRAM**
- **VERY FEW SENSOR NUISANCE FAULTS**
- **NO EXCEPTIONS TO FAIL-OP OR FAIL-SAFE DESIGN**

CONTRACTOR AND UNIVERSITY STUDIES/GRANTS

In addition, a large number of supporting studies have been conducted by universities and contractors in support of various advanced concepts addressed by the F-8/DFBW program.

ADVANCED CONTROL LAW CONCEPTS	MIT RENSSELAER INSTITUTE (RPI) COLLEGE UNIVERSITY OF N.Y. (C.U.N.Y.) WILLIAM AND MARY VIRGINIA POLYTECHNIC *CSDL *HONEYWELL
● PHASE II CONCEPTUAL DESIGN	HONEYWELL
● FAULT-TOLERANT COMPUTER DESIGN	ULTRASYSTEMS
● DIGITAL FLIGHT CONTROL ACTUATION	ROCKWELL
● DFBW CERTIFICATION REQUIREMENTS	CSDL

*CONCEPTS FLIGHT TESTED

CONTRACTOR SUPPORT

Over 11 separate contractors have been involved directly in support of the F-8/DFBW program. This broad scope of involvement has contributed greatly to the program's transfer of digital fly-by-wire technology to industry in a timely manner.

CHARLES STARK DRAPER LAB	SOFTWARE AND INTERFACE HARDWARE
DELCO	INTERFACE HARDWARE
IBM	COMPUTER HARDWARE
RAYTHEON.....	COMPUTER HARDWARE
SPERRY FLIGHT SYSTEMS.....	ANALOG BYPASS SYSTEM
HYDRAULICS RESEARCH & MANUFACTURING ...	ACTUATORS
LING, TEMCO, VOUGHT.....	AIRCRAFT INTERFACE
BOEING.....	SNEAK CIRCUIT ANALYSIS
G.E.....	LIGHTNING TESTS
LIGHTNING TECHNOLOGIES, INC.....	LIGHTNING TESTS
AIR FORCE FLIGHT DYNAMICS LAB.....	LIGHTNING TESTS

JOINT NASA CENTER RESPONSIBILITIES FOR PHASE II PROGRAM

Overall program management responsibility for the F-8/DFBW program, including flight qualification and flight testing, rests at Dryden Flight Research Center. Advanced control law and system architectural concepts developed at Langley Research Center have been an integral part of the F-8/DFBW program. Considerable support of the space shuttle control system development has taken place through joint efforts with the Johnson Space Center. A joint NASA/FAA workshop on digital flight controls, sponsored by the Ames Research Center, was also supported by the program in 1979.

DRYDEN FLIGHT RESEARCH CENTER

- PROGRAM MANAGEMENT
- SYSTEM SPECIFICATION AND PROCUREMENT
- OVERALL SYSTEMS INTEGRATION
- SOFTWARE VERIFICATION
- FLIGHT QUALIFICATION
- FLIGHT TESTS

LANGLEY RESEARCH CENTER

- ADVANCED CONTROL LAW DEVELOPMENT
- PHASE II CONCEPTUAL STUDY
- DIGITAL ACTUATOR DEVELOPMENT STUDY

JOHNSON SPACE CENTER

- SPECIFY SHUTTLE SUPPORT TASKS
- SUPPORT SHUTTLE SOFTWARE FLIGHT TEST

AMES RESEARCH CENTER

- JOINT NASA/FAA WORKSHOP

F-8/DFBW CONTROL LAWS

Several advanced control law algorithms were developed and implemented in the F-8/DFBW system. The primary objective was to address the type of algorithms that might be applicable to future systems employing active control concepts. The goal was to tax the system as heavily as possible in order to identify limitations encountered in a realistic implementation of advanced control techniques.

ACTIVE CONTROL LAWS

INVESTIGATE PERFORMANCE AND INTEGRATION OF PROJECTED ACTIVE CONTROL FUNCTIONS

- **COMMAND AUGUMENTATION SYSTEM**
- **BOUNDRY CONTROLLER (α -LIMITER)**
- **AUTOPILOT FUNCTIONS**
- **RIDE SMOOTHING SYSTEM/MANEUVER FLAPS**
- **LOW SAMPLE RATE EXPERIMENT**

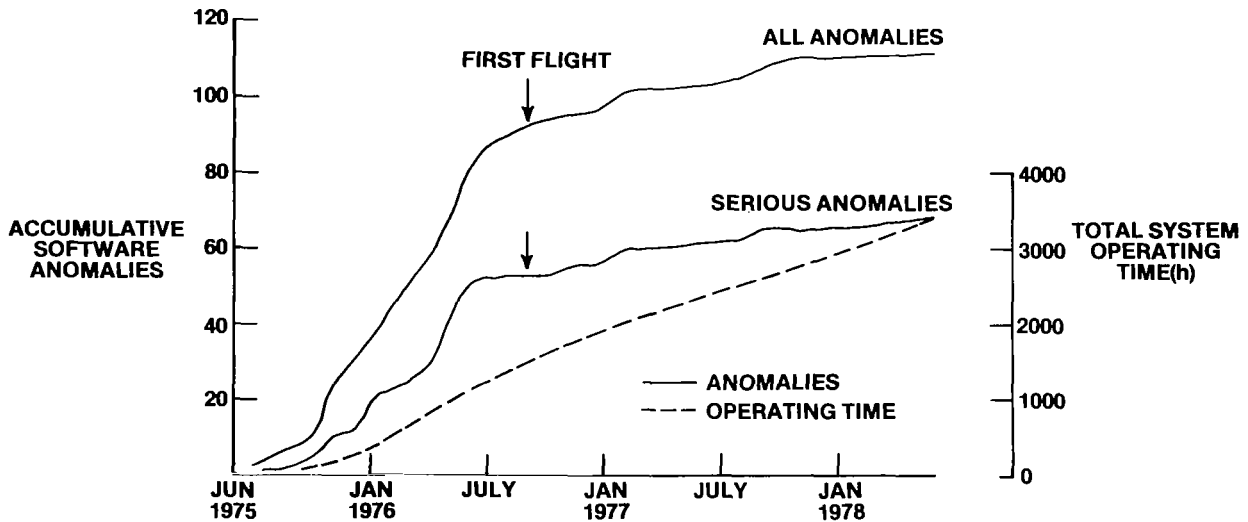
ADAPTIVE CONTROL LAWS

USE MODERN IDENTIFICATION THEORY TO ESTIMATE AIRCRAFT PARAMETERS FOR ADAPTIVE GAIN SCHEDULING

- **MAXIMUM LIKELIHOOD ESTIMATION**
- **ESTIMATE DYNAMIC PRESSURE, α**
- **IDENTIFICATION ALGORITHM ON GROUND COMPUTER**

SOFTWARE ANOMALY EXPERIENCE

Almost one year of verification testing was required before the system reached a level of maturity satisfactory for first flight. 1750 hours of system operating time were required during this period. Of significance is that even after extensive software verification testing, software anomalies occurred after the system was flight qualified, pointing to the fact that it is impossible to tell whether or not all latent software bugs have been identified and corrected.



SUMMARY OF DIGITAL SUBSYSTEM GROUND TEST EXPERIENCE

The amount of ground and verification testing required to bring the F-8/DFBW to a level of maturity was largely underestimated. Many problems requiring software changes and resultant verification were identified. The greatest number of changes occurred after initial integration of all subsystems. Many interrelating effects not identifiable in the early design phase were manifested, resulting in degraded operation.

Sufficient automated testing techniques were also lacking, especially those required to monitor and interrogate simultaneously operating redundant digital computers.

Overall system performance finally achieved, however, was excellent as validated by the flight test results.

- **COMPUTER REDUNDANCY MANAGEMENT EFFORT UNDERESTIMATED**
- **GROUND TEST TOOLS FOUND TO BE LACKING (MULTI-COMPUTER OPERATION)**
- **GENERIC COMPUTER HARDWARE PROBLEMS**
- **FAIL OP-FAIL SAFE OPERATION VERIFIED**
- **CONTROL LAW VERIFICATION ROUTINE ONCE BASIC OPERATIONAL ASPECTS OF SYSTEM MATURED**
- **NO EMI PROBLEMS**
- **NO STRUCTURAL MODE INTERACTIONS**
- **EXCELLENT SYSTEM PERFORMANCE ACHIEVED**

SMALL TRANSPORT AIRCRAFT TECHNOLOGY

Thomas L. Galloway
NASA Ames Research Center

ABSTRACT

The commuter airlines have experienced very high growth rates during the past two years. This strong growth is anticipated to continue as the U.S. air transportation system is reshaped by deregulation. The regulatory changes, coupled with the increasing market for commuter air travel have resulted in a strong demand for new, improved small transport aircraft and have significantly improved the opportunities for the application of advanced technology to the design of these aircraft.

This paper reviews NASA's recent and proposed research on Small Transport Aircraft Technology (STAT). The results of contracted studies identifying the potential benefits of advanced technology are presented. Current in-house studies and research efforts are discussed. An overview of the proposed technology elements in STAT research is presented.

SMALL TRANSPORT AIRCRAFT TECHNOLOGY

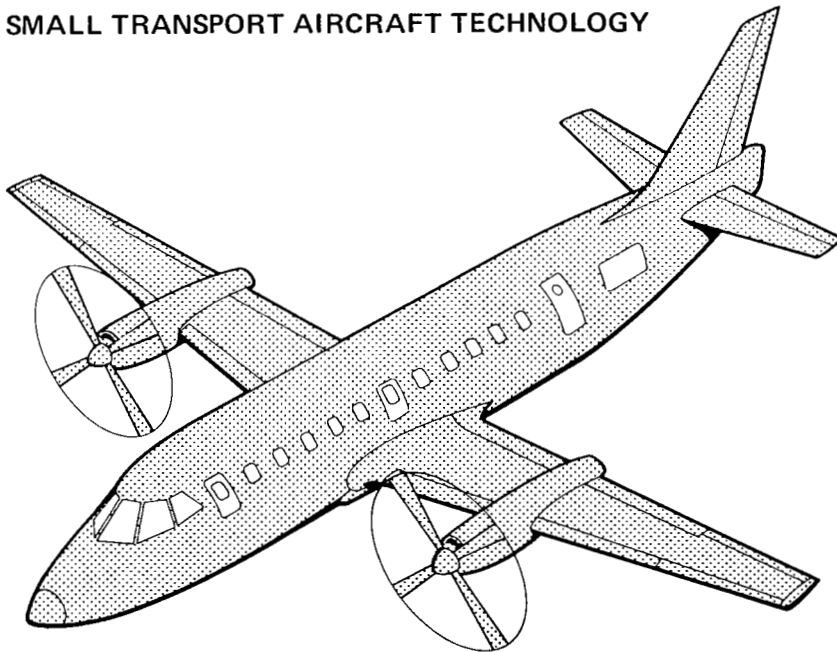


Figure 1 shows the growth in U.S. commercial air transport service dating from the Ford Tri-motor era, with the introduction dates of some of the more significant transport aircraft. The Civil Aeronautics Board (CAB) has been instrumental in the classification of carriers. The Civil Aeronautics Act of 1938 granted certificates to the carriers in operation at that time which formed the cadre of trunk airlines. As the trunk airlines grew, they obtained larger aircraft and reduced service to smaller communities. In response, the CAB instituted the "local-service" airlines experiment in 1944 to provide better air service to the smaller communities. Following the pattern of the trunk airlines, the local-service airlines expanded and upgraded their fleet to larger jet-powered aircraft. Again because these larger aircraft are inefficient for short-haul, low density air service, a number of the smaller communities were faced with a loss of air service. In 1969 the CAB established the "Commuter Carriers" classification for operations with aircraft of less than 5674 kg (12,500 lb) gross weight. Whereas local-service carriers were able to start service in the 1940's with aircraft the same size as the trunk airlines (the DC-3's), commuter airlines were restricted to the 12,500 lb takeoff weight limit. In late 1972, the CAB restriction on commuters was revised to allow up to 30 passengers or 3404 kg (7500 lb) payloads. The "Airline Deregulation Act of 1978" and subsequent rulings have raised the limitations on commuter air carriers up to 60 passengers or 8170 kg (18,000 lb) maximum payload. Rising fuel costs and deregulation have resulted in trunk and local service carriers continuing to abandon the lower density, short-haul routes.

HISTORY OF U.S. COMMERCIAL AIR TRANSPORTATION

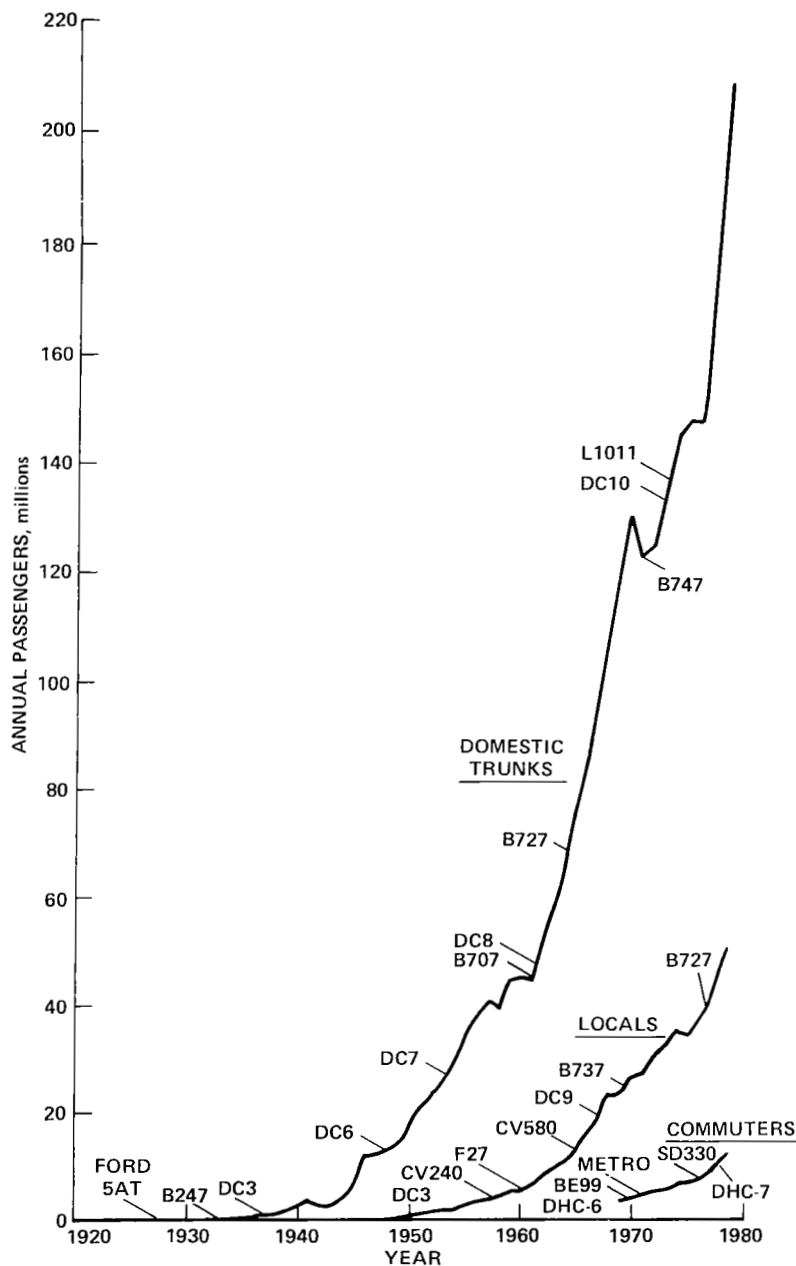


Figure 1

The U.S. trunk airlines have now transitioned completely to jet powered transport aircraft and three-fourths of the local service airlines fleet is jet powered. Unfortunately, jet transport aircraft are less energy efficient for short flights than longer flights where the speed and altitude capability of the jet engine can be used more effectively. The reduced fuel efficiency of jet transport aircraft for short-haul service was tolerable at cheap fuel prices. However, from 1973 to 1979 the average price of jet fuel for the U.S. trunk airlines has increased (figure 2) from 3.4 cents/liter (13 cents/gal) to over 18.5 cents/liter (70 cents/gal). In 1973, fuel accounted for about 25% of the direct operating cost for a B727-200 aircraft. By 1979 this percentage had risen to over 50% of the direct operating cost.

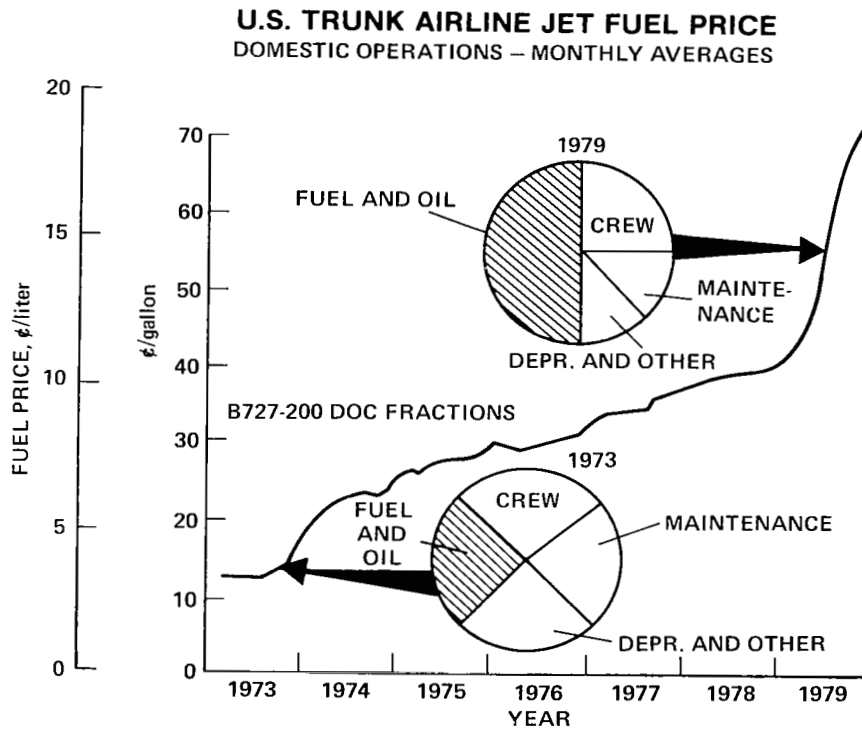


Figure 2

The effect of fuel cost on the trunk airline direct operating cost elements is shown historically in figure 3 (reference 1). The influence of fuel price and its dominance since 1973 over the other direct operating cost elements is clearly evident. Because fuel costs are expected to continue to dominate aircraft operating cost, increasing aircraft fuel efficiency has become the major new transport aircraft design objective.

INFLUENCE OF FUEL PRICES
DIRECT OPERATING COST ELEMENTS

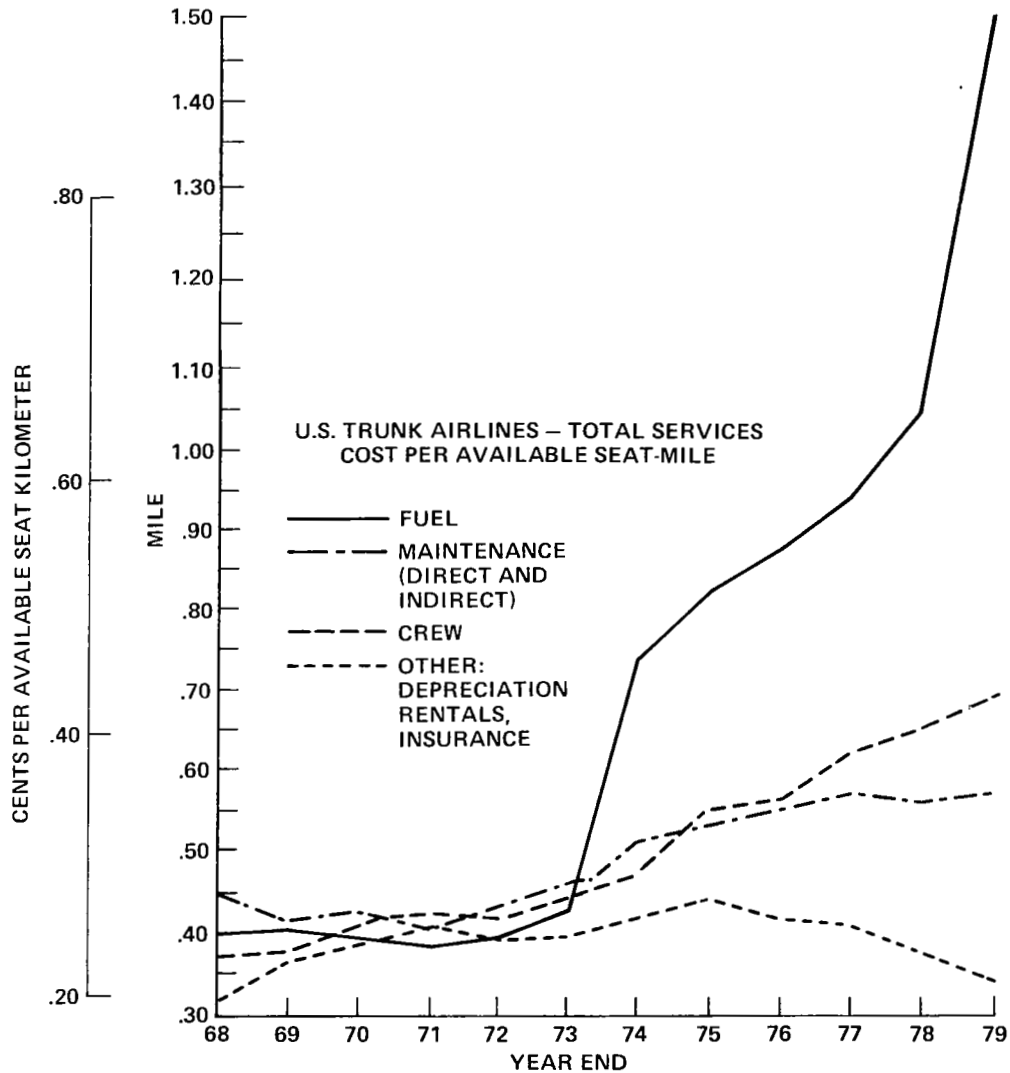


Figure 3

The Airline Deregulation Act of 1978, bringing with it easier market entry and exit provisions, along with the sky-rocketing fuel costs, have resulted in trunk and local service airlines improving their operating efficiency by moving their jet transport aircraft to the longer, high density routes where they are more efficient. This transition is most noticeable by the increase in average stage length (figure 4, from Reference 2) since deregulation. This transition has resulted in the smaller communities being faced with more reductions in service by the carriers using the larger jet powered transports.

AVERAGE STAGE LENGTH
 U.S. TRUNK AND LOCAL SERVICE CARRIERS
 OCTOBER 1975-1979

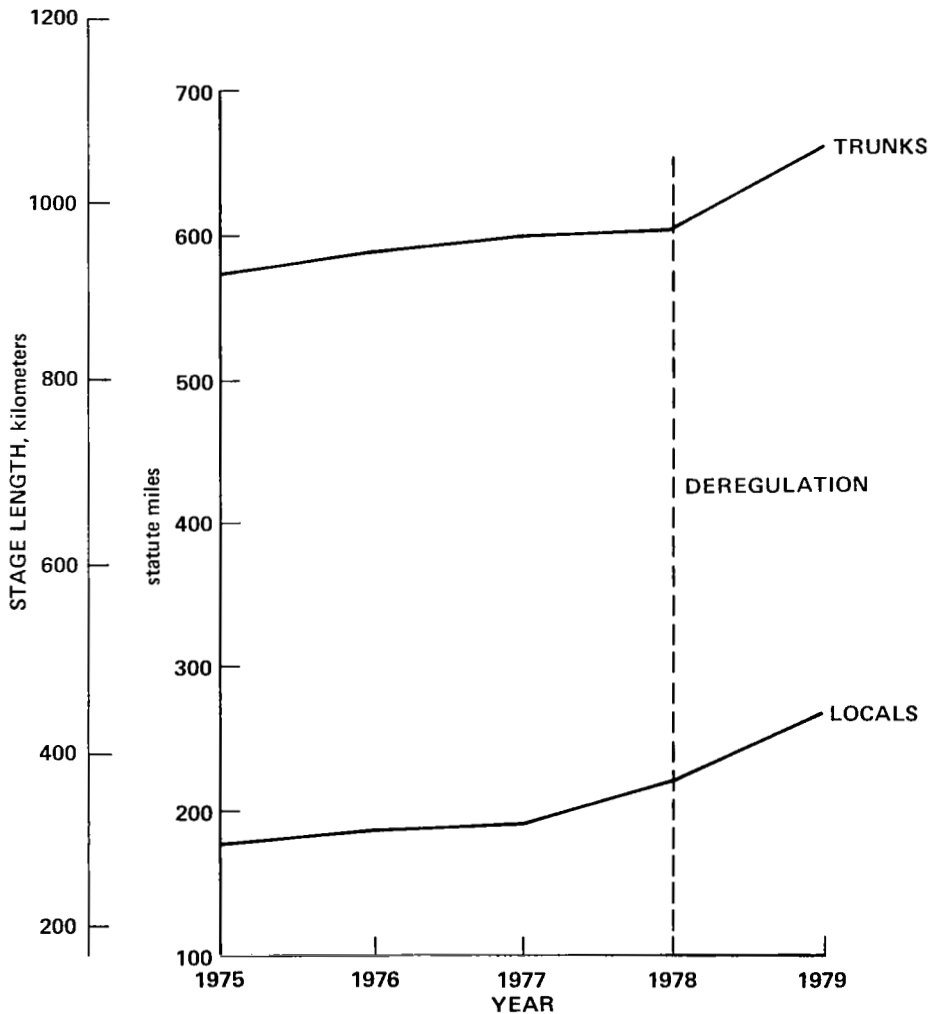
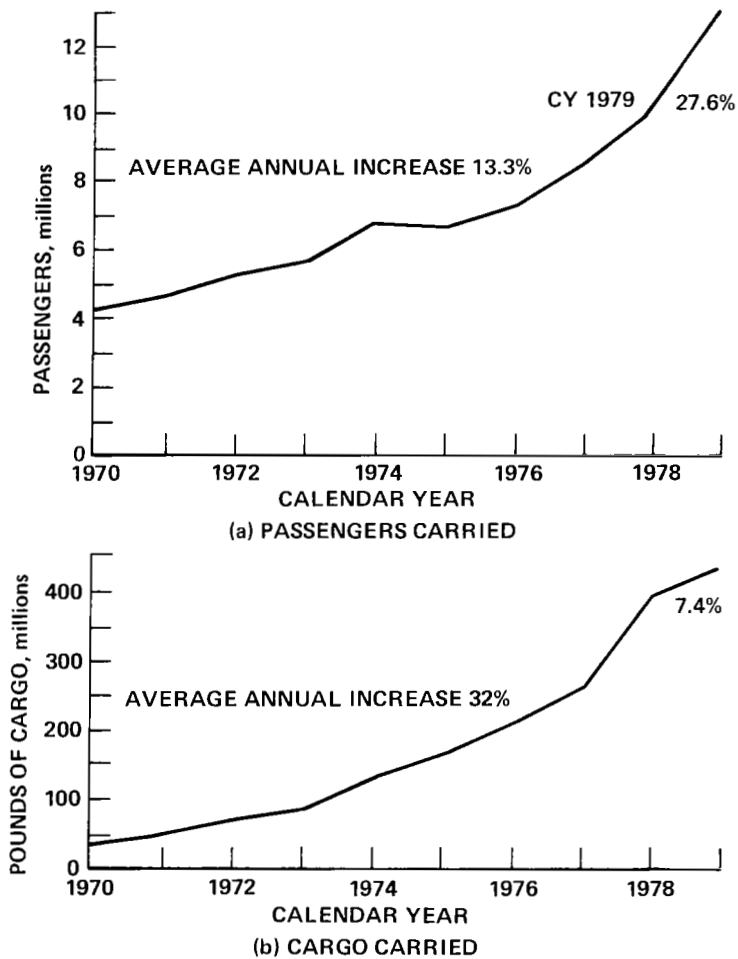


Figure 4

The U.S. commuter airlines have expanded their operations in order to provide service on the short-haul lower density routes abandoned by the trunk and local service airlines. The resulting rapid growth in commuter airline service (Figure 5) has made them the fastest growing segment of air transportation. In 1979, commuter airline activity increased by 27.6% in passengers carried and 7.4% in cargo. The transition to commuter airlines and smaller commuter aircraft for short-haul air transportation is evident at most airports. The dramatic expansion in short-haul service with turboprop-powered commuter aircraft represents a remarkable change in the last few years, particularly since these aircraft are so different from the larger jet transports to which the public has become accustomed.

**COMMUTER AIRLINE GROWTH
DECEMBER 1970 TO 1979***



*1979 VALUES INCLUDE CARRIERS THAT WERE COMMUTERS IN 1978 AND OBTAINED CERTIFICATES IN 1979

Figure 5

The current turboprop powered commuter aircraft, although representing older technology and some sacrifices in passenger comfort, use 15 to 25% less fuel per seat mile at short stage lengths than the larger jet transports they are replacing. This efficiency improvement coupled with the smaller aircraft ability to provide a better match with passenger demand results in a significant overall system efficiency improvement. In recognition of the expanding role of the U.S. commuter airlines, several manufacturers have initiated the development of new, improved commuter transport aircraft. One of the most recently announced new aircraft development is the Fairchild/Saab-Scania 30-34 passenger aircraft shown in Figure 6. Scheduled for introduction into service in 1984, this aircraft will incorporate the best current technology available and will be powered by the General Electric CT7-5 turbo-prop engine.

FAIRCHILD/SAAB-SCANIA 30 PASSENGER COMMUTER AIRCRAFT

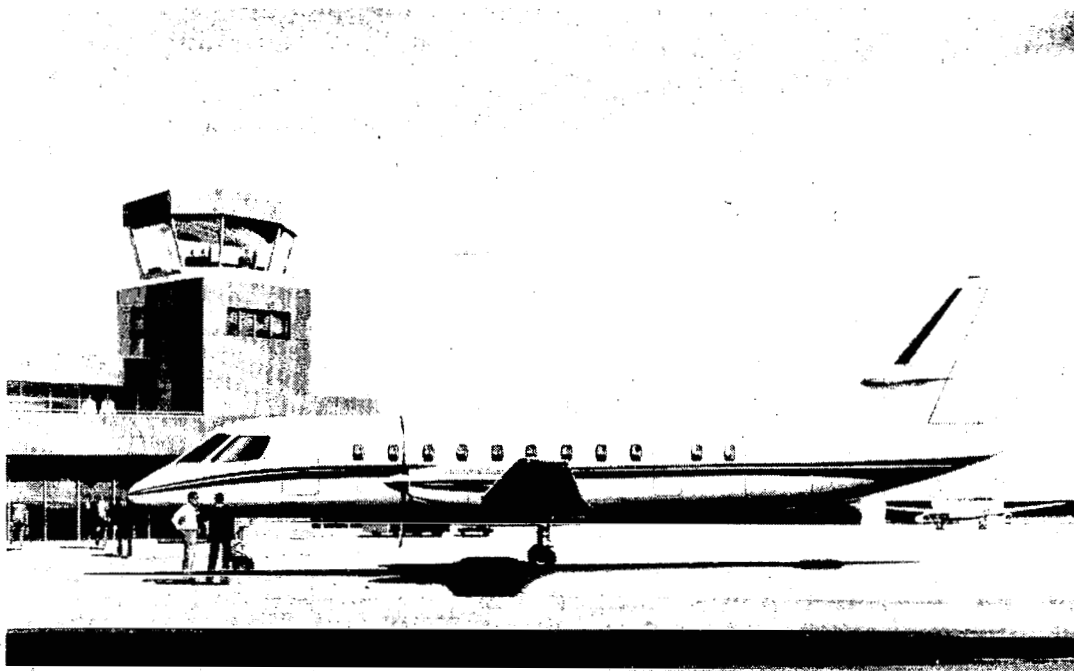


Figure 6

In order to develop the advanced technology that can be applied to future small transport aircraft, focused research and technology efforts are required. NASA has initiated a Small Transport Aircraft Technology (STAT) aeronautics research activity to provide this focus. Figure 7 depicts the elements of this activity to enhance the development of significantly improved small short-haul transport aircraft. Technologies that can improve public acceptance and operational economies are important research areas.

SMALL TRANSPORT AIRCRAFT TECHNOLOGY (STAT)

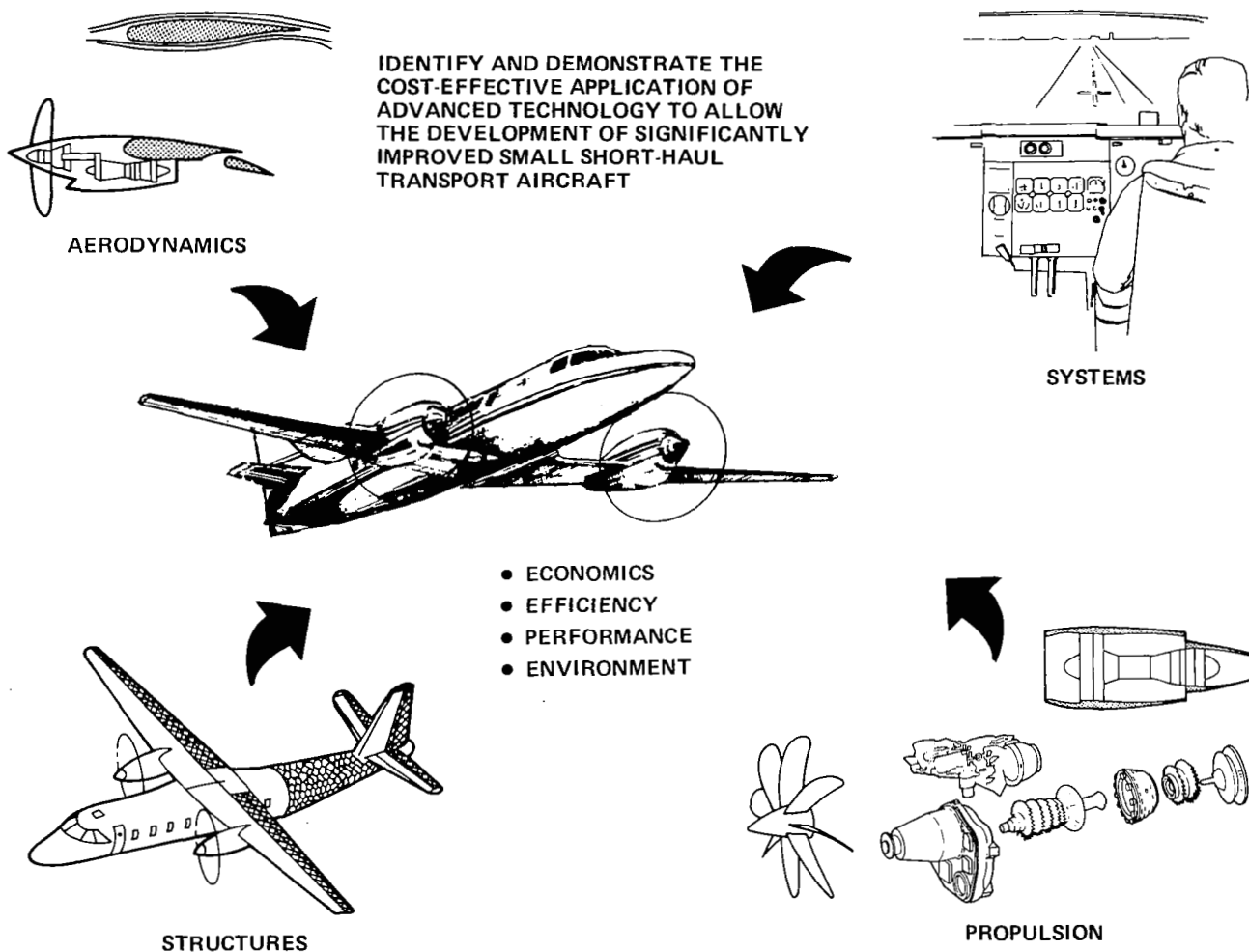
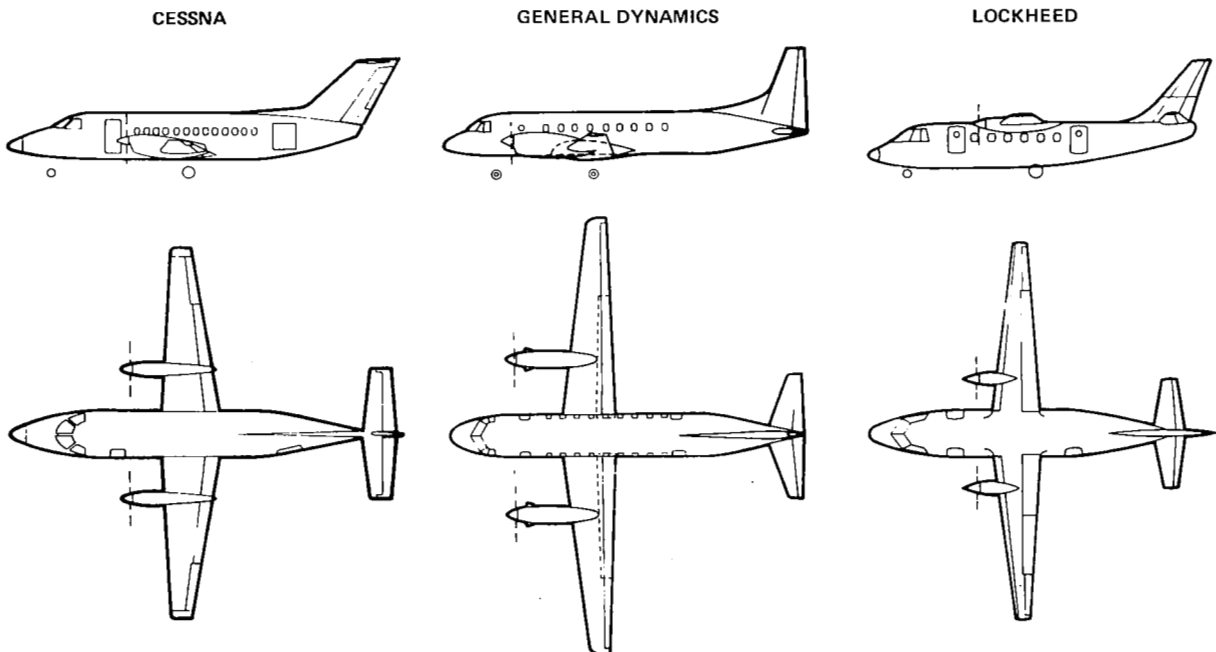


Figure 7

To assist in formulating the STAT research activity, a broad range of advanced technology application studies have been initiated with airframe, engine, and propeller manufacturers. Recently completed studies by Cessna (unpublished), General Dynamics-Convair (Reference 3), and Lockheed-California Company (Reference 4) investigated small transport aircraft designs with 19, 30, and 50 seat capacity. Initially, current technology baseline designs were established for use as a reference against which the benefits of advanced technology could be measured. Figure 8 shows the general arrangement of each manufacturer's 30 passenger baseline. Cessna's design has stand-up headroom, a cruise speed of Mach 0.456 (250 KIAS), Citation business jet airframe technology, Pratt & Whitney of Canada PT6 turboprop engine technology, and has been optimized to minimize direct operating cost (DOC) for fuel at \$1.00 per gallon. However, the design did not consider meeting the jet transport interior noise goals of the specification. Cessna also studied a 19 passenger configuration. General Dynamics-Convair designed 30 and 50 passenger current-technology baseline aircraft similar to Cessna's except for the addition of acoustical cabin wall treatment to achieve the interior cabin noise goal of 85 overall sound pressure level, typical of current jet transports. The acoustical treatment weight was estimated to be 1044 kg (2300 lb) for the Convair 30 passenger design of Figure 8. Lockheed-California chose higher design cruise speeds of Mach 0.6 and 0.7 for their 30 and 50 passenger aircraft respectively.

BASELINE AIRCRAFT CONFIGURATIONS

30 PASSENGERS 1219 m (4000 ft) FIELD LENGTH

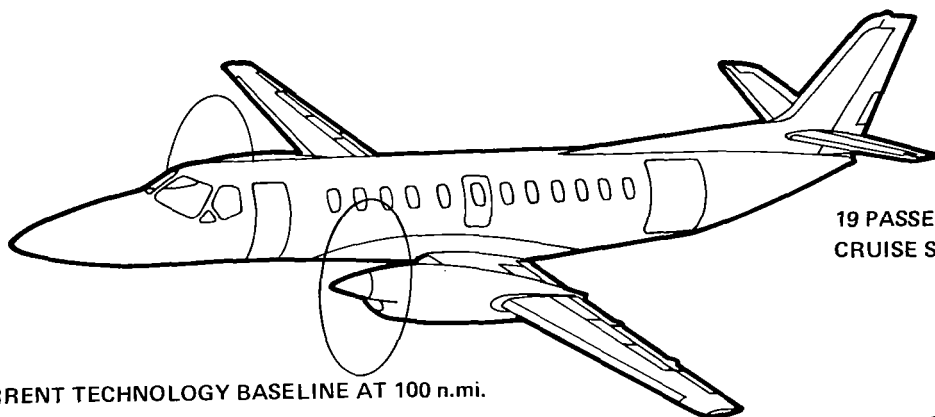


	CESSNA	GENERAL DYNAMICS	LOCKHEED
GROSS WEIGHT, kg (lb)	10982 (24210)	13427 (29600)	12976 (28606)
POWER/ENG., kW (hp)	1439 (1930)	1747 (2343)	1792 (2403)
PROPELLER diam, m (ft)	3.05 (10.0)	3.50 (11.5)	3.23 (10.6)
DESIGN MACH NO.	0.456	0.456	0.600
DESIGN CRUISE ALT., m (ft)	3048 (10000)	3048 (10000)	8534 (28000)
DESIGN RANGE, km (n.mi.)	1112 (600)	1112 (600)	1112 (600)
DOC @ 100 n.mi., \$/Skm (#/Sn.mi.)	5.66 (10.48)	5.64 (10.45)	5.37 (9.95)

Figure 8

Figure 9 shows the improvement in fuel usage and direct operating cost for Cessna's 19 and 30 passenger advanced technology designs. The utilization of bonding along with the use of composites in secondary structural components had the major impact on improving aircraft weight, cost and operating economics. The major improvements resulting from advances in propeller, engine and aerodynamic technology were in fuel usage followed by significant savings in direct operating cost. Combining all the technologies resulted in advanced technology aircraft designs that used 38 to 40% less fuel on a 100 n.mi. trip compared with the current technology baseline. These improvements resulted in a 21% reduction in direct operating cost on the 100 n.mi. trip. The general arrangement of Cessna's advanced designs are the same as their baseline configurations. As such, the 2 abreast 19 passenger design does not offer the passenger comfort levels of the 3 abreast 30 passenger design.

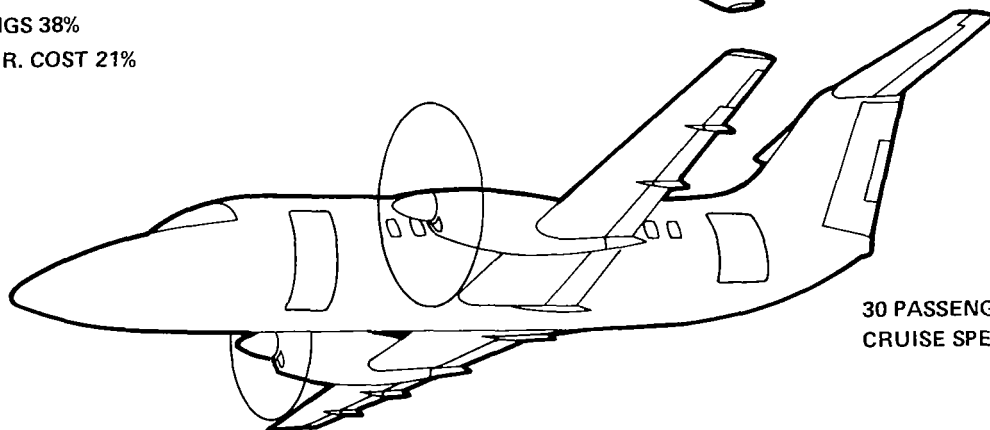
**ADVANCED TECHNOLOGY SMALL TRANSPORT
AIRCRAFT DESIGN
CESSNA AIRCRAFT**



**19 PASSENGER
CRUISE SPEED = 0.5 MACH**

RELATIVE TO CURRENT TECHNOLOGY BASELINE AT 100 n.mi.

FUEL SAVINGS 38%
DIRECT OPER. COST 21%



**30 PASSENGER
CRUISE SPEED = 0.5 MACH**

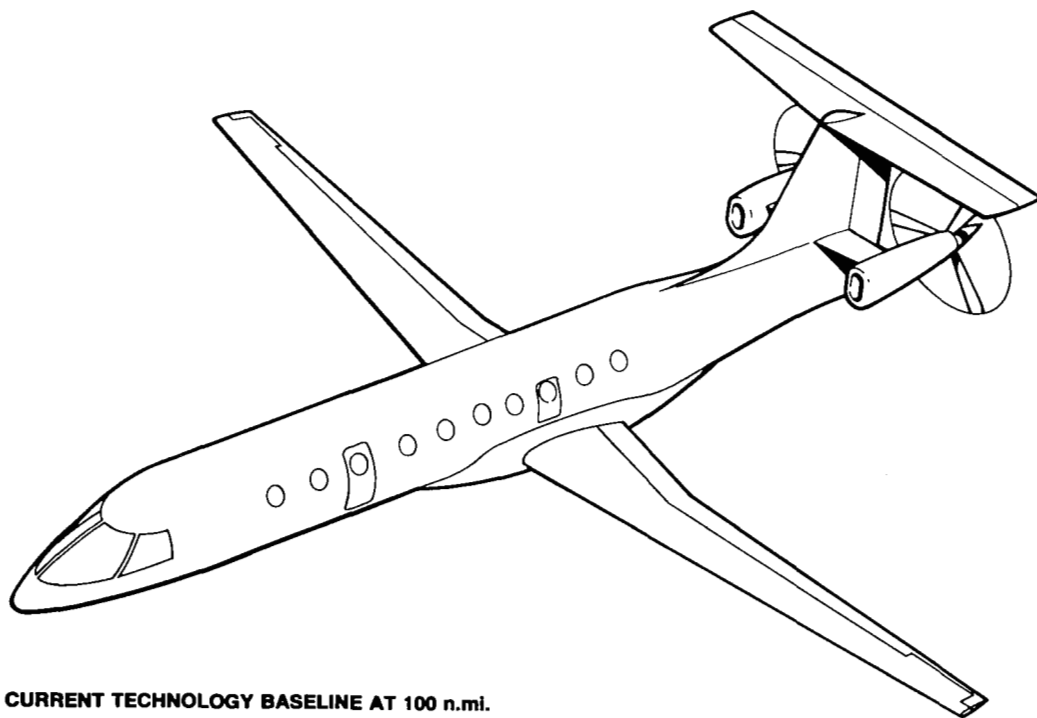
RELATIVE TO CURRENT TECHNOLOGY BASELINE AT 100 n.mi.

FUEL SAVINGS 40%
DIRECT OPER. COST 21%

Figure 9

In the Convair study, advanced technologies in aerodynamics, structures, systems, and propulsion were applied individually and those with the greatest payoff were incorporated in a combined advanced technology design. All the Convair aircraft were designed for cruise speed of 250 knots indicated airspeed. The advanced 30 passenger short-haul aircraft design (Figure 10) incorporates a new high-lift wing design using low-drag airfoils, composite structure, active controls, and improved propeller/engine technology. Compared with the current technology baseline, the Convair advanced technology 30 passenger aircraft is 22% lighter in gross weight, has 51% less wing area, requires 37% less power, and uses 31% less fuel on a 100 n. mi. trip. These improvements result in a 24% reduction in direct operating cost for a 100 n.mi. trip with fuel at 26¢/liter (\$1/gal). The advanced technology configuration has the engine mounted on pylons at the back of the fuselage. Because a major design goal is to provide a low cabin interior noise level equal to what the passenger is used to in large jet transports, the aft location avoids the large fuselage acoustic treatment penalties that are required for a configuration with wing mounted engines. The aft fuselage location also reduces engine-out lateral control requirements, provides much of the desired longitudinal static stability, improves the wing efficiency by removing the engine nacelle from the wing, and places the propeller and engine in an improved position to be idled safely and avoid damage from aircraft servicing equipment at the terminal.

**ADVANCED TECHNOLOGY
SMALL TRANSPORT AIRCRAFT DESIGN
GENERAL DYNAMICS — CONVAIR**



RELATIVE TO CURRENT TECHNOLOGY BASELINE AT 100 n.mi.

FUEL SAVINGS 31%

DIRECT OPERATING COST SAVINGS AT \$1/gallon 24%

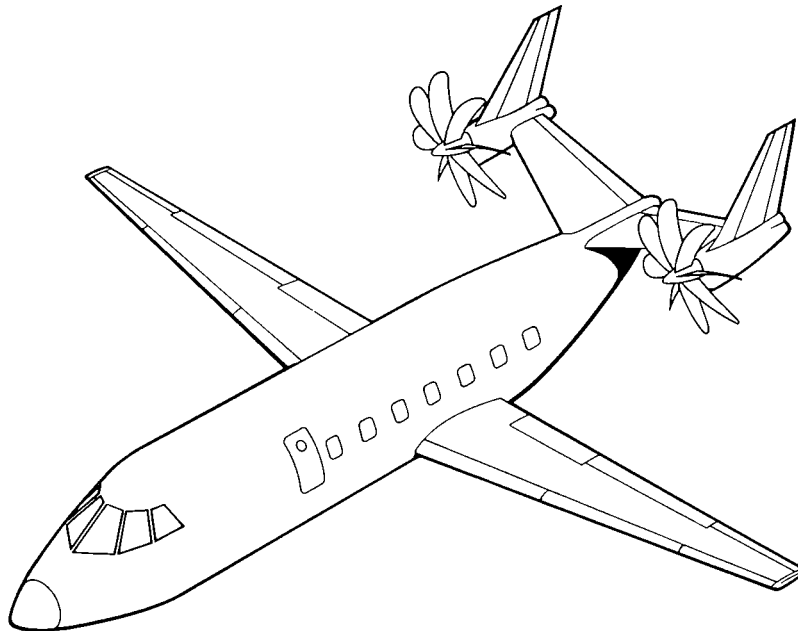
**30 PASSENGER
CRUISE SPEED = 0.5 MACH**

Figure 10

In the Lockheed-California study a major emphasis was placed on reducing airframe manufacturing costs. Alternative fuselage and wing structural concepts were investigated using both aluminum and composite materials compared to the skin-stringer aluminum structure of the baseline design. Lockheed's orthogrid or isogrid composite structural concept utilizing laminated bars built up of alternating layers of syntactic resin and high-strength fibers appears very attractive. Prepregged graphite and syntactic resin tape can be obtained in combined form so that both layers can be wound together on automatic machines. This manufacturing technology gives the structural designer considerable flexibility in choosing grid size and pattern to meet specific load distribution and fail-safe requirements. Since the resulting stiffened skin is very stable, much of the substructure normally required for stiffness is minimized. This saves both parts and labor. For a 30 passenger design this concept resulted in a 25% structural cost savings relative to conventional aluminum skin-stringer design practice. One of the most promising advanced technology designs resulting from this study (Figure 11) incorporates an improved high-lift, low drag wing design, composite structures, active controls and propulsion system improvements. This design also has aft mounted engines—for the same reasons as the Convair 30 passenger aircraft design. The Lockheed advanced technology 30 passenger aircraft design uses 26% less fuel on a 100 n.mi. trip and has a 16% reduction in DOC over their current technology baseline.

**ADVANCED TECHNOLOGY SMALL TRANSPORT
AIRCRAFT DESIGN**

LOCKHEED - CALIFORNIA COMPANY



RELATIVE TO CURRENT TECHNOLOGY BASELINE AT 100 n.mi.
FUEL SAVINGS 26%
DIRECT OPERATING COST SAVINGS 16%

30 PASSENGER
CRUISE SPEED = 0.6 MACH

Figure 11

General Electric, Garrett AiResearch, and Detroit Diesel Allison are investigating advanced engine technologies for engines in the 1000 to 5000 horsepower class for NASA's Lewis Research Center. Since these studies started well after the airframe studies, NASA utilized their in-house aircraft synthesis capability with airframe manufacture inputs to design optimized baseline aircraft. These aircraft were optimized around current technology engine cycles furnished by the engine companies and scaled to meet common aircraft design requirements. Figure 12 presents an example for cruise speed selection for the three different engine cycles representing different types of compressors and a range of turbine inlet temperature (TIT). Each contractor is now investigating engine cycle characteristics and component technologies that can increase engine life, improve fuel efficiency, and lower maintenance cost for this class of engine. Some of the advanced technologies being investigated for larger engines as part of NASA's ACEE program may be utilized. These studies will be completed in the next couple of months.

ENGINE INFLUENCE ON CRUISE MACH NUMBER SELECTION

50 PASSENGER 1219 m (4000 ft) FIELD LENGTH

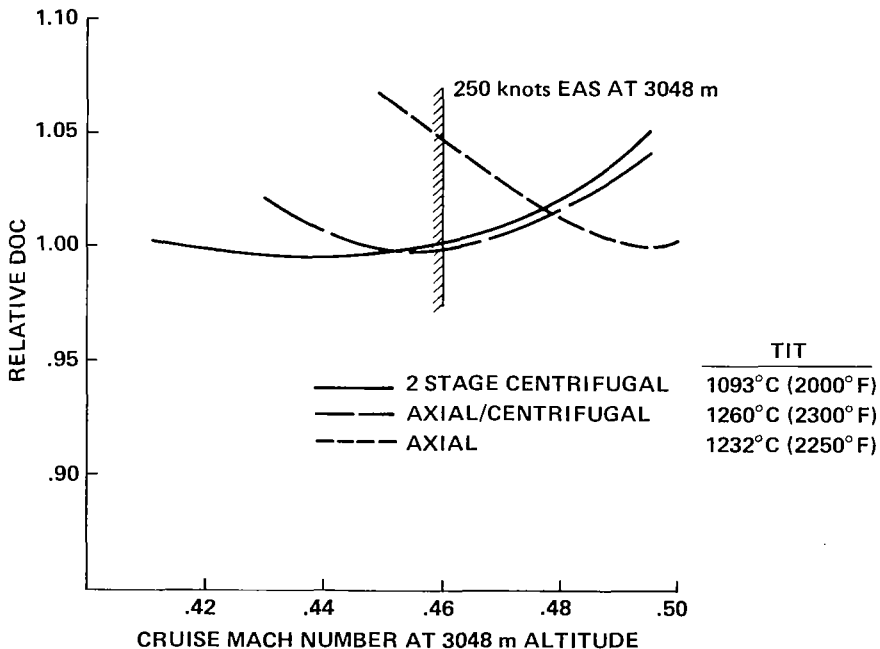


Figure 12

Potential improvements in small transport aircraft propellers are being studied by United Technologies--Hamilton Standard Division and Cessna's McCauley Accessory Division. To compliment these studies, NASA has performed various trade-off studies to investigate the influence of noise goals, field length requirements and cruise speed capability on propeller selection. Figure 13 shows the influence of number of blades on some selected performance criteria and acoustical treatment weight requirements for 30 and 50 passenger configurations. The magnitude of weight to meet the 85 dB overall sound pressure level goal is about the same for both sizes. However, it represents 3-5.5% of the 30 passenger gross weight compared to 2 - 4% of the 50 passenger gross weight. The power is determined by the 1219 meter (4000 ft.) field length requirement for 3 and 4 blades, and the 250 knot indicated cruise airspeed for the 6 blade case. The 5 blade case is an equal match. In terms of minimum direct operating cost, the 30 passenger design shows a definite optimum with 5 blades while the 50 passenger is about the same for 4, 5, or 6 blades.

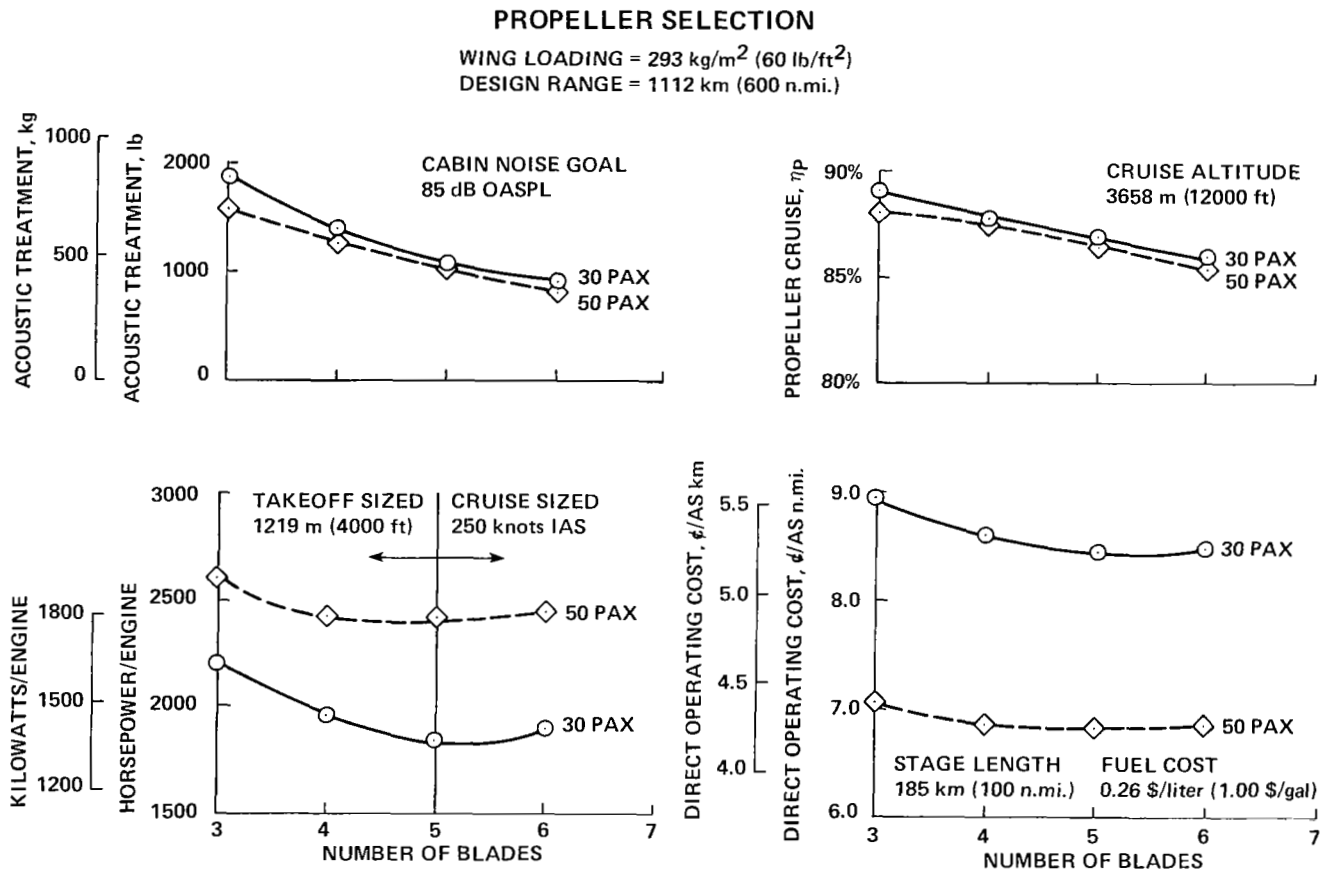


Figure 13

In addition to the broad technology studies for small transport aircraft, NASA is also considering needs that may be met by results from on-going research efforts. Aerodynamic research on natural laminar flow airfoils and low-speed lift to drag improvements are examples. Figure 14 shows one of NASA-Ames most promising advanced natural laminar flow airfoils compared to the older NACA 65A laminar flow airfoil, along with analytically predicted pressure distributions and drag. The advanced airfoil design has a blunter nose, and its maximum thickness occurs farther aft than for the NACA 65A airfoil. The pressure distribution is shown for a Mach number of 0.65 and a lift coefficient of 0.588, which corresponds to the design point for the advanced airfoil. The drag comparison was determined from a viscous-flow computational code that accounted for boundary-layer growth. Transition was assumed to occur at the point where the upper-surface pressure gradient became unfavorable on the respective airfoils. The reduction in drag is about 28%. Recent boundary layer stability analysis by Lockheed-Georgia has indicated a stable boundary layer to 59% chord on the upper surface and 41% chord on the lower surface at the design Mach number and lift coefficient.

NATURAL LAMINAR FLOW AIRFOIL DESIGN

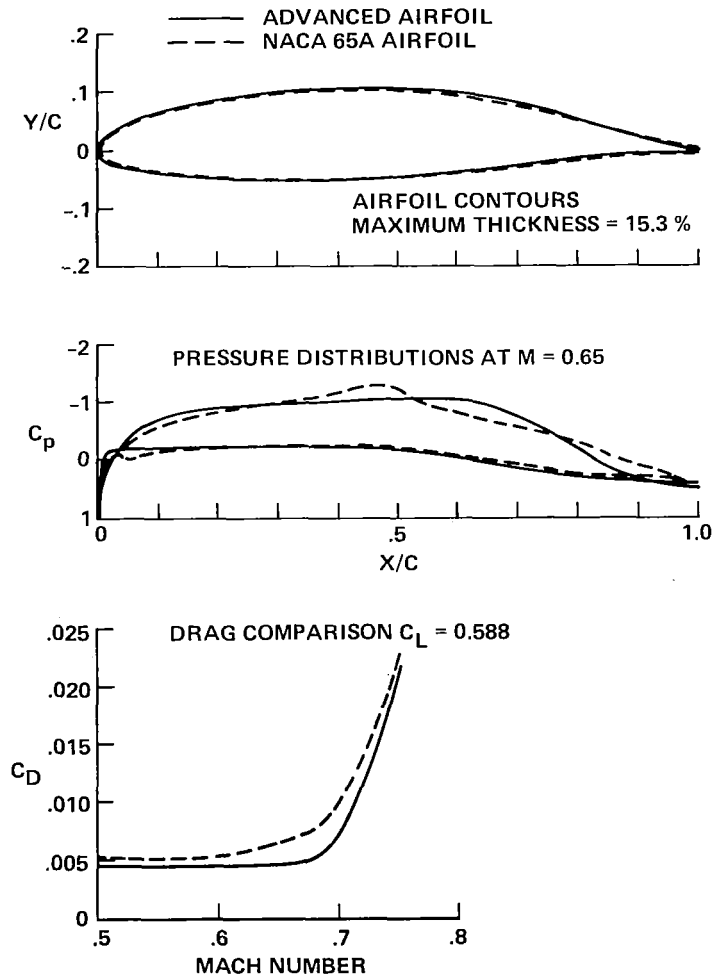


Figure 14

In order to validate the natural laminar flow airfoil design concept, utilizing practical manufacturing techniques, a large-scale, 1.27 meter (50 inch) chord, two-dimensional airfoil test is planned in the Ames 12-foot pressure wind tunnel. By using the bonded aluminum honeycomb structural concept, an airfoil can be constructed with a practical manufacturing technique that will maintain its shape and have a smooth rivet-free surface. Figure 15 shows an example of such a section built by the Boeing Commercial Airplane Co. (Reference 5). In connection with this airfoil research, a report (Reference 6) summarizing experience with natural laminar flow and the potential for resilient leading edges to reduce insect contamination was published in May 1979. Other concepts to protect the leading edge from contamination so that laminar flow can be maintained will also be evaluated. Some of these concepts have been investigated in NASA's ACEE program as part of the laminar flow control research.

SAMPLE BONDED ALUMINUM HONEYCOMB CONSTRUCTION

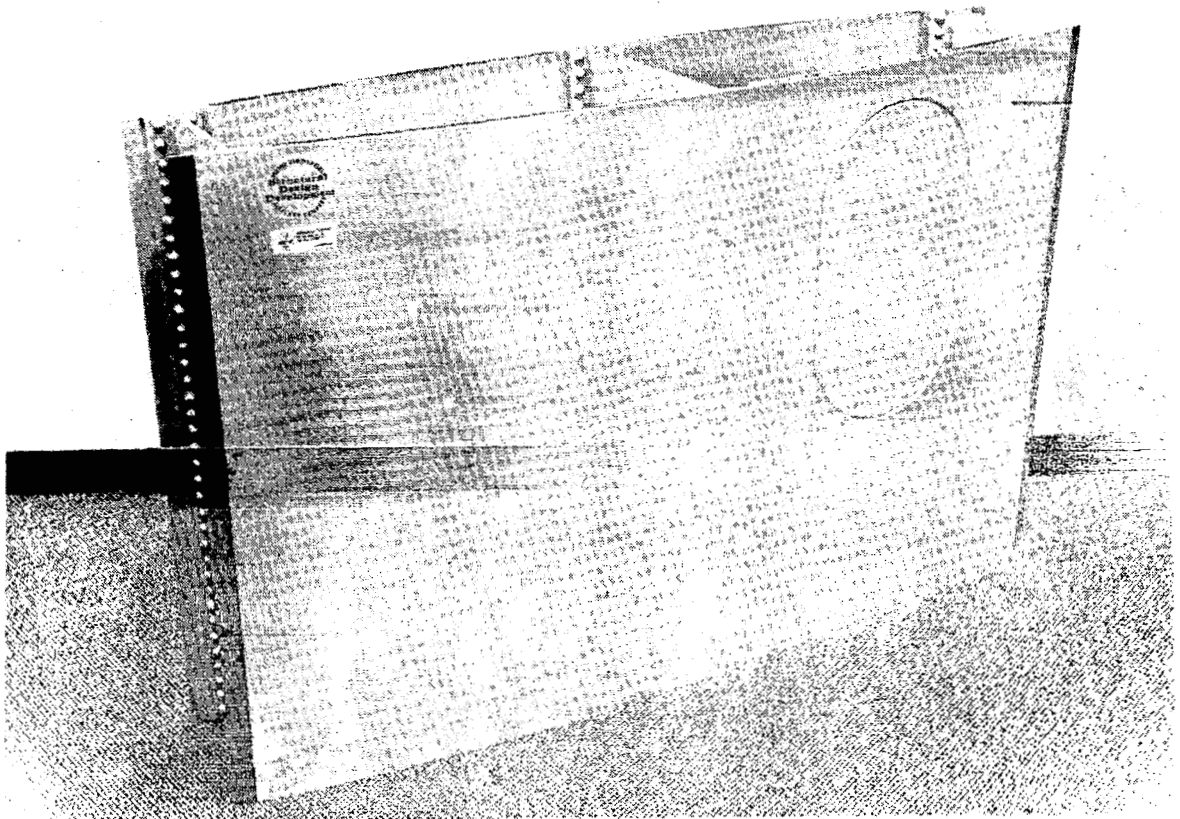


Figure 15

To establish an aerodynamic data base representative of current technology, unpowered and powered small transport aircraft wind tunnel tests of a 15%-scale model of the Swearingen Metro transport are being conducted by NASA-Ames under a cooperative research agreement with Swearingen Aviation Corporation. The first series of unpowered tests were completed in the Ames 12-foot pressure wind tunnel in June of 1980. These tests consisted of aircraft component drag build-up; low, mid, and high nacelle locations on the wing; modified wing leading edges; and an alternate flap design. A limited amount of wing flow visualization and pressure distributions (using pressure belts) was obtained with the engine nacelles on and off the wing. Figure 16 illustrates the aircraft drag build-up configurations and their contributions to total model drag. The body and wing have almost equal drag contributions, about 120 counts. The tail assembly added 48 counts and the nacelle contribution was mainly at the higher lift coefficients. When the landing gear was extended with the gear doors open, this added 548 counts of drag for the flaps up configuration.

DRAG BUILDUP

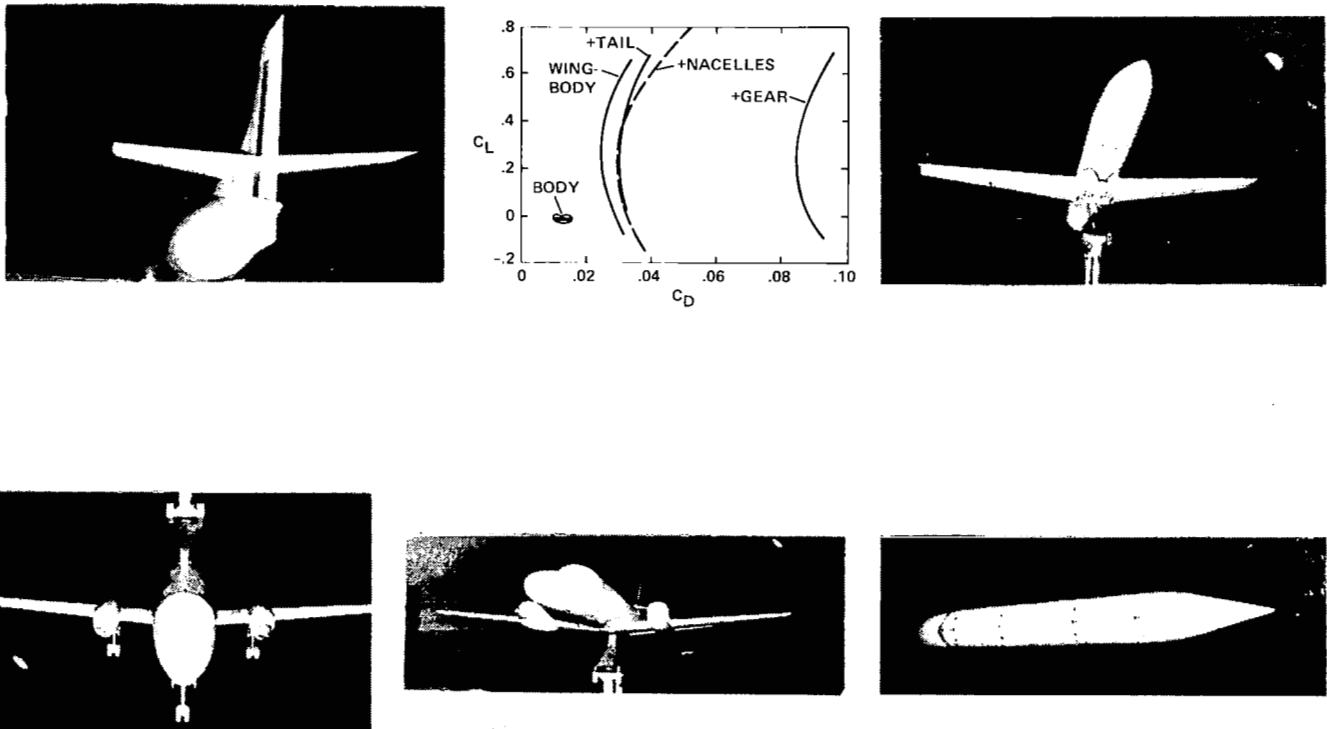


Figure 16

During the testing of the basic Swearingen Metro configuration alternate engine nacelle locations were investigated for general research interest. Figure 17 shows the influence of the nacelle location on the maximum lift coefficient of the model. All nacelles had the same general shape except for the aft fairing. The low nacelle showed the least degradation in maximum lift compared to the clean wing. However, for a low wing configuration, the mid-nacelle location offers a more practical compromise for other design considerations.

NACELLE LOCATION

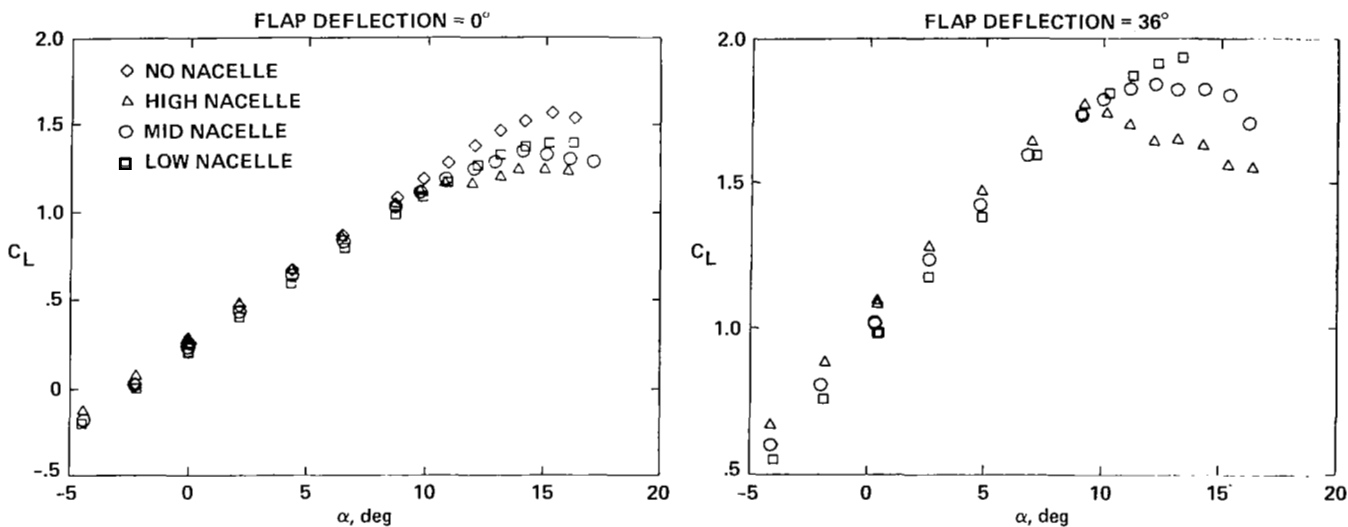
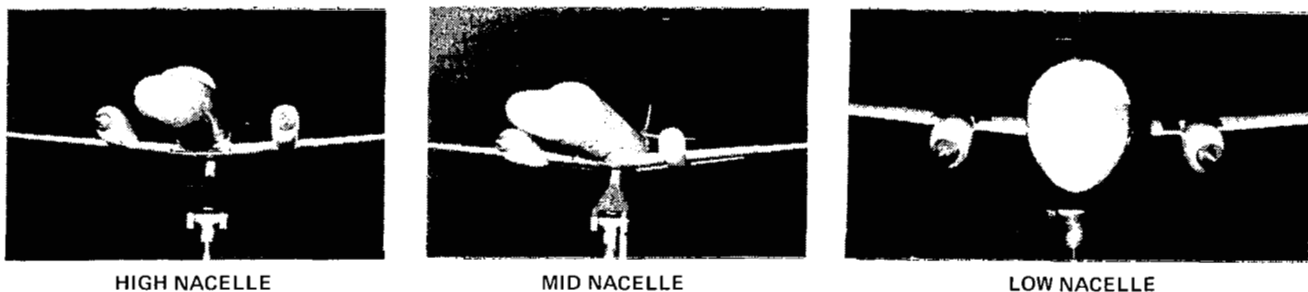


Figure 17

The STAT technology elements are along disciplines similar to the large aircraft technologies of the ACEE program. The short stage length and lower altitude operations, however, result in different design considerations. In aerodynamics, climb performance is as important as cruise performance. Turbo-prop installation aerodynamics and propeller efficiency are major propulsion system considerations. The small size of engine components results in different engine design limitations. In structure, minimum gage requirements mean different tradeoffs in composite utilization. Active control systems and icing protection can enhance ride quality and safety in the low altitude operating environment. Unconventional configurations such as aftmounted turboprops, lifting tails, or canards may offer significant benefits.

Recent studies have indicated advanced technology can offer aircraft with passenger space and comfort levels comparable to the larger jet transports with significant improvements in economics. Estimates in direct operating cost savings ranged from 16 to 24 percent with initial aircraft costs reduced from 5 to 18%. Fuel savings range from 26 to 40 percent.

IMPORTANT TECHNOLOGY ELEMENTS

AERODYNAMICS	PROPULSION	STRUCTURES	SYSTEMS
LOW DRAG AIRFOILS	PROPELLERS	COMPOSITES	ACTIVE CONTROLS
HIGH-LIFT DEVICES	ENGINE COMPONENTS	BONDING	ICING PROTECTION
ENGINE/AIRFRAME INTEGRATION	CONFIGURATION		CONFIGURATION

TECHNOLOGY BENEFITS

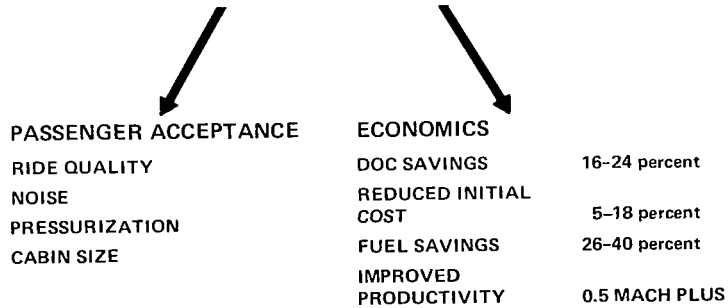


Figure 18

REFERENCES

1. Spencer, Frank A.: Factors Affecting the Retirement of Commercial Transport Jet Aircraft, NASA CR-152308, August 1979.
2. Schlansky, Mark H.: Restructuring of the Airline Industry Under Deregulation: The Domestic Route Network. Presentation to the 59th Annual Meeting of the Transportation Research Board Committee on Aviation Demand Forecasting, Washington, D.C., January 1980.
3. Adcock, C.; Coverston, C.; and Knapton, B.: Application of Advanced Technologies to Small, Short-Haul Air Transports. NASA CR-152364, 1980.
4. Coussens, T. G.; and Tullis, R. H.: Application of Advanced Technologies to Small, Short-Haul Transport Aircraft. NASA CR-152363, 1980.
5. Andrews, D. G.; Brubaker, P. W.; Bryant, S. L.; Clay, C. W.; Giridharadas, B.; Hamamota, M.; Kelly, T. J.; Proctor, D. K.; Myron, C. E.; and Sullivan, R. L.: Application of Advanced Technologies to Small, Short-Haul Aircraft. NASA CR-152089, 1978.
6. Carmichael, B. H.: Summary of Past Experience in Natural Laminar Flow and Experimental Program for Resilient Leading Edge. NASA CR-152276, 1979.

STATUS REPORT ON AN INVESTIGATION OF POWERED NACELLES ON A
HIGH ASPECT RATIO NASA SUPERCRITICAL WING - PHASE II

Stuart G. Flechner, James C. Patterson, Jr., and Paul G. Fournier
NASA Langley Research Center

ABSTRACT

This is a status report on Phase II of an investigation of powered nacelles on a high aspect ratio NASA supercritical wing. Several separate flow and mixed flow nacelles were tested to determine the effect of nacelle and pylon cant angle variations and longitudinal and vertical position variations. Results are presented for the cruise condition: 0.82 Mach number and 0.55 lift coefficient.

INTRODUCTION

This is a status report on Phase II of the Langley propulsion/airframe integration investigation where several powered nacelles were installed on a proposed energy efficient transport having a high aspect ratio NASA supercritical wing and tested in the Langley 8-Foot Transonic Pressure Tunnel. The Phase I investigation compared short and long core separate flow nacelles, long duct and energy efficient engine (E³) nacelles, symmetrical and cambered pylons, and several longitudinal and vertical nacelle locations. The Phase II investigation utilized a modified wing with the long core separate flow nacelle and several E³ nacelles. The effects of nacelle and pylon cant angles and nacelle longitudinal and vertical location were investigated in detail. The investigation was conducted over a Mach number range from 0.70 to 0.83 although only the results at the cruise condition, 0.82 Mach number and 0.55 lift coefficient, are presented in this status report.

MODEL

Figure 1 shows a picture of the semispan model in the Langley 8-Foot Transonic Pressure Tunnel. The model was all-metric; that is, the fuselage was not attached to the tunnel sidewall. The fuselage was mounted on the balance which was located just outside the tunnel test section wall. Figure 2 is a dimensioned drawing of the model. The wing had a quarter chord sweep of 30° , an aspect ratio 10, and was 12 percent thick at the nacelle location which is 40 percent of the semispan.

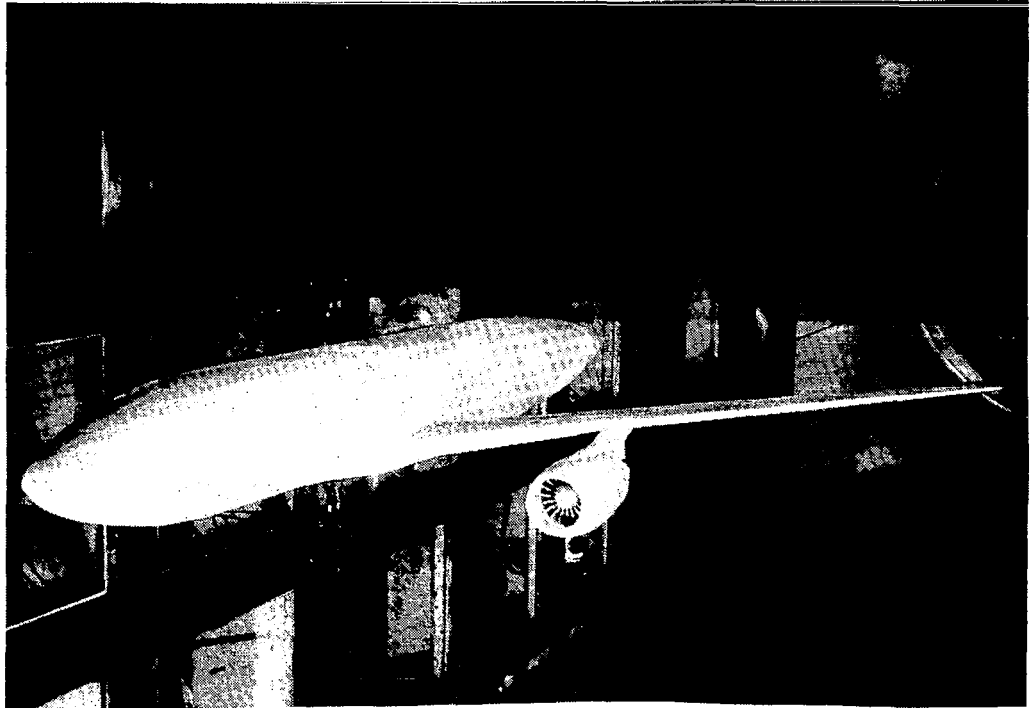


Figure 1

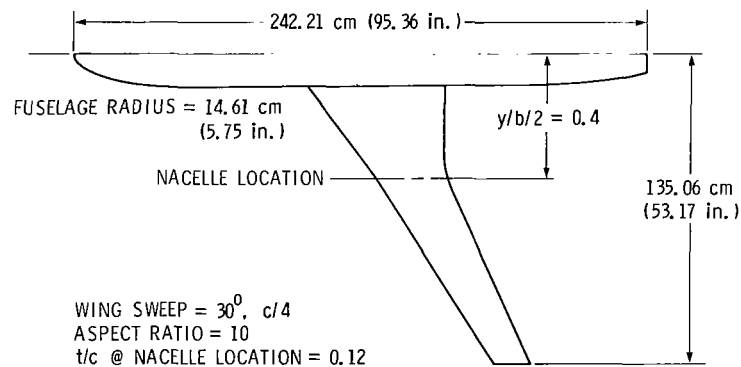


Figure 2

SCOPE OF PHASE II

The results obtained in Phase I indicated the changes required for the Phase II investigation. (See fig. 3.) A new outer wing panel was fabricated having 2.5° more wingtip washout and incorporating the latest modification to the supercritical airfoil section. These modifications consisted of a re-shaping of the lower surface of the airfoil section, at the engine location, near the leading edge and a reduction in the camber in the cusp region.

The wing-pylon attachment was also modified to provide a -2° nacelle "toe-in" capability for each nacelle pylon configuration and to reduce the nacelle incidence angle by 1° . Phase I results had indicated that a nacelle cant angle of -2° and a forward nacelle position was more desirable. Because of the increased wingtip washout, the cruise lift coefficient would be obtained at a higher angle of attack. Thus, the nacelle incidence angle was reduced 1° in an attempt to maintain the same nacelle alignment with the local flow.

SCOPE OF SECOND PHASE INVESTIGATION

- INCREASED WING TWIST
- WING LOWER SURFACE AIRFOIL RESHAPED
- NACELLE CANT OF -2 DEGREES (TOE-IN), Δ INCIDENCE -1°
- NACELLES IN FORWARD POSITION
- LIMITED TO LONG CORE AND E^3 NACELLES

Figure 3

EFFECT OF TWIST ON SPANWISE LOAD DISTRIBUTION

The effect of the increased wing twist on the spanwise load distribution for the wing fuselage configuration without pylons and nacelles is shown in figure 4. The data presented, at the cruise Mach number of 0.82 and at 2.5° angle of attack, are the normalized load at each spanwise wing station. The lift coefficient at this constant angle of attack was reduced by 0.02 due to the additional outboard twist. The loading on the outboard portion of the wing is reduced from the nacelle location to the wingtip as expected. In order to increase the lift coefficient of the new wing by this 0.02, an increase in angle of attack of approximately 0.3° was required.

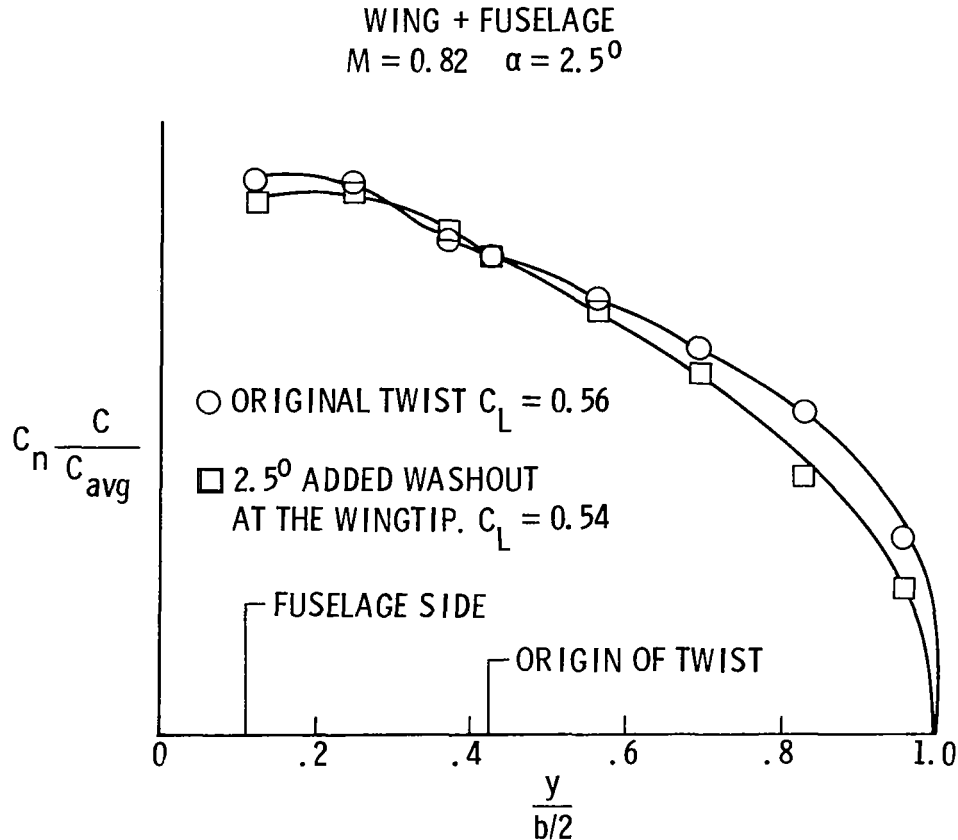


Figure 4

EFFECT OF AIRFOIL RESHAPING ON WING PRESSURE DISTRIBUTION

The chordwise pressure distribution measured just inboard of the nacelle location for the same configurations and conditions as for figure 4 is presented in figure 5. On the forward portion of the lower surface the velocities were reduced for the modified wing, as intended. On the upper surface of this airfoil section there are some changes that were not favorable as well as some that were. There is a stronger shock near the leading edge followed by a weaker shock at the 50 percent chord location followed again by an unfavorable shock recovery at the 70 percent chord location. While the causes of these differences have not yet been identified, several factors must be looked at. The airflow over the wing at this station was directly affected by the change to the lower surface shape near the leading edge and indirectly by the changes to the outboard wing panel. The new airfoil, incorporating the modified cusp and the start of the additional washout, starts just outboard of this station. The transition region between the airfoil shapes may have extended over the upper surface of this station. Accurate measurements of the wing will provide insight into the differences between the pressure distributions for the two phases.

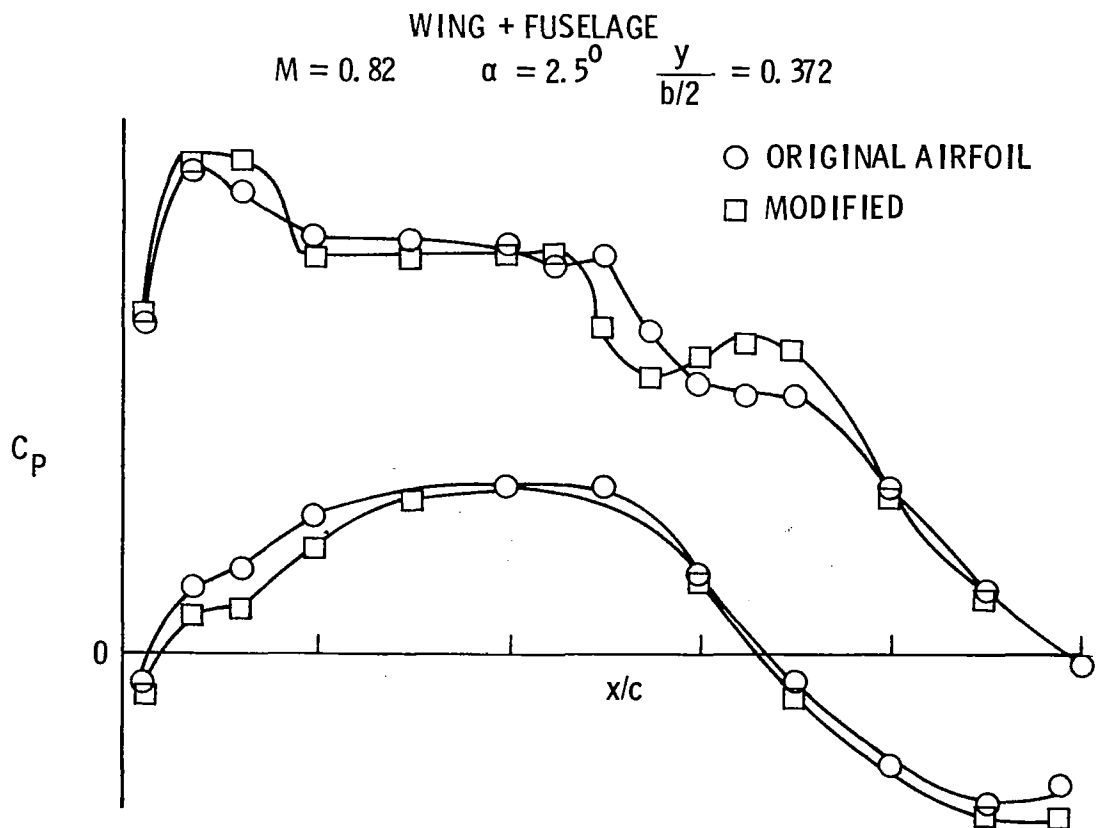


Figure 5

INCREMENTAL DRAG

The rest of this paper discusses the several powered nacelle configurations in terms of incremental drag (either installed drag or interference drag). Computing incremental drag requires testing four different configurations: the complete model; the wing and fuselage; the pylon and nacelle on an isolated strut; and the isolated strut alone. (See fig. 6.)

The installed drag is obtained by subtracting the drag of the wing fuselage configuration from the drag, adjusted for the calculated thrust, of the complete model configuration. The interference drag is obtained by subtracting the drag of the pylon and nacelle on the isolated strut, adjusted for the calculated thrust and the isolated strut tare, from the installed drag. A pylon and nacelle mounted on the isolated strut is shown in figure 7.

METHOD FOR DETERMINATION OF INCREMENTAL DRAG

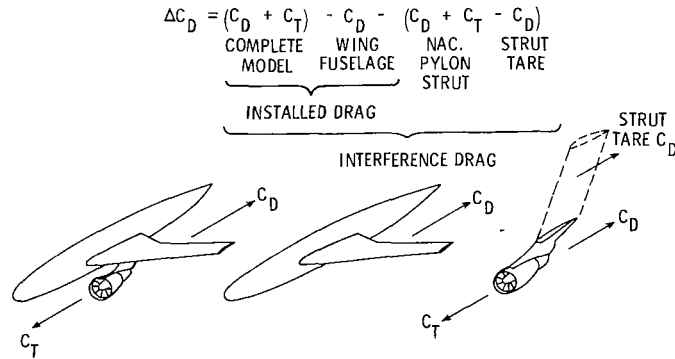


Figure 6

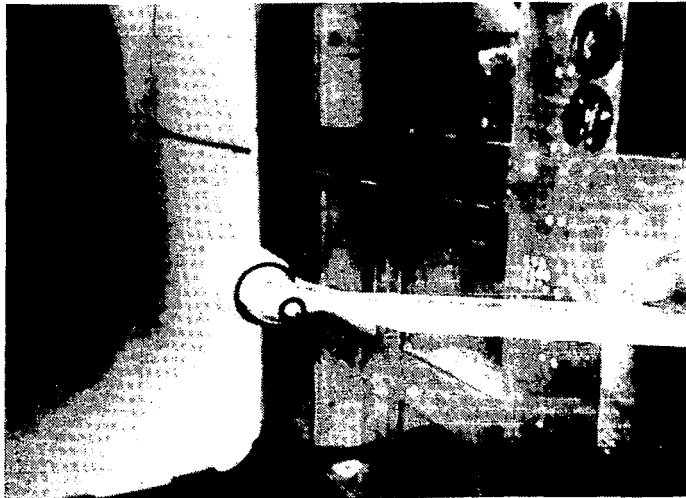


Figure 7

NACELLE CONFIGURATIONS

Figure 8 is a summary of the configurations that were investigated. The top two nacelles, the long core and the advanced E³ nacelles were tested in Phase I as well as in this second test phase. The long core nacelle represents current technology; it is representative of the 50,000 pound thrust class engines. The advanced E³, mixed flow nacelle represents advanced fan jet engine technology; at this time this engine is in the 37,000 pound thrust class which is expected to be increased to a thrust level comparable to that of the long core engine. The E³ nacelle fan cowl has been extended to provide a more complete mixing of the fan and primary flows which has been shown to result in a 5 percent reduction in fuel consumption. This nacelle was tested in this second test phase. To compare separate and mixed flow nacelles effects, a separate flow nacelle comparable in size to the E³ nacelle was also tested. This nacelle had a conical primary nacelle and plug.

Tests were conducted with different pylon and nacelle cant angles with the nacelles at several longitudinal and vertical positions. A sketch of the nacelle at a cant angle of -2° ("toe-in") is shown in figure 9 along with a view of nacelle position. The cambered pylon was tested at 0° and +2° cant angles. Phase I results indicate that there is a reduction in drag associated with the cambered pylon compared to the symmetrical pylon. The cambered pylons produce the desired side forces even at 0° cant angle. The nacelle's primary exit is located longitudinally with respect to the wing leading edge by the distance "X" (figure 9). The nacelle's centerline is located vertically with respect to the wing chord by distance "Z." The different nacelle configurations tested are presented in figure 10.

NACELLE CONFIGURATIONS

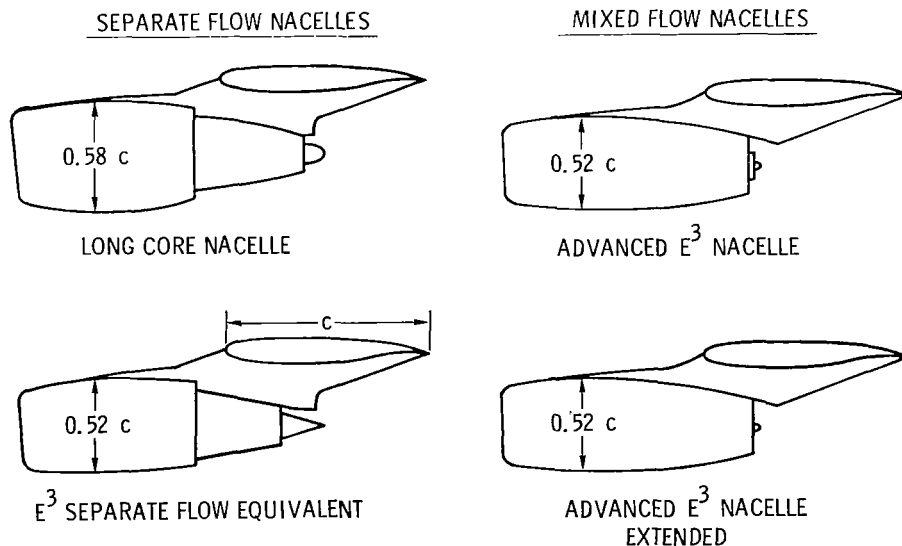


Figure 8

VARIATION OF ENGINE NACELLE POSITION AND ALIGNMENT

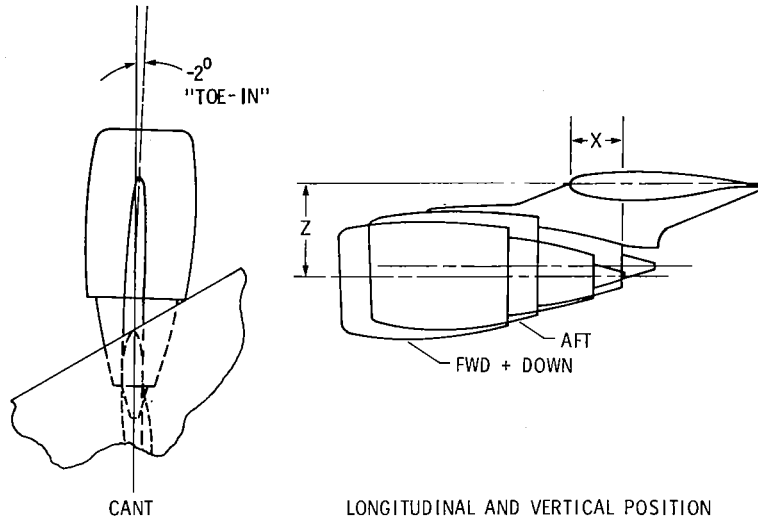


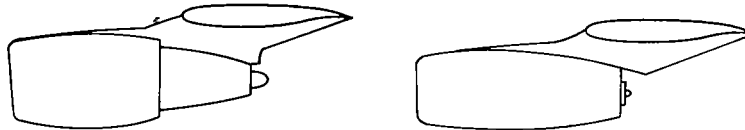
Figure 9

PROPULSION/AIRFRAME INTEGRATION INVESTIGATION

TEST CONFIGURATIONS

SEPARATE FLOW NACELLES

MIXED FLOW NACELLES



NACELLE CONFIG	PHASE	PYLON SHAPE		CANT ANGLE DEG		CORE EXIT	
		SYM	CAM	PYLON	NAC	LONGIT	VERTICAL
LONG CORE NAC (SEPARATE FLOW)	II	X		0	0	.40c	.40c
	II	X		0	-2	.40c	.40c
	II	X		0	-2	.25c	.45c
	II	X		0	-4	.40c	.40c
	II	X		+2	0	.40c	.40c
	II	X		+2	-2	.40c	.40c
E ³ CONICAL CORE NAC (SEPARATE FLOW)	II	X		0	-2	.29c	.40c
E ³ NAC (MIXED FLOW)	II	X		0	-2	.17c	.40c
	II	X		0	-2	.17c	.45c
	II	X		0	-2	.27c	.40c
	II	X		+2	0	.27c	.40c
E ³ EXTENDED NAC (MIXED FLOW)	II	X		0	-2	.29c	.40c

Figure 10

EFFECT OF LONG CORE NACELLE AND PYLON CANT

The effect of the nacelle and pylon cant angle variations on interference drag for the long core separate flow nacelle is presented in figure 11. Lower interference drag was obtained with a nacelle cant angle of -2° than with either 0° or -4° cant angles. The pylon cant angle of 0° in combination with the nacelle cant angle of -2° was shown to be more favorable than the $+2^\circ$ pylon cant angle.

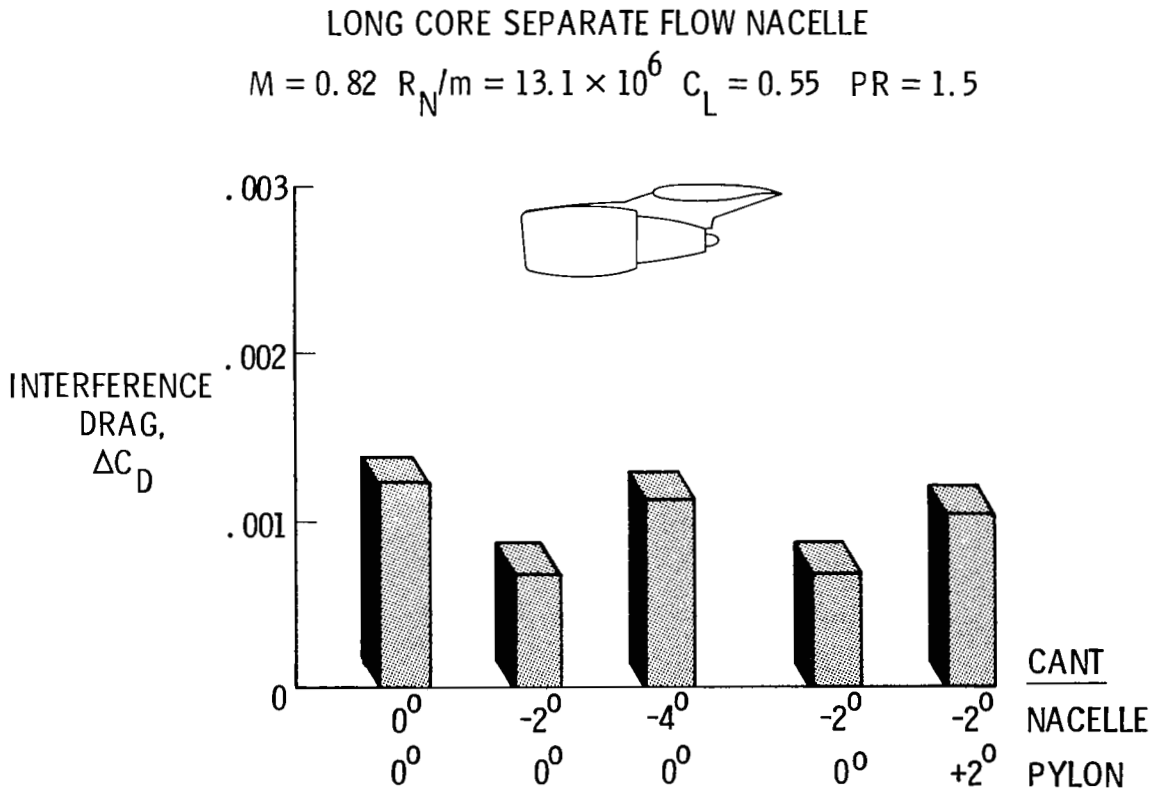


Figure 11

EFFECT OF LONG CORE NACELLE CANT ON PRESSURE DISTRIBUTION

The chordwise pressure distribution for the wing station just inboard of the nacelle is presented in figure 12. The -2° nacelle cant angle configuration has significantly lower velocities on the lower surface than either the 0° or -4° configurations. The 0° nacelle cant angle configuration also has a significant loss in lift at this station. The upper surface pressures near the wing trailing edge indicate there is some separation for the 0° nacelle cant configuration compared to that of the -2° or -4° configurations.

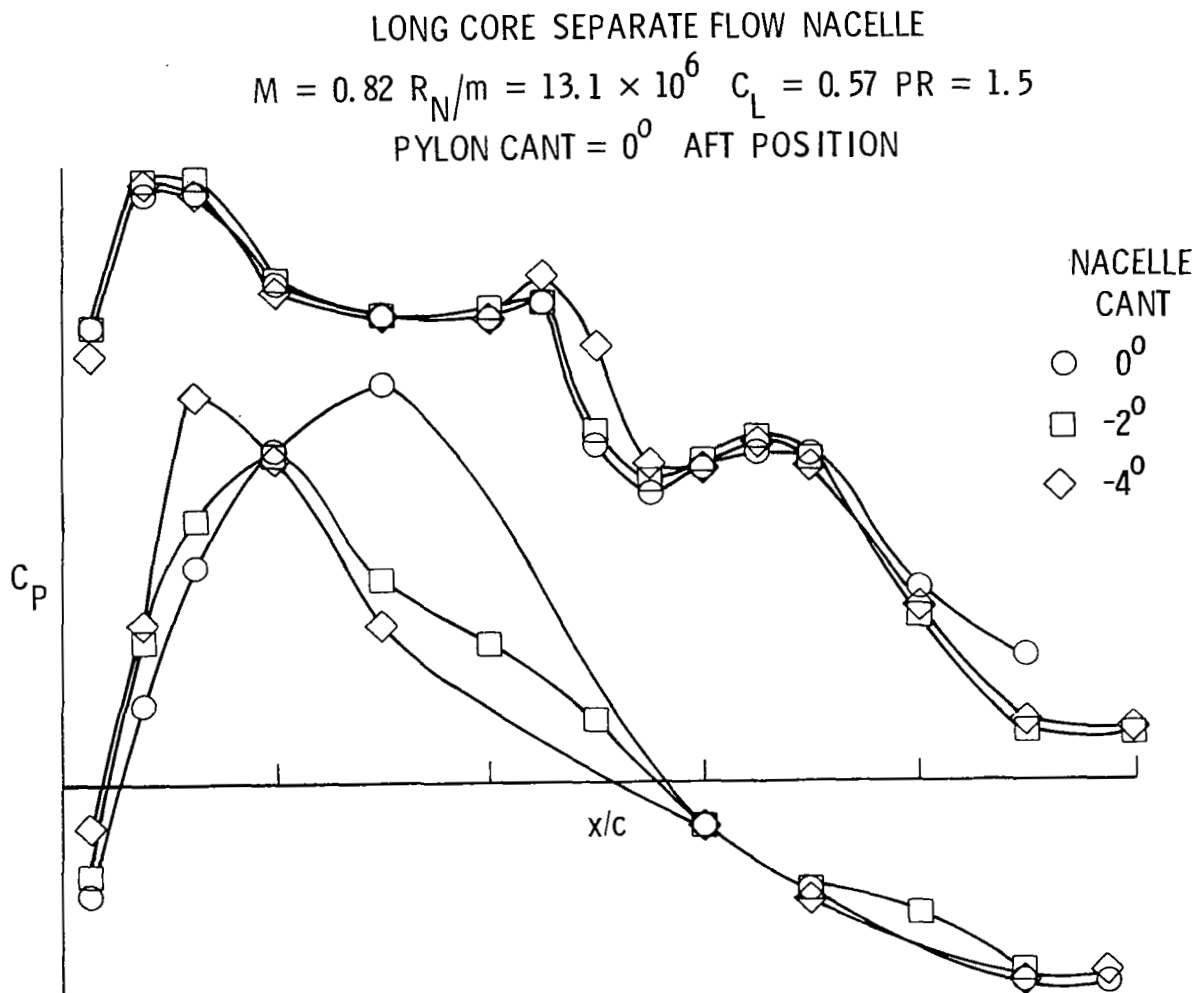


Figure 12

EFFECT OF LONG CORE NACELLE POSITION

Figure 13 presents the effect of the nacelle position on interference drag. Moving the nacelle from the aft position to the forward and down position resulted in an unexpected increase in interference drag. Results from previous powered nacelle tests had indicated that a forward position was more favorable than an aft position. A pylon was not available to produce a forward but not down position.

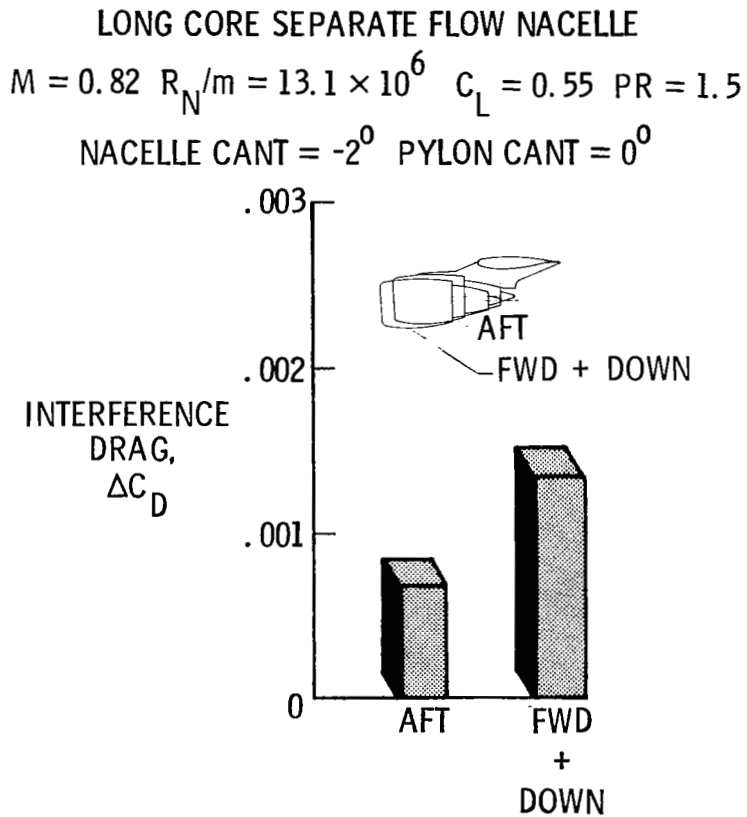


Figure 13

EFFECT OF E³ NACELLE POSITION AND CANT

Figure 14 shows the effect of position and cant of the E³ mixed flow nacelle. The forward position, as expected from Phase I results, had lower interference drag than either the aft or forward and down positions. These three positions were at the -2° nacelle cant angle and 0° pylon cant angle. The last two data columns show that the -2° nacelle cant angle and the 0° pylon cant configuration has less drag than the 0° nacelle cant and 2° pylon cant configuration. Again, there was no pylon available to test the intermediate configuration.

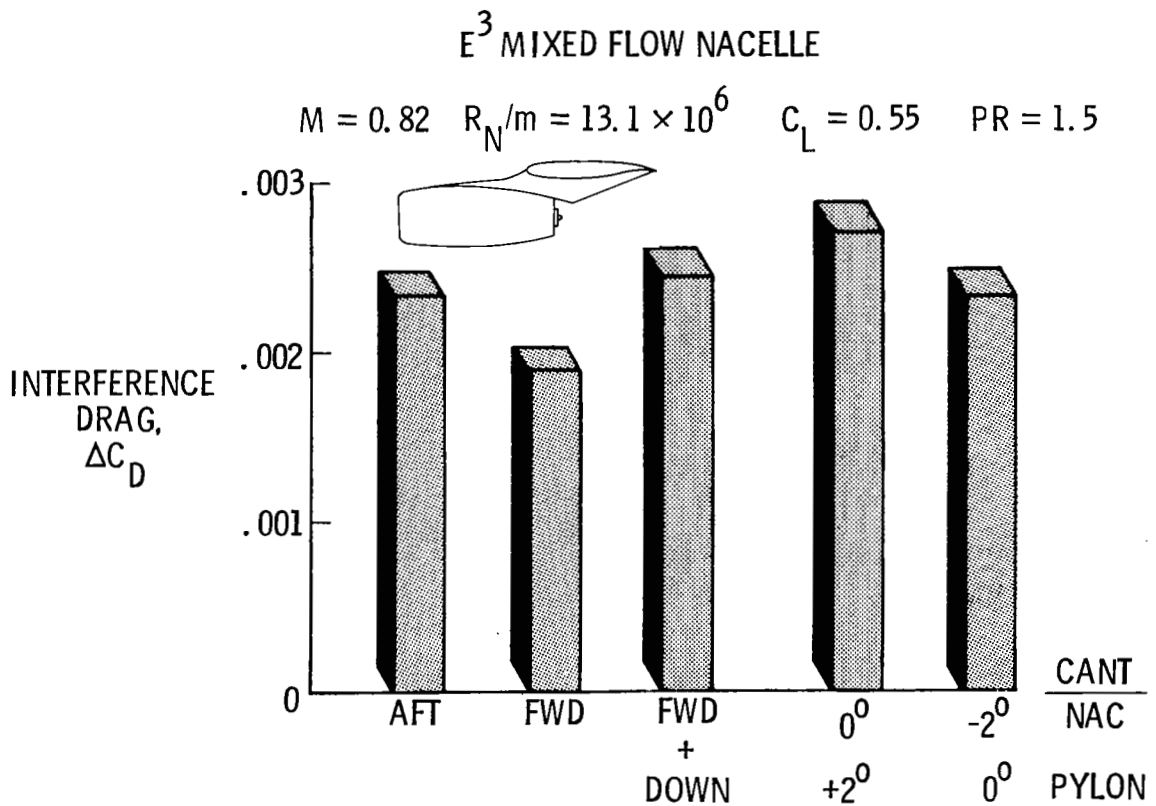


Figure 14

EFFECT OF E³ NACELLE POSITION ON PRESSURE DISTRIBUTION

The pressure distribution over the wing chord just inboard of the nacelle, presented in figure 15, indicates the effects of nacelle position. The pressures on the wing lower surface for the aft position indicate a significant lift loss. The peak pressures along the lower surface are not very different for the three configurations although the two forward positions probably have a shock wave near the leading edge. The upper surface pressures indicate that the aft configuration has a lift loss over the rear portion but a lift gain over the forward portion of the wing. Near the trailing edge there probably is some separation with the forward and down position having a little more separation than either the aft or forward positions.

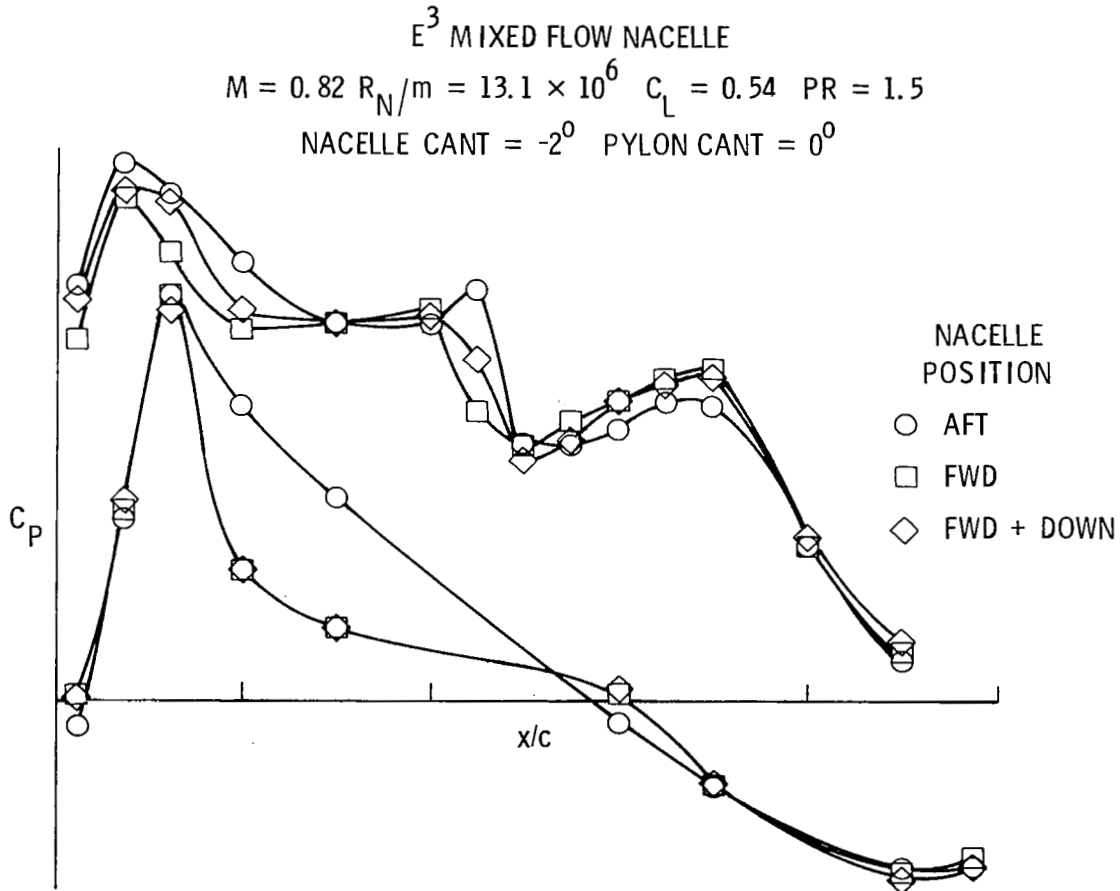


Figure 15

SUMMARY OF E³ NACELLE TYPES

Figure 16 compares the several E³ nacelle configurations, each with -2° nacelle cant, 0° pylon cant, and in the aft position. The results with the nacelle in the forward position are presented as the thin data column attached to the wider aft position column. The mixed flow configuration was improved, as expected, by going to an extended mixed flow configuration, but the separate flow configuration is still a better configuration than either mixed flow configuration.

$$M = 0.82 \quad R_N/m = 13.1 \times 10^6 \quad C_L = 0.55 \quad PR = 1.5$$

NACELLE CANT = -2° PYLON CANT 0° AFT POSITION

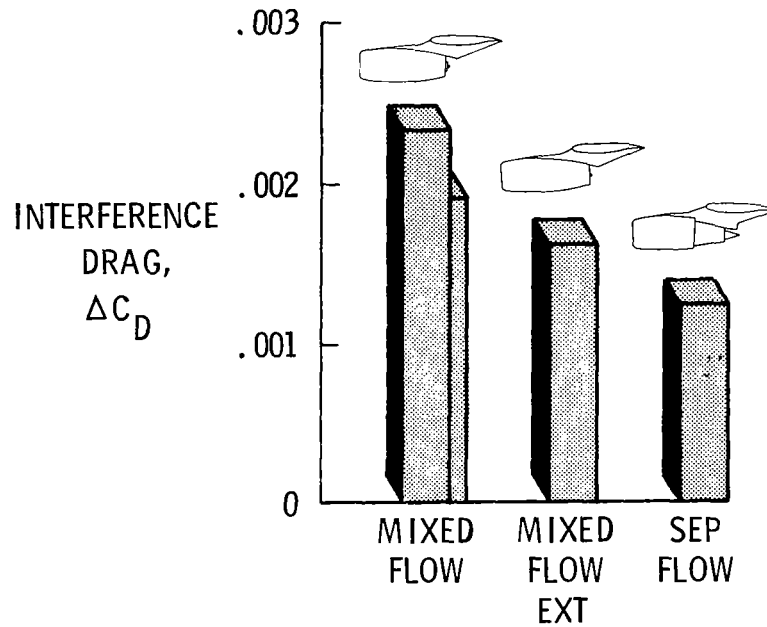


Figure 16

EFFECT OF E³ FLOW-THROUGH NACELLE POSITION

Figure 17 shows the effect of the nacelle position for an E³ flow-through nacelle. The nacelle has the same external shape as the E³ mixed flow nacelle. The internal duct diameter decreased linearly from the inlet to the exit. Again, the forward position is better than either the aft or the aft and up position.

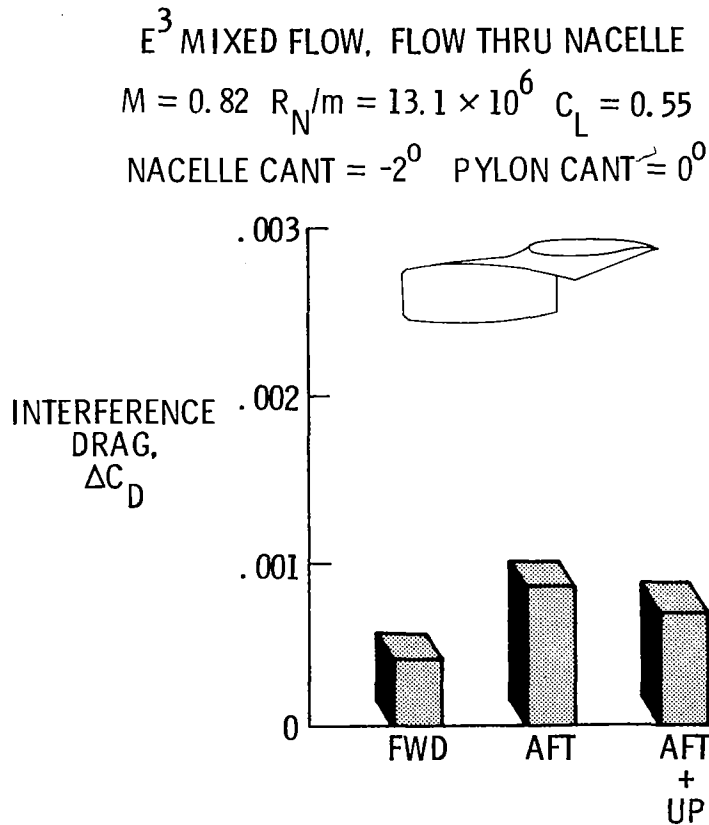


Figure 17

SUMMARY OF NACELLE TYPES

Both the installed drag, the drag of the complete model less the drag of the wing plus fuselage, and the interference drag, the installed drag less the drag of the engine-pylon configuration, are presented, for each nacelle tested, in figure 18. Each configuration has the same nacelle and pylon cant angles, -2° and 0° , respectively, and the data presented is for the nacelles in the aft position. In two cases the results obtained with the nacelles in the forward position are presented as thin data columns attached to the wider aft position columns. A comparison of the relative drag penalty associated with the installation of the various nacelles may be seen as well as that portion of the installation drag that is due to interference.

These data indicate that the long core separate flow nacelle has the lowest installation drag, with less interference drag than the other powered nacelle configurations tested, even though the nacelle length and frontal area are somewhat greater. The longer primary core of this nacelle allows reduced boattail slopes resulting in reduced boattail drag. There may possibly be a favorable effect of the nacelle fan wake compared to the mixed flow nacelles that may also contribute to the lower drag of this configuration. The installation drag of the E³ conical core separate flow nacelle is less than that of the mixed flow nacelle, half of which is interference drag. This is possibly a result of a reduction in the wing upper surface shock and reduced velocities associated with the separate flow nacelle on the forward portion of the wing lower surface, both inboard and outboard of the pylon. The extended mixed flow nacelle, extended for more complete mixing of the primary and fan flows, also is shown here to have a lower installation drag than the basic E³ mixed flow nacelle. The thrust calibration of the basic E³ nacelle has been in question and therefore it is planned to recalibrate this nacelle. It is conjectured, based on a similar circumstance, that the recalibration will result in a reduction in the installed drag coefficient of approximately 0.0004. This would reduce the drag level of the basic E³ nacelle to just below the extended nacelle as would be expected.

The E³ flow-through nacelle results are also presented on this figure, reduced by an internal drag coefficient of 0.00061. These data are compared with the basic E³ nacelle and are shown to be approximately 30 percent less than the powered nacelle case. The installation and interference drag values for the flow-through and the E³ powered nacelle in the forward position are also presented. In both cases there is a reduction in installation and interference drag in the forward position as shown in earlier powered nacelle investigations.

EFFECT OF NACELLE TYPE

$$M = 0.82 \quad R_N/m = 13.1 \times 10^6 \quad C_L = 0.55 \quad PR = 1.5$$

- ▣ INSTALLED DRAG = $\Delta C_D = C_D \text{ COMPLETE MODEL} - C_D \text{ WING} + \text{FUSELAGE}$
- ◻ INTERFERENCE DRAG = $\Delta C_D = \text{INSTALLED DRAG} - C_D \text{ ISOLATED NACELLE}$

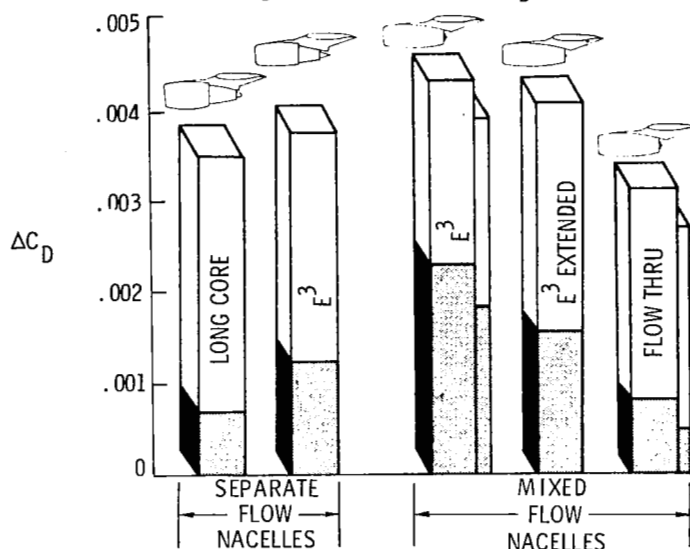


Figure 18

SUMMARY

The Phase II investigation was conducted with several separate flow and mixed flow nacelles. The effects of nacelle and pylon cant angle variations and longitudinal and vertical variations were investigated in detail. The results of the investigation, at the cruise condition, 0.82 Mach number and 0.55 lift coefficient, indicate that:

- Separate flow nacelles have less installation and interference drag than mixed flow nacelles
- Long core nacelles, representing current technology, have less installation and interference drag than the E³ mixed flow and conical-core separate flow nacelles, representing advanced design technology.
- Best nacelle position and alignment:
 - Forward position
 - 2° nacelle cant angle ("toe-in")
 - 0° pylon cant angle



STATUS REPORT ON THE EET HORIZONTAL TAILS INVESTIGATION AND
THE EET LATERAL CONTROLS INVESTIGATION

Peter F. Jacobs and Dennis W. Bartlett
NASA Langley Research Center

ABSTRACT

In the late 1980's or early 1990's, jet transports will be highly fuel efficient configurations, utilizing high-aspect-ratio supercritical wings and other advanced aerodynamic concepts to reduce drag. While much preliminary work has been done in the development of practical airplane configurations, two areas of interest need to be investigated further. First, the impact of the increased nose-down pitching moments, characteristic of supercritical wings, on trim drag must be assessed. Second, the effect of the highly aft-cambered supercritical wing sections on the performance of lateral-control systems needs to be determined. These two areas are not unrelated. An aircraft employing an advanced lateral/active control system with gust and maneuver load alleviation, flutter suppression, and relaxed static stability may have a smaller horizontal tail which, in turn, may reduce the trim drag increment for the aircraft. Experimental data in these important areas were obtained in two separate wind tunnel investigations recently conducted in the Langley 8-Foot Transonic Pressure Tunnel as a part of the NASA Energy Efficient Transport Program.

In the EET Horizontal Tails Investigation, aerodynamic data were measured for five different horizontal tails on a full-span model with a wide-body fuselage. Three of the horizontal tails were low-tail configurations and two were T-tail configurations. All five tails were tested in conjunction with two wings, a current wide-body wing and a high-aspect-ratio supercritical wing. Local downwash angles and dynamic pressures in the vicinity of the tails were also measured using a yaw-head rake. The results of this investigation will provide a comparison of the aerodynamic characteristics of the two wing configurations at trimmed conditions for Mach numbers between 0.60 and 0.90.

In the EET Lateral Controls Investigation, the control effectiveness of a conventional set of lateral controls was measured over a Mach number range from 0.60 to 0.90 on a high-aspect-ratio supercritical wing semispan model. The conventional controls included a high-speed aileron, a low-speed aileron, and six spoiler segments. The wing was designed so that the last 25 percent of the chord is removable to facilitate testing of various control systems, for example, active controls.

Because these investigations have only recently been completed, data are not yet available. The current status and an indication of the data obtained in these investigations will be presented.

OBJECTIVES OF EET HORIZONTAL TAILS INVESTIGATION

The main objective of this program was to assess the trim drag of a high-aspect-ratio supercritical wing configuration relative to the trim drag of a current wide-body configuration. Included in the investigation were tests to study the effects of horizontal-tail position (low-tail versus T-tail), horizontal-tail camber, elevator effectiveness, and a survey of the flow field in the vicinity of the horizontal tails with a yaw-head rake to determine local flow angles and dynamic pressures. Figures 1 and 2 show the models used in this investigation in the Langley 8-Foot Transonic Pressure Tunnel.

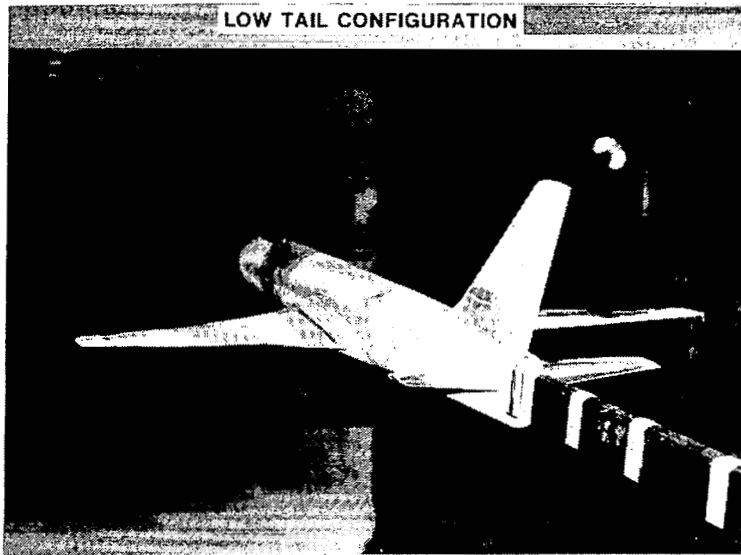


Figure 1.

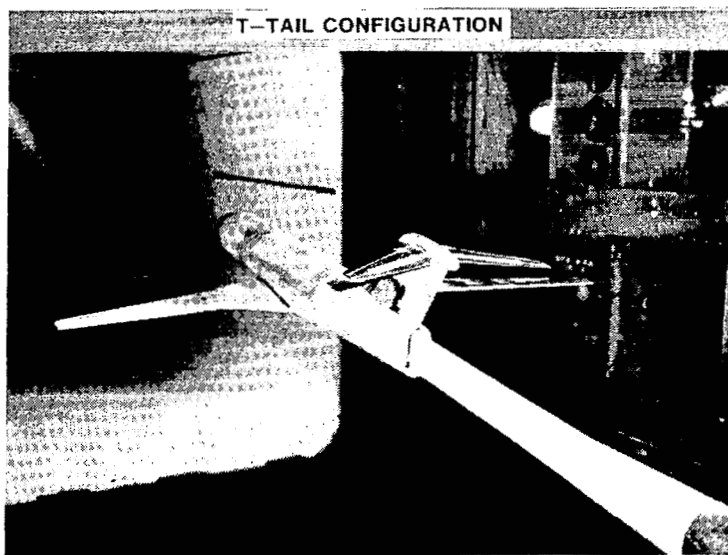


Figure 2.

LOW-TAIL WIND TUNNEL MODEL

A sketch of the model with the three low horizontal tails is shown in figure 3. H_1 and H_3 , shown by the solid line, have a smaller planform area than H_2 , shown by the dashed line. H_1 and H_2 have cambered supercritical airfoil sections and H_3 has a symmetrical supercritical section. The horizontal tails used incidence blocks which allowed rotation of the tail from -4° to 4° in 0.5° increments. Additionally, the cambered horizontal tails H_1 and H_2 had 30-percent-chord full-span elevators with angle brackets for deflections up to $+5^\circ$. These brackets are visible in the photograph of the model in the wind tunnel (see fig. 1).

LOW TAIL CONFIGURATION

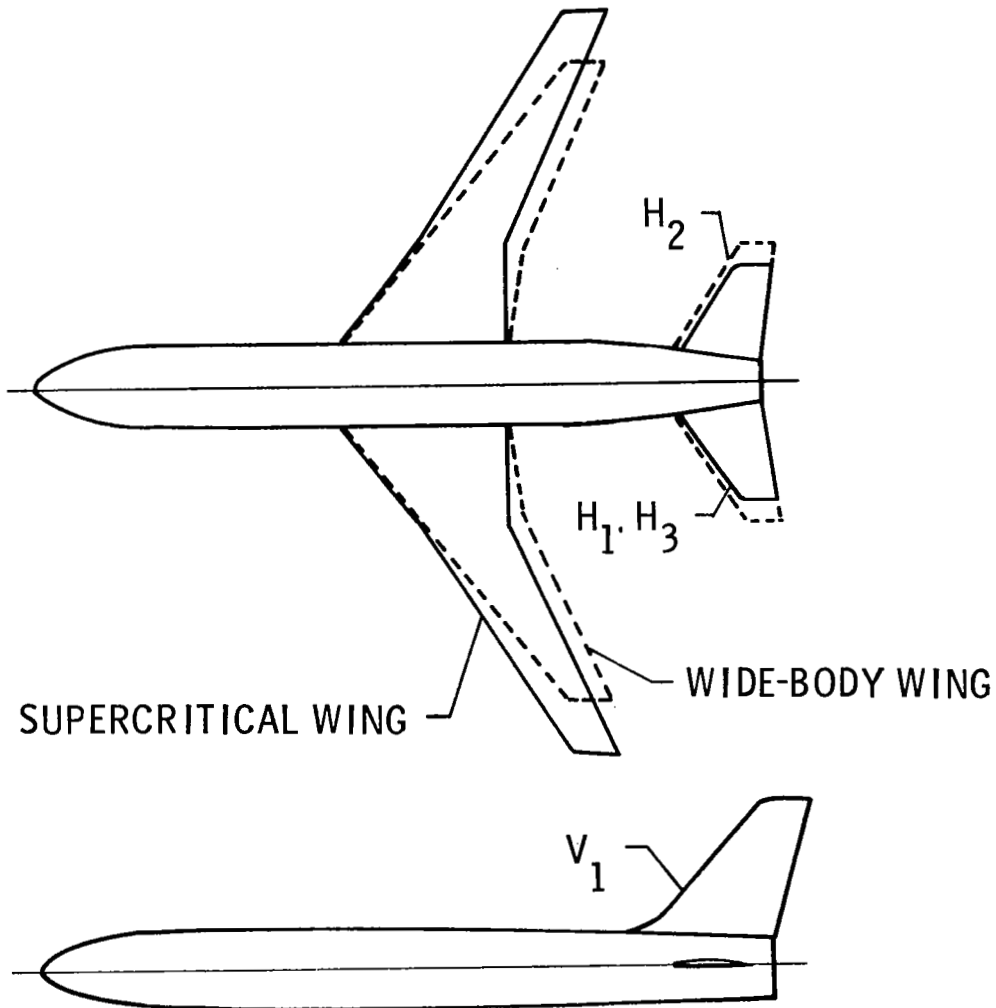


Figure 3.

T-TAIL WIND-TUNNEL MODEL

A sketch of the model in the T-tail configuration is shown in figure 4. H_4 has a cambered supercritical airfoil section and H_5 has a symmetrical section. The horizontal tails for the T-tail also had incidence blocks which allowed rotation between -4° and 4° in 0.5° increments. The cambered tail, H_4 , had an elevator with angle brackets similar to H_1 and H_2 . A photograph of the T-tail configuration is shown in figure 2.

T-TAIL CONFIGURATION

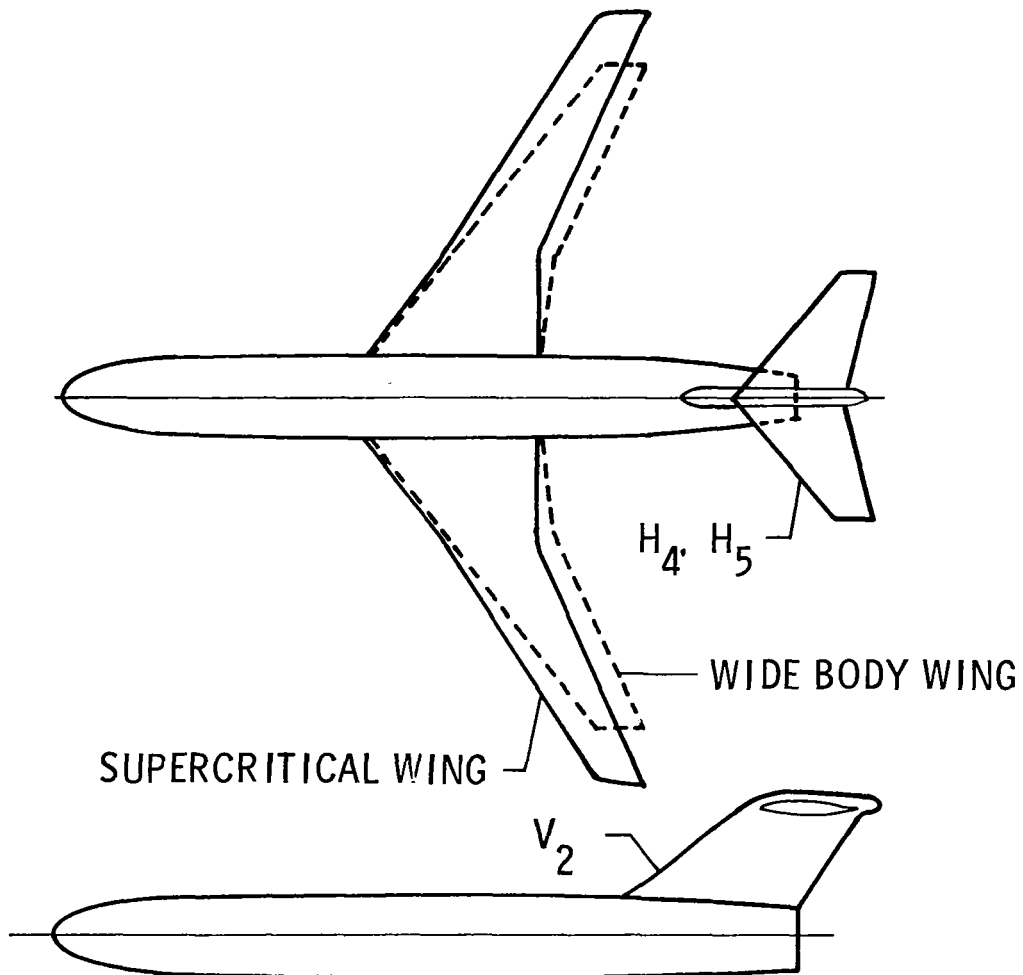
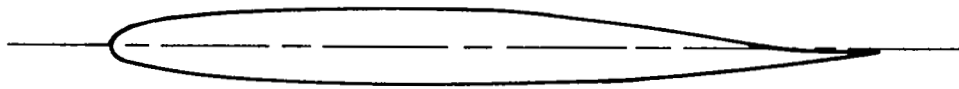


Figure 4.

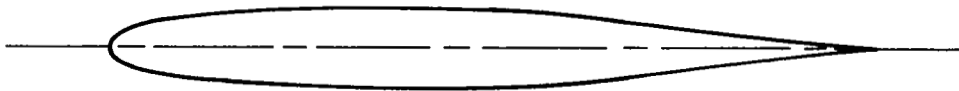
HORIZONTAL- AND VERTICAL-TAIL AIRFOILS

Figure 5 shows sketches of the airfoil sections used for the horizontal and vertical tails. A 10-percent-thick cambered supercritical airfoil was used for horizontal tails H_1 , H_2 , and H_4 . A 10-percent-thick symmetrical supercritical airfoil was used for horizontal tails H_3 and H_5 and was also used for the low-tail vertical V_1 . A 12-percent-thick symmetrical supercritical airfoil was used for the T-tail vertical V_2 .

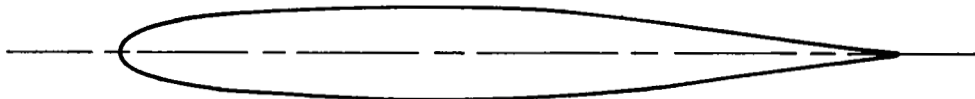
HORIZONTAL AND VERTICAL TAIL AIRFOILS



10% THICK CAMBERED



10% THICK SYMMETRICAL



12% THICK SYMMETRICAL

Figure 5.

TAIL CHARACTERISTICS

Several important tail parameters are presented in figure 6 for each tail. The tail area listed for the horizontal tails is the trapezoidal area extended to the fuselage center line, but for the vertical tails, the area shown is exposed area. Tail volume coefficient gives an indication of the tail contribution to overall stability level and is defined as

$$C_t = \frac{l_t S_t}{\bar{c}_w S_w}$$

where l_t = the distance from the center of gravity to the aerodynamic center of the tail

S_t = tail planform area

\bar{c}_w = mean aerodynamic chord of the wing

S_w = wing planform area

These tails were designed to have approximately the same relative size and tail volume coefficient as current technology aircraft. However, because the mean aerodynamic chord for the wide-body configuration was larger than for the supercritical wing configuration, the tail volume coefficients for the wide body are less.

Neglecting tail dihedral, horizontal tails H_1 , H_3 , H_4 , and H_5 have the same geometry and planform area. H_2 , which is slightly larger than the other horizontal tails, was designed to have the same exposed area and tail volume coefficient as the T-tail horizontal tails H_4 and H_5 .

TAIL CHARACTERISTICS

	TAIL	AIRFOIL	AREA m ² (ft)	TAIL VOLUME COEFFICIENT	
				SCW	WIDE BODY
LOW TAIL	H ₁	10% THICK CAMBERED	.05 (.55)	.90	.69
	H ₂	10% THICK CAMBERED	.07 (.70)	1.12	.86
	H ₃	10% THICK SYMMETRICAL	.05 (.55)	.90	.69
	V ₁	10% THICK SYMMETRICAL	.04 (.42)	.67	.51
T-TAIL	H ₄	10% THICK CAMBERED	.05 (.56)	1.09	.84
	H ₅	10% THICK SYMMETRICAL	.05 (.56)	1.09	.84
	V ₂	12% THICK SYMMETRICAL	.04 (.47)	.68	.52

Figure 6.

YAW-HEAD RAKES

The two yaw-head rakes used to measure local flow angles and dynamic pressures are shown in figures 7 and 8. Data were measured at two spanwise tail locations for each set of wing panels in both the low-tail and T-tail configurations. The data from these rakes will be helpful in separating the effects of the wing downwash field and wing wake energy losses on horizontal-tail efficiency.

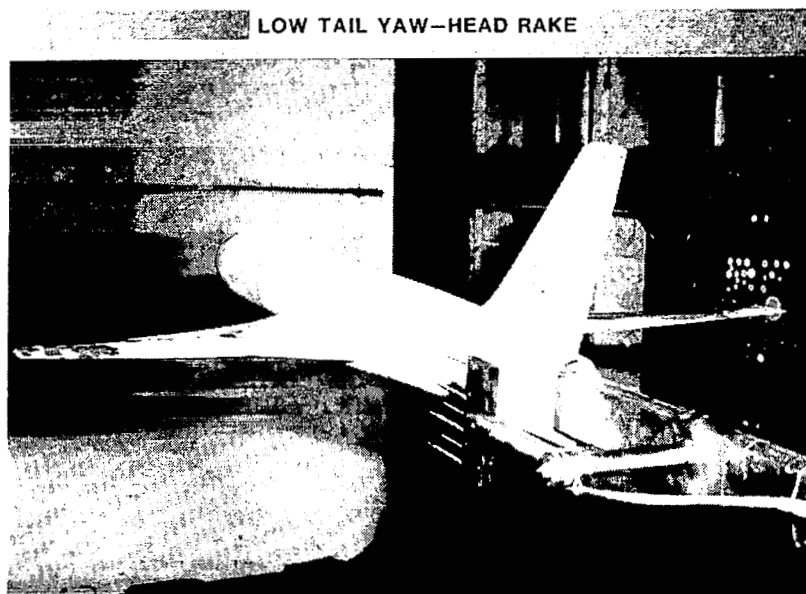


Figure 7.

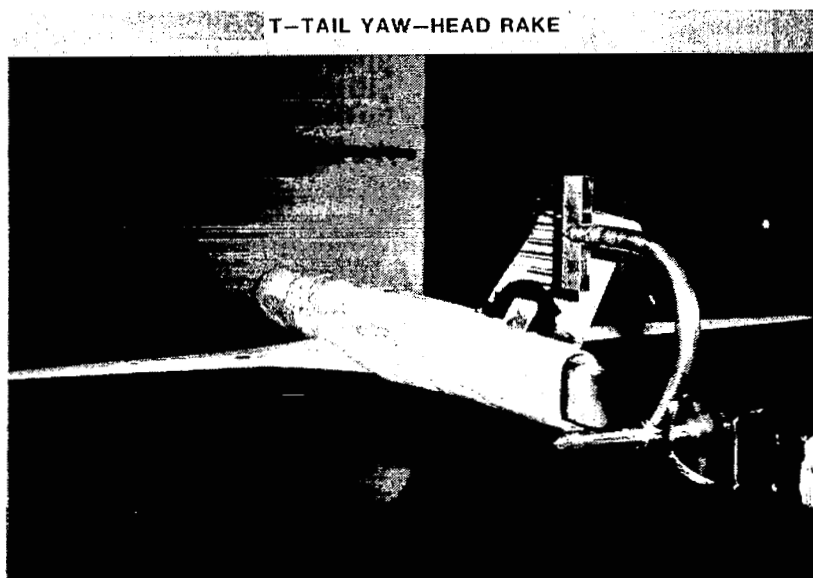


Figure 8.

SUMMARY OF DATA ACQUIRED

A summary of the data acquired in this investigation is shown in figure 9. Aerodynamic data were taken for each set of wing panels in combination with each of the five horizontal tails. Data with elevator deflected were taken for both wings with tails H₁, H₂, and H₄, as well as yaw-head rake data at two spanwise tail locations for both the low-tail and T-tail configurations. Aerodynamic data with the wing panels removed were taken to determine the lift and drag of each tail. The large amount of data from this recent investigation has not been fully analyzed and will not be presented at this time.

EET TAILS INVESTIGATION DATA ACQUIRED

WING	TAIL	ELEVATOR	YAW HEAD RAKE
SCW-4	H ₁ H ₂ H ₃ H ₄ H ₅	YES YES YES	 LOW-TAIL (2 POSITIONS) T-TAIL (2 POSITIONS)
WIDE BODY	H ₁ H ₂ H ₃ H ₄ H ₅	YES YES YES	 LOW TAIL (2 POSITIONS) T-TAIL (2 POSITIONS)
WING OFF	H ₁ H ₂ H ₃ H ₄ H ₅		

Figure 9.

OBJECTIVE OF EET LATERAL CONTROLS INVESTIGATION

The objective of this investigation is to determine the lateral-control effectiveness parameters for ailerons and spoilers on a high-aspect-ratio supercritical wing configuration. Initially a conventionally sized lateral-control system with high- and low-speed ailerons and spoilers was tested. More advanced control systems (e.g., active controls) may also be tested in the future. Figure 10 shows the semispan model used in this investigation in the Langley 8-Foot Transonic Pressure Tunnel.

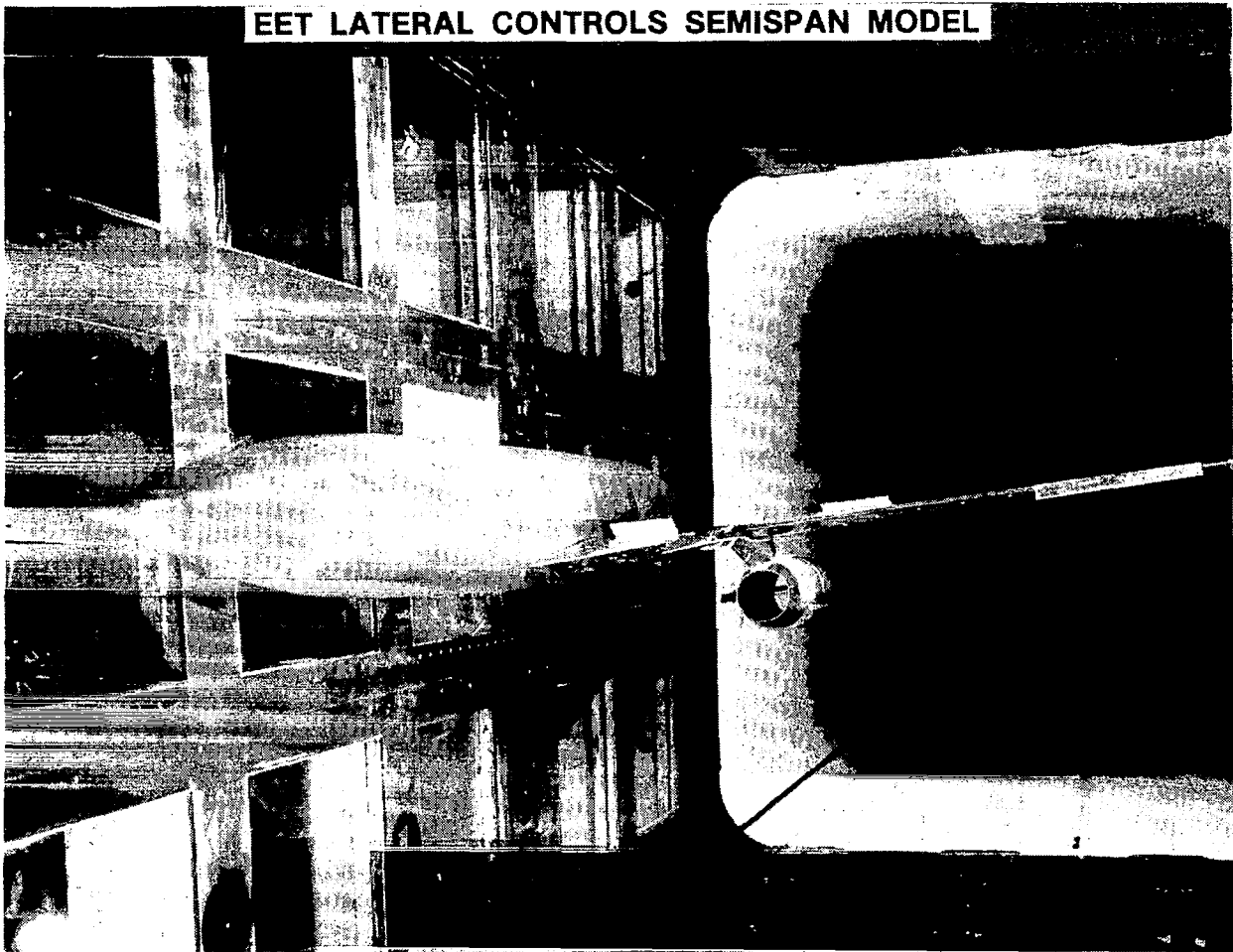


Figure 10.

WIND TUNNEL MODEL

A sketch of the high-aspect-ratio supercritical wing semispan model with a conventional set of lateral controls is shown in figure 11. The model has a high-speed and a low-speed aileron and six spoiler segments. A flow-through nacelle and pylon are located at 40 percent of the wing semispan and the model has the capability of testing winglets. The wing is instrumented with seven rows of pressure tubes and has hinge moment gauges for both ailerons. An important feature of the model is that the last 25 percent of the wing chord is removable, and therefore different control system configurations can be tested.

CONVENTIONAL LATERAL CONTROLS ON SEMISPAN MODEL

A. R. = 9.8 QUARTER-CHORD SWEEP = 30°

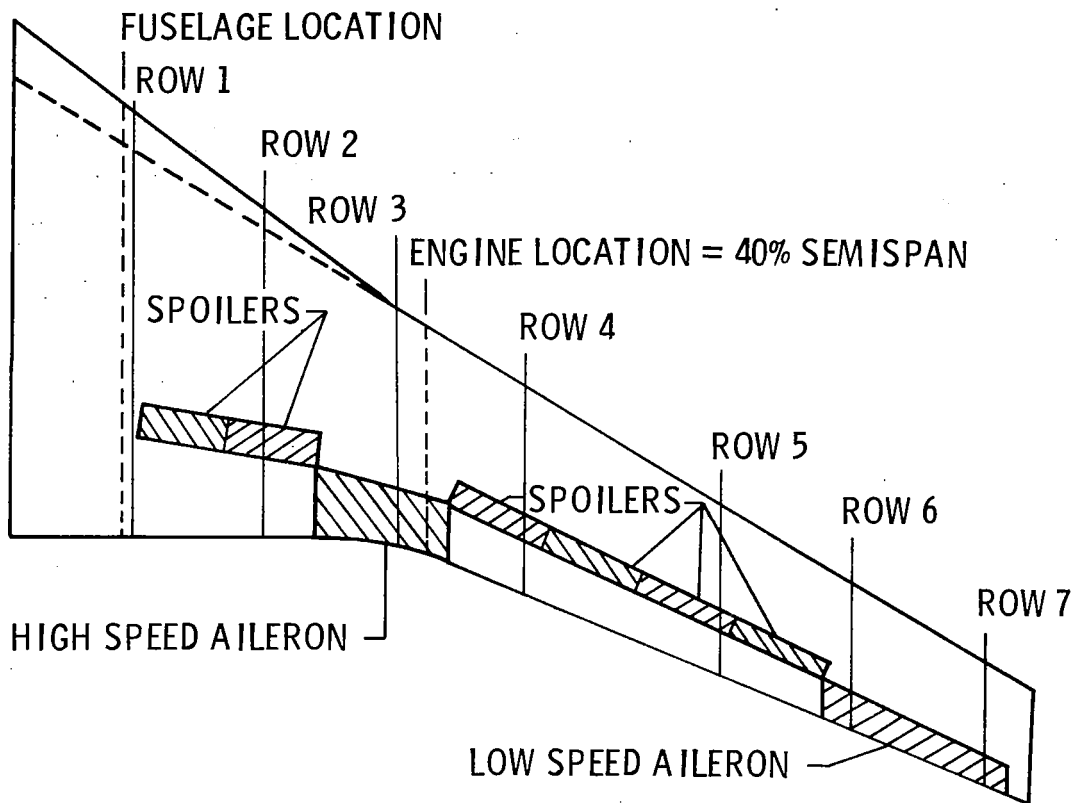


Figure 11.

MODEL CONTROL SURFACES

Detail photographs of the control surfaces are shown in figures 12 and 13. In the initial wind tunnel test of the conventional lateral-control system, data were measured for individual deflections of the high-speed aileron (-12.5° to 12.5°), the low-speed aileron (-17.5° to 17.5°), and the fourth spoiler segment (5° , 10° , 20° , 60°). Individual deflections of the remaining spoilers and combinations of controls will be tested in future wind tunnel entries. Again, because this investigation was only recently completed, data are not available and will not be presented.

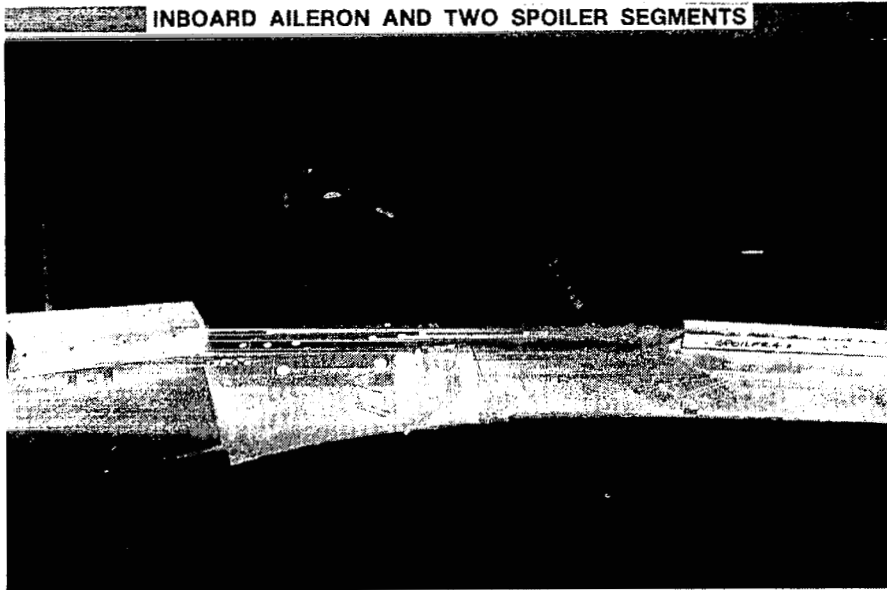


Figure 12.

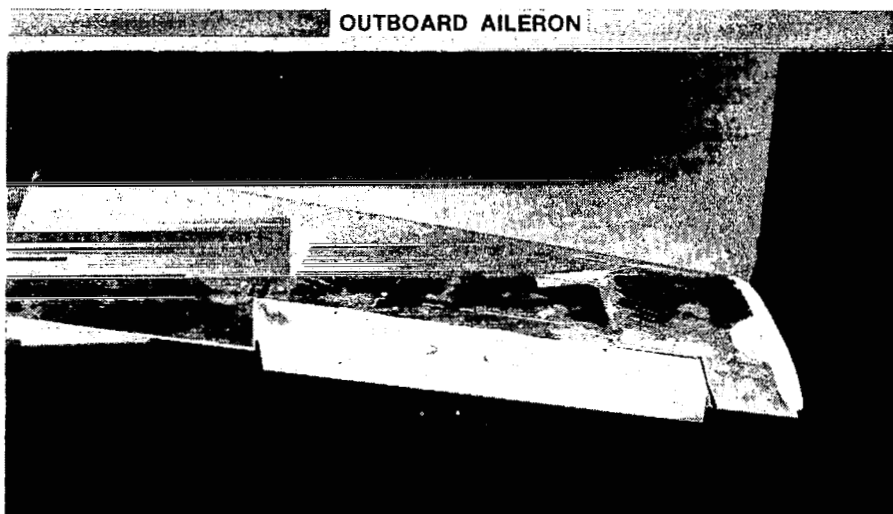


Figure 13.

NATURAL LAMINAR FLOW FLIGHT EXPERIMENT

Louis L. Steers
NASA Dryden Flight Research Center

ABSTRACT

Significant improvements in cruise efficiency of transport aircraft can be obtained if the flow over the wings is laminar. Active laminar flow control can prevent turbulent flow over most of the wing, but such systems add weight, cost, and complicate maintenance.

A possible alternative to active laminar flow control is natural laminar flow (NLF). Natural laminar flow utilizes an airfoil shape which encourages laminar flow to extend further over the airfoil than conventional shapes. The airfoil shape must maintain a favorable pressure gradient over most of the chord. While the advantages of laminar flow for significantly improving aerodynamic efficiency are well known, the problem of maintaining natural laminar flow has not previously been addressed at the higher Reynolds numbers and Mach numbers associated with commercial aircraft operations.

As a part of the NASA Aircraft Energy Efficiency Program, a joint Dryden Flight Research Center/Langley Research Center research effort has been conducted to investigate the feasibility of maintaining natural laminar flow on lifting surfaces. A supercritical airfoil section has been designed with favorable pressure gradients on both the upper and lower surfaces. Wind-tunnel tests in support of this experiment were conducted in the Langley Research Center 8-Foot Transonic Pressure Tunnel.

The outer wing panels of the F-111 TACT airplane were modified to incorporate partial span test "gloves" having the natural laminar flow profile. Instrumentation was installed to provide surface pressure data as well as to determine transition location and boundary-layer characteristics.

The flight experiment encompassed 19 flights. These flights were conducted with and without transition fixed at several locations for wing leading-edge sweep angles which varied from 10° to 26° at Mach numbers from 0.80 to 0.85 and altitudes of 7620 meters (25,000 feet) and 9144 meters (30,000 feet). Data analysis is underway. Preliminary results indicate that a large portion of the test chord experienced laminar flow. A quantitative measure of transition location cannot be provided at this time.

TEST BED AIRPLANE

The F-111 TACT airplane was used as the test bed for the natural laminar flow (NLF) experiment. Both wings were fitted with built-up partial span gloves having the NLF supercritical airfoil shape.

The F-111 TACT baseline wing also had a supercritical profile and variable sweep. In addition to the partial span gloves it was necessary to add fairing material inboard of the gloves to reduce the effects of shocks, characteristic of the carrier vehicle, which would otherwise have interfered with the experiment.

Test chord Reynolds numbers of 28 million were obtained with this experiment over a Mach number range from 0.80 to 0.85 and wing leading-edge sweep angles from 10° to 26° .



NLF CONCEPT

The NLF concept utilizes an airfoil shape that maintains the necessary favorable pressure gradient over a large percentage of the test chord. This concept is an alternative to active laminar flow control systems which would be more expensive, heavier, and would require more maintenance. It should be mentioned, however, that the NLF airfoil concept may also be used to enhance the performance of an active laminar flow control system.

Airfoils designed to encourage natural laminar flow have been flown on aircraft before—sailplanes and World War II and various post-war military aircraft. However, the present experiment addresses a significantly higher cruise Mach number than earlier efforts. In addition, earlier studies did not experience the problem of leading-edge crossflow effects on transition to the extent that the present study did.

NATURAL LAMINAR FLOW

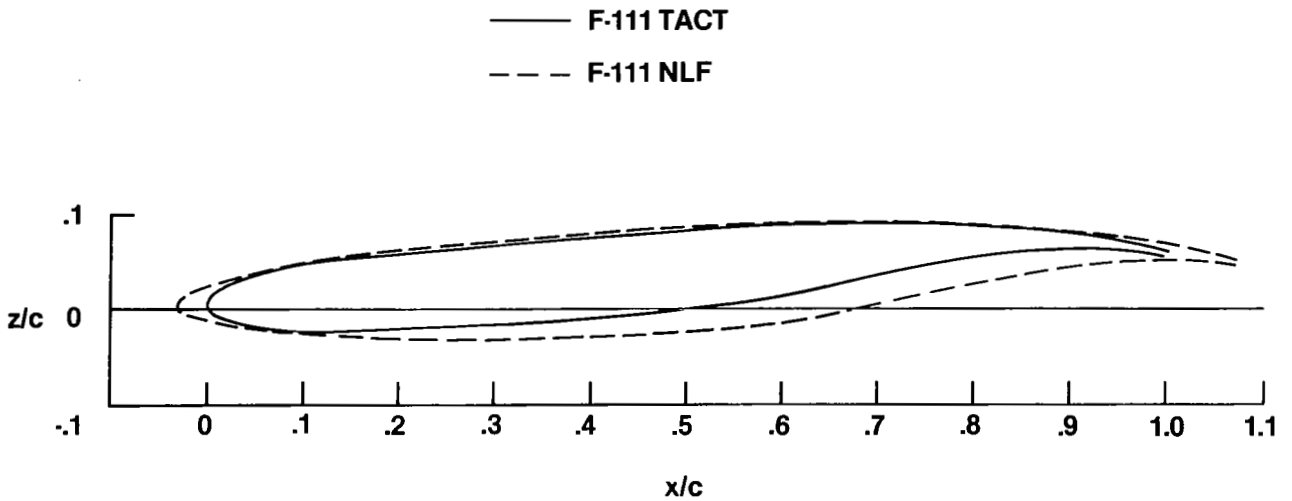
- **AVOIDS COMPLICATED SYSTEMS BY DESIGNING FOR FAVORABLE PRESSURE GRADIENTS**
 - **REDUCED WEIGHT**
 - **REDUCED MAINTENANCE**
 - **REDUCED COMPLEXITY**

- **BUT**
 - **RESTRICTED TO MODERATE WING SWEEP ANGLES**

NLF AIRFOIL

The NLF airfoil of the present experiment was initially a theoretical, two-dimensional shape designed for the required favorable pressure gradients. The theoretical shape was then fitted around the outer wing panels of a 1/24-scale model of the F-111 TACT carrier vehicle. In order to fit the test airfoil to the carrier vehicle wing, it was necessary to slightly thicken the trailing-edge region from the "ideal" shape.

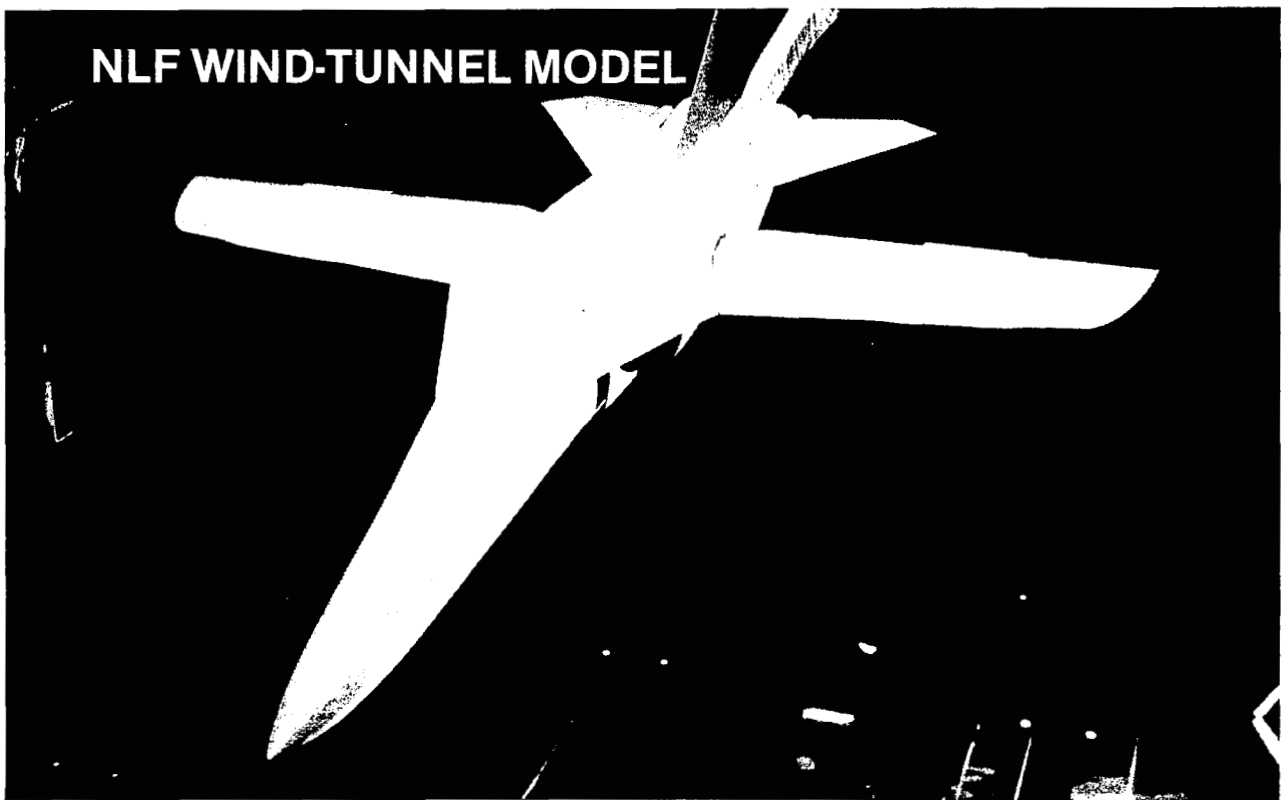
NATURAL LAMINAR FLOW AIRFOIL



NLF WIND-TUNNEL MODEL

The wind-tunnel tests were conducted to assess the stability and control characteristics of the modified configuration, establish the pressure gradients, and develop the interface (fairing) between the F-111 TACT airplane and the test glove. (The fairings were necessary for maintaining the quasi-two-dimensional flow characteristics required for the NLF experiment.)

These refinements, achieved during the 1/24-scale model tests, provided favorable pressure gradients over 65 and 50 percent of the model test chord for the upper and lower surface, respectively.

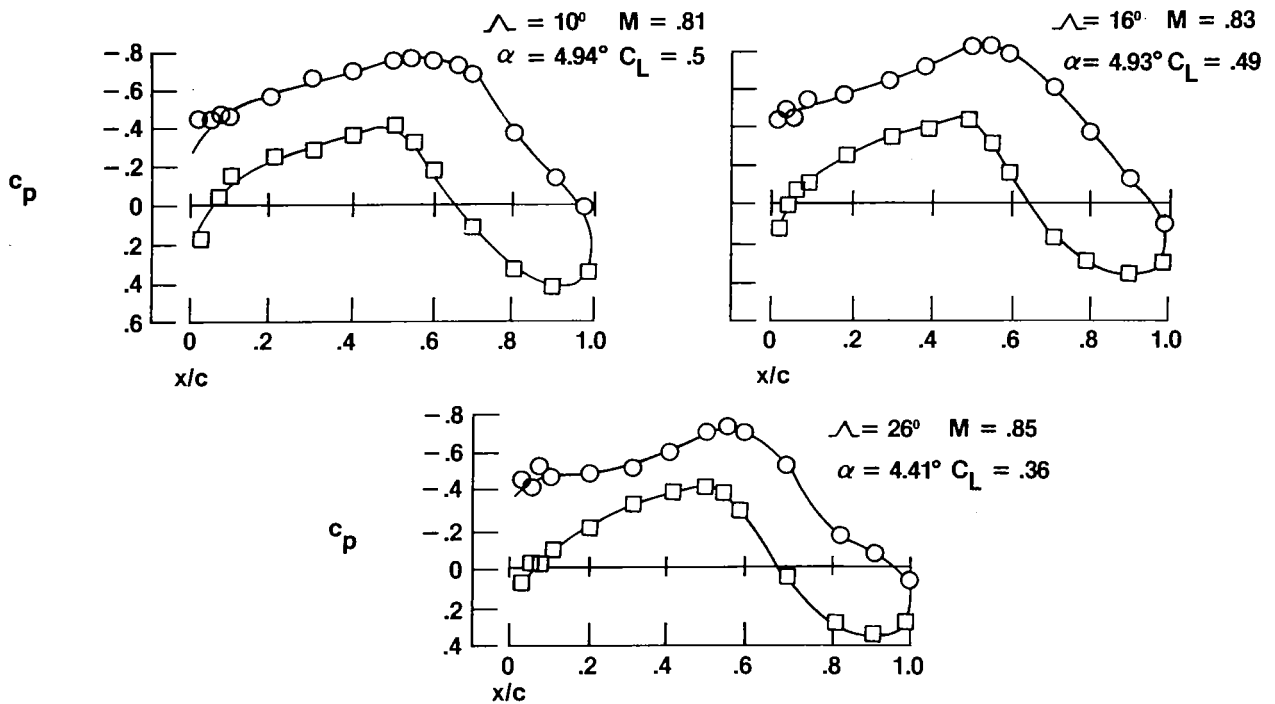


WIND-TUNNEL TEST RESULTS

The wind-tunnel model tests provided data for leading-edge sweep angles of 10° , 16° , and 26° , Mach numbers from 0.6 to 0.85 (with limited data at $M = 0.3$), and unit Reynolds numbers from 8.2 million to 16.4 million per meter (2.5 million to 5.0 million per foot). Force, pressure distribution, and flow visualization data were obtained.

These tests, conducted in the Langley 8-Foot Transonic Pressure Tunnel, resulted in acceptable stability and control characteristics and verified that the flow over the test glove region was free of undesirable three-dimensional effects or shocks emanating from the carrier vehicle environment. Favorable pressure gradients could be maintained over a large portion of the test chord at the higher Mach numbers ($M > 0.8$) for all sweep angles, angles of attack, and Reynolds numbers for which data were obtained.

WIND TUNNEL PRESSURE DISTRIBUTIONS

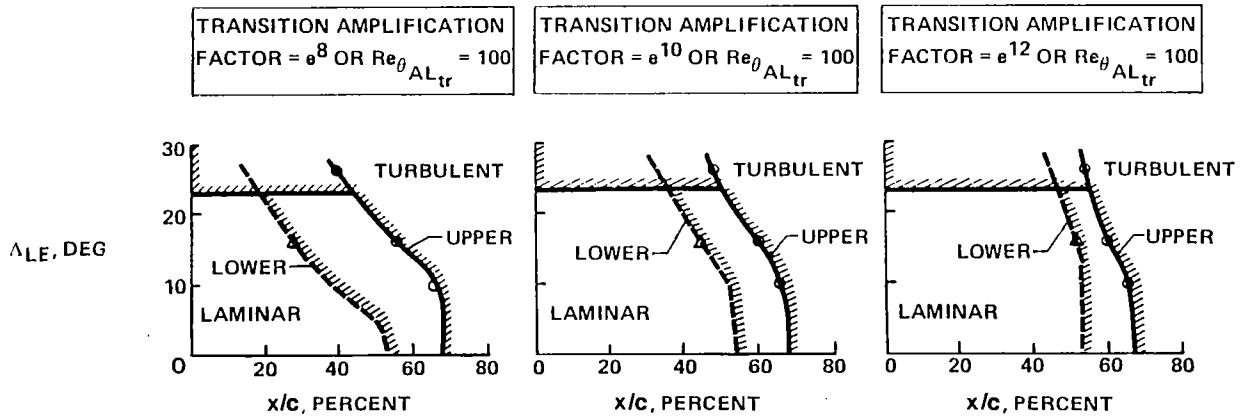


SUPPORTIVE THEORETICAL STUDY

In the fall of 1979, the Boeing Aerospace Company calculated transition location for three design conditions: leading-edge sweep angles of 10° , 16° , and 26° and Mach numbers of 0.81, 0.83, and 0.85, respectively. The compressible flow analysis incorporated the effects of the Tollmien-Schlichting disturbance amplification, cross-flow disturbance amplification, and leading-edge attachment line contamination on the predicted transition location at a chord Reynolds number of 25 million. The results indicated that laminar flow can be maintained over a large extent of the chord.

PREDICTED LOCATION OF FULLY TURBULENT FLOW COMPRESSIBLE STABILITY

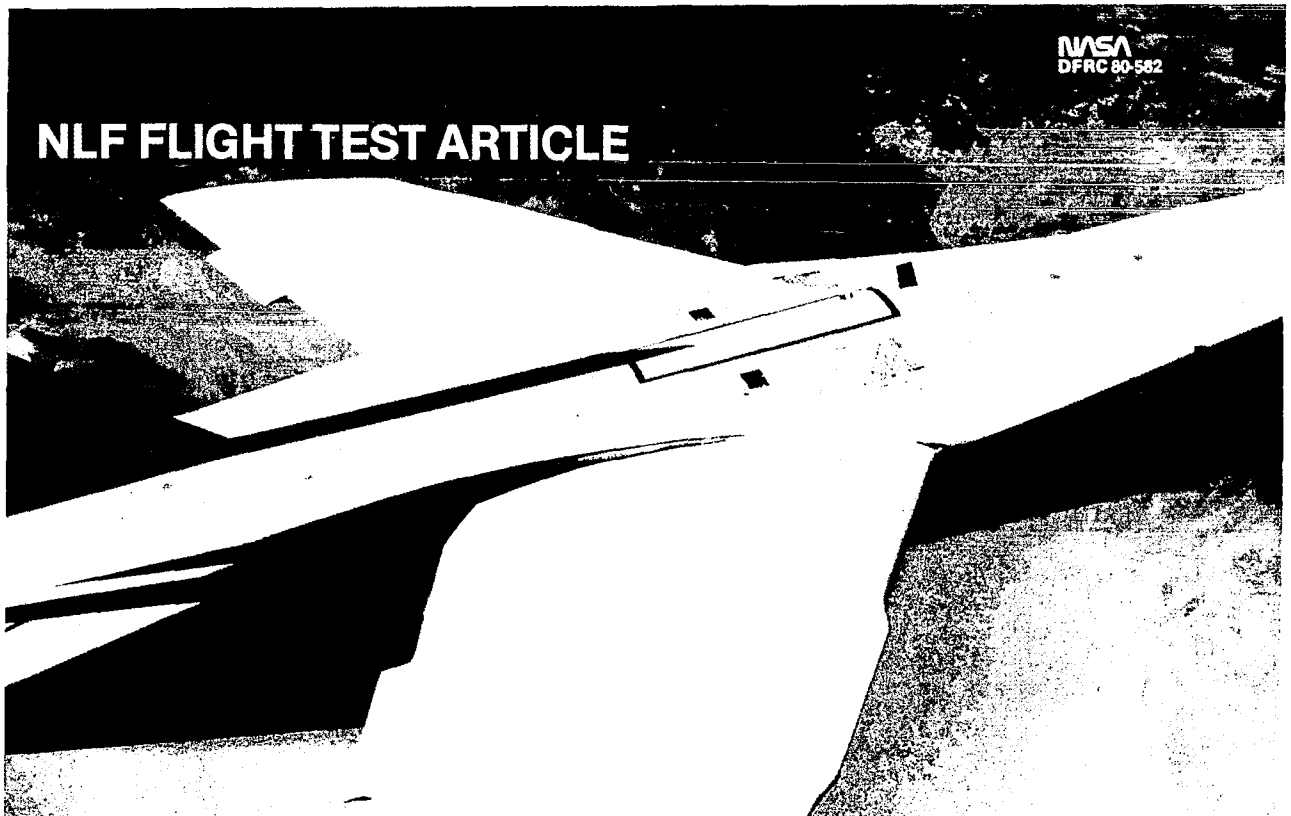
- $Re_c = 25.0 \times 10^6$
- $\bar{c} = 3.057\text{m (10.03 ft)}$
- $M_\infty = 0.81$ AT $\Lambda_{LE} = 10$ deg
- $M_\infty = 0.83$ AT $\Lambda_{LE} = 16$ deg
- $M_\infty = 0.85$ AT $\Lambda_{LE} = 26$ deg



FLIGHT TEST ARTICLE

The NLF "gloves" were fabricated on the flight vehicle using fiber glass, high density foam, microballoons, and body putty. The use of these materials aided in achieving the aerodynamically smooth surface desired for this experiment. As with the wind-tunnel model, both the left and right wings were fitted with the NLF airfoil, but only the right test section was instrumented.

The instrumentation included 15 flush surface pressure orifices, a boundary-layer rake, and transition strips on both the upper and lower surfaces. The boundary-layer rake was located at 90 percent of the chord on both surfaces. The transition strips were strategically placed at several different spanwise chord locations—one location per flight.



FLIGHT PRESSURE DISTRIBUTIONS

In-flight pressure distribution data were obtained over a matrix of Mach numbers and angles of attack in an attempt to define the flight conditions for the optimum extent of favorable pressure gradient.

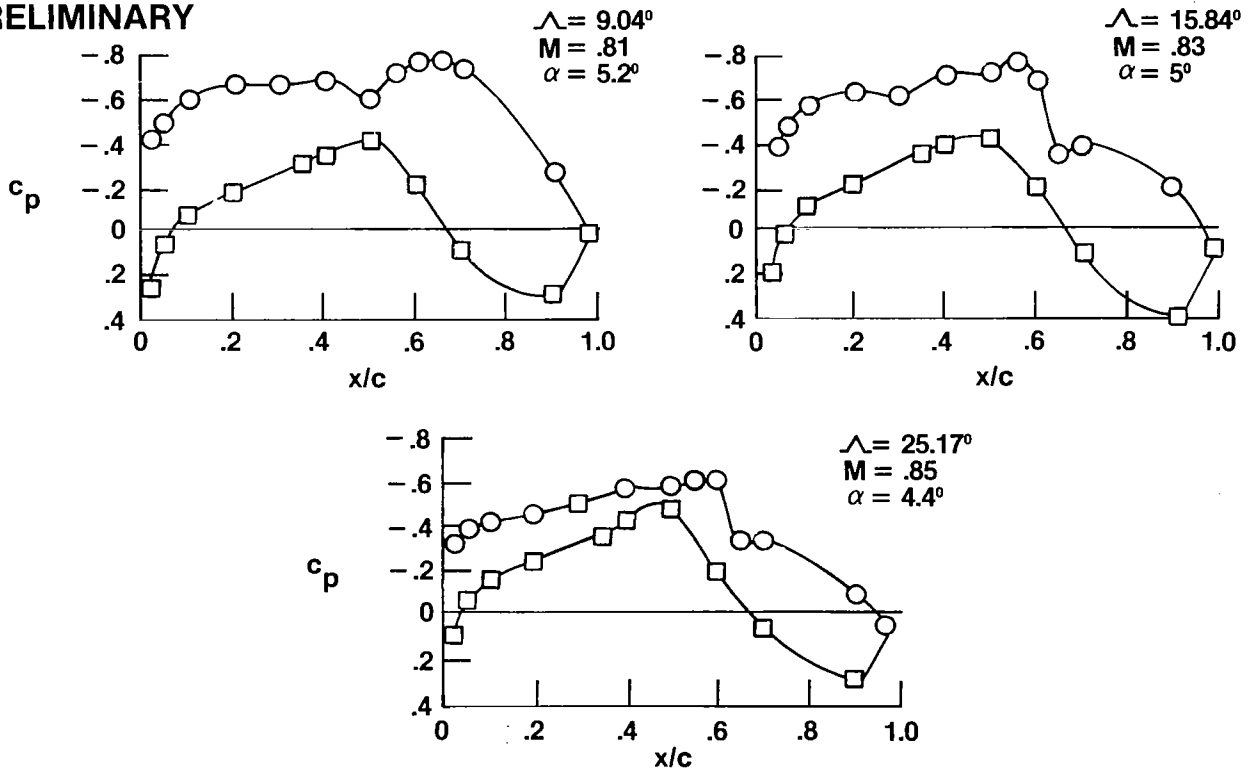
Preliminary data consistently demonstrated a significant extent of favorable pressure gradient for the same range of wing sweep angles tested in the wind tunnel.

The actual extent of laminar flow attained in flight will be determined through the study of boundary-layer profile data obtained from the upper and lower surface rakes. Fixed transition was used on some of the flights to aid in the interpretation of the boundary-layer data obtained from flights with free transition.

Preliminary analysis showed that laminar flow was maintained over a large part of the test section, but a quantitative measure of transition location could not be proclaimed at this stage of the analysis.

NLF FLIGHT PRESSURE DISTRIBUTIONS

PRELIMINARY



POTENTIAL FOLLOW-ON EFFORT

The current NLF experiment was hampered by not being conducted on a dedicated flight vehicle. A joint U.S. Air Force/NASA program (AFTI/F-111) forced termination of the NLF experiment before other factors could be assessed.

The present NLF experiment was conducted to determine the feasibility of the natural laminar flow concept for supercritical flow conditions.

Follow-on work should assess how practical the concept will be for real world operating conditions. The susceptibility of the concept to fabrication tolerances, operational blemishes, contamination, and moisture should be determined. An assessment should also be made of the requirement for leading-edge protection and maintenance. Any follow-on work deserves a dedicated test bed facility.

RECOMMENDATIONS

STUDY NATURAL LAMINAR FLOW PHENOMENA ON A DEDICATED BED FACILITY TO

- DETERMINE SENSITIVITY OF TRANSITION TO
 - SURFACE MATERIAL, MOISTURE, CONTAMINATION, ETC.
 - SURFACE DETERIORATION FROM OPERATIONAL BLEMISHES
 - SURFACE FABRICATION TOLERANCES
- DETERMINE REQUIREMENTS FOR
 - SURFACE MAINTENANCE
 - LEADING-EDGE PROTECTION

KC-135 WINGLET FLIGHT RESULTS

Lawrence C. Montoya
NASA Dryden Flight Research Center

ABSTRACT

Winglets are small, nearly vertical aerodynamic surfaces which are designed to be mounted at the tips of aircraft wings. They are found in nature on all soaring birds who cant their tip feathers when attempting to achieve a high-lift flight condition.

Design optimization studies and wind-tunnel tests led by Richard Whitcomb of the NASA Langley Research Center have shown that these extensions can produce significant increases in the lift-to-drag ratios on some of today's transport aircraft. The application of winglets to the U.S. Air Force (USAF) KC-135 tanker aircraft is predicted to increase its cruise lift-to-drag ratio by 8 percent. This increase would result in an average fuel savings of 227.1 kiloliters per airplane per year. If retrofitted to the KC-135 fleet, more than a billion dollars worth of fuel could be saved over the next 20 years. Therefore, the USAF and NASA have embarked on a joint program to obtain a full-scale evaluation of winglets on the KC-135 aircraft. The Boeing Company, under USAF contract, has constructed a set of flight-test winglets. NASA Dryden Flight Research Center has instrumented a test airplane.

To date, three KC-135 winglet configurations have been flight tested for cant/incidence angles of $15^\circ/-4^\circ$, $15^\circ/-2^\circ$, and $0^\circ/-4^\circ$, as well as the basic wing. The flight results for the $15^\circ/-4^\circ$ and basic wing configurations confirm the wind-tunnel-predicted 7-percent incremental decrease in total drag at cruise conditions. The $15^\circ/-4^\circ$ configuration flight-measured wing and winglet pressure distributions, loads, stability and control, flutter, and buffet also correlate well with predicted values. The only unexpected flight result as compared with analytical predictions is a flutter speed decrease for the $0^\circ/-4^\circ$ configuration.

The $15^\circ/-2^\circ$ configuration results show essentially the same incremental drag reduction as the $15^\circ/-4^\circ$ configuration; however, the flight loads are approximately 30 percent higher for the $15^\circ/-2^\circ$ configuration. The drag data for the $0^\circ/-4^\circ$ configuration show only a slight drag reduction.

Present planning through October, which is the projected flight program completion date, will complete the range factor testing for the above configurations. These range factor flights are being performed to fulfill a primary Air Force objective to obtain hard data for the proposed fleet retrofit. Two flutter flights have been proposed for a $7.5^\circ/-4^\circ$ configuration to obtain some insight into the structural dynamics anomaly found at the $0^\circ/-4^\circ$ configuration.

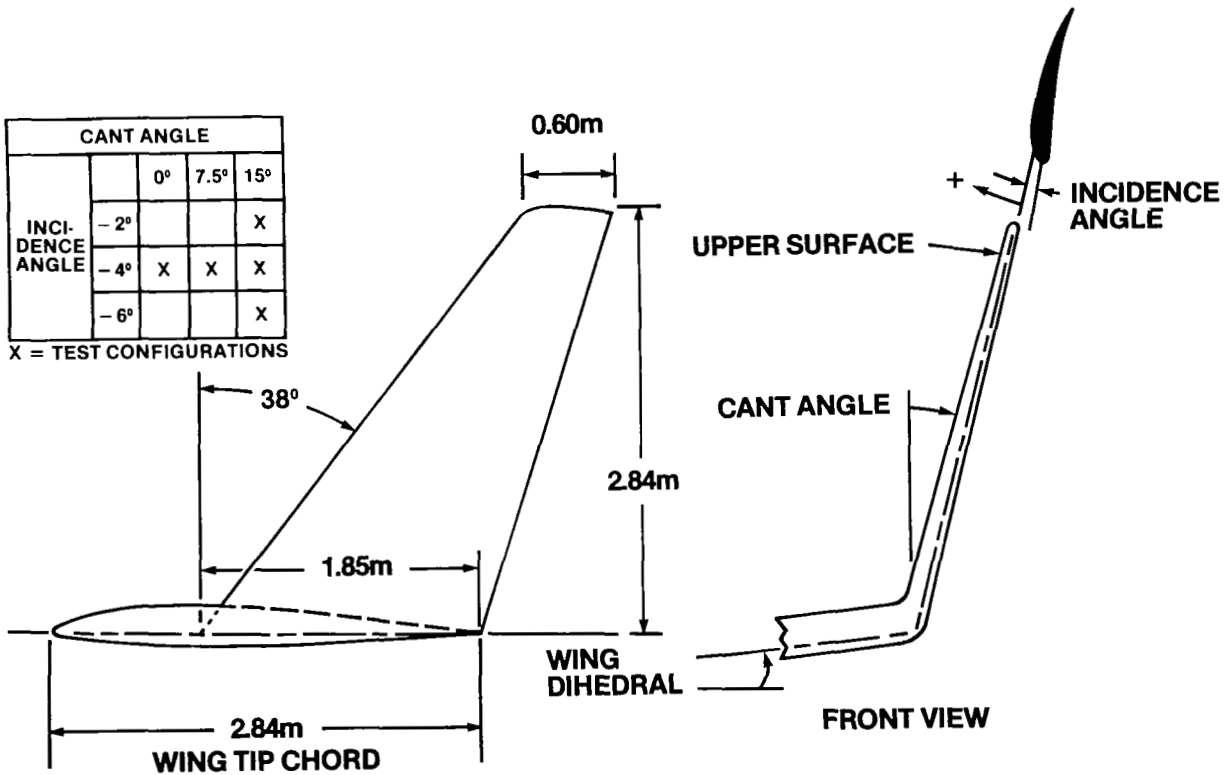
PROGRAM OBJECTIVES

The primary objective of the KC-135 winglet flight program was to define the full-scale performance gains provided by winglets for comparison with wind-tunnel test results. To accomplish this, the airplane was instrumented to measure wing and winglet pressure distributions, total lift and drag, loads, stability and control, flutter, buffet, and range factor. The test conditions covered the Mach number range from 0.30 to 0.82 at altitudes between 10,363 meters and 11,887 meters. The test winglets were designed to investigate a matrix of cant/incidence angles. The design test condition was $M = 0.78$ and $C_{L} = 0.42$ for a $15^{\circ}/-4^{\circ}$ winglet configuration.



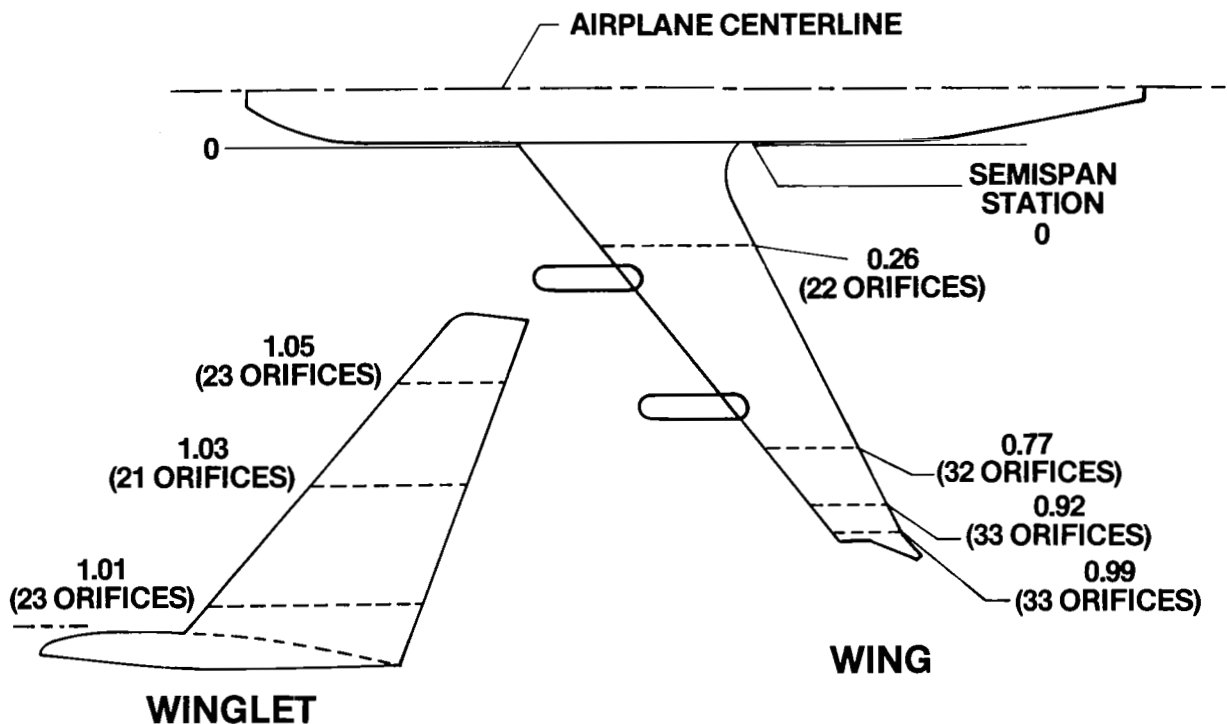
WINGLET GEOMETRIC CHARACTERISTICS

The test winglet consisted of an 8-percent thick General Aviation Airfoil and was designed to be tested over a matrix of cant/incidence angles. It had a span of 2.83 meters, a tip chord of 0.60 meter, and a leading-edge sweep angle of 38° . This geometry was derived from the wind-tunnel model coordinates with the exception of some slight wing/winglet juncture fairing differences, which resulted from the addition of the cant/incidence angle mounting hardware to the flight winglets.



WING AND WINGLET PRESSURE ORIFICE LOCATIONS

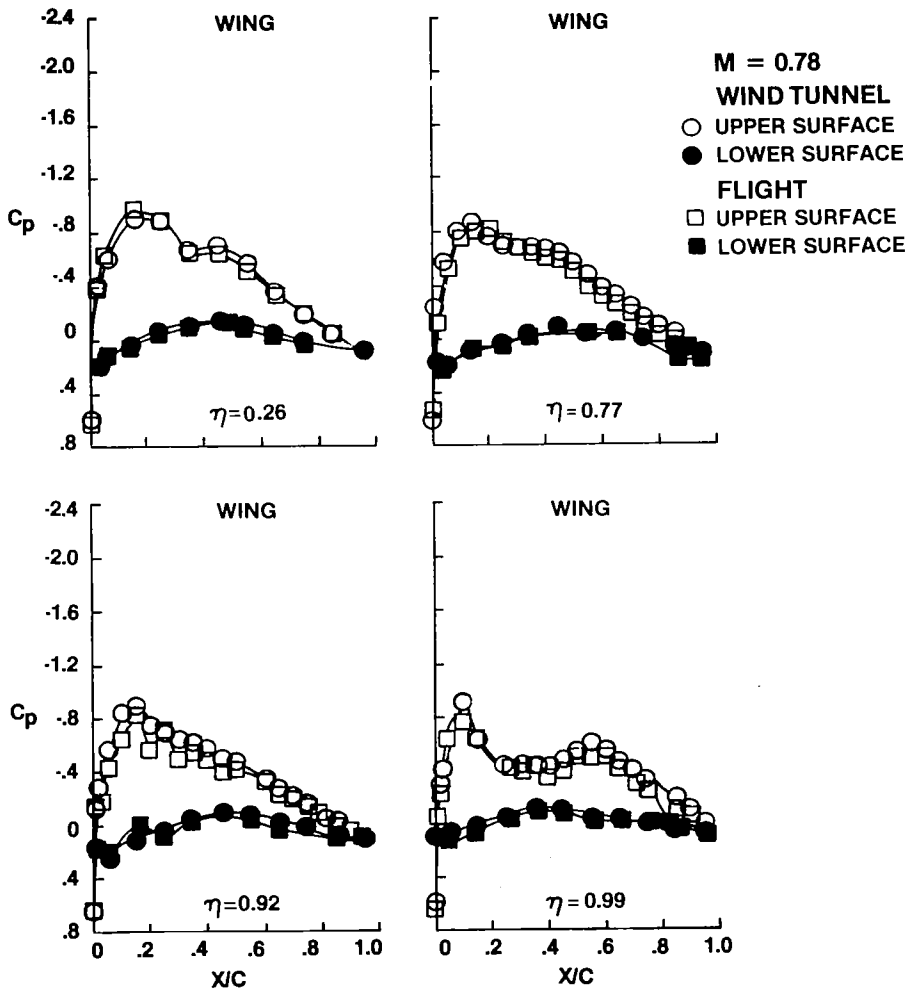
Wing and winglet pressure distributions were obtained along four orifice rows on the wing (semispan stations 0.26, 0.77, 0.92, and 0.99) and three orifice rows on the winglet (semispan stations 1.01, 1.03, and 1.05). The number of orifices per row varied from 22 to 33 on the wing and from 21 to 23 on the winglet. All wing orifices except leading-edge orifices were externally mounted; all winglet orifices were mounted flush. The orifice row locations and the number of orifices were essentially the same for the wind-tunnel model and the full-scale airplane.



WING PRESSURE DISTRIBUTIONS

At the design test condition of Mach 0.78 and angle of attack of approximately 2° , the flight and wind-tunnel wing pressure distributions show good agreement. Small differences between the measurements of various rows could be attributed to the airplane surface conditions and the fact that the orifices were externally mounted.

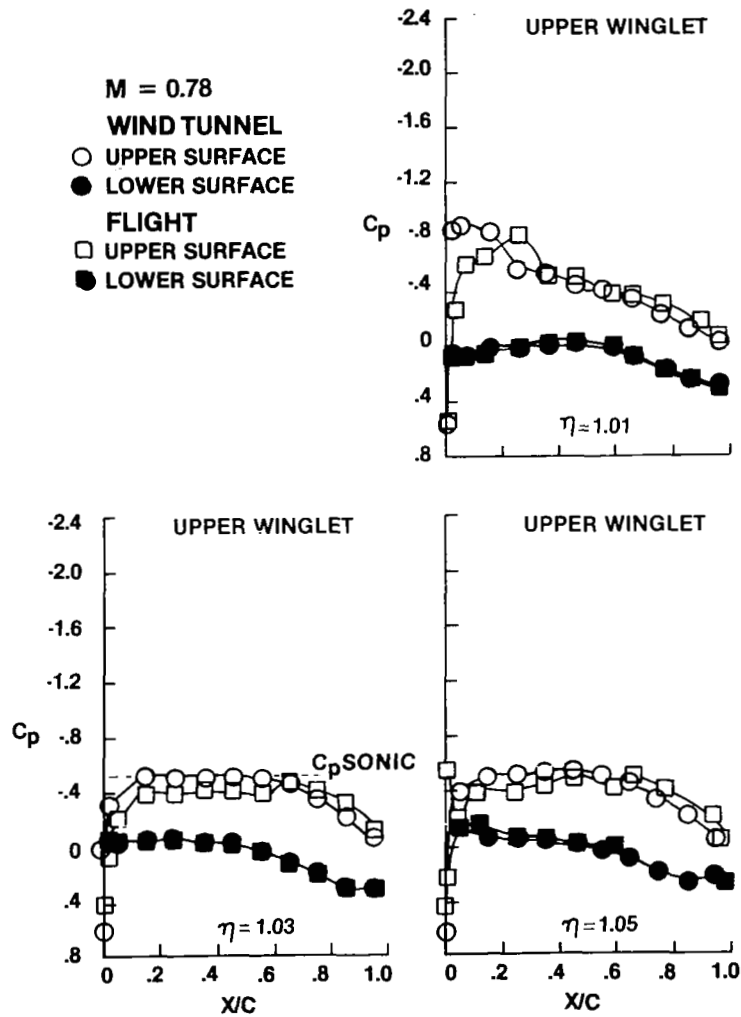
In general, the flight and wind-tunnel pressure distributions showed good agreement at all the conditions tested.



WINGLET PRESSURE DISTRIBUTION

At winglet semispan station 1.01 (winglet span station 0.15) and the design test condition, flight and wind-tunnel pressure distributions show significant differences on the upper surface near the leading edge. These differences are attributed to "oilcanning" (skin deflection) which occurred in flight in this area. Distributions for the remainder of the station show good agreement.

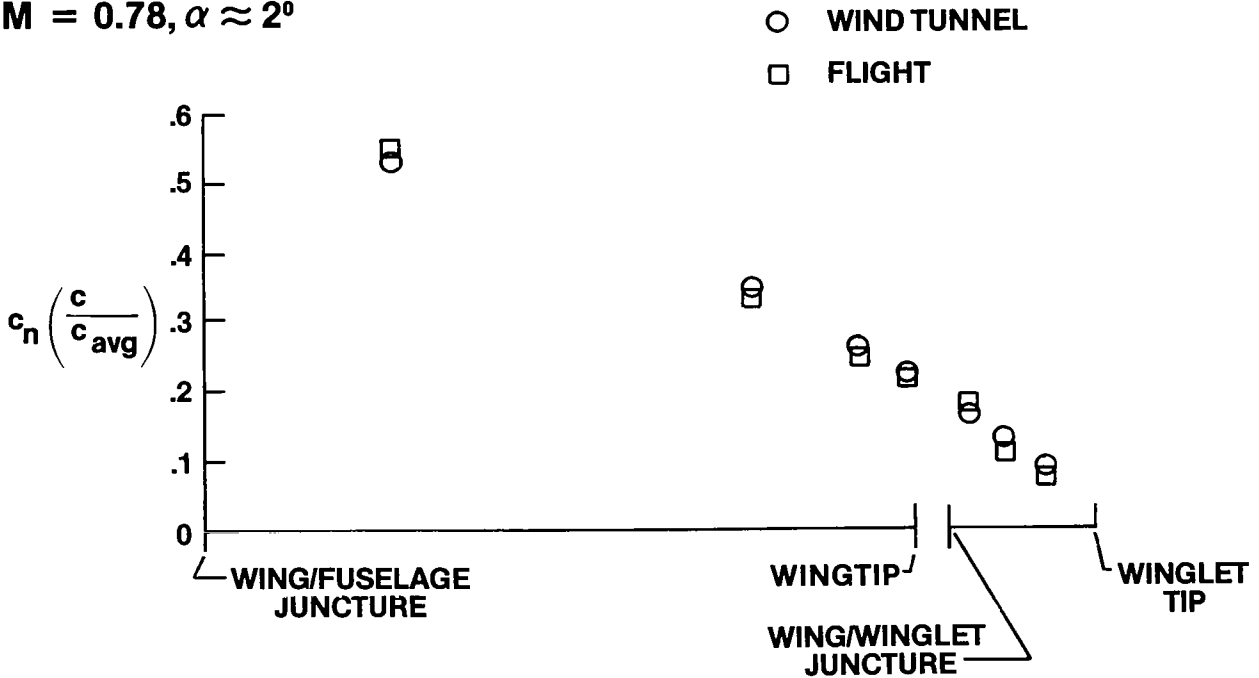
At semispan stations 1.03 and 1.05 (winglet span stations 0.50 and 0.90, respectively) the lower surface flight and wind-tunnel pressure distributions show good agreement; however, differences are noted in the data for the upper surface along the entire chord. These differences are also attributed, at least in part, to "oilcanning." Apart from the "oilcanning," which would not necessarily occur on a production winglet design, flight and wind-tunnel winglet pressure distributions show good agreement.



WING AND WINGLETS SPAN LOAD DISTRIBUTION

The flight and wind-tunnel model span load distribution at the design test condition show good agreement. These data are typical of the results obtained at other test conditions indicating that the semispan model provided a good simulation of the full-scale wing deflections.

$M = 0.78, \alpha \approx 2^\circ$

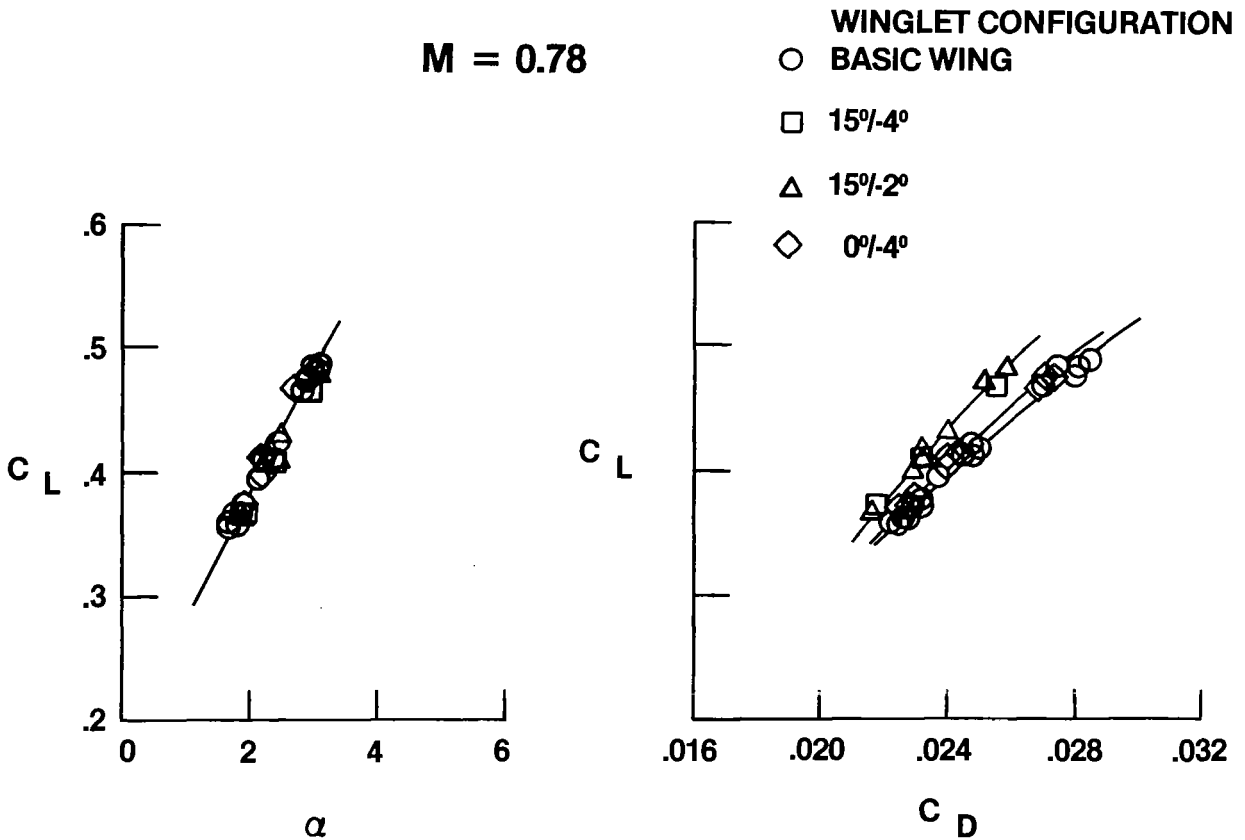


LIFT AND DRAG

Lift and drag data were obtained by measuring gross thrust and ram drag, normal and longitudinal accelerations at the aircraft center of gravity, and appropriate air data parameters.

For all Mach numbers tested, the trends in the data are the same as for the design Mach number. Installation of the winglets does not influence the lift curve slopes. All winglet configurations show a decrease in drag coefficient at a given lift coefficient when compared to the basic wing configuration. The largest decrease in drag coefficient was provided by the $15^\circ/-4^\circ$ and the $15^\circ/-2^\circ$ configurations. The $0^\circ/-4^\circ$ configuration decreases the drag coefficient only slightly.

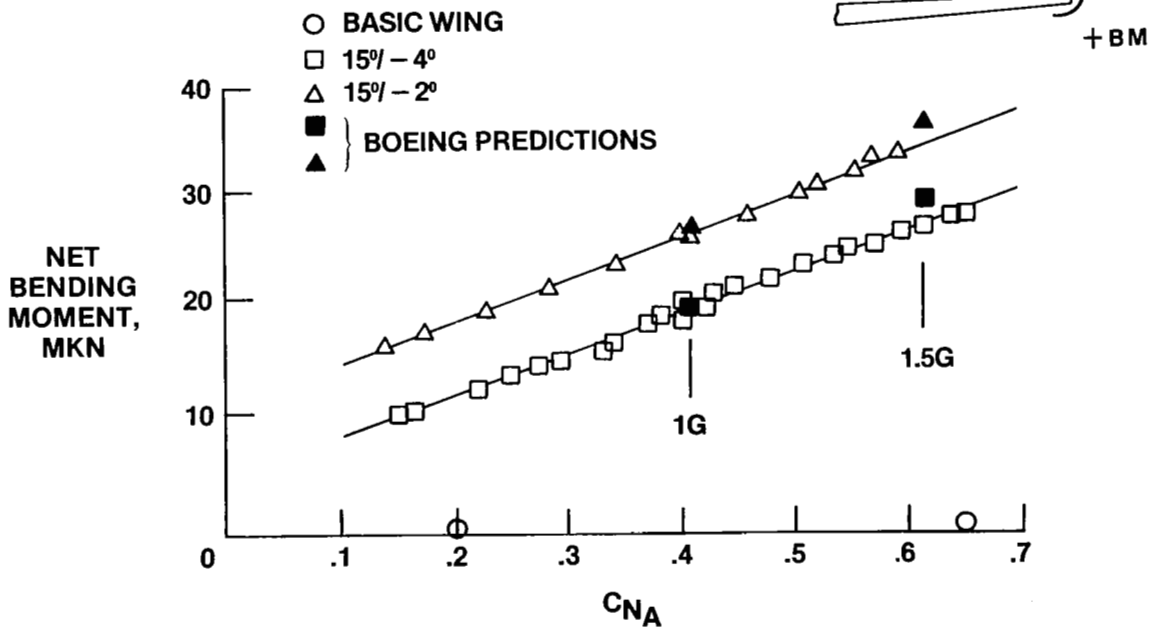
For Mach numbers greater than 0.70, the data show the drag reduction between winglet configurations and basic wing configuration to increase with increasing lift coefficient.



WING/WINGLET JUNCTURE BENDING MOMENT LOADS

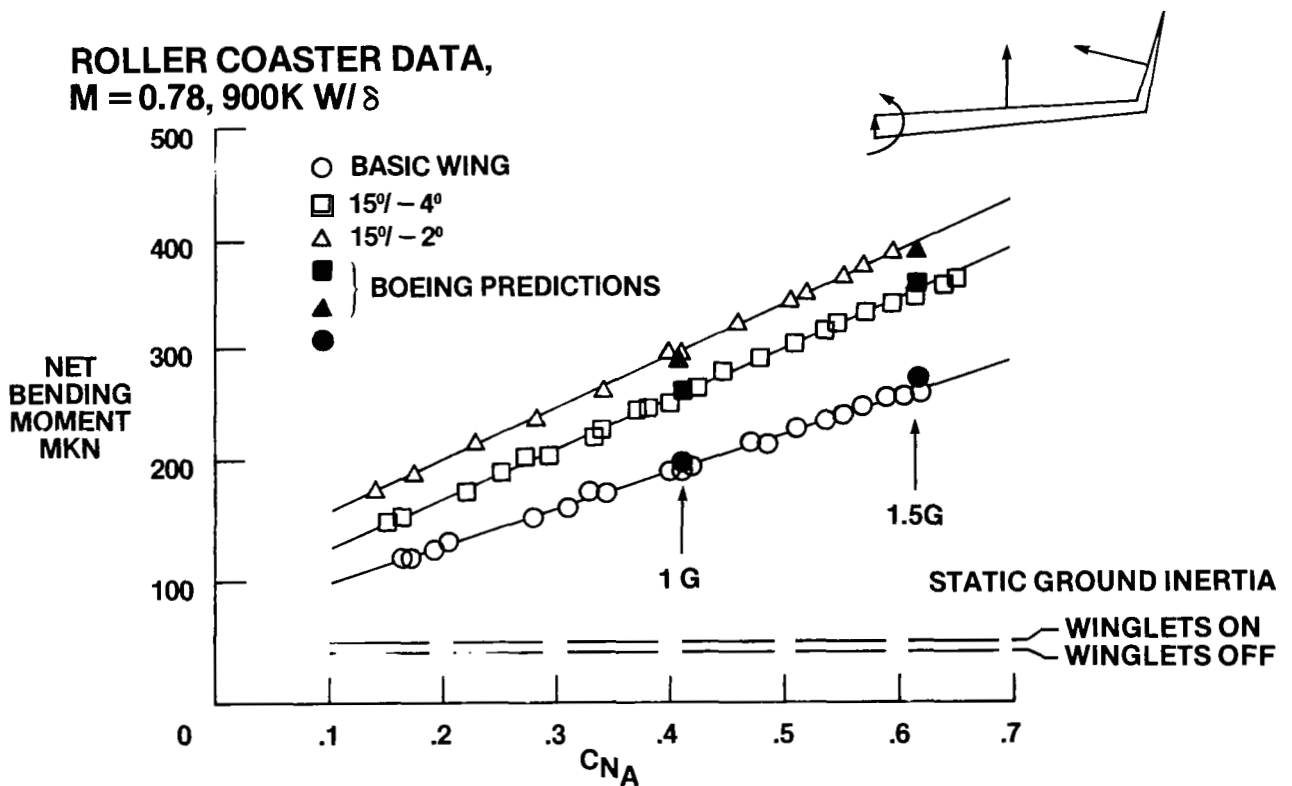
The flight wing/winglet juncture bending moment loads as a function of airplane normal force coefficient were compared with Boeing aeroelastic prediction data at the design test condition. The airload at 1 g for the 15°/-2° winglet configuration is about 34 percent higher than the 15°/-4° configuration, indicating the desirability of the 15°/-4° configuration. A comparison of the flight data with the Boeing prediction data shows good agreement at the 1 g condition, but predictions are somewhat higher than flight data at the 1.5 g condition.

ROLLER COASTER DATA, $M = 0.78, 900K W/\delta$



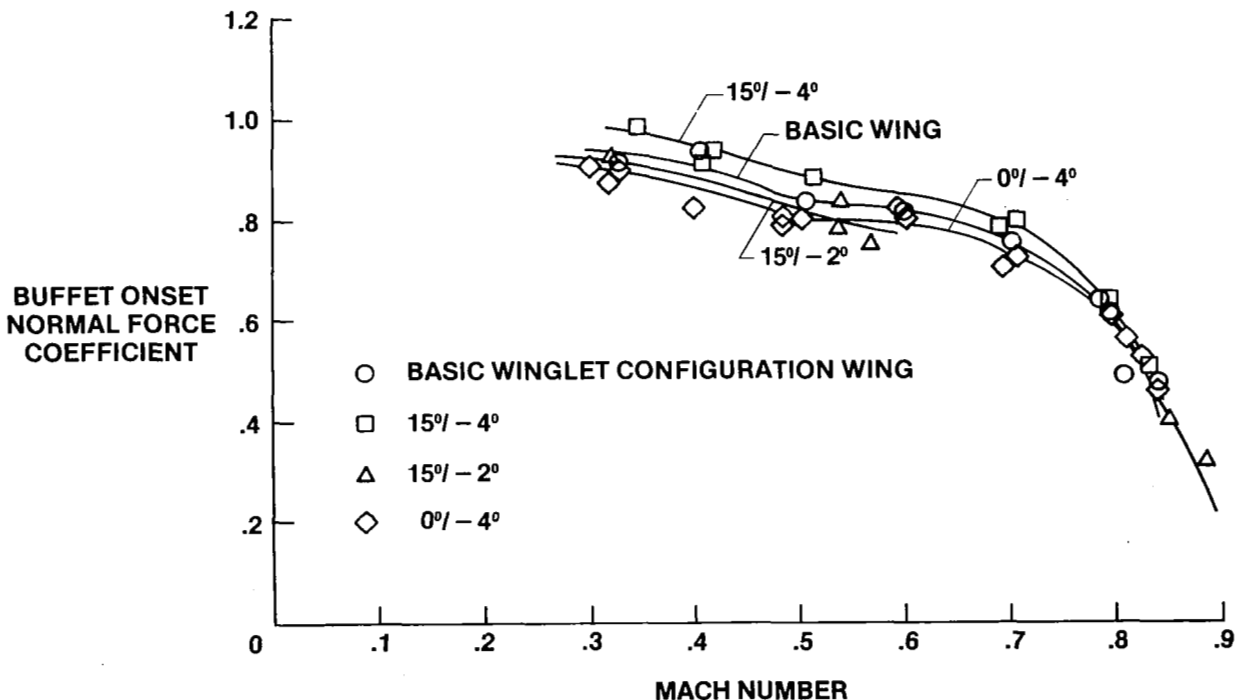
OUTBOARD WING BENDING MOMENT LOADS

The flight wing bending moment loads measured at the outboard wing station as a function of airplane normal force coefficient were compared with Boeing aeroelastic prediction data at the design test condition. At 1 g, the 15°/-4° configuration shows a 32-percent increase in airload over the basic wing while the 15°/-2° configuration exceeds the basic wing by 50 percent. Comparison between the measured flight loads and the Boeing prediction data is considered quite good at both 1 g and 1.5 g. The average bending stresses measured at the wing root for the design winglet configuration (not shown) were only 2.5 percent higher than the basic wing stresses.



BUFFET CHARACTERISTICS

Buffet characteristics were assessed by analyzing the output of high frequency response accelerometers mounted in the cockpit on the elastic axis of the left and right wingtips at the left and right winglet tips and left and right horizontal tail tips. Both buffet onset boundaries and buffet intensity rise characteristics have been compared between winglet configurations $15^\circ/-4^\circ$, $15^\circ/-2^\circ$, and $0^\circ/-4^\circ$ and the basic wing. The winglets produced only minor variations in the basic wing buffet onset boundary at low subsonic speeds and no significant differences in the cruise Mach number region. Intensity rise characteristics were essentially invariant with winglet configuration. The winglets produced no significant changes in the cockpit and horizontal tail accelerometer outputs.



SUMMARY

The KC-135 winglet flight program has shown the following results to date: the wind-tunnel-predicted 7-percent drag reduction was confirmed, the wing and winglet wind-tunnel and flight pressure distributions show good agreement, the predicted and measured flight loads show good agreement, and the winglets produced only minor variations in the buffet onset boundary at low subsonic speeds and no significant differences in the cruise Mach number region.

At present, additional range factor flights are in progress with an expected flight program completion date of October 1980.



OVERVIEW OF ADVANCED WING DESIGN

Raymond M. Hicks

NASA Ames Research Center

ABSTRACT

Several recent examples of experiment-theory correlation are presented to give an indication of the capabilities and limitations of wing design and analysis for transonic applications by potential-flow theory. The examples include correlations of experimental pressure distributions with theoretical results from isolated wing codes and wing-body codes. Both conservative and non-conservative differencing as well as body and boundary layer corrections are considered. The results show that a full potential isolated wing code correlates well with data from an isolated wing test but may give poor prediction of the aerodynamic characteristics of some wing-body configurations. Potential-flow wing body codes were found to improve the correlation for the wing-body configurations considered.

ISOLATED WING WIND TUNNEL MODEL

The swept wing shown in Figure 1 was tested in the Ames 12-foot pressure tunnel at Mach .8 and at Reynolds number of 2 million based on the M.A.C. (ref. 1). The model was mounted on the tunnel wall and hence is useful for evaluating isolated wing codes.

$S = 0.77M^2$ (8.283 ft²)
 $AR = 6.04$
TAPER RATIO = 0.5
NACA 64₁ - 212 SECTION
NORMAL TO L.E.
 $b/2 = 1.52M$ (5 ft)

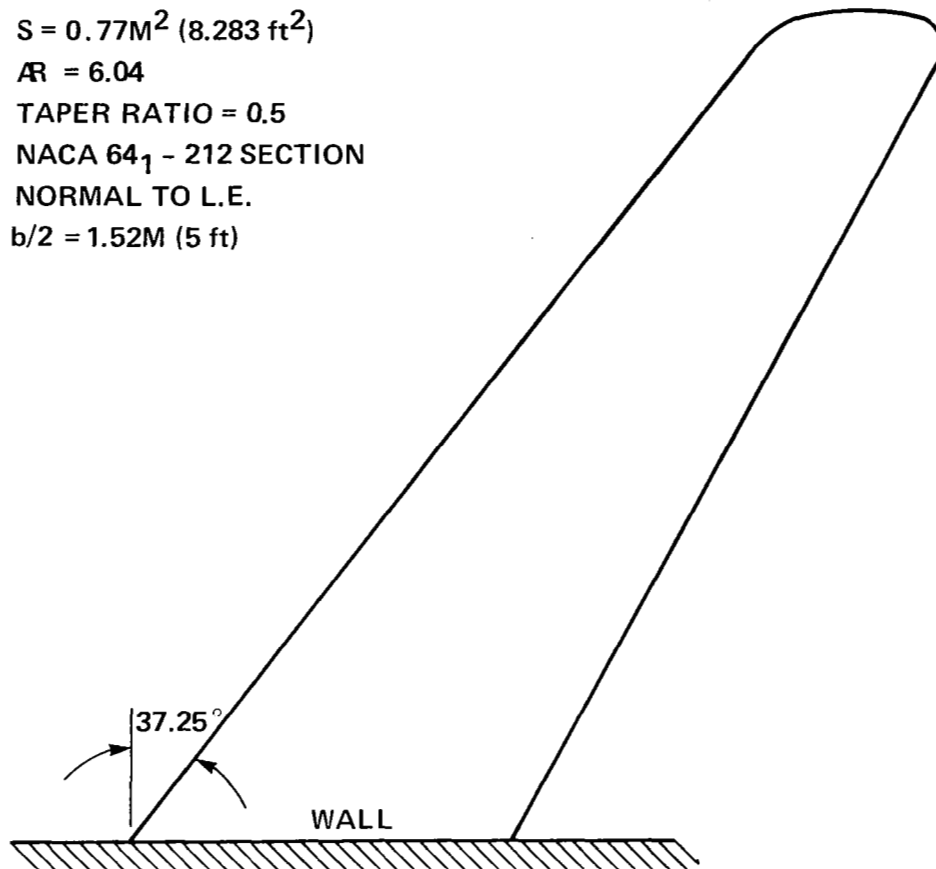


Figure 1

EXPERIMENT-THEORY CORRELATION FOR AN ISOLATED WING

The experiment-theory correlation for the isolated wing is shown in Fig. 2. The code FLO22NM solves the transonic potential equation in non-conservative form with an iterated Nash-McDonald boundary layer correction. The boundary layer subroutine was coupled with FLO22 by P. A. Henne of Douglas Aircraft Company. The results shown in the figure indicate that good experiment-theory correlation of wing pressures can be expected for most isolated wings with 6-series sections at span stations greater than $\eta \sim .15$. The correlation might be expected to be less satisfactory at span stations closer to the wall due to the close proximity to the tunnel wall boundary layer.

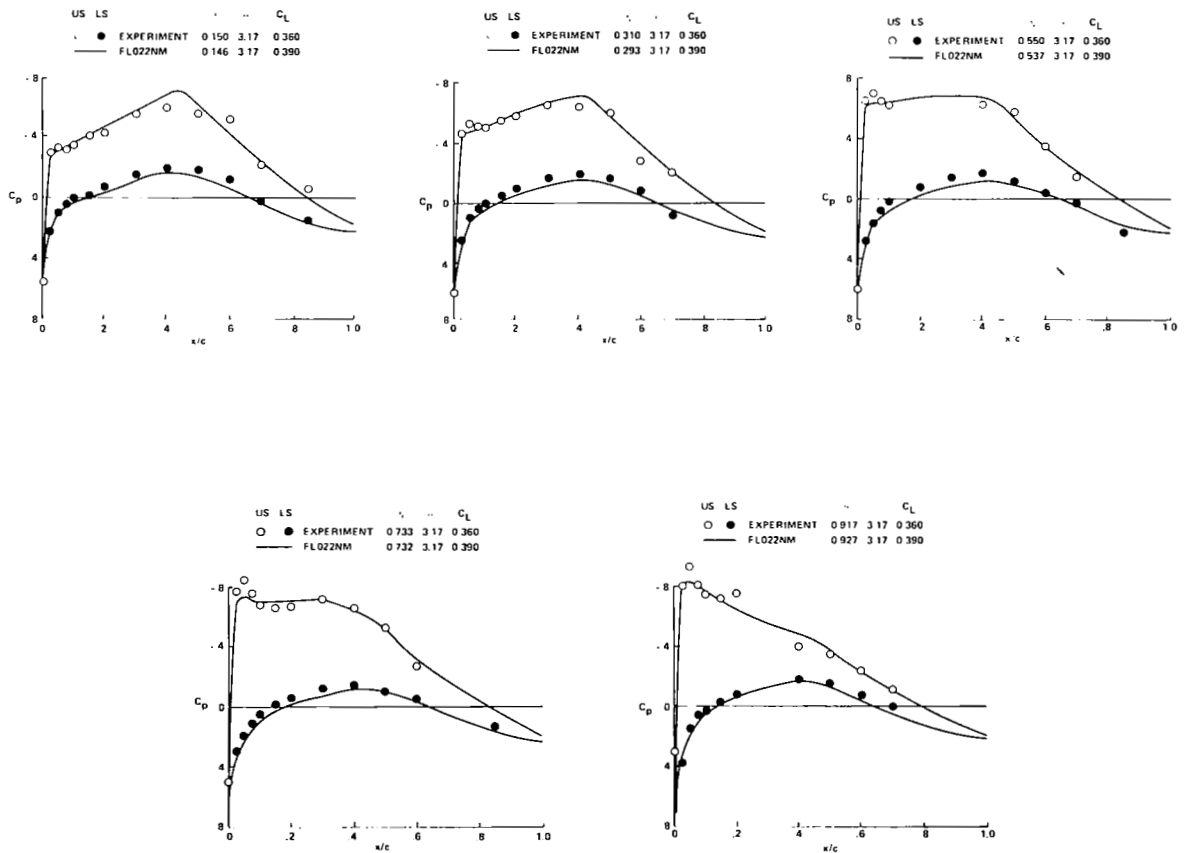


Figure 2

VOUGHT A-7 FIGHTER WIND TUNNEL MODEL

A model of the Vought A-7 fighter was tested in the Ames 11-foot transonic wind tunnel to evaluate the capability of FLO22 to predict the surface pressures for a low aspect ratio wing mounted in the high position on a low fineness ratio body. A sketch of the wind tunnel model is shown in Figure 3. The wing has an average thickness of 12 percent of the chord.

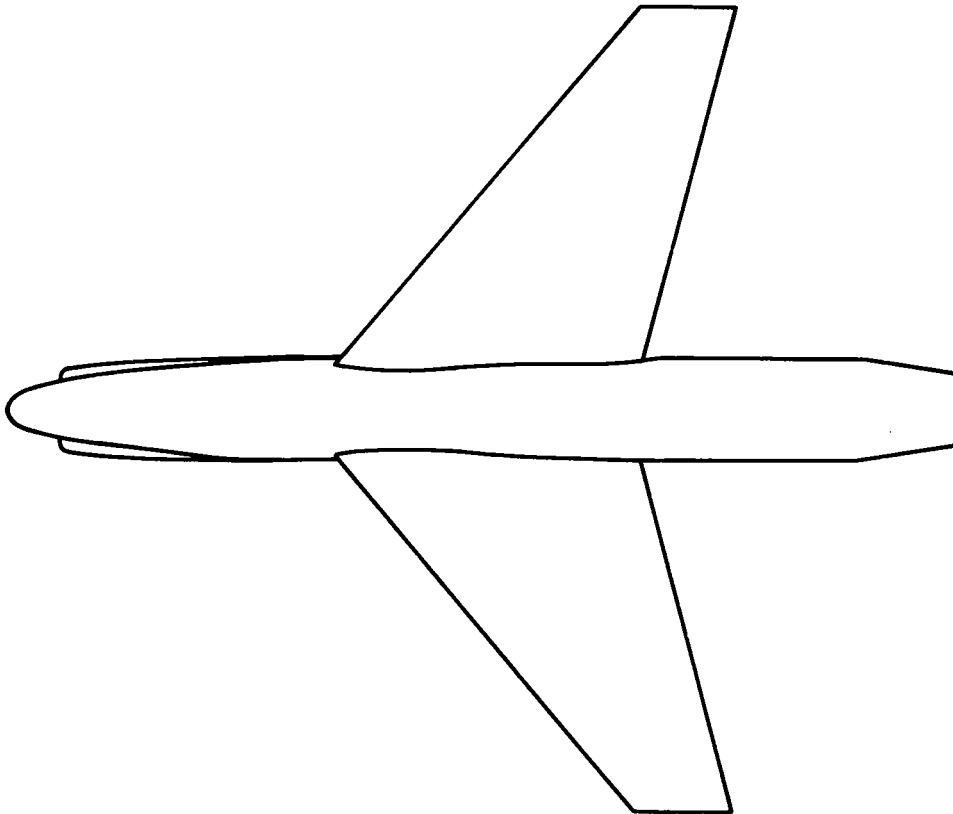


Figure 3

EXPERIMENT-THEORY CORRELATION FOR THE A-7 FIGHTER

The experiment-theory correlation for the A-7 fighter at Mach .85 and a Reynolds number of 8.7 million is shown in Figure 4. Note that FLO22 predicts a shock position which is farther forward than the experiment at all span stations. The FLO22 calculation includes a passive boundary layer correction but no body correction.

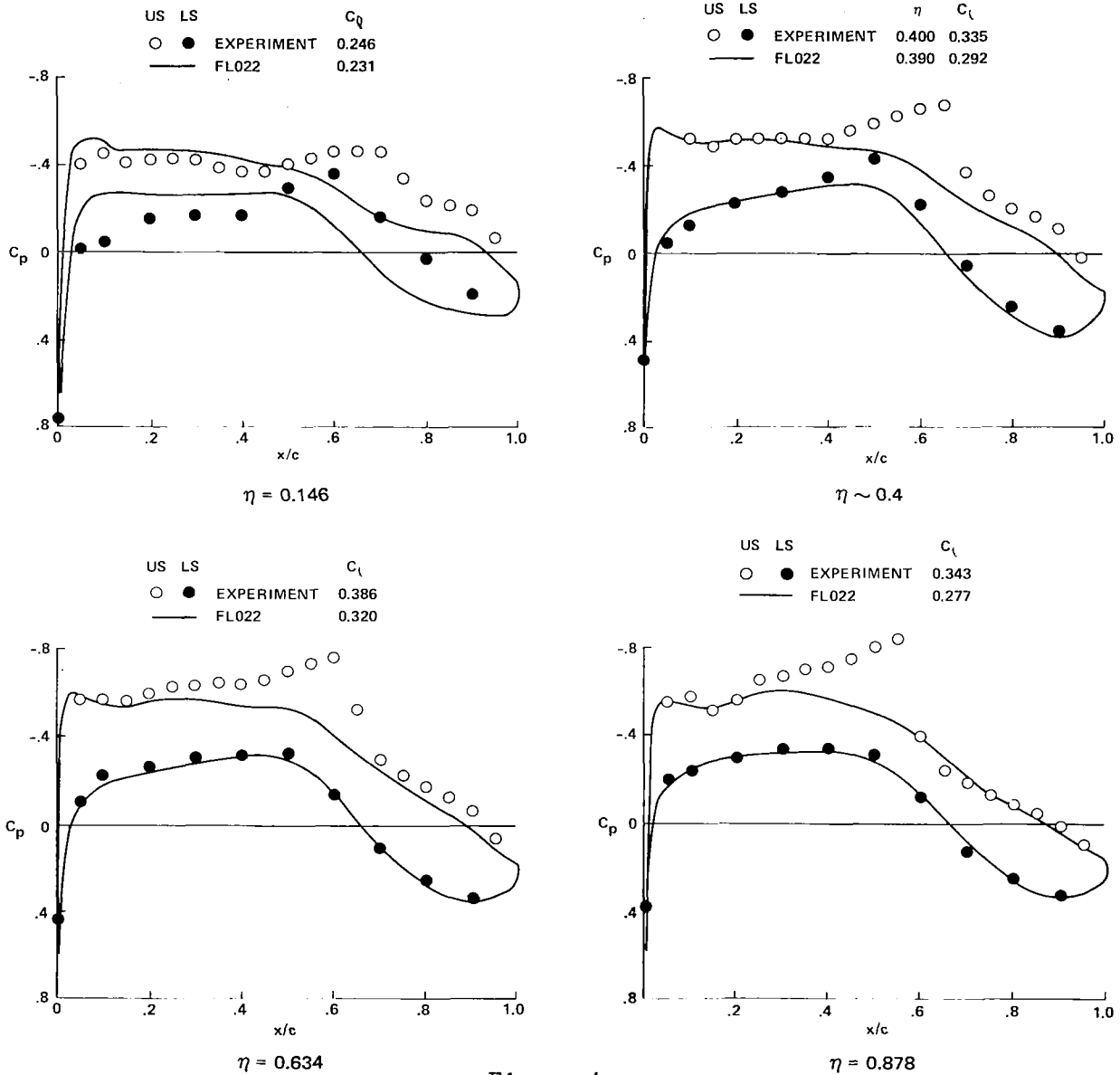


Figure 4

TRANSONIC WING-BODY WIND TUNNEL MODEL

The wind tunnel model shown in Figure 6 was tested in the Ames 14-foot transonic wind tunnel. This configuration has been included to show that the results shown previously for the A-7 fighter are not peculiar to high wing, low aspect ratio fighter aircraft.

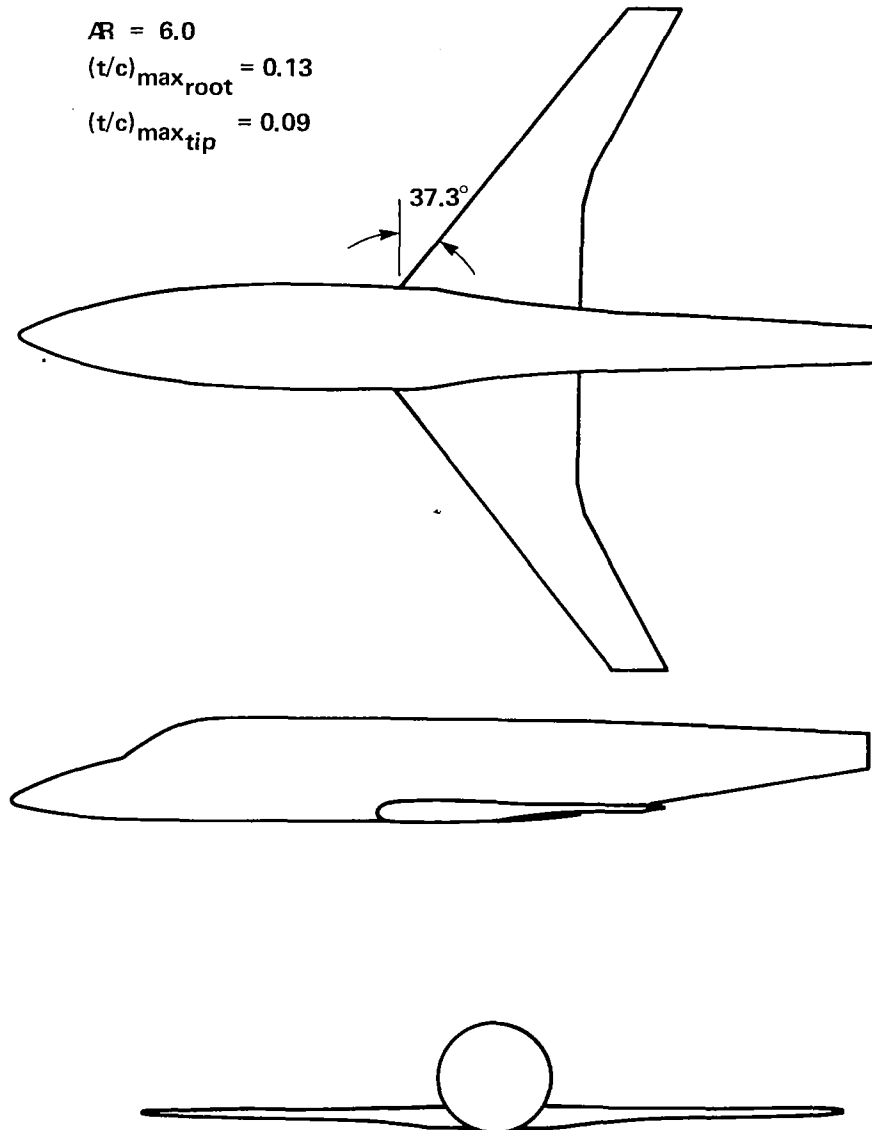


Figure 6

EXPERIMENT-THEORY CORRELATION FOR A TRANSONIC WING-BODY

A comparison of experimental wing pressures with those predicted by FL022 for Mach .8 and a Reynolds number of 2.3 million is shown in Figure 7 for a transonic wing-body configuration. The calculations included an iterated boundary layer correction and a twist distribution determined by a panel code analysis to correct for body effects. The poor correlation at the inboard stations indicates an inadequate body correction.

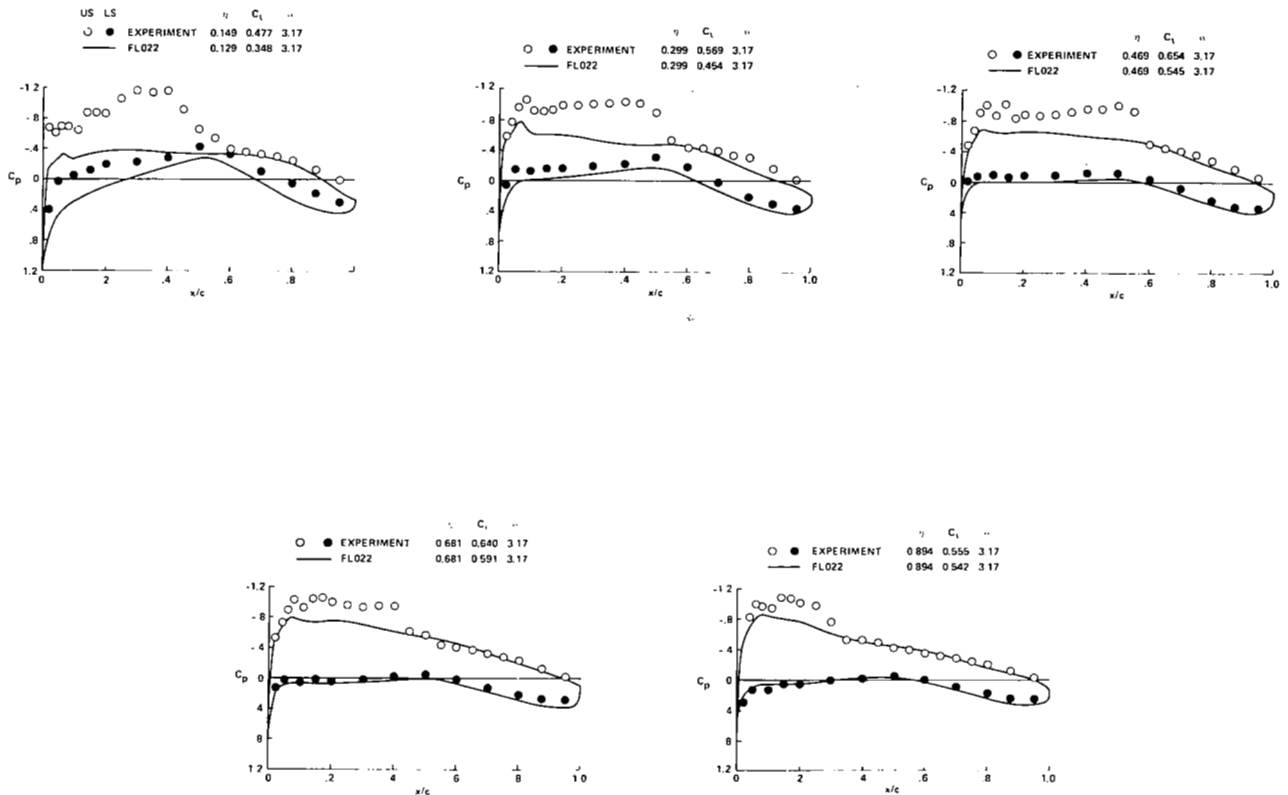


Figure 7

EXPERIMENT-THEORY CORRELATION FOR A TRANSONIC WING-BODY

The experimental pressures for the transonic wing-body configuration are compared with calculations from the wing-body code, FL030, in Figure 8. Note that the correlation is substantially improved over that observed with FL022 in Figure 7, particularly for the inboard stations.

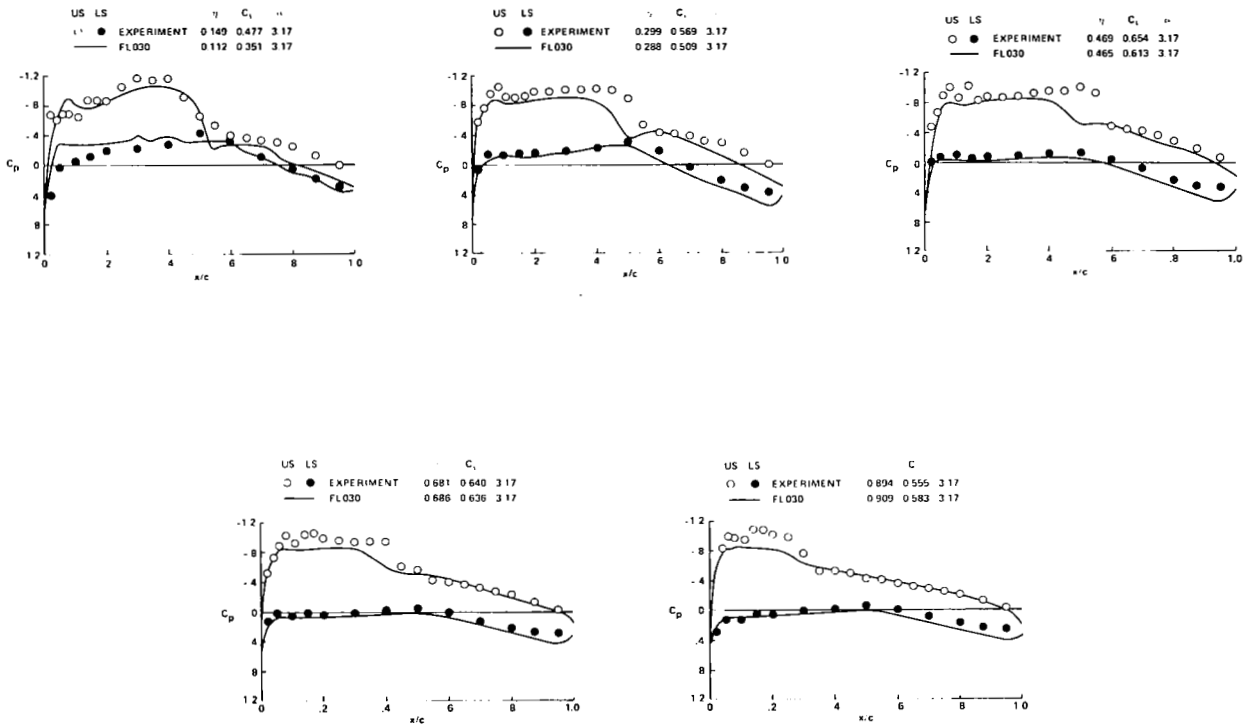


Figure 8

TRANSONIC BIZ-JET WIND TUNNEL MODEL

Tests of the transonic biz-jet configuration shown in Figure 9 permitted an evaluation of the ability of the wing-body code, FL028, to predict the effect of body mounted engines on the wing pressure distribution.

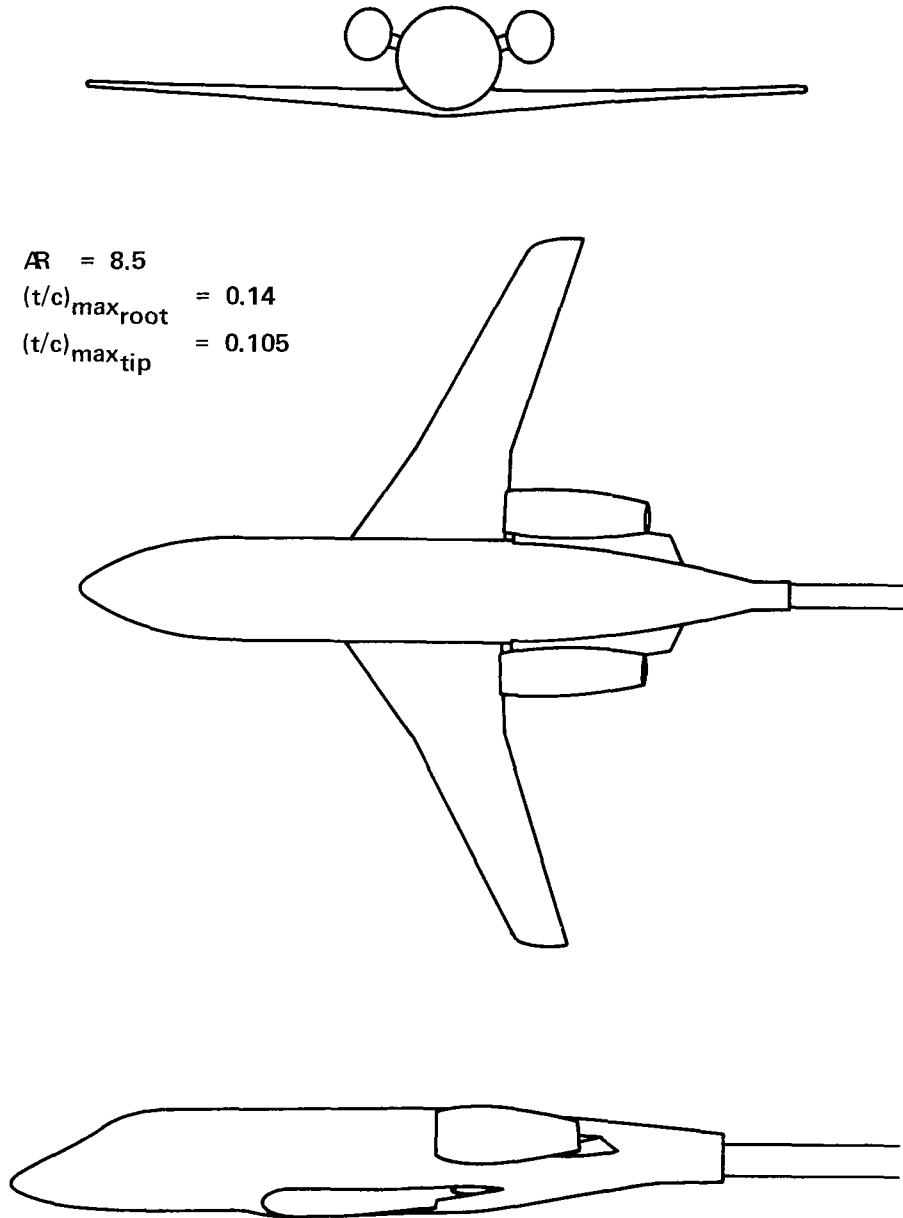


Figure 9

TRANSONIC BIZ-JET MATHEMATICAL MODEL

The mathematical model used to describe the transonic biz-jet configuration for input to FLO28 is shown in Figure 10. The engine installation was simulated by a large "bump" on the side of the body with a cross-sectional area equal to the engine plus pylon minus capture area.

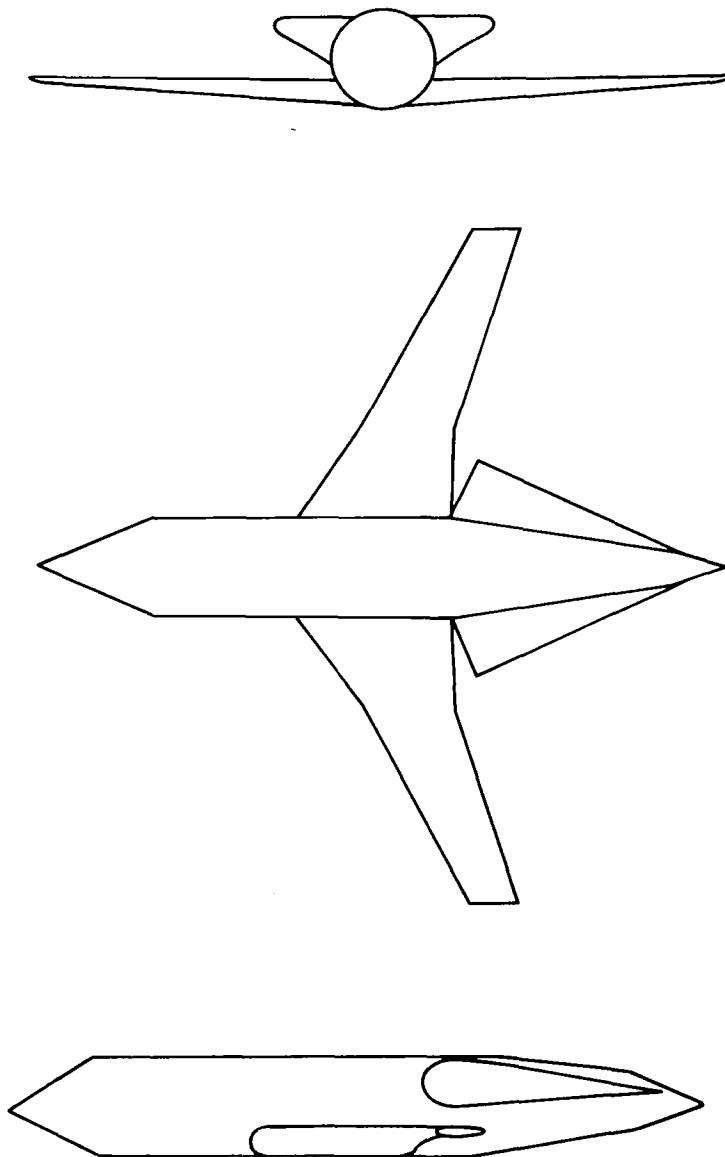


Figure 10

EXPERIMENT-THEORY CORRELATION FOR A TRANSONIC BIZ-JET

The experimental and theoretical pressure distributions with and without the engine installation are shown in Figure 11. The predicted pressures show the correct trend with engine installation but the magnitude of the effect is underestimated.

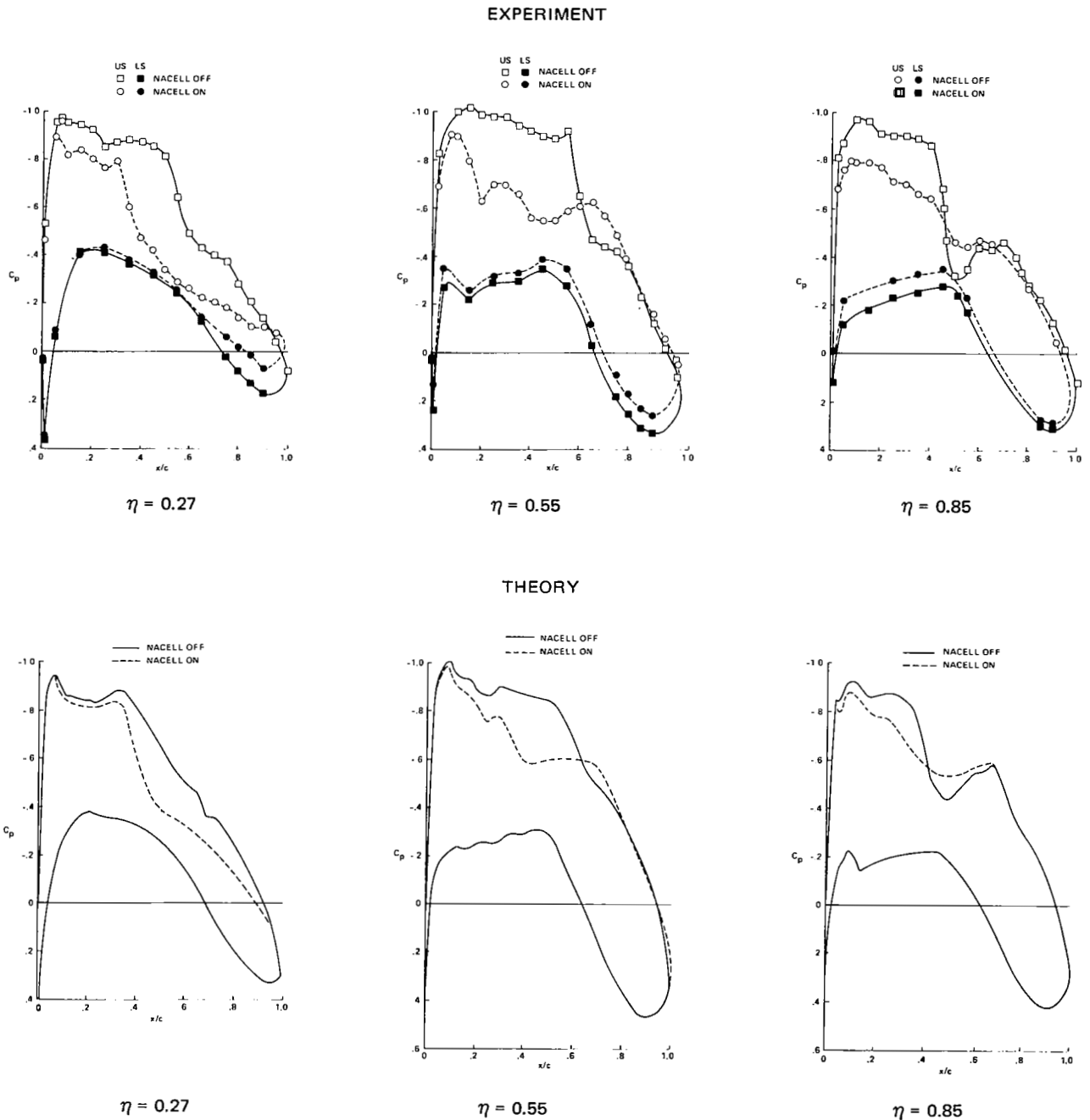


Figure 11

REFERENCE

1. Edwards, George G.; and Boltz, Fredrick W.: An Analysis of the Forces and Pressure Distribution on a Wing with the Leading Edge Swept Back 37.25° . NACA RM A9K01, Mar. 1950.



ADVANCED TURBOPROP INSTALLATION AERODYNAMICS

R. C. Smith
NASA Ames Research Center

PROBLEM DEFINITION

The expected aerodynamic effects of a propfan installed on a thick supercritical wing are summarized qualitatively on this figure.

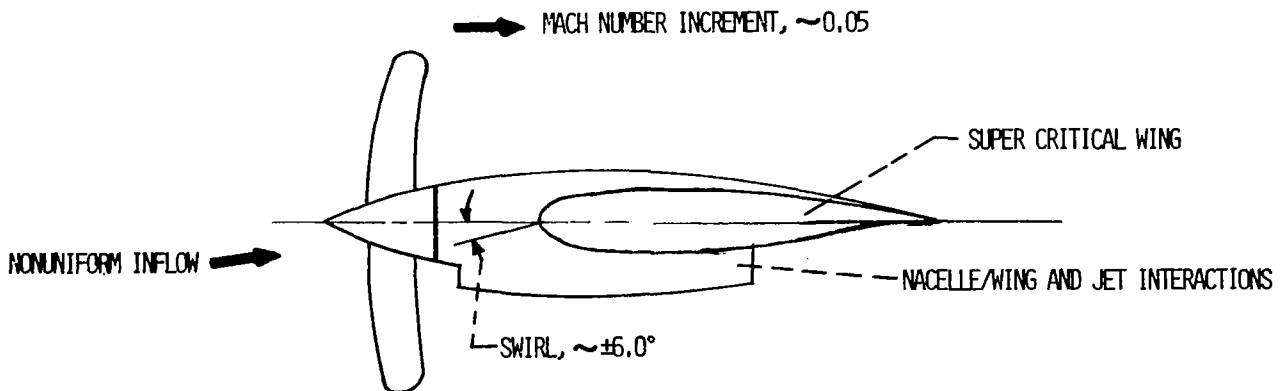
Nacelle/wing and jet interactions.- The nacelle/wing interaction affects the local profile drag and induced drag by altering the basic-wing pressure distribution in the vicinity of the nacelle. This effect can be minimized by proper contouring and filletting. The jet adds a scrubbing drag increment which may be reduced by separating the jet from the wing surface.

Slipstream incremental velocity.- Off-design operation of the wing segment inside the slipstream could add a drag-rise increment corresponding to $M + \Delta M$ for that segment. Leading edge extensions could help this. The velocity increment also produces a friction or scrubbing drag increment.

Nonuniform inflow.- The airframe induces 2P and higher cyclic variations in the propeller onset flow which may reduce the propeller efficiency. The cyclic inflow will also impact the blade design from the standpoint of fatigue life.

Swirl loss recovery.- The presence of the wing is expected to recover some of the swirl energy wasted by the uninstalled propeller. The wing acting as exit guide vane may be contoured to maximize this benefit.

PROBLEM DEFINITION FOR WING-MOUNTED ENGINES



INSTALLATION DRAG ESTIMATE

The summary of drag increments prepared by Lockheed-Georgia Co. for NAS1-15701 (ref. 1) gives an idea of how bad the propeller installation might be. The swirl/drag divergence increment shown is from a slipstream simulator test reported in NASA CR-152138. The 18 count increment is the largest measured in the test and might therefore be considered the worst case. Examination of those test results indicates a negative 10 count increment is equally likely. This might be considered the best case, thereby bounding the total effect of installation between 7.4 percent adverse and 1.9 percent favorable.

NASA/LOCKHEED NAS1-15701 COMPROMISE A/C #1

	<u>WORST CASE (ref.1)</u>	<u>BEST CASE</u>
$C_{DA/C}$ (no props)	0.02796	0.02796
$\Delta C_{D_{INDUCED}}$	0.00030	0.00030
$\Delta C_{D_{SCRUB}}$	0.00018	0.00018
$\Delta C_{D_{SWIRL/DRAG DIVERG.}}$	0.00176	-0.0010
$\Delta C_{D_{PROP EFFECTS}}$	0.00224	-0.00052
 <u>EFFECT OF INSTALLATION</u>		
$\frac{\Delta C_{D_{IND}} + \Delta C_{D_{SCRUB}} + \Delta C_{D_{SW/DD}}}{C_{D_{TOT}}} =$	7.4%	(-)1.9%

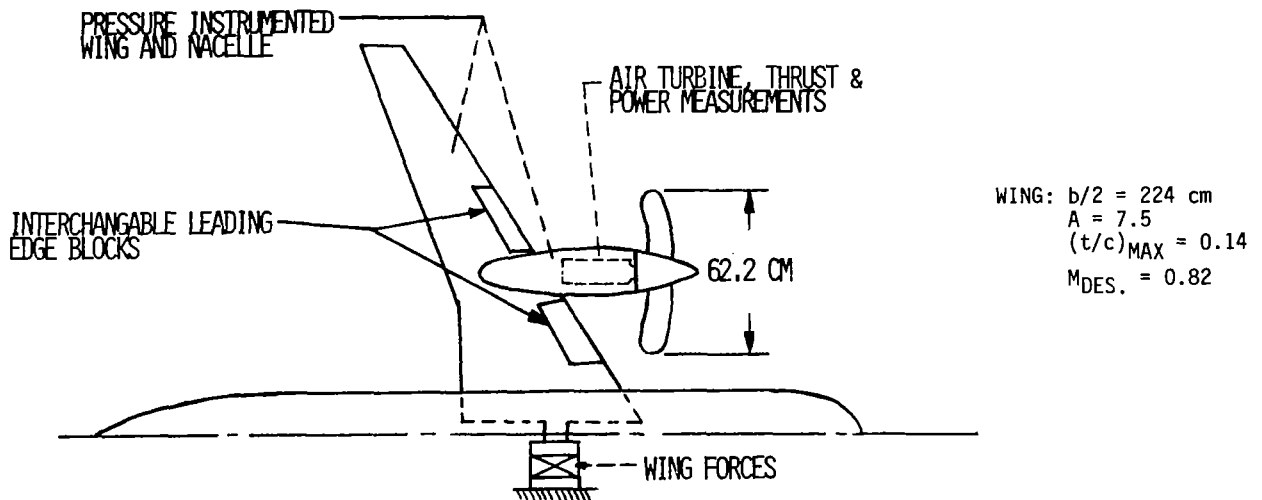
AMES APPROACH

The ejector-powered simulator test (ref.2) was intended to get an early first-order assessment of propfan installation losses. Although the results were not as accurate as expected, their magnitude should not be completely discounted. The half-model tests planned at Ames for 1980, 81 and 82 are intended to provide high-quality data on the installation losses including diagnostic measurements of normal surface pressure distributions and wake surveys. Initially, a baseline propeller/wing/nacelle model will be tested (1980) followed by a modified-leading-edge test (1981) and finally an optimized wing/nacelle configuration will be tested (1982) to assess the benefit of optimization. Later in the program a stability and control model will be tested (1985) to help assess the trade-offs between wing-mounted and fuselage-mounted engines. Efforts to develop improved analysis techniques will be continued. A inviscid small disturbance code solving the wing in the slipstream with swirl has been completed by Flow Research Corp. A new method including viscous effects will be attempted in subsequent years starting in 1981.

1. SLIPSTREAM SIMULATOR TEST - ORDER OF MAGNITUDE
2. ACTIVE PROPELLER HALF-MODEL TESTS
 - INITIAL TEST (1980)
 - Scope the installation problem
 - Incident noise on cabin wall
 - Blade structural response
 - FOLLOW-ON TEST (1981)
 - Wake diagnostics
 - Reynolds number effects
 - Wing-leading-edge mods
 - OPTIMIZED WING/NACELLE (1982) (CONTRACTOR)
 - Determine optimization benefit
3. STABILITY AND CONTROL MODEL (CONTRACTOR)
 - 1ST TEST - WING-MOUNTED ENGINES (1985)
 - 2ND TEST - AFT-FUSELAGE MOUNTED ENGINES (1985)
4. ADVANCED ANALYSIS (CONTRACTOR)
 - SMALL DISTURBANCE WITH SLIPSTREAM (1979)
 - HYBRID CODE - N.S. PLUS TRANSONIC POTENTIAL (1983)

POWERED SEMI-SPAN MODEL

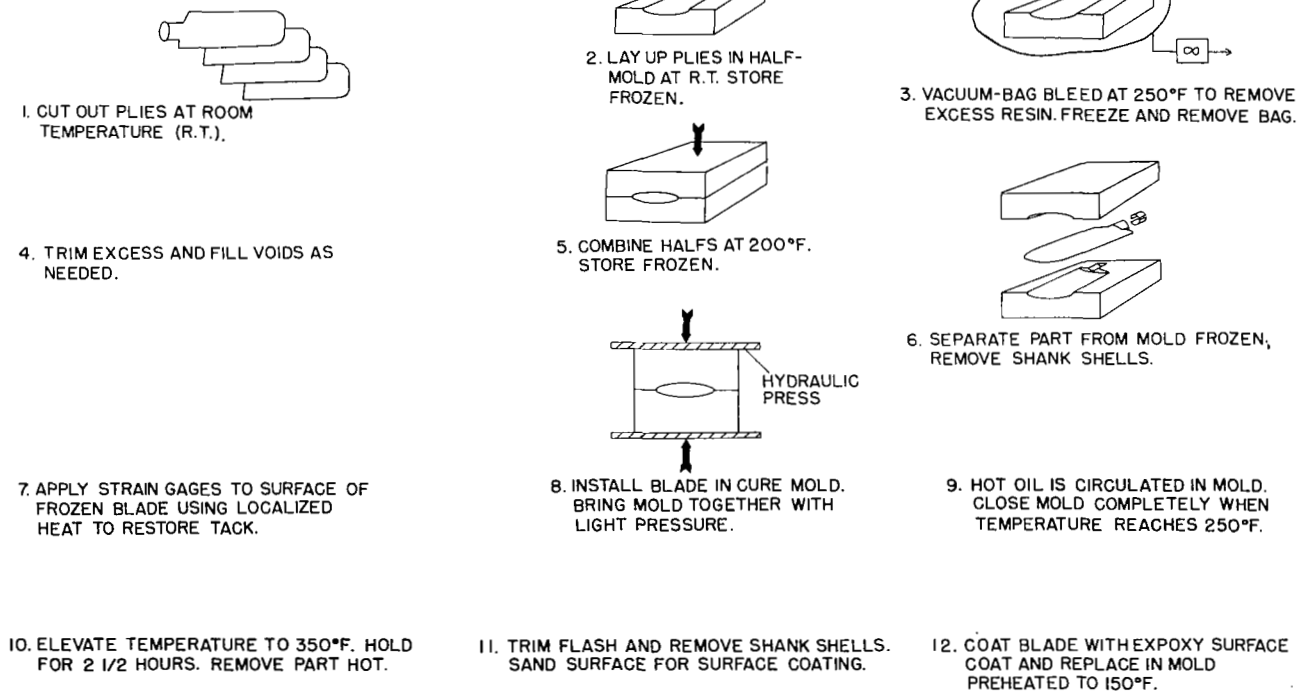
The powered model developed for the half-model testing consists of a pressure-instrumented supercritical wing, a non-metric half-body and the powerplant nacelle. A 62.2 cm 8-bladed propfan will be driven by a 550 kW air motor. The air motor exhaust exit area matches the exhaust exit on the transport installation so that the external nacelle contours are representative except for the faired-over inlet. The exhaust duct is instrumented and calibrated to provide accurate measurements of exhaust thrust which is to be subtracted from model forces measured by the floor balance. The propfan is the Hamilton Standard SR-2 configuration fabricated in graphite composite. The graphite blades have strain gages molded into the surfaces for measuring blade structural responses. Propeller thrust, torque and lateral forces are measured by a six-component balance mounted in the hub. In addition to the propeller model shown, a jet effects configuration with no propeller will be tested to provide the baseline data needed to get slipstream-induced increments. The fuselage and wing have been instrumented with dynamic pressure cells to measure incident acoustic pressures.



GRAPHITE BLADE PROCESS

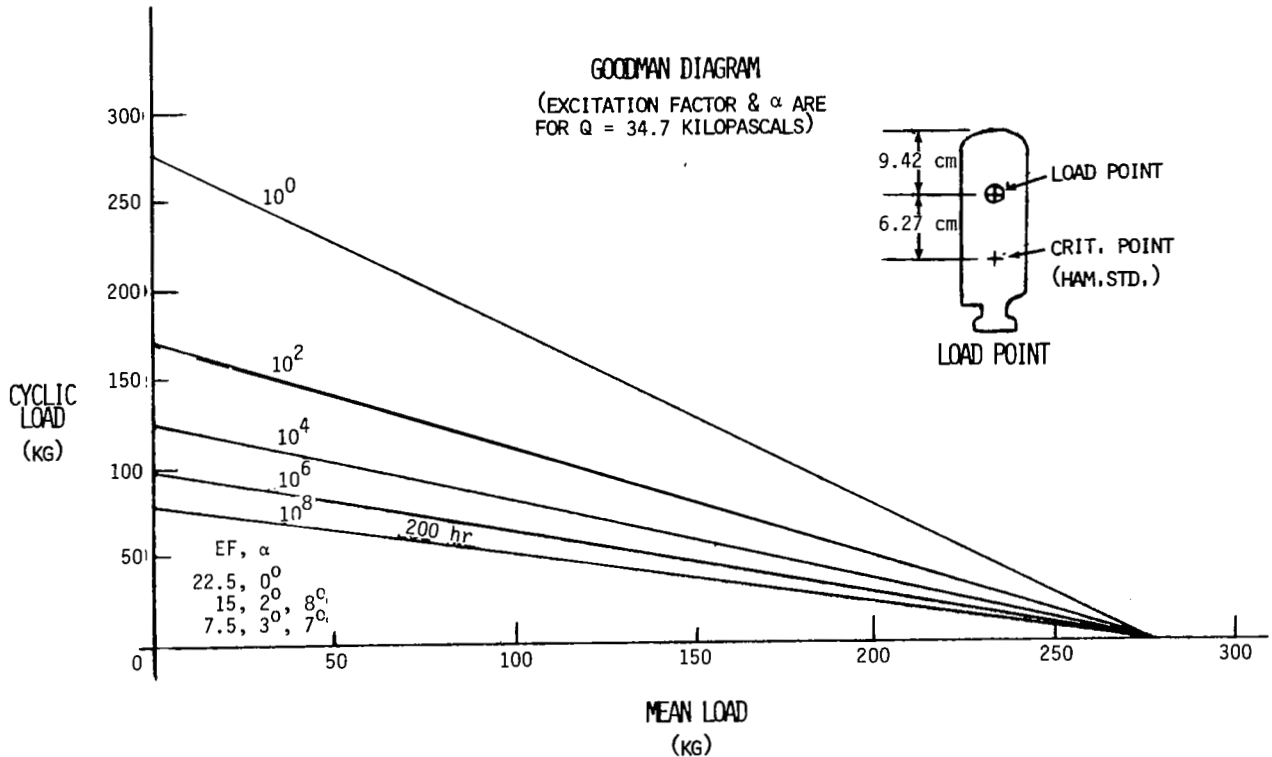
The manufacturing process developed for the graphite SR-2C blades is shown in this figure. The lay-up is composed of preimpregnated plies of unidirectional graphite tape in the ratios 1/4-bias and 3/4-longitudinal. The prebleeding is done to draw off most of the preimpregnated epoxy resin so that the lay-up will fit into the mold without excessive pressure thus avoiding fiber crushing. The technique has resulted in a blade structure with excellent mechanical properties.

MANUFACTURING PROCESS FOR GRAPHITE MODEL PROPELLER BLADE



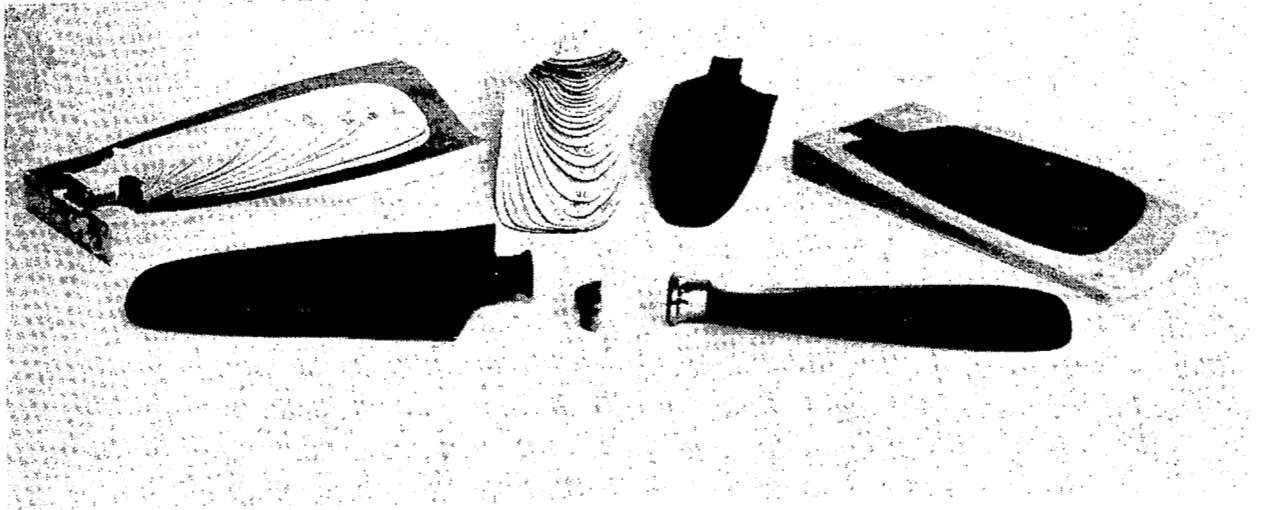
SR-2C PROPERTIES

Extensive destructive testing was done to determine the fatigue properties of production blades. This slide shows the Goodman diagram obtained from the tests. Our most severe anticipated operating condition is the point labeled excitation factor (EF) = 22.5 which occurs at zero airplane lift. Because of the large safety margin exhibited by the test results, no further attempt was made to optimize the structure.

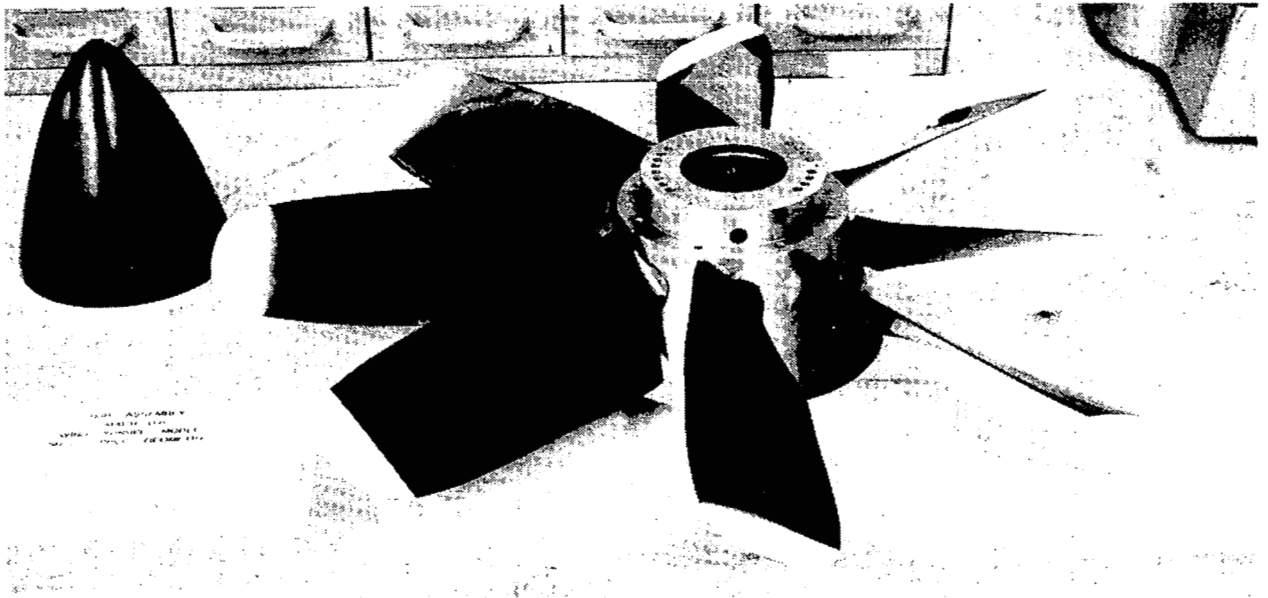


REFERENCES

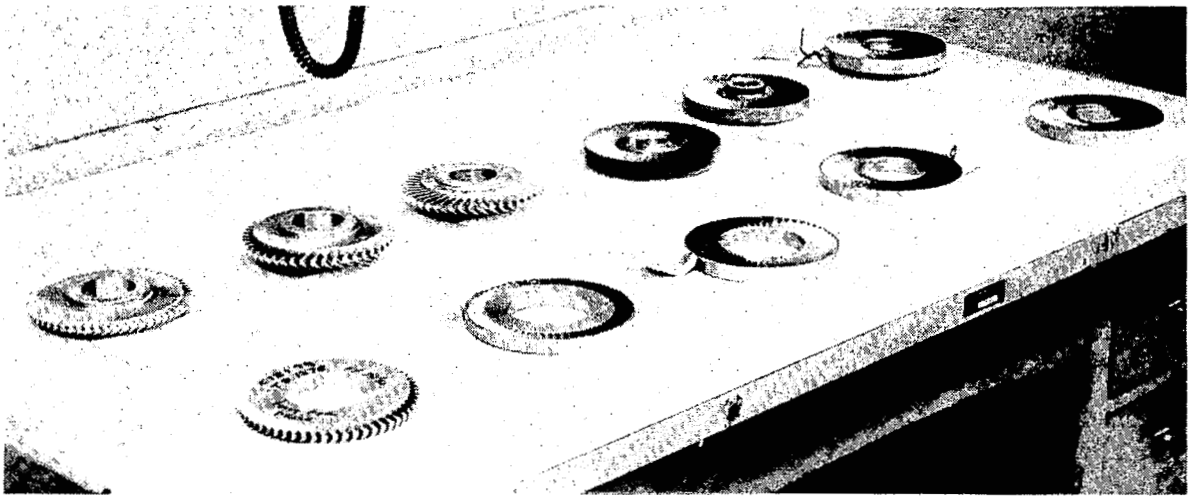
1. Final Oral Review Of Results From Lockheed-Georgia Study. "Turboprop Cargo Aircraft Systems Study". NASA Contract NAS1-15708, July 29, 1980.
2. Welge, H. Robert; and Crowder, James P.; Simulated Propeller Slipstream Effects On A Supercritical Wing. NASA CR-152138



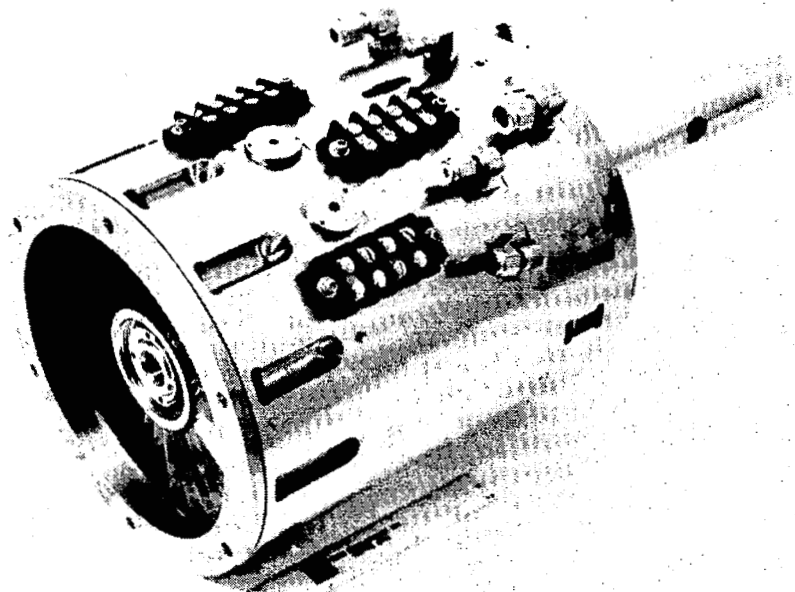
Blade fabrication stages.



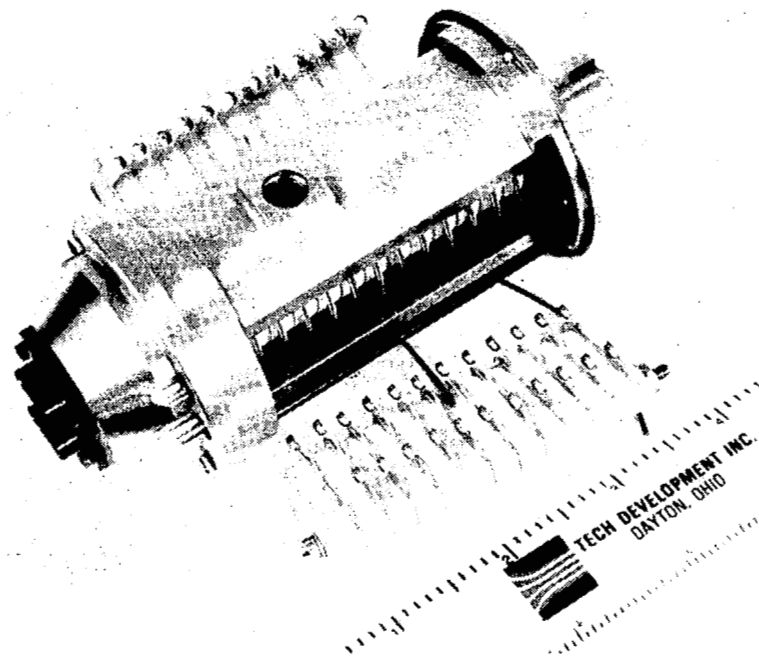
Model hub/propfan assembly.



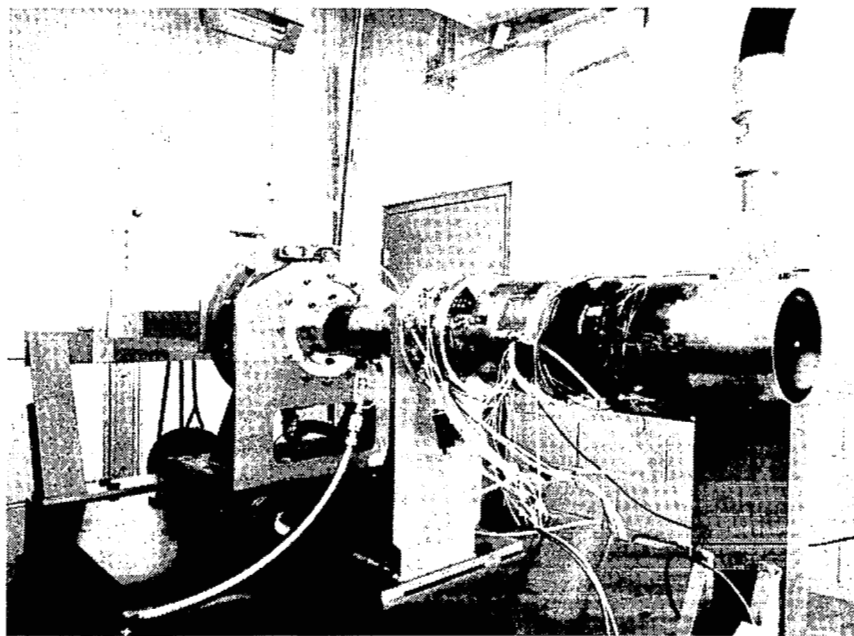
TDI turbine motor components.



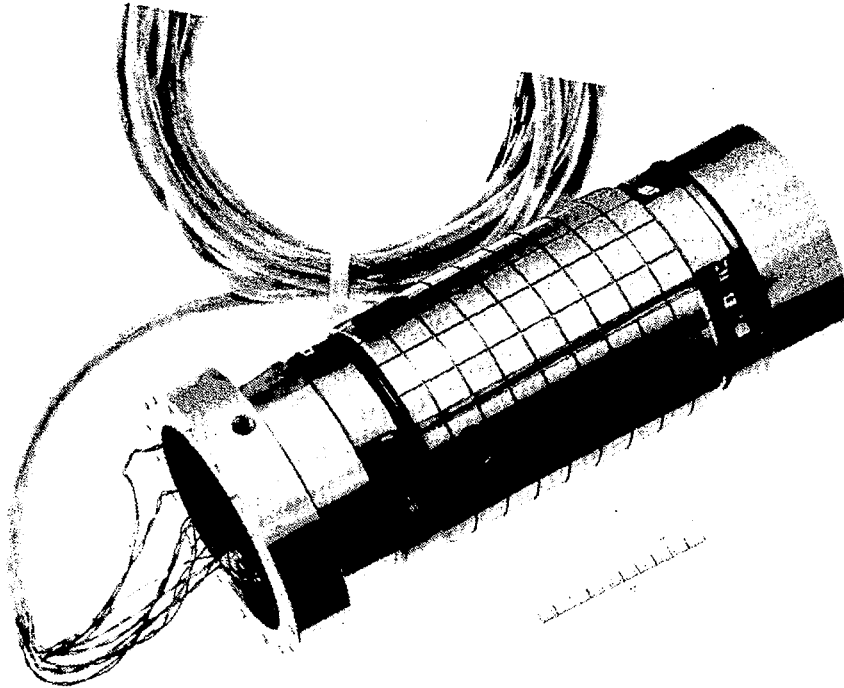
TDI turbine motor assembly.



TDI motor slipring assembly.



Motor and prop balance on dynamometer test stand.



Component propeller balance.

1. Report No. NASA CP-2172		2. Government Accession No.		3. Recipient's Catalog No.	
4. Title and Subtitle ADVANCED AERODYNAMICS AND ACTIVE CONTROLS - SELECTED NASA RESEARCH				5. Report Date February 1981	
				6. Performing Organization Code 534-02-13-01	
7. Author(s)				8. Performing Organization Report No. L-14278	
9. Performing Organization Name and Address NASA Langley Research Center Hampton, VA 23665				10. Work Unit No.	
				11. Contract or Grant No.	
12. Sponsoring Agency Name and Address National Aeronautics and Space Administration Washington, DC 20546				13. Type of Report and Period Covered Conference Publication	
				14. Sponsoring Agency Code	
15. Supplementary Notes This status review (fourth annual) is the first to be documented by an NASA Conference Publication.					
16. Abstract This Conference Publication contains selected NASA papers that were presented at the Fourth Annual Status Review of the NASA Aircraft Energy Efficiency (ACEE) Energy Efficient Transport Program held in Mountain View, California, October 7-9, 1980. These papers describe the status of several in-house research activities in the areas of advanced aerodynamics and active controls.					
17. Key Words (Suggested by Author(s)) Active controls Aerodynamics Flight controls			18. Distribution Statement Unclassified - Unlimited Subject Category 01		
19. Security Classif. (of this report) Unclassified		20. Security Classif. (of this page) Unclassified		21. No. of Pages 185	22. Price A09